CD20 as a prognostic biomarker and as a potential therapeutic target of oncolytic measles virus in adult acute lymphoblastic leukaemia

Katharine Elizabeth Bailey

The degree for which the thesis is submitted:

Doctor of Philosophy

University College London

2019

Signed Declaration

I, Katharine Elizabeth Bailey confirm that the work presented in this thesis is my own. Where information has been derived from other sources, I confirm that this has been indicated in the thesis.

Acknowledgements

I would like thank Professor Adele Fielding for her time, help and support with the work that has gone into this thesis. To laboratory colleagues for friendship, advice and for splitting my cells so I could go on holiday. To all my friends, in particular Emma Fosbury, Maria Marzolini, and Alison Thomas, who's understanding and support has helped me through. I would like to thank my parents and sisters for their unquestioning support and encouragement through my many, many years of further education. To my partner, Phil Mayers, who has never doubted my career choices and has lovingly supported me through every challenge along the way.

Abstract

Adult Acute lymphoblastic leukaemia (ALL) is an aggressive haematological malignancy with a poor outcome for 50% of patients. CD20 is an important target antigen in ALL. I have examined the role of CD20 as a biomarker in ALL and investigated whether an oncolytic measles virus (MV) targeted to CD20 is therapeutically relevant.

In Chapter 3, I analysed CD20 expression in primary specimens from the UKALL14 trial. Increasing CD20 expression - whether measured by the percentage of positive ALL cells or as CD20 antigen density - conferred inferior survival. I developed a RT-qPCR assay to quantify the gene expression of CD20 for use in specimens without stored cells. This correlated well with the flow cytometry data with a similar relationship to outcome.

ALL cells are known to be sensitive to MV oncolysis. Chapter 4 of my thesis investigated the therapeutic potential of a MV genetically modified to target entry via CD20. MVHαCD20 was more effective than the native MV at killing CD20 positive cells *in vitro*. A MV 'blinded' to the native MV receptors by ablation of the residues necessary for receptor-binding also demonstrated efficacy suggesting it would have therapeutic efficacy whilst avoiding off-target effects.

In Chapter 5 I investigated the underlying mechanism of the MV oncolysis previously demonstrated. Neutrophils are effector cells in MV-oncolysis but not by antibody-dependent cellular cytotoxicity, as previously shown by my lab, so I explored their role in antibody-mediated phagocytosis after CD20 targeted MV infection of ALL cells. I demonstrated that true phagocytosis was a rare event. However, neutrophils demonstrated an antibody-dependent cellular process called 'trogocytosis'. Trogocytosis did not result in target cell death, however it appeared to increase neutrophil activation, which suggests that activated neutrophils may orchestrate additional immune responses following MV oncolysis.

Impact Statement

Adult acute lymphoblastic leukaemia is an aggressive haematological malignancy with a poor outcome for 50% of patients. Typically, treatment involves several cycles of cytotoxic chemotherapy, long stays in hospital, and often requires an allogeneic haematopoietic stem cell transplant (HSCT). This can place an enormous emotional, and often economic burden on the individual patient and their family. There is a significant financial cost for the NHS from days in hospital and the treatments themselves. Improving ALL treatment will positively impact these burdens.

Improving the ability to identify those patients with a good or bad prognosis helps to decide the most appropriate treatment. My thesis has shown that increasing CD20 confers a poor prognosis and therefore this knowledge will benefit patients in tailoring their treatment. I have also developed an assay for measuring CD20 gene expression which will offer an alternative method which will have a potential impact both nationally and internationally. The quality of the assay could also have an impact locally by improving the robustness of similar qPCR assays.

The Edmonston-B, vaccine strain of measles virus has oncolytic activity in numerous preclinical tumour models with safety and some clinical efficacy also being demonstrated in clinical trials. My project has shown that a CD20 targeted virus has therapeutic potential. This could be of future benefit to ALL patients.

The mechanism of MV oncolysis is gradually being unravelled. It is important to understand the mechanisms in order to present a safe product and also to inform the likely modifications which could result in enhanced efficacy. This thesis has investigated the role of neutrophils and shown that neutrophil trogocytosis occurs in MV oncolysis. Given that ALL is treated with multi-agent chemotherapy regimens, an understanding of the mechanism will help to determine the correct place for this novel treatment.

This work has already been disseminated with four poster presentations at three international conferences: American Society of Haematology, European Haematology Association and American Society of Gene and Cellular Therapy. The work is intended for

publication in peer reviewed journals of high impact factor, thus benefiting the scientific community as a whole.

The project has been funded by the charity Bloodwise. It has received specific interest from a number of their funders who visited our laboratory and were very engaged by the process. This project improved the ability of Bloodwise to raise funds for translational research in haematological malignancies. I have also given two presentations of this work to the Bloodwise fundraisers.

Probably the most excitement for a new treatment in ALL in recent years are the CAR-T cells. However, this is a complex product that requires expertise and expense to administer, with the possibility of life-threatening side effects, and is also specific to individual patients. An advantage of oncolytic MV is that it could potentially be freeze-dried, as vaccines, and safely distributed to less-developed countries. Thus, in the future MV could have huge international benefit to patients with ALL and other malignancies.

Publications and Abstracts

Publications and abstracts arising from the work described in this thesis at the time of submission:

European Haematology Association 23rd Congress, June 2018, Stockholm, Sweden, Bailey K, Beaton B, Kirkwood AA, Aguiar M, Alapi K, Clifton-Hadley L, Patrick P, Lawrie E, Douglas A, Marks DI, McMillan A, Rowntree CJ, Menne T, Wrench B, Moorman AV, Fielding AK Re-thinking the prognostic relevance of a CD20 expression cut-off of 20% in Acute Lymphoblastic Leukaemia: Initial results from the UKALL14 Trial . Poster presentation.

American Society of Gene and Cell Therapy 21st Annual Meeting, May 2018, Chicago,IL,USA Bailey K, Aref S, Mitchell R, Alapi K, Aguiar M, Dey A, Burt R, Lee S, Muirhead C, Naughton T, Fielding AK. CD20 Targeting of Oncolytic Measles Virus in the Treatment of Adult Acute Lymphoblastic Leukemia. Poster Presentation.

American Society of Hematology 59th Annual Meeting and Exposition, December 2017, Atlanta, USA Bailey K, Aref S, Dey A, Mitchell RJ, Burt R, Naughton TJ, Okasha D, Alapi K, and Fielding AK Oncolytic measles virus and CD20 targeting in the treatment of adult ALL. Poster Presentation

American Society of Gene and Cell Therapy 19th Annual Meeting, May 2016, Washington DC, USA Bailey K, Dey A, Aref S, Boyer L, and Fielding, AK. Can Oncolytic Measles Virus Targeted to CD20 Recapitulate any of the Effects of Rituximab in the Treatment of Acute Lymphoblastic Leukaemia? Poster Presentation

Buatois V, Johnson Z, Salgado-Pires S, … Bailey K, Fielding AK, Eissenberg L, Ritchey J, Rettig M, DiPersio JF, Kosco-Vilbois MH, Masternak K, Fischer N, Shang L, Ferlin WG. Preclinical development of a bispecific antibody that safely and effectively targets CD19 and CD47 for the treatment of B cell lymphoma and leukemia. Mol Cancer Ther. 2018 May 9. [Epub ahead of print]

Bailey K, Burt R, Fielding AK. (2018) The Future of Haematology: The Impact of Molecular Biology and Gene Therapy pp 93-98 in Edited by Provan D. ABC of Clinical Haematology (4th Ed), John Wiley & Sons Ltd.

Aref S, Bailey K, Fielding A. Measles to the Rescue: A Review of Oncolytic Measles Virus. Viruses. 2016 Oct 22;8(10). Pii:E294

Dey A, Zhang U, Castleton AZ, Bailey K, Beaton B, Patel B, Fielding AK. The role of neutrophils in measles virus-mediated oncolysis differs between B-cell Malignancies and is not always enhanced by G-CSF. Molecular Therapy. 2016 Feb;24(1):184-92. doi: 10.1038/mt.2015.149. Epub 2015 Aug 17.

Statement of Work Undertaken

Sample processing of UKALL14 specimens was undertaken by members of the MRD laboratory. Flow cytometry of 67 UKALL14 specimens was carried out and analysed Dr Brendan Beaton, Clinical Research Fellow. Flow cytometry acquisition of the remaining UKALL14 specimens was carried out by a laboratory technician, Melanie Aguiar who was trained and supervised by the author.

Outcome statistics for UKALL14 specimens were analysed by Amy Kirkwood, Senior Statistician, CRUK and UCL Cancer Trials Centre.

Table of Contents

Declaration……2

Acknowledgements……3

Abstract……4

Impact Statement……5

Publications and Abstracts……7

Statement of Work Undertaken……9

Table of Contents……10

List of Figures……15

List of Tables……18

List of Abbreviations……19

Chapter 1 Introduction 22

1.1 Acute Lymphoblastic Leukaemia 22

1.2 Prognostic and predictive factors in ALL 24

1.2.1 Minimal Residual Disease in Acute Lymphoblastic Leukaemia 26

1.3 CD20 29

1.3.1 Relevance of CD20 expression in Acute Lymphoblastic Leukaemia 31

1.3.2 CD20 targeting with Rituximab 34

1.3.3 Mechanisms of action of rituximab 34

1.4 Cancer therapeutics – historical context. 36

1.4.1 Oncolytic virotherapy – a novel cancer therapeutic 37

1.4.2 Measles and its vaccine 40

1.4.3 MV Structure 41

1.4.4 MV Receptors 42

1.4.5 Antiviral host defence against MV 45

1.4.6 Measles virus as oncolytic virotherapy 47

1.4.7 Genetically modified MV 47

1.4.8 MV Targeting 49

1.4.9 CD20 targeted oncolytic MV 50

1.4.10 MV receptor 'blinding' 50

1.4.11 Measles Virus Clinical Trials 51

1.5 Mechanisms of oncolysis 55

1.5.1 Role of the Immune System 56

1.6 Neutrophils 58

1.6.1 Neutrophil Biology 58
1.6.2 Neutrophils and phagocytosis 58
1.6.3 Neutrophils and cancer 59
1.7 Hypothesis and aims of this thesis 60

Chapter 2 Methods 62
2.1 General Cell and Tissue Culture Methods 62
2.1.1 Tissue culture 62
2.1.2 Cell lines 62
2.1.3 Cell culture reagents 63
2.1.4 Cryopreservation and cell recovery 63
2.1.5 Cell counting and viability 64
2.2 Flow Cytometry Methods 64
2.2.1 General method 64
2.2.2 Compensation 67
2.2.3 Estimating molecules per cell (MPC) 67
2.2.4 Fluorescent activated cell sorting 67
2.2.5 Imaging Flow cytometry - Imagestream® 68
2.3 Measles Virus Methods 68
2.3.1 Measles Virus strain 68
2.3.2 MV rescue from cDNA 68
2.3.3 MV propagation and $TCID_{50}$ 69
2.3.4 MV Infection 69
2.4 Neutrophil Extraction Methods and Cellular Assays 70
2.4.1 Neutrophil Isolation from Peripheral Blood – Traditional Method 70
2.4.2 Neutrophil Isolation from Peripheral blood – Magnetic Beads - MACSxpress® - Method 71
2.4.3 Complement Dependent Cytotoxicity (CDC) assay 72
2.4.4 Neutrophil Mediated Antibody-Dependent Cellular Phagocytosis (ADCP) Assay 72
2.5 Microscopy Methods 73
2.5.1 Confocal Microscopy 73
2.6 Molecular Biology Methods 74
2.6.1 mRNA extraction – TRIzol® method 74
2.6.2 mRNA extraction – QIAamp® RNA Blood Mini Kit (Quiagen) 74
2.6.3 First strand cDNA synthesis – Method A (Used in MV experiments) 75
2.6.4 First strand cDNA synthesis – Method B (MRD lab method – used for UKALL14 primary patient specimens) 75
2.6.5 First strand cDNA synthesis – Method C (RT^2 First Strand Kit - Qiagen® – For use with RT^2 Profiler assays) 76

2.7 Cloning Methods....76

2.7.1 Cloning and Retroviral Transduction of Nalm6 to make Nalm6-CD20....76

2.7.2 Extraction of DNA Fragments from TAE Agarose Gel....77

2.7.3 Restriction Digest....78

2.7.4 Ligase Reaction....78

2.7.5 Retroviral Transfection....79

2.8 RT qPCR Methods....81

2.8.1 MV-N (nucleocapsid) mRNA relative quantification by PCR....81

2.8.2 GeNorm analysis....82

2.8.3 Real-Time PCR for RT^2 Profiler PCR Arrays....83

Chapter 3 CD20 as a prognostic biomarker in Acute Lymphoblastic Leukaemia 85

3.1 Introduction....85

3.1.1 Prognostic, predictive and therapeutic biomarkers in cancer....85

3.1.2 Prognostic and predictive factors in ALL....85

3.1.3 CD20 as a prognostic marker in BCP-ALL....86

3.1.4 Rituximab in the treatment of ALL....86

3.1.5 UKALL14 and Rituximab....87

3.1.6 Clarifying the difference between prognostic and predictive biomarkers....88

3.1.7 How to monitor CD20 expression.....89

3.1.8 Rationale for developing a RT-qPCR assay to measure CD20 expression....89

3.2 Hypotheses:....90

3.3 Aims:....90

3.4 Methods....91

3.5 Results....94

3.5.1 Baseline characteristics of patients analysed for CD20 expression by flow cytometry 94

3.5.2 Distribution of CD20 expression across patient samples in UKALL14....96

3.5.3 CD20 antigen density increases with the proportion of CD20 positive blasts.....97

3.5.4 Higher CD20 expression is associated with inferior outcomes in UKALL14....97

3.5.5 Event Free Survival and CD20....99

3.5.6 Overall survival and CD20....101

3.5.7 Increasing CD20 antigen density negatively impacts survival....103

3.5.8 CD20 expression does not affect outcome in UKALL14 patients with BCR-ABL1....104

3.5.9 Multivariable analysis....107

3.5.10 Including antigen density improves CD20 as a prognostic biomarker....109

3.5.11 CD20 expression together with cytogenetic risk factor can identify very good and very poor risk patients. 112

3.5.12 Developing a molecular method to determine CD20 expression 114

3.5.13 GeNorm analysis enables the identification of stable reference genes. 114

3.5.14 Avoiding increased CD20 expression from normal B-cells – Can CD20 splice variants help exclude normal B-cells? 116

3.5.15 CD20 RT-qPCR assay results correlated strongly with CD20 flow cytometry results 119

3.5.16 Further Optimising RT-qPCR Assay performance 121

3.5.17 Patient characteristic in patients with RT-qPCR data are similar to those with flow cytometry data. 122

3.5.18 RT-qPCR CD20 expression is strongly correlated to flow cytometry CD20 124

3.5.19 CD20 measured by RT-qPCR does not significantly predict event free survival in UKALL14 BCP-ALL patients 125

3.5.20 Comparison of RT-qPCR method to flow cytometry methods 126

3.6 Discussion 128

3.6.1 CD20 measured by RT-qPCR is a potential prognostic biomarker in BCR-ABL1 negative patients 129

3.6.2 Comparing flow cytometry and RT-qPCR 129

3.6.3 BCR-ABL1 and CD20 130

Chapter 4 A CD20 targeted Oncolytic Measles Virus 132

4.1 Introduction 132

4.1.1 CD46 133

4.1.2 SLAM (CD150) 134

4.1.3 'Blinding' MV to Native receptors 135

4.2 Purpose of this chapter. 136

4.3 Hypotheses 136

4.4 Aims 136

4.5 Results 137

4.5.1 NALM6 cells can be retrovirally transduced to stably express CD20 137

4.5.2 CD20 expression on ALL cells can show a broad range of intensity within a leukaemic blast population. 140

4.5.3 MVHαCD20can infect and replicate in ALL cells 141

4.5.4 MVHαCD20 infection results in greater cell death in ALL cells expressing CD20 ... 143

4.5.5 NALM6 cells expresses CD46 but do not express SLAM or Nectin4. 145

4.5.6 ALL cells universally express CD46 but rarely express SLAM or Nectin 4. 146

4.5.7 CD46 expression, as measured by mean fluorescent intensity (MFI) is significantly lower in leukaemic blasts than in normal lymphocytes. 148

4.5.8 MVHαCD20 has greater oncolytic efficacy than MVHαCD20CD46blind 150

4.5.9 MVHαCD20SLAMblind has similar oncolytic efficacy to MVHαCD20 152

4.5.10 Blinding MV to CD46 results in reduced complement dependent cytotoxicity 154

4.5.11 MVHαCD20CD46blind infection induces less neutrophil-medicated antibody dependent cellular phagocytosis (ADCP) than MVHαCD20 when complement is present. 157

4.6 Discussion 159

Chapter 5 Antibody-Dependent Neutrophil-Mediated Oncolysis 163

5.1 Introduction 163

5.1.1 Neutrophils and oncolytic virotherapy 164

5.1.2 Antibody dependent cellular phagocytosis (ADCP) 165

5.2 Hypothesis: 166

5.3 Aims: 166

5.4 Results 167

5.4.1 Neutrophil mediated antibody dependent cellular phagocytosis (ADCP) as a mechanism of MV oncolysis 167

5.4.2 MVNSe and MVHαCD20 infection result in a positive finding in the ADCP assay .. 168

5.4.3 The proportion of positive cells in the ADCP assay is dependent on the quantity of anti-MV IgG 171

5.4.4 Imaging flow cytometry and confocal microscopy show true phagocytosis to be a rare event 173

5.4.5 Neutrophils had increased mobility, morphological changes and showed trogocytosis when ALL cells had previously been infected with MV. 176

5.4.6 Trogocytosis does not directly result in increased target cell death. 180

5.4.7 Relationship of trogocytosis and neutrophil activation 181

5.4.8 Exploring targeted gene expression profiles of neutrophils after trogocytosis. 187

5.5 Discussion 192

Chapter 6 General Discussion 195

6.1 CD20 as a prognostic marker. 195

6.2 Redefining the 'positive' cut-off for CD20 196

6.3 Improving the quantification of CD20 expression 197

6.4 RT-qPCR vs flow cytometry 197

6.5 Exploring the use of a CD20 targeted oncolytic MV 198

6.6 Conclusions 200

References 201

Appendix I: Full gating strategy for ADCP assay 217

Appendix II: RT^2 profiler gene lists 218

List of Figures

Figure 1-1 Acute Lymphoblastic Leukaemia (ALL) Average Number of New Cases per Year and Age-Specific Incidence Rates per 100,000 Population, UK, 2013-2015. 22
Figure 1-2 Detection thresholds for measurable residual disease detection..... 27
Figure 1-3 A schematic representation of CD20. 29
Figure 1-4 Putative mechanisms of action of rituximab. 35
Figure 1-5 Measles virus Edmonston vaccine lineage 41
Figure 1-6 Schematic diagram of measles virus structure and genome. 42
Figure 1-7 Schematic representation of measles virus receptors 43
Figure 1-8 Measles virus rescue from cDNA. 49
Figure 3-1 UKALL14 Trial Schema 88
Figure 3-2 Flow cytometry antibody panel used for UKALL14 patient specimens 91
Figure 3-3 Flow cytometry gating strategy for determining CD20 percentage. 93
Figure 3-4 Samples from UKALL14 available for flow cytometry. 94
Figure 3-5 CD20 percentage positive blasts in UKALL14 specimens 96
Figure 3-6 Antigen Density of CD20 on B-ALL blasts..... 98
Figure 3-7 Percentage of CD20 positive blasts is significantly associated with inferior event free survival..... 100
Figure 3-8 Percentage of CD20 positive blasts is significantly associated with inferior overall survival. 102
Figure 3-9 Percentage of CD20 positive blasts multiplied by CD20 antigen density (MPC) is significantly associated with inferior event free survival. 103
Figure 3-10 Clinical Outcomes in BCR-ABL1 positive and negative groups. 105
Figure 3-11 Clinical Outcomes in BCR-ABL1 positive and negative groups including CD20 antigen density..... 106
Figure 3-12 Comparing flow methods: ROC analysis. 110
Figure 3-13 Clinical outcome when Youden's cut-off is used to determine CD20 positive groups. 111
Figure 3-14 Clinical Outcomes in for CD20 and standard/high risk groups. 113
Figure 3-15 geNorm analysis to identify the most stable reference genes and the optimum number of reference genes. 115
Figure 3-16 Schematic representation of CD20 variant coding transcripts. 117
Figure 3-17 Expression of CD20 variants in comparison to wild type CD20. 118
Figure 3-18 CD20 gene expression shows a strong correlation to flow cytometry data. 119

Figure 3-19 Histograms of Flow cytometry and RT-qPCR CD20 expression for UKALL14 specimens in pilot study. 119
Figure 3-20 Concordance of RT-qPCR data to flow data is strengthened when bone marrow samples alone are analysed. 120
Figure 3-21 Samples from UKALL14 available for RT-qPCR. 122
Figure 3-22 59 bone marrow specimens had CD20 data by both flow cytometry (x-axis) and RT-qPCR (y-axis). 124
Figure 3-23 Clinical outcome Youden's cut-off is used for RT-qPCR CD20 to determine groups. 126
Figure 4-1 Schematic representation of MVHαCD20. 133
Figure 4-2 Schematic of MSCV-IK6-IRES-mRFP replication defective retroviral vector indicating restriction sites and insertion of CD20 gene. 137
Figure 4-3 Schematic of retroviral transduction using Phoenix™-AMPHO packaging cells. 138
Figure 4-4 CD20 expression of NALM6 cells, Raji, NALM6-low-CD20, NALM6-medium-CD20, and NALM6-high-CD20. 139
Figure 4-5 Examples of CD20 expression in primary ALL specimens. 140
Figure 4-6 One-step growth curves for MV-NSe and MVHαCD20 141
Figure 4-7 MV-N mRNA expression of NALM-6 and NALM6-high-CD20 cells following MV infection. 142
Figure 4-8 Live cells as a proportion of uninfected cells following MVHαCD20 infection or MV-NSe on NALM6 cells with differing CD20 expression. 144
Figure 4-9 NALM6 cells express CD46 but not SLAM or Nectin 4. 145
Figure 4-10 Expression of MV receptors CD46, Nectin 4 and SLAM of primary ALL cells. .. 147
Figure 4-11 CD46 expression has a significantly lower MFI in normal lymphocytes compared to ALL blasts in paired patient UKALL14 specimens. 149
Figure 4-12 Live cells over time following infection with CD46 blind MV. 151
Figure 4-13 Live cells over time following infection with SLAM blind MV. 153
Figure 4-14 Complement Dependent Cytotoxicity (CDC) assay following infection with CD46 blind MV. 155
Figure 4-15 Neutrophil mediated Antibody dependent cellular phagocytosis (ADCP) assay with CD46 blind MV. Comparing the % phagocytosis in samples +/-complement. 158
Figure 5-1 Representative flow cytometry dot plot of antibody dependent phagocytosis (ADCP) assay with CD15-APC stained neutrophils as effector cells and PKH67 stained NALM6 highCD20 cells 167

Figure 5-2 Neutrophil phagocytosis is increased in higher expressing CD20 cells in the presence of Rituximab at different concentrations. 168
Figure 5-3 A positive neutrophil mediated ADCP assay reached similar levels following MV infection to rituximab in the presence of both anti-MV antibody and complement. 170
Figure 5-4 CD20 MFI decreases following 24 hours post infection MVHaCD20 MOI 1.0. ... 171
Figure 5-5 ADCP assay result is related to concentration of anti-MV IgG 172
Figure 5-6 Imagestream analysis of ADCP assay – rituximab condition. 174
Figure 5-7 Imagestream analysis of ADCP assay – MV infected NALM6 cells. 175
Figure 5-8 Neutrophils showed acquisition of of PKH67 dye from NALM6 cells, and greater activity when in co-culture with NALM6-high-CD20 infected by MV-HαCD20 than with uninfected targets alone. 177
Figure 5-9 Neutrophils showed greater morphological changes when in co-culture with NALM6-high-CD20 infected by MVHαCD20 than with uninfected targets alone. 178
Figure 5-10 Confocal imaging Z-stack indicates internalization of PKH67 staining by neutrophil. 179
Figure 5-11 Live/dead analysis of NALM6-high-CD20 cells and neutrophils in ADCP assays. 180
Figure 5-12 Neutrophils become more activated when co-cultured with infected target cells and this is greater in the presence of anti-MV IgG. 182
Figure 5-13 RT^2 qPCR Human Phagocytosis gene array. 188
Figure 5-14 RT^2 qPCR Human Cytokine and Chemokine array. 189

List of Tables

Table 1-1 EGIL classification of B-ALL 23
Table 1-2 Published Studies Investigating the Impact of CD20 expression on Outcome in B-ALL. 32
Table 1-3 Selected Oncolytic Viruses in Clinical Trials 38
Table 1-4 Oncolytic Measles Virus Clinical trials 52
Table 2-1 Antibodies and Isotype Controls used in flow cytometry 65
Table 3-1 Baseline characteristics of patients with CD20 data by flow cytometry compared to all BCP-ALL patients. 95
Table 3-2 Multivariable analysis of Event Free Survival 108
Table 3-3 Baseline characteristics of patients with CD20 data by RT-qPCR and flow cytometry compared to all BCP-ALL patients. 123
Table 3-4 Comparing flow data to RT-qPCR data. 127
Table 4-1 SLAM expression of normal B-cells 134

List of Abbreviations

ADCC	Antibody-dependent cell-mediated cytotoxicity
ADCP	Antibody-dependent cellular phagocytosis
ALL	Acute lymphoblastic leukaemia
ATP	Adenosine triphosphate
AUC	Area under the curve
BM	Bone marrow
BSA	Bovine serum albumin
CDC	Complement-dependent cytotoxicity
CDV	Canine distemper virus
CML	Chronic myeloid leukaemia
CNS	Central nervous system
CXCR	C-X-C motif receptor
DC	Dendritic cell
DMEM	Dulbecco's modified eagle medium
DMSO	Dimethyl sulfoxide
DNA	Deoxyribonucleic acid
dsRNA	Double stranded RNA
EFS	Event free survival
EGF	Epidermal-derived growth factor
ELISA	Enzyme-linked immunosorbent assay
FBS	Foetal bovine serum
GBM	Glioblastoma multiforme
GCSF	Granulocyte colony stimulating factor
GFP	Green fluorescent protein
GM-CSF	Granulocyte-monocyte colony stimulating factor
GIMEMA	Gruppo Italiano Malattie EMatologiche dell'Adulto
GMP	Good manufacturing practice
GRAALL	Group for Research in ALL
hpi	Hours post infection
HSCT	Haematopoietic stem cell transplant
IFN	Interferon
Ig	Immunoglobulin

IL	Interleukin
IV	Intravenous
JAK	Janus kinase
MFI	Mean flourescent intensity
MHC	Major histo-compatability
MOI	Multipicity of infection
MRD	Minimal residual diesease
MSC	Mesenchymal stromal cells
MV	Measles virus
NDV	Newcastle disease virus
NILG	Northern Italy Leukaemia Group
NIS	Sodium iodide symporter
NK	Natural killer cell
OD	Optical density
OS	Overall Survival
PAMP	Pathogen associated molecular patterns
PBS	Phosphate buffered saline
PCR	Polymerase chain reaction
PETHEMA	Programa Español de Tratamientos en Hematología
PFU	Plaque forming unit
PI	Propidium iodide
PRR	Pattern recognition receptors
PVRL4	Poliovirus receptor-related 4
RDA	Food & Drug Administration
RNA	Ribonucleic acid
ROC	Receiver operating characteristic
ROS	Reactive oxygen species
RT	Room temperature
ScFV	Short chain fragment variable
SEM	Standard error of the mean
SLAM	Signalling lymphocyte activation molecule
ssRNA	Single stranded RNA
STAT	Signal transduction & activator of transcription
T-VEC	Talimogene Laherparepvec
TCID50	50% tissue culture infectious dose

TKI	Tyrosine kinase inhibitor
TLR	Toll-like receptor
VEGF	Vascular endothelial growth factor
VSV	Vesicular stomatitis virus

Chapter 1 Introduction

1.1 Acute Lymphoblastic Leukaemia

Acute lymphoblastic leukaemia (ALL) is a clonal disorder resulting from genetic abnormalities arising in lymphoid progenitor cells leading to the transformation and proliferation of malignant cells within the bone marrow and peripheral blood. ALL has a bi-modal age distribution, with 75% of cases occurring in children less than six years at diagnosis and a much lower peak in adults over the age of 70 [1, 2][See Figure 1-1]. In children, ALL is the most common malignancy diagnosed accounting for 20% to 30% of childhood cancer incidence and with modern therapy 80% to 90% of patients achieve a long-term cure [3, 4]. However, in adults ALL is a rare disease and often has a poor outcome with only 30-40% reaching long term cure, despite 85-95% having a good response to induction therapy[5] .

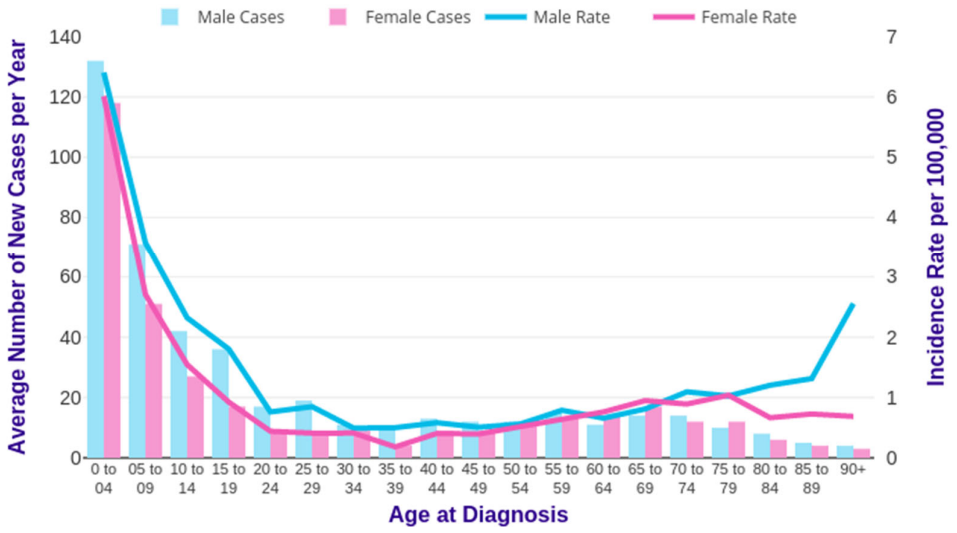

Figure 1-1 ***Acute Lymphoblastic Leukaemia (ALL) Average Number of New Cases per Year and Age-Specific Incidence Rates per 100,000 Population, UK, 2013-2015.*** *Source: cruk.org/cancerstats*

Predicting the likely outcome from presenting clinical, cellular and molecular features, is important to identify those patients who would benefit from more intensive therapy, such as haematopoietic allogeneic stem cell transplant, and also those who could be cured with

less intensive treatment in order to reduce long term unwanted effects - a particular concern in children and young adults. Increasingly, targeted non-chemotherapy agents are being employed to treat haematological malignancies. These have the benefit of efficacy whilst often avoiding the toxic unwanted effects of conventional chemotherapy - such as bone marrow suppression. This is particularly desirable in older patients who tolerate conventional chemotherapy poorly.

Traditionally, acute leukaemia was classified by cellular morphology of Romanowsky-stained peripheral blood and bone marrow aspirates smears using light microscopy. A uniform system of classification and nomenclature was first proposed by the French-American-British (FAB) Co-operative Group in 1976 [6]. The FAB classification formally divided leukaemia into 'lymphoblastic' and 'myeloid' leukaemias and provided further subdivisions dependent on appearances of maturation. Myeloid leukaemias were categorised into 6 main types (M0 to M6) and lymphoid leukaemia to 3 types (L1 to L3) where the 'M' or 'L' number increases with cellular maturation. Whereas this classification remains of use for describing the acute myeloid leukaemias, it is now only of historical interest for describing acute lymphoblastic leukaemia.

With the advent of flow cytometry, acute lymphoblastic leukaemia could be further subclassified to B-ALL and T-ALL according to cell markers that enabled lineage and maturation stage to be more definitely defined. A system for immunological classification was proposed in 1995 by the European Group for the Immunological Characterization of Leukemias (EGIL) [7]. Approximately 75% of ALL cases are B-ALL and can be identified by the expression of early B-cell markers (eg, CD19, cytoplasmic CD79a, cytoplasmic CD22) and the lack of T-cell markers (cytoplasmic CD3 and CD7). B-ALL can be further subdivided by flow cytometry based on the maturity of the progenitor cell according to the EGIL classification. CD20 is not seen in pro B-ALL but is variably expressed beyond B-I.

Table 1-1 EGIL classification of B-ALL

		Positive cell markers	Negative cell markers	% of ALL cases
B-I	Pro B-ALL	HLA-DR, TdT, CD19	CD10, CyIg	10
B-II	Common ALL	CD10, TdT	CyIg	50
B-III	Pre-B-ALL	CyIg, CD10, TdT		10
B-IV	Mature B-ALL	SmIg	TdT, CD34	4 (Majority Burkitts)

Although the EGIL classification remains a useful tool it has been superseded by the World Health Organisation (WHO) classification which is largely based on cytogenetic and genetic abnormalities. The WHO classification was published in 2001 and revised in 2008 and 2016 [8].

WHO classification of acute lymphoblastic leukaemia[a]

B-cell lymphoblastic leukaemia/lymphoma, not otherwise specified

B-cell lymphoblastic leukaemia/lymphoma, with recurrent genetic abnormalities

- B-cell lymphoblastic leukaemia/lymphoma with hypodiploidy
- B-cell lymphoblastic leukaemia/lymphoma with hyperdiploidy
- B-cell lymphoblastic leukaemia/lymphoma with t(9;22)(q34;q11.2)[BCR-ABL1]
- B-cell lymphoblastic leukaemia/lymphoma with t(v;11q23)[MLL rearranged]
- B-cell lymphoblastic leukaemia/lymphoma with t(12;21)(p13;q22)[ETV6-RUNX1]
- B-cell lymphoblastic leukaemia/lymphoma with t(1;19)(q23;p13.3)[TCF3-PBX1]
- B-cell lymphoblastic leukaemia/lymphoma with t(5;14)(q31;q32)[IL3-IGH]
- B-cell lymphoblastic leukaemia/lymphoma with intra-chromosomal amplification of chromosome 21 (iAMP21)b
- B-cell lymphoblastic leukaemia/lymphoma with translocations involving tyrosine kinases or cytokine receptors ('BCR-ABL1–like ALL')[b]

T-cell lymphoblastic leukaemia/lymphomas Early T-cell precursor lymphoblastic leukaemia[b]

[a] On the basis of The 2016 revision to the World Health Organization classification of myeloid neoplasms and acute leukemia.

[b] Provisional entity

1.2 Prognostic and predictive factors in ALL

Clinical features of increasing age and elevated white blood cell count at diagnosis have long been associated with a poor prognosis in ALL. Age over 60 years confers a particularly poor prognosis with only 10-15% surviving for 5 years [9]. The advent of cytogenetics

dramatically changed our understanding both of the disease and prognosis. The translocation t(9;22) resulting in the Philadelphia chromosome and the *BCR-ABL1* gene transcript is the most common cytogenetic abnormality seen in ALL and its presence indicates a very poor prognosis without targeted treatment. The prevalence of *BCR-ABL1* is less than 5% in children and between 15-30% in adults [10-12] and increases with increasing age [13]. The prognosis has improved with the addition of tyrosine kinase inhibitors (TKIs) to conventional treatment. Although there are no randomized trials comparing the combination of a TKI with conventional chemotherapy to chemotherapy alone, the UKALLX11/ECPG2993 trial compared groups from the pre-imatinib era with patients treated with chemotherapy and imatinib. The addition of imatinib resulted in a higher complete remission rate (92% versus 82%), a greater number of patients receiving a allogeneic haematopoietic stem cell transplant (46% versus 31%) and a superior 4 year overall survival (38% versus 22%) [14]. It is now standard practice to include a TKI with chemotherapy in the treatment of patients with *BCR-ABL1* positive ALL, and the role of second and third generation TKIs is also being explored. Early relapses with TKI inhibitors are almost always associated with point mutations in the *BCR-ABL1* kinase domain, the third generation Ponatinib has shown promise in treating patients who have become resistant to TKIs and is now being investigated as a first line treatment by the Gruppo Italiano Malattie EMatologiche dell'Adulto (GIMEMA) group [15, 16].

Genetic abnormalities other than the Philadelphia chromosome that indicate a poor prognosis were identified from the MRC UKALL XII/ECOG E2993 trial. This was a large multicentre international treatment trial of adult ALL which recruited a total of 1522 patients for whom pre-treatment cytogenetics was available for 90%. In addition to the Philadelphia chromosome, cytogenetics indicative of a poor outcome included the *KMT2A* (*MLL*) gene rearrangement t(4;11), complex karyotype and low hypodiploidy (30-39 chromosomes)/near triploidy (60-78 chromosomes) (Ho-Tr). Patients with t(4;11) represented 9% of the *BCR-ABL1* negative group, and had a significantly reduced 5 year event free survival of 24% [95% CI, 13%-36%] and overall survival of 24% [95% CI, 13%-36%] compared with *BCR-ABL1* negative patients, and they tended to die from relapse or other causes within a year of diagnosis. This was not true for patients with other MLL/11q23 translocations whose survival was comparable to that of other *BCR-ABL1* negative patients. A total of 5% of patients had a complex karyotype with five or more chromosomal abnormalities. They had a five-year overall survival of 28% [95% CI, 15%-43%]. The most favourable cytogenetics were high hyperdiploidy (HeH), which was also the most prevalent

chromosomal abnormality, other than the Philadelphia chromosome, forming 10% of the *BCR-ABL1* negative group. The overall survival for HeH was 53% [95% CI, 41% - 64%]. Del(9p) was also marginally associated with an improved event free survival and overall survival in this trial, however this abnormality has proven to be associated with poor outcome in patients who are also *BCR-ABL1* positive [17, 18].

Whole genome analysis of gene expression in ALL cells has provided further insight into genetic subtypes of ALL. A new subtype of ALL was described in children by Mullighan *et a*l in 2009 termed 'Philadelphia chromosome like', or '*BCR-ABL1*-like ALL', due to the gene expression profile being similar to that of *BCR-ABL1* positive ALL [19-21]. *BCR-ABL1*-like ALL shows a diverse array of kinase-activating alterations and is now included in the WHO classification. There is a high frequency of deletions of *IKZF1* – the gene that encodes the IKAROS protein - a lymphoid transcription factor – and rearrangements or mutations of other transcription factors such as *CRLF2* and *JAK*. *BCR-ABL1*-like ALL is indicative of poor outcome in both children and adults however, the array of abnormalities offers an exciting opportunity for precision medicine as known inhibitors to many of the affected pathways are already available in clinical practice, such as the *JAK* inhibitor ruxolitinib to target *JAK/STAT* pathway lesions, dasatinib to target *ABL* class alterations, and *MEK* inhibitors to target Ras/*MAPK* pathway [22, 23]. Currently no drugs that can target *IKZF1* are known, however there has been conflicting evidence that certain chemotherapeutic strategies are more advantageous to patients harbouring *IKZF1* abnormalities than others – such as pulses of prednisolone and vincristine. In preclinical studies retinoic acid compounds and *FAK* inhibitors are showing some promise [24, 25]. Although the chromosomal and genetic abnormalities are important in determining the best treatment options by risk stratifying patients with ALL, today the most significant prognostic biomarker is the presence of minimal residual disease (MRD) [26].

1.2.1 Minimal Residual Disease in Acute Lymphoblastic Leukaemia

Establishing that a patient with acute leukaemia is in remission has traditionally relied upon morphological assessment of a bone marrow specimen demonstrating less than 5% of nucleated cells as lymphoblasts. Although this is a marked reduction from the baseline diagnostic level of ≥20% lymphoblasts, it does not predict the likelihood of relapse. More sensitive methods have been developed to detect leukaemic cells below the limit of

conventional detection and termed 'minimal residual disease' or 'measurable residual disease' (MRD). The relevance of MRD has been increasingly understood and used in a range of haematological diseases, it was originally developed as a means of monitoring CML patients during TKI treatment as expression of the *BCR-ABL1* gene could be detected by RT-qPCR.

MRD can be measured by examining the expression of cell surface and cytoplasmic markers by flow cytometry or by molecular methods using the polymerase chain reaction (PCR) to analyse DNA or mRNA. The sensitivity of different methods can be compared to morphology assessment as illustrated in figure 1-2 [27]. Flow cytometric analysis of the blast population at diagnosis can establish a leukaemia associated immunophenotype (LAIP) so that at subsequent time points this clone can be detected and monitored. This technique has been widely used to monitor MRD in childhood ALL and has improved with technology enabling the use of 8 to 10 colour panels as standard – i.e. to measure increasing numbers of markers simultaneously.

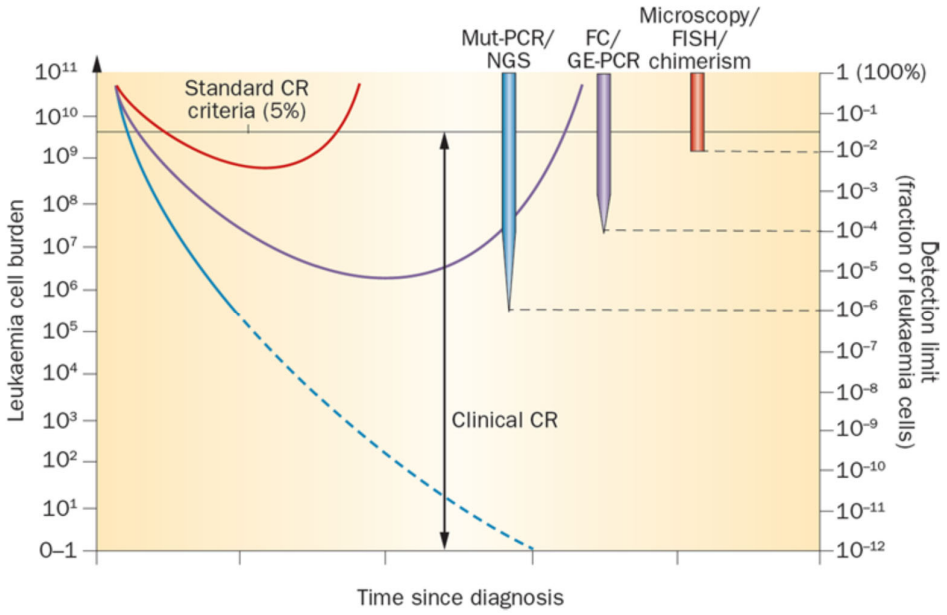

Figure 1-2 ***Detection thresholds for measurable residual disease detection*** *(adapted from Zach 2014 [27]).*
Mut-PCR - PCR fro fusion transcripts and gene mutations, NSG next-generation sequencing, FC flow cytometry, GE-PCR PCR for overexpressed genes.

Molecular techniques are based on the ability to find tumour-specific DNA or messenger RNA targets and amplify these by polymerase chain reaction (PCR). In ALL, leukaemia specific rearrangements of the immunoglobulin heavy gene or T-cell receptor gene can be detected and/or gene -fusion transcripts such as *BCR-ABL1* or *MLL*. These can then be amplified by RT-qPCR. Today, molecular methods are widely used in the management of adult ALL patients and a marker is available in >95% patients [26]. It should be noted that molecular methods are more laborious than detecting an aberrant LAIP by flow cytometry, however they have the benefit of about 1 $\log_{10}$ greater sensitivity. Recently there has also been interest in developing next generation sequencing to detect MRD. A NGS assay has been approved in 2018 by the FDA for its use in both ALL and myeloma. There is some evidence that NGS may provide greater sensitivity than previously described methods in both paediatric and adult ALL[28] [29].

In adult ALL, most studies have measured MRD following induction or in early consolidation. The Group for Research in ALL (GRAALL), the Northern Italy Leukaemia Group (NILG) and Programa Español de Tratamientos en Hematología (PETHEMA) groups have all confirmed MRD to have a strong and independent prognostic impact after induction and early consolidation treatment[30-34]. The German Multicentre ALL (GMALL) group showed that MRD negativity following induction II, or following consolidation I, at day 71 and week 16, was associated with a clinical benefit irrespective of clinical and cytogenetic risk factors. In contrast, detectable MRD $\geq 10^{-4}$ after consolidation I identified a new high-risk group [33]. In the NILG study an MRD level of 1 $x10^{-4}$ to $<10^{-3}$ correlated with inferior disease-free survival after allogeneic HSCT, compared to MRD negative, and those with an MRD $\geq 1x10^{-3}$ did very poorly [34]. In contrast, patients with MRD $\leq 1x10^{-4}$ after ≥3 intensive treatments had a good outcome. The PETHEMA group were able to successfully avoid HSCT in high risk patients who were MRD negative $<5x10^{-4}$ at week 17 with a good early morphological response. The GRAALL group also showed that measuring MRD $<1x10^{-4}$ at day 11 identified a group with excellent prognosis [32].

MRD has proven to be a powerful independent predictor of outcome in ALL. As described, evidence from recent clinical trials that incorporate MRD monitoring have indicated that early negative MRD is predictive of an excellent outcome, and that MRD monitoring helps to stratify treatment and can be used to pre-emptively salvage patients at later time points.

1.3 CD20

CD20 is a membrane bound non-glycosylated phosphoprotein expressed on the surface of both normal and malignant B-lymphocytes from early pre-B development until it is lost at terminal plasma cell differentiation [35, 36]. Of CD19 positive normal bone marrow cells approximately 60% express CD20 with approximately 20% of those also expressing CD10, a marker normally expressed on early lymphoid cells and the common form of ALL [37]. Expression density of CD20 is known to increase with cell maturation [38]. Following the initial use of anti-CD20 monoclonal antibodies it was thought that CD20 did not undergo antigen modulation [39], however it has subsequently been seen that following anti-CD20 binding the antigen can be rapidly internalised [40]. CD20 is highly expressed on most B lymphocyte cell lines at 100 000 to 200 000 antigens per cell [38].

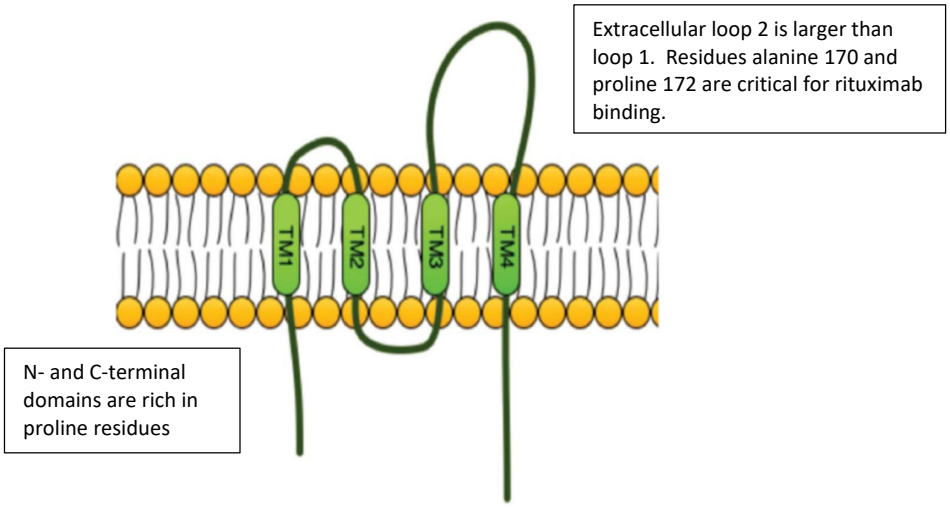

Figure 1-3 A schematic representation of CD20. As a member for the membrane spanning 4-A family it passes through the cell membrane four times resulting in the N- and C- terminal ends within the cytoplasm. Adapted from Eon Kuek et al.[42]

CD20 belongs to the membrane spanning 4-A (MS4A) family, its structure passes through the cell membrane four times resulting in the long N- and C- terminal ends within the cytoplasm and a small exposed portion on the cell surface. The larger extracellular loop is critical to the binding of the anti-CD20 monoclonal antibody rituximab [see figure 1-3] [41, 42]. Within the cell membrane CD20 organizes into dimers and tetramers. Reports suggest

that it localizes with CD40, MHC class II and the B-cell receptor antigen (BCR) although precise details of its interaction are currently unknown. CD20 has been shown to be down-modulated following CD40 engagement resulting in internalisation of CD20 and enhanced calcium signalling [43]. The function of CD20 is not yet fully understood. From the initial studies leading to its discovery using monoclonal antibodies it was discovered that binding to CD20 can augment B-cell function, inhibit proliferation and B cell differentiation. It also forms a component of a cell surface complex involved in Ca^{2+} trans-membrane regulation. By regulating Ca^{2+} homeostasis it is involved in cell cycle progression which, when activated, can lead to apoptosis. Engagement of CD20 can lead to various effects however experiments with different monoclonal antibodies have given opposing results. These include, increased phosphorylation of many targets, up-regulation of CD18, CD58, CD95 and MHC class II molecules, increased c-myc and b-myb. Despite evidence of the importance in B-cell development and calcium homeostasis, $CD20^{-/-}$ mice have normal lifespans and immunity. They are also able to reproduce successfully. The main finding from these animal models was of a reduced calcium response following IgM ligation [44].

Human and murine CD20 are structurally similar with 73% amino acid homology. The B-cells of CD20 deficient mice develop and function normally however their Ca^{2+} responses to CD19 and the B-cell receptor (BCR) are abnormal in the spleen [44, 45]. In humans, a rare case of CD20 deficiency in a Turkish girl has been described due to a homozygous compound mutation of the non-canonical splice donor sequence of exon 5, resulting in complete deletion of exon 5 with insertion of intronic sequences in transcripts [46]. The patient presented at 4 years of age with recurrent respiratory infection, however, showed normal numbers and differentiation of B-cells, a significant abnormality was that she was found to be severely hypo-gammaglobulinaemic. Analysis also showed a severe reduction of class switched $sIgD^{-}CD27^{+}$ memory B cells. The patient had impaired responses to vaccination.

1.3.1 Relevance of CD20 expression in Acute Lymphoblastic Leukaemia

Appoximately 30-50% of patients with ALL express CD20 on at least 20% of their leukaemic blasts. There have been conflicting reports with regards to the prognostic implications of CD20 expression in ALL, as summarised in table 1-2. The first investigation into CD20 expression was in children and young adults. Borowitz *et al* carried out a large study of 1314 patients, age range 1 yr and 21.9 years, entered into the Pediatric oncology group (POG) with newly diagnosed B-ALL [47]. Immunophenotyping was carried out at a central laboratory using fresh patient samples and the flow cytometers were calibrated daily with a set of standardised beads. Their results showed that when using a 20% cut off for positivity there was a modest relationship between CD20 positive expression and adverse outcome. They also established that CD20 intensity (i.e. antigen density), measured as mean fluorescence intensity (MFI) was an independent prognostic factor for poor outcome. This finding was not supported by Jeha *et al* who describe 353 children treated on St Jude's protocols between December 1991 and May 1999 where those who were CD20 positive and had slightly better outcomes than those not expressing CD20 [48].

In adults the impact of CD20 expression on prognosis is equally uncertain. Thomas *et al* [49] at the MD Anderson Cancer Centre report 254 patients with B-ALL treated with VAD/CVAD or hyper-CVAD. Pre-treatment characteristics for both CD20 positive (>20%) and CD20 negative patients was similar except performance status, thrombocytopenia and the presence of lymphadenopathy. They concluded that CD20 expression appeared to be a poor prognostic feature in B-ALL, particularly in younger patients. They also analysed their data looking at different levels of CD20 expression. The outcome of those with 10-19% CD20 expression initially declined rapidly at a similar rate to those with those >20% CD20 expression, the curve levelled off to a similar survival rate of 50% to the <10% CD20 cohort. They did not show a direct correlation between increased levels of CD20 expression based on percentage, and poorer outcome.

Table 1-2 Published Studies Investigating the Impact of CD20 expression on Outcome in B-ALL.

Trial group or Institution	Author/year	Age (years)	n	Treatment protocol	Dates of ALL treatment	% CD20 positive	Outcome
Paediatric Oncology Group	Borowitz 1997 [47]	1-21.9	1231	POG9005 and 9006	1991-1994	Not specified	CD20 adverse both by % but more by intensity
St Jude's Research Hospital, USA	Jeha 2006 [48]	0-18	353	St Jude's protocols Total 13A, 13B, 14	1991- 1999	48	CD20+ do slightly better
University of Texas MD Anderson USA	Thomas 2009 [49]	15-80	253	VAD Hyper CVAD	1985-2000	47	3yr CRD (20%v55%) and OS (27% v 40%) significantly worse in CD20+
GRAALL-2003 Phase II trial	Maury 2010 [50]	15-60	143	GRAALL 2003	2003 –2005	32	CD20+ assoc with increased CIR at 42m Impact of CD20+ when WBC >30 (70% v 24%)
University of Minnesota USA	Bachanova 2011 [51]	0.6-66	157	HSCT	1999 - 2009	52 children 39 adults	CD20 positivity had no impact on outcome.
NILG 09-2000	Mannelli 2012 [52]	16-68	172	NILG 09-2000	2000 –2008	30.2	If MRD neg CD20+do same as CD20-. Post allo CD20+ do slightly worse
University of Toronto, Canada.	Naithani 2012 [53]	1-18	259	Various including POG 9904,9905	2004 –2009	51	CD20+ confers worse EFS, but not significant.
Nafang Hostpial, Guangzhou. China	Xu 2016 [54]	18-65	135	NCCN v 1.2014	2008 – 2014	39	Pt with CDKN2 del with CD20+ had inferior OS and DFS. No sig diff in relapse
Peking University Institute of Haematology, China	Yang 2017 [55]	18-64	217	CODP+/-L After 2010 hyperCVAD	2000 –2015	34	CD20+ increased CIR and decreased DFS and OS
Chiba prefecture Japan	Isshiki 2017 [56]	16-70	96	Various - determined locally.	2001 –2014	34	CD20+ associated with inferior EFS.

CIR: cumulative incidence of relapse, OS: Overall survival; EFS: Event free survival; DFS: Disease free survival; MRD: Measurable residual disease; EM: Extramedullary; HSM: Hepatosplenomegaly; LN: lymph node; CNS: central nervous system; TKI: tyrosine kinase inhibitor GRAALL: Group of Research on Adult Acute Lymphoblastic Leukaemia; NCCN: National Comprehensive Cancer Network; POG: Paediatric oncology Group; NILG: Northern Italy Leukaemia Group. All clinical trials used 20% as cut-off unless otherwise state. *Green: CD20 expression improves outcome; Orange: CD20 expression confers worse outcome*

The Group for Research on Adult Acute Lymphoblastic Leukemia 2003 (GRAALL-2003) trial recruited 255 patients between November 2003 and November 2005 with *BCR-ABL1* negative B-ALL. Immunophenotyping was performed at local centres although there was central review of the CD20 flow cytometry scatter-grams. Their results showed a higher cumulative incidence of relapse in patients with >20% ALL blasts positive for CD20 however this did not confer a difference in event free survival or overall survival [50]. They also found that the negative impact of CD20 expression was only observed in patients with higher WBC at diagnosis (70% [95%CI, 42-93] vs. 24% [95% CI, 12-46] at 42 months; p=0.006) but not with a lower WBC (33% [95% CI, 19-53] vs 31% [95% CI, 21-44] at 42 months; p=0.77). This could not be explained by differences in post-remission therapy. Chang *et al*, University Health Network, Canada. compared this with their results of 119 patients diagnosed with BCP-ALL between the ages of 18 and 60 who were treated with a modified paediatric protocol including L-asparaginase, similar to that in GRAALL-2003. Unlike the previous study they did not find an effect of CD20 expression on overall survival, cumulative incidence of relapse, or event free survival (p=0.18, p=0.40, and p=0.15 respectively). Following subgroup analysis no association between CD20 positivity and adverse outcome in a high WBC group was found [57]. Mannelli *et al* also did not show a prognostic impact of CD20 expression in their B-ALL, *BCR-ABL1* negative cohort of 172 adult patients from the Northern Italian Leukaemia Group (NILG) 09-2000, enrolled between March 2000 and September 2008. Unlike previous studies they were able to look for correlations between CD20 expression and MRD course. It was noted that there was a trend, albeit non-significant, for more MRD markers being available in the CD20 negative subset. Overall, they found no impact of CD20 expression on EFS and OS. They also found the rate of MRD negativity was similar for CD20 positive and negative patients [52]. More recent retrospective studies from China and Japan have tended to indicate a worse outcome in CD20 positive patients. Interesting one reported that although there was no significant difference in relapse of CD20 positive and negative patients in their *BCR-ABL1* positive patient cohort, they saw an inferior survival in patients who were CDKN2 deleted and were also positive for CD20 [54].

Results from the GRAALL trial and the MD Anderson were sufficient to support the inclusion of the CD20 targeted monoclonal antibody – rituximab - to treat CD20 positive patients in

their subsequent *BCR-ABL1* negative trials. The results of these trials have been published and both show an improvement in survival. The MD Anderson showed an improved survival in the rituximab group however this was not randomised [58]. The GRAALL trial was published in 2016 and showed a significantly longer event-free survival in the rituximab group than in the control group (hazard ratio, 0.66; 95% CI 0.45-0.98; P=0.04) after 30 months [59].

1.3.2 CD20 targeting with Rituximab

Rituximab is a mouse/human chimeric CD20 monoclonal antibody and was the first chimeric monoclonal antibody to be approved by the U.S. food and Drug Administration (FDA) in 1997. It has been successfully used to treat B-Non-Hodgkin Lymphoma (NHL) and has been found to be most efficacious in combination with combination chemotherapy, resulting in improved long-term survival with an excellent toxicity record. It is now successfully been used for the treatment of several autoimmune conditions including rheumatoid arthritis and Wegener's granulomatosis. As discussed above, the first phase 3 results using rituximab in the treatment of ALL are from the French GRAALL 2005 clinical trial showing improved event free survival. Rituximab was administered to those patients with 'CD20 positive' ALL which was taken as ≥20% positive leukaemic blasts.

1.3.3 Mechanisms of action of rituximab

Rituximab has several mechanisms of action which are summarised in figure 1-4. Following binding to CD20 it is effective via four main mechanisms, complement dependent cytotoxicity (CDC), antibody dependent cytotoxicity (ADCC), antibody dependent cellular cytotoxicity (ADCP) and induction of apoptosis[60]. The pharmacokinetics of rituximab are similar to human IgG and can be present in the circulation of patients for months following intravenous administration [61]. Rituximab can induce death of malignant B-cells *in vitro* without immune effector cells. This direct killing can be either via caspase dependent or caspase-independent pathways. Caspase-dependent apoptosis can possibly result from rituximab causing rearrangement of lipid rafts which in turn triggers a *src* family kinase dependent process [62]. The mechanisms have been explored and changes have included

inhibition of antiapoptotic pathways p38 MAPK activated protein kinase, NF-ΚB, extracellular signal-regulated kinase 1 / 2 (ERK 1 /2) and AKT [63, 64].

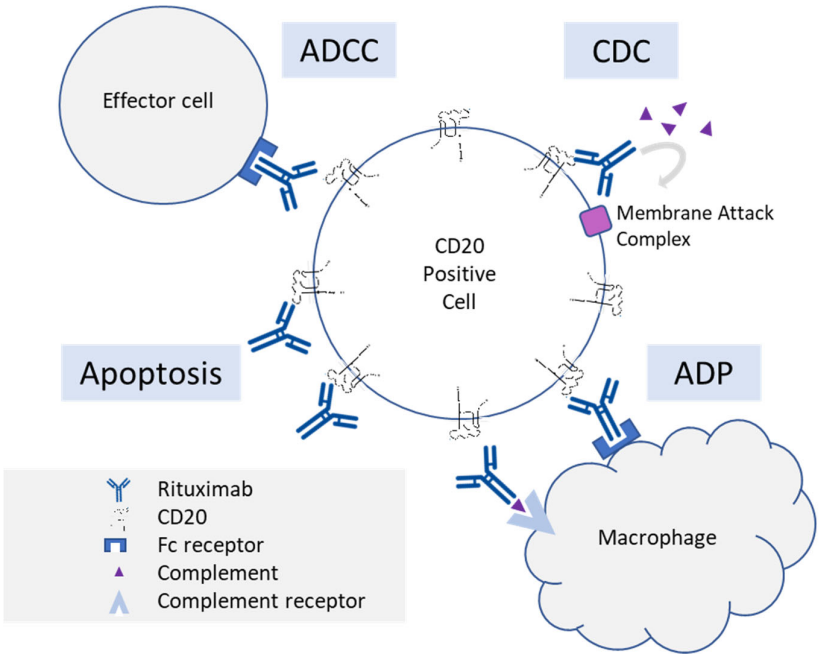

Figure 1-4 Putative mechanisms of action of rituximab. *ADCC – antibody dependent cellular cytotoxicity; CDC – complement dependent cytotoxicity; Apoptosis; ADP – antibody dependent phagocytosis. Adapted from Kasi et al 2012[60]*

Monoclonal antibodies, including rituximab, can induce antibody dependent cellular cytotoxicity (ADCC) that is mediated by immune effector cells that include NK cells, neutrophils and macrophages [65, 66]. The Fc of the monoclonal antibody binds to an activating Fcγ receptor on the effector cell thus triggering immune cell activation and killing of the target cell. In NK cells this binding triggers the release of granules containing perforin with resultant permeabilization of the target cell membrane. Granzyme B is also released which infiltrates the now permeabilized membrane of the target cell inducing apoptosis [67]. Evidence that ADCC is a likely mechanism is supported by clinical studies that polymorphisms of FcγRIIIa are associated with the clinical response to Rituximab. Patients with follicular lymphoma who are homozygotes for having valine at position 158 (VV) have a superior clinical response to rituximab than patients who are heterozygotes or homozygotes for having phenylalanine at that position (VF or FF) [68, 69].

In vitro studies have implicated complement dependent cytotoxicity (CDC) in the action of rituximab. In CDC, the C1 complex binds to cells opsonized by rituximab thus triggering the complement cascade which terminates in the insertion of the membrane attack complex (MAC) causing cell lysis. Complement inhibitory molecules (CD55 and CD59) expressed at high levels on malignant B-cells appeared to reduce the extent of rituximab-mediated *in vitro* lysis [70, 71]. However, expression of these complement inhibitory molecules was not found to be predictive of rituximab efficacy in patients with follicular lymphoma [72]. *In vivo* studies involving the depletion of complement using Cobra Venom Factor reduced the survival of SCID mice that had been injected with Daudi or EHRB cells and subsequently treated with rituximab [73]. Also, rituximab appeared to be ineffective in syngeneic C1q knock-out animals with EL4-CD20+ lymphoma [73, 74]. Conversely, in murine studies genetic deficiencies for complement components did not affect the ability of murine anti-CD20 to kill circulating cancer cells suggesting that complement is unlikely to be important *in vivo* [75].

Antibody-dependent phagocytosis is the most recent mechanism involved in the action of rituximab to be described. Opsonised target cells are phagocytosed by macrophages or neutrophils. There is some evidence that in knockout mouse models macrophage specific FcγRIV are required for rituximab to kill cancer cells [76]. Recently it has been suggested that the effector cells for rituximab mediated ADP are a specific subgroup of monocytes and macrophages that express the slan antigen, a carbohydrate modification of P-selectin glycoprotein ligand 1 [77].

One of the difficulties in fully understanding the mechanism of rituximab action is appreciating the relative importance of these known mechanisms in patients. For example, there is evidence that there is a competitive relationship between ADCC and CDC[78].

1.4 Cancer therapeutics – historical context.

Since the mid twentieth century, the landscape for cancer therapeutics has been dominated by chemotherapy. One of the great success stories in oncology is the treatment of childhood acute lymphoblastic leukaemia (ALL). Prior to the 1950s ALL was universally fatal, however, due to the pioneering work of Sidney Farber, antifolates were trialled in children resulting in the first remissions [79]. Subsequent multi-agent chemotherapy

regimens saw the survival rate increase sequentially decade upon decade to achieve the 90% cure rate in children with ALL [80]. Sadly, the same is not true for adults, where fewer than 50% achieve long term survival. The reason for this disparity is multifactorial and includes the increasing number of adverse cytogenetic factors that are apparent in adults and also a reduced tolerance for intensive treatment with increasing age. Thus, medical research has turned its attention towards developing treatments that specifically target cancer cells leaving normal cells unharmed in an effort to mitigate unwanted effects whilst enhancing treatment efficacy.

1.4.1 Oncolytic virotherapy – a novel cancer therapeutic

Effective oncolytic viruses are replicating viruses that preferentially infect transformed cells resulting in their death but leaving normal cells unharmed. Viral infection has been known to have anti-cancer effects at least since the mid-nineteenth century and is known to induce the host's anti-tumour immune responses [81, 82]. In order to be a suitable virotherapy, transformed cells need to be both susceptible and permissive to the virus however there should be minimal toxic effects. Candidate viruses are either viruses that do not cause significant disease, for example, Newcastle disease virus and reovirus or viruses that have been attenuated such as the vaccine strain in the case of measles virus. An added attraction of oncolytic virotherapy is our ability to genetically engineer viruses thus providing the opportunity for enhancing the killing ability, specifically targeting the virus to transformed cells and also to track the virus *in vivo*. Table 1-3 lists a selection of oncolytic viruses in clinical trials. [83]

Table 1-3 Selected Oncolytic Viruses in Clinical Trials

Virus	Modification	Trial Phase	Tumour	Notes
Adenovirus				Entry receptor: CAR
CG0070	E3 deletion; GM-CSF insertion	1	Non-muscle invasive bladder carcinoma[84]	Minor toxicity, CR 48.6%; median duration of response 10.4 months
ICOVIR-5	Modified DNX-2401-E2F promoter optimized	1	Diffuse intrinsic pontine glioma Melanoma	MSC loaded; intra-arterial injection, safe. Single IV dose failed to induce regression. [85]
VCN-01	PH20 hyaluronidase insertion; RGD targeting	1-2	Advanced solid tumours	In combination with Abraxane and iv gemcitabine.
DNX-2401	Δ24RGDInsertion	1	Malignant gynaecological disease[86]	Intraperitoneal; Safety and potential; MTD not reached.
Enadenotucirev		1	CRC, UCC, SCCHN, salivary gland carcinoma, and RCC	IV and intratumoural well tolerated. CD8 infiltrate. [87]
Herpesvirus				Entry receptors: HVEM, nectin 1, nectin 2
Talimogene laherparepvec T-Vec	ICP34.5 deletion; US11 deletion; human GM-CSF insertion.	3 Licenced	Melanoma[88]	Intratumoural. 16.3% DRR; safety 2015 FDA approved for unresectable metastatic melanoma. Jan 2016 EC approved.establish[ed][89]
HSV-1716	ICP34.5 deletion	1	Melanoma [90]; high-grade glioma[91]	Safety and responses reported.
HF10	UL56 deletion; single copy of UL52	1-2	Pancreatic carcinoma[92] Melanoma	Multiple intratumoral injections; safe and potential responses.
G207	ICP34.5 deletion; UL39 disruption	1	Glioma[93]	Resection cavity injection plus irradiation.

Coxsackie				Entry receptors: CAR, ICAM-1, DAF
Cavatak	Wt coxsakievirus A21	1-2	Melanoma; SCCHN; Breast cancer, Prostate cancer	
Measles virus			See Table 1-4	Entry receptors: CD46, Nectin 4
Vaccinia Virus				Entry receptors: none specific
PexaVec (JX594)	TK deletion; GM-CSF insertion	2 1b	Advanced hepatocellular carcinoma[94] Colorectal carcinoma [95]	Oncolytic and immunotherapeutic effects No toxic effects, 10 patients 67% had stable disease
Prostvac	Expresss PSA and TRICOM	1-3	Prostate carcinoma	Well tolerated, results expected 2019
Parvovirus				Entry receptors: Sialic Acid
ParvOryx	Parvovirus H1 (Wt)	1-2	Glioblastoma	Insert to prevent neurotoxic side effects
Polio virus				Entry receptors: CD155
PVS-RIPO	IRES replaced with HRV2 IRES		Glioblastoma	
Reovirus				Entry receptors: NgR1, JAM-A
Reolysin	WT virus, serotype 3	1-2 2	Glioma peritoneal cancer; colorectal cancer; sarcoma; SCCHN; pancreatic cancer; lung melanoma	
Vesicular	**stomatitis virus**			Entry receptors: LDLR
VSV-hIFNβ	Insertion of IFNβ	1-2	Solid tumours; SCCHN; hepatocellular carcinoma	

1.4.2 Measles and its vaccine

Measles is a exanthematous disease for which humans are the sole host. Measles virus (MV) is highly infectious with a high reproduction number [R_0] 14-18. The reproduction number is the average number of secondary cases produced by one infected individual in a population of susceptible individuals [96]. This compares to a R_0 of 3.8 for the 1918 Spanish flu in Geneva and 2.06 for the recent outbreak of Zika in South America in 2015-16. Measles virus infects via the respiratory tract and then spreads systemically, resulting in a characteristic rash and a febrile illness that normally lasts between 10 and 14 days. Of note, following initial infection, MV has long been known to result in several weeks of immunosuppression with deaths occurring due to secondary infections, typically bacterial bronchopneumonia. There are potentially fatal, late effects, such as measles inclusion body encephalitis and subacute sclerosing panencephalitis, however, these are now extremely rare thanks to successful vaccination programs [97].

Following isolation of MV by Enders and Peebles in 1954 [98], their laboratory successfully developed a live attenuated vaccine via multiple passages in chicken eggs of wild type virus from a patient called Edmonston [99]. The lineage is shown in Figure 1-5. The MV vaccine has successfully protected millions of people worldwide over the past 50 years and has an excellent safety record. In 5-15% of recipients, mild symptoms such as rash, fever, and conjunctivitis can occur, however severe complications are rare and confined to immunosuppressed patients [100, 101].

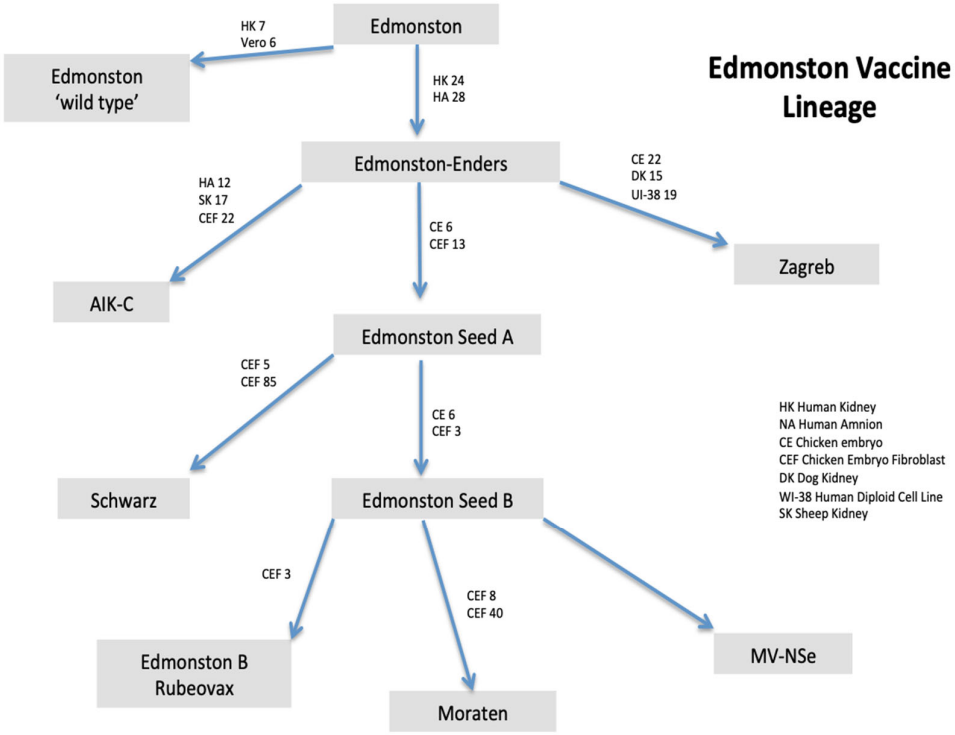

Figure 1-5 Measles virus Edmonston vaccine lineage *(adapted from Rota et al 1994[102]). A schematic representation of the Edmonston vaccine strains indicating the number of tissue culture passages taken to create each strain. Moraten is available in the USA and in the combined MMR measles/mumps/rubella vaccine; Schwartz is produced in Brail and Europe; Zagreb is the most frequently used in WHO programs including India, Croatia, and Switzerland; AIK-C strain is used in Japan.*

1.4.3 MV Structure

Measles virus (MV) is an enveloped, non-segmented, negative strand RNA virus from the genus *morbillivirus* and family *paramyxoviridiae*. The MV genome consists of 15 894 RNA nucleotides comprising six transcription units separated by trinuclear intergenic sequences, and encoding 6 proteins that form the virion. The genome is protected by a nucleocapsid composed of 2649 copies of the N protein. Associated with this are the RNA polymerase - large (L) protein and its co-factor phosphoprotein (P). Together, N, L and P form the ribonucleoprotein complex (RNP). Surrounding the RNP is the matrix (M) and within the membrane are Haemagglutinin (H) protein and the Fusion (F) protein. The proteins V and C are non-structural proteins that are expressed from an alternative RNA transcript of the P

gene. They are implicated in protecting the virus from type 1 interferon host immune responses. [See Figure 1-6]

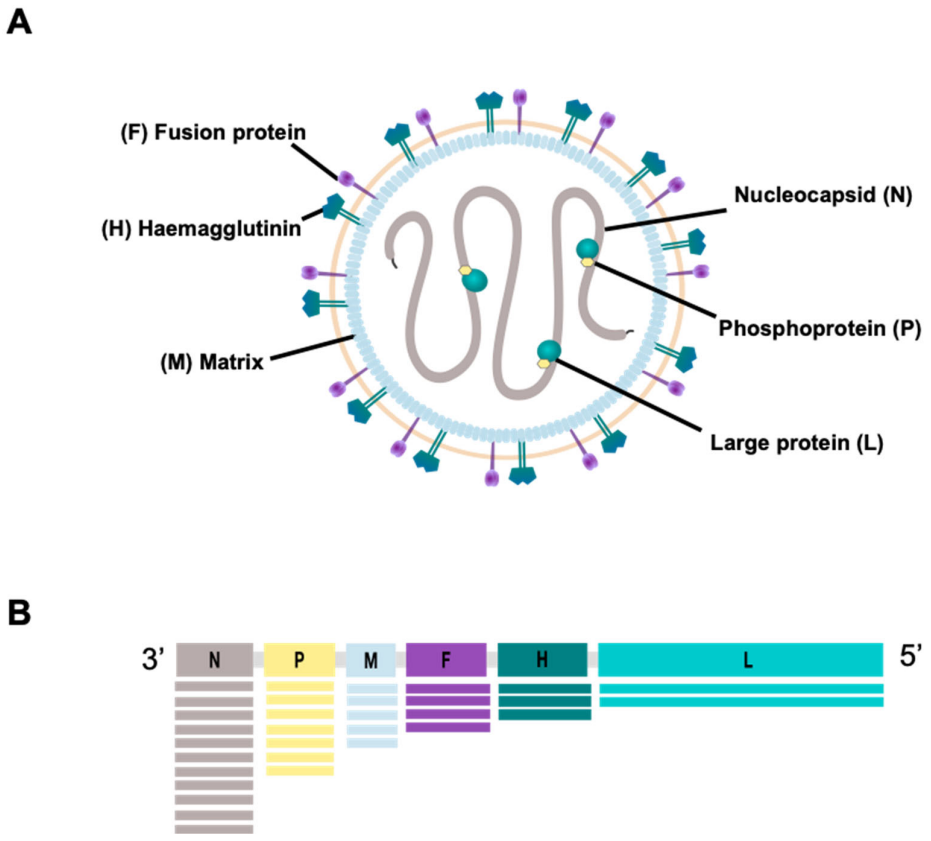

Figure 1-6 Schematic diagram of measles virus structure and genome. *[A] Virion: The virion has a lipid bilayer envelope from which the two glycoproteins F and H protrude. The single-stranded negative sense RNA genome is encapsidated by the N protein to form the ribonucleoprotein complex. The Large protein is a viral RNA-dependent RNA polymerase. P acts as a co-factor. [B] Genome: The genome encodes six structural and two non structural proteins. Organisation of MV genome and MV transcription gradient showing mRNA of the genes at the 3' end are more abundantly produced than the 5' end.*

1.4.4 MV Receptors

To infect host cells the H protein – a 617-amino acid type II transmembrane glycoprotein [103] - initially interacts with a MV receptor on the host cell membrane. The resulting conformational change of H activates the trimeric fusion protein F thereby mediating membrane fusion and entry of the ribonucleoprotein complex into the cell. Subsequent expression of the F and H proteins on the host cell leads to fusion with adjacent non-

infected cells resulting in giant multinucleated cells known as syncytia [104]. These are the hallmark of MV infection. The paramyxoviridae are unusual in that the functions of attachment and fusion are carried out by separate glycoproteins in contrast to many enveloped viruses where these are combined. This leads to a high degree of flexibility for modification of the virus [105].

Three MV receptors have been identified: signalling lymphocyte-activation molecule (SLAM) or CD150 [106], Nectin-4 [107] and CD46 [108]. [See Figure 1-7]

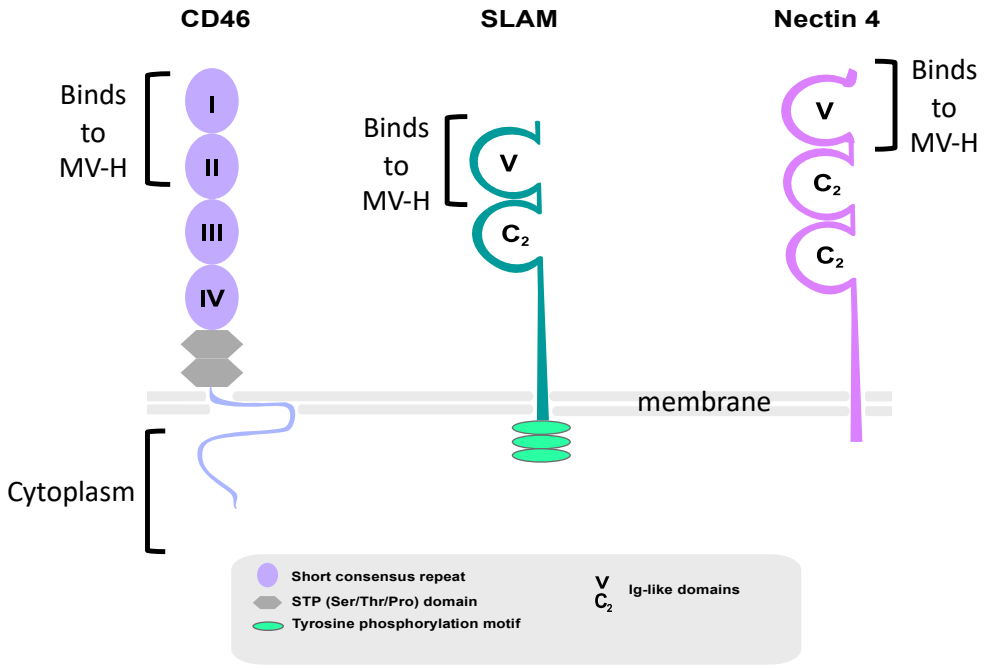

Figure 1-7 Schematic representation of measles virus receptors *[adapted from Noyce et al (2012)[109]]. CD46 contains 4 short consensus repeat domains (SCR), a serine-threonine-proline (STP) rich domain, a transmembrane domain and a cytoplasmic region. SLAM contains cytoplasmic tyrosine phosphorylation sites, a variable region and a type 2 constant region. Nectin 4 contains a V region and two C2 regions.*

1.4.4.1 CD46 – Membrane cofactor protein

The primary receptor for vaccine strain MV is CD46, a type-1 membrane cofactor glycoprotein that negatively regulates complement and is expressed ubiquitously on human nucleated cells. CD46 belongs to regulators of complement activation (RCA) proteins and acts as a cofactor for the serine protease factor I, mediating cleavage of C3b and C4b. It is thus a key regulator in the classical and alternative complement pathways, maintaining

homeostasis by protecting cells from autologous complement attack [110]. More recently CD46 has been found to have a role in T-cell regulation and inflammation. Co-engagement of CD46 and the T-cell receptor induces IFN-gamma secreting T-helper type 1 cells. These then switch into interleukin-10 secreting T regulatory cells [111] . There have been several genetic association studies that implicate CD46 in the regulation of humoral immunity after measles vaccination, for example an Australian study indicated that the CD46 polymorphism was significantly associated with measles IgG levels, [112] and a Danish study revealed a high correlation between the CD46 intronic SNP rs2724384 and MMR-related seizures [113]. Following MV binding CD46 is internalized and results in altered intracellular processing and antigen presentation. Measles is not alone in exploiting CD46 as an entry receptor, there are at least eight other human pathogens including three other viruses and five bacterial species [114].

CD46 is overexpressed on transformed cells, a factor thought to provide a survival advantage by protecting them from autologous complement destruction. There is a correlation between the level of CD46 expression and MV-Edm infection with non-transformed human cells being minimally infected compared to their transformed counterparts. [115]

CD46 is not expressed on murine cells, other than spermatozoa [116]. In order to limit research using non-human primates, several CD46-transgenic mouse models have been developed. Initially such models were not susceptible to MV infection due to the host's antiviral response however by crossing the huCD46-transgenic mice with mice deficient in type 1 IFN receptor (IFNAR1) the antiviral response can be mitigated and viral spread enhanced. The resultant mice strains such as CD46GexIFNARKO although susceptible to MV infection cannot sustain human malignancy [117, 118].

1.4.4.2 Signaling lymphocyte Activation Molecule [SLAM] – CD150

Wild-type MV strains enter host cells predominantly via the membrane glycoprotein SLAM. The receptor is a member of the immunoglobulin gene superfamily and is expressed on B-cells, T-cells, dendritic cells, haemopoietic stem cells, and immature thymocytes, and thus may account for the immunosuppressive properties of MV [119, 120]. It is a CD2-related

receptor and it functions to enhance T cell proliferation and gamma interferon production (IFN-γ). SLAM engagement also augments the cytotoxic activity of CD4+ and CD8+ T cells [121, 122].

SLAM is widely expressed on human B-cells, De Salort *et al* 2011 measured the expression level of SLAM on normal B cells from human bone marrow (see Table 4-1 in Chapter 4) [119]. Given that nearly 50% of pre-B cells expressed SLAM it is likely that expression in ALL will vary. Although murine SLAM displays 60% structural and functional homology to human SLAM it does not bind MV [123].

1.4.4.3 Nectin 4 (Poliovirus receptor-like 4; PVRL-4)

Nectin-4 is the most recently discovered MV receptor [107, 109]. The observation that several cell lines negative for SLAM and CD46 could be infected by wild type MV led to its discovery by two independent groups in 2011. A microarray approach was used to analyse the membrane protein genes in those cell lines that were susceptible to MV infection [107]. Nectin 4 is a type 1 transmembrane protein of the immunoglobulin superfamily and is normally localized on the basolateral surface at the adherens junctions of epithelial cells. Contact with the C beta-sheet and the FG loop of Nectin 4 are critical for binding to the H protein of MV [124]. Nectin 4 is expressed in placental trophoblasts, brain, lung, testis, stomach and is overexpressed in many adenocarcinomas such as lung, breast and colon. It is released in soluble form in blood [125]. Nectins mediate calcium-independent cell-to-cell adhesion and have a role in cell proliferation and tumour metastasis. Their stimulation increases Rac1 activity in regulating lung cell migration but the signalling pathway has not yet been determined [126].

1.4.5 Antiviral host defence against MV

Invading viruses are recognised by host cells that activate a strong antiviral response. Rapid initial recognition of pathogen-associated molecular patterns (PAMPs) which include viral RNA or protein, is achieved by pattern recognition receptors (PRRs). This eventually results in cellular antiviral inflammatory responses and type 1 interferon responses. RNA viruses

are recognized by PRRs such as transmembrane Toll Like Receptors (TLR) 7 and 8, and by cytosolic PRRs retinoic acid inducible gene –I (RIG-I) which recognizes 5'-triphosphate-ended RNA. MDA-5 detects dsRNA but also contributes to the recognition of MV. Upon binding to viral RNA, RIG-I is dephosphorylated by protein phosphatase 1. TRIM25 then recognizes the dephosphorylated RIG-I and adds ubiquitin moieties onto its caspase recruitment domains (CARD) allowing for interaction with mitochondrial antiviral-signalling protein (MAVS). This leads to the activation of transcription factors such as interferon regulatory factor 3 (IRF3), IRF7 and nuclear factor kappa B(NF-κB) which together activate the transcription of type 1 interferons (IFN) and pro-inflammatory cytokines.

Increased interferon and interferon induced proteins have been detected in patients infected with MV Edmonston [127]. Interferon activates the IFN-α receptor (IFNAR) of neighbouring cells to in turn activate the JAK/STAT signalling pathway resulting in the induction of IFN-stimulated genes (ISG) thus limiting the spread of the virus. An example is the protein Mx1 which interferes with the formation of the RNP complex thus inhibiting the early steps of viral replication [128].

The MV-P gene products – P, V, and C proteins – are viral virulence factors that modulate the antiviral response. All can counteract the IFN mediated JAK/STAT pathway with V being particularly important. The P and V proteins bind STAT1 via the N-terminal domain and interfere with nuclear importation [129, 130]. V also binds STAT2 and JAK1 via the V C-terminal domain. V also prevents MDA5 mediated IFN induction by binding PRRs, MDA5 and LGP2 but not RIG1 [131] [132]. By binding IKKα and IRF7 it prevents TLR7/9 mediated induction of IFNα. C is also involved by preventing type 1 IFN mediated expression of ISG [133].

The ability for the vaccine strain to induce the host's IFN response can explain, at least to some extent, its lack of pathogenicity compared to the wild type virus. Recombinant wild-type MV bearing the H protein from the Edmonston vaccine strain induced IFN-α in macaques whereas this was not seen in wild-type MV [134].

1.4.6 Measles virus as oncolytic virotherapy

Reports that measles virus can have anti-cancer effects began to appear in the mid-twentieth century with a case report of a tumour regression in Hodgkin lymphoma [135]. Other reports followed of similar effects in several cases of Hodgkin Lymphoma, ALL, and also Burkitt lymphoma [136].

The non-segmented genome renders MV stable with a low risk of mutation thus making it unlikely to revert to the pathological form. This is supported by the elucidation of the crystal structure which shows the H protein epitopes are highly conserved, and the clinical evidence that the vaccine has remained protective during the 5 decades of use. The vaccine produces long term immunity with protective antibodies being readily detectable. Neutralizing antibodies to all the MV proteins - except M, C and Ls2 - have been detected using high-throughput microarray technology [137]. Antibodies to H and F have been considered the most relevant as their depletion results in abrogation of the virus neutralization, with greater effect from the depletion of H[138]. Of relevance to this work, this poses some concerns regarding its efficacy as an oncolytic as these antibodies can neutralize the virus rendering it ineffective.

1.4.7 Genetically modified MV

The development of systems to 'rescue' MV from cDNA has enabled genetically modified strains of MV to be successfully developed [See figure 1-8] [139, 140]. This has enabled the virus to be targeted to specific antigens increasing specificity, to track the virus, or to enhance the oncolytic effect. MV has been modified to enable tracking by imaging *in vitro* with green fluorescence protein (GFP) expression or *in vivo* with luciferase or sodium iodide symporter (NIS) where viral replication can be detected with single photon emission computed tomography (SPECT). Alternatively, reporter genes such as carcinoembryonic antigen (CEA) or IgG kappa have been incorporated into the MV genome to enable monitoring by their detection in patients' serum [141, 142]. Inserting 'suicide' genes is a means to combine the tropism of the oncolytic MV with chemotherapy. The *Escherichia coli* purine nucleoside phosphorylase (PNP) is a prodrug convertase. This converts fludarabine and 6-methylpurine-2'-deoxyriboside into the more toxic 2-fluoroadenine and

6-methylpurine respectively and a CD20 targeted MV with PNP has shown efficacy in murine models of Burkitt Lymphoma treated with fludarabine [143]. The NIS transgene also enables the potential for combination with radiotherapy when beta-emitting iodine-131 can be pumped into the transformed cells, thus limiting the effect to the tumour microenvironment [144-146]. Strategies have been developed to attempt to improve the immune response to the oncolytic MV. Several models involving 'arming' the virus with growth factors have shown mixed results: models with granulocyte-macrophage colony stimulating factor (GM-CSF) enhanced tumour regression in some and an increase in infiltrating neutrophils and T-cells however results were mixed in murine models with B-cell malignancies treated with MV-hGCSF where oncolytic effect was increased in Raji – a Burkitt lymphoma cell line – but not in NALM6 [147-149]. Of note, the US and European licensed oncolytic virus T-Vec, Talimogen laherparepvec, is a herpes virus modified to express GM-CSF for the treatment of advance melanoma. Other strategies have included MV expressing IFNβ, MV expressing *Helicobacter pylori* neutrophil activating protein to stimulate the release of proinflammatory cytokines, and more recently incorporating antibodies against the immune checkpoint inhibitors cytotoxic T-lymphocyte antigen-4 (CTLA-4) and programmed cell death -1 (PD-1) [150].

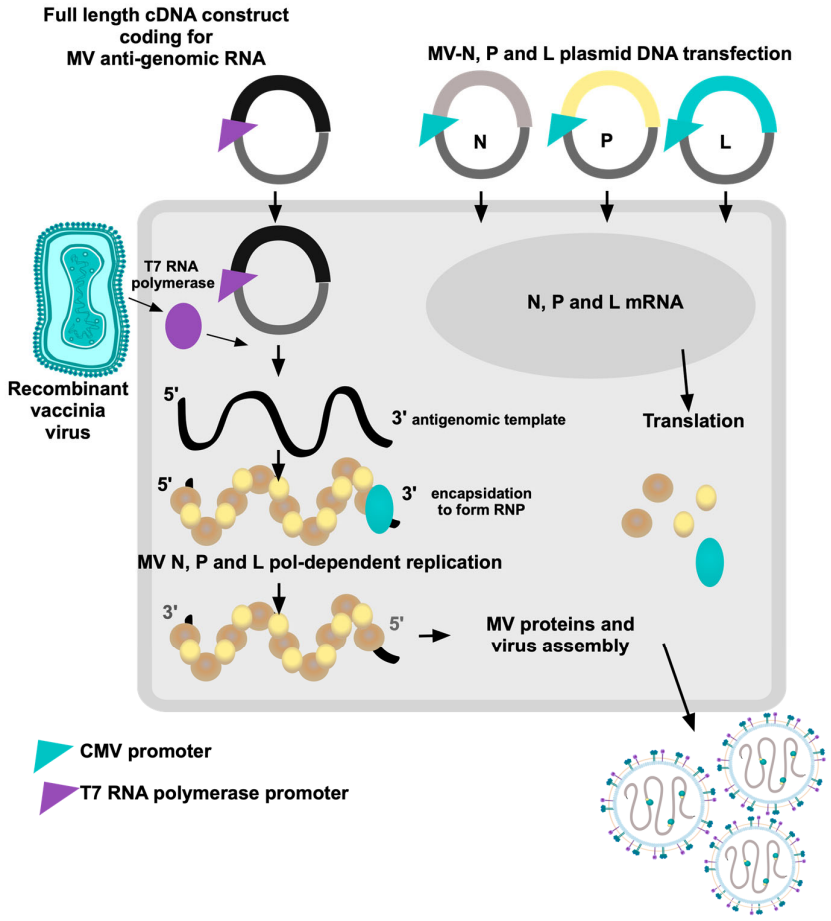

Figure 1-8 Measles virus rescue from cDNA. *Schematic representation of method for rescuing MV using vaccinia MVA-T7 virus expressing T7 RNA polymerase. Full length anti-genomic MV RNA and simultaneously mRNAs encoding the viral N, P and L proteins in order to replicationally and transcriptionally active nucleocapsids.*

1.4.8 MV Targeting

Despite the natural tropism to transformed cells, increasing the specificity of oncolytic MV to malignant cells has been a strategy employed by many different research groups since the discovery of MV's oncolytic potential. The H protein can be modified by inserting cell or

tumor-specific ligands to its carboxyl-terminal extension. For example, single-chain antibodies including scFvαCD20 anti scFvαCEA, anti scFvαCD38 have been cloned and displayed on MV-H giving it targeted entry to NHL, epithelial carcinomas and myeloma respectively [151-153].

1.4.9 CD20 targeted oncolytic MV

Bucheit *et al* engineered a MV where a single-chain variable fragment (ScFv) anti-CD20 was displayed on MV-H. This MVHαCD20 was engineered from cDNA encoding murine anti-CD20 antibody B9E9 with an 18-mer linker between the V_H and V_L domains and tailed with *Sfi*I and *Not*I restriction sites. It was fused to the C terminus of MV-H with a G_4S noncleavable linker. Bucheit demonstrated that the scFv anti-CD20 construct resulted in CD20 binding, cell-cell fusion and that the ability of the rescued virus to infect cells is mediated through an interaction between the scFv anti-CD20 and human CD20. The targeted virus suppressed the growth of human CD20 expressing tumours with greater efficiency than the parent MV. [151]

1.4.10 MV receptor 'blinding'

The targeting strategies discussed do not prevent the modified MV from entering via the native receptors CD46 , SLAM and Nectin 4. To create 'blinded', or fully retargeted, viruses mutations can be introduced into the MV-H protein. These were painstakingly identified by iterative cycles of mutant protein production followed by functional assays. Several residues were identified that are required for CD46 – dependent fusion (451, 481) and SLAM-dependent fusion(529,533). The first demonstration of the oncolytic efficacy of a targeted and then 'blinded' MV was a fully retargeted to CD38. Paired mutations at positions 451 and 529 or 481 an 533 supported fusion via the CD38 but not CD46 or SLAM[154]. In order to rescue such fully 'blinded' virus on vero cells a system whereby a His-Tag – a peptide containing 6 histidine residues at the C terminus of the mutated H protein - is used [149-155]

1.4.11 Measles Virus Clinical Trials

Oncolytic measles virus (MV) entered Phase 1 clinical trials over a decade ago; completed and current trials are listed in Table 1-5. The first clinical trial was a small, open-label, Swiss study enrolling 5 patients with cutaneous T-cell lymphoma stage IIb or higher who had relapsed or were resistant to therapy. MV was injected intra-tumourally following treatment with subcutaneous IFNα. The results were mixed but encouraging as several of the tumours regressed, one disappeared completely, and in two patients distant lesions improved, with limited adverse effects to the MV injections [156]. Further trials have involved the intraperitoneal and systemic routes. An ongoing Phase I trial in multiple myeloma has reported 2 cases where heavily pre-treated patients have successfully entered a complete remission following systemic MV treatment. Despite high viral titre of up to $1x10^{11}$ given intravenously, reported side effects were mild and largely confined to the time of the infusion [157].

Table 1-4 Oncolytic Measles Virus Clinical trials

Author/year	Trial phase	No of patients	Type of cancer	Virus strain	Route/Dose	Protocol	Side effects	Efficacy
Heinzerling et al 2005 [156]	1	5	CTCL	MV-Zagreb	Intratumoural $TCID_{50}$ - 10^2-10^3	16 injections Max 2 cycles Pre treatment IFNα	Grade 1	5 of 6 lesions clear regressions, one disappearance, untreated lesions improved in two. One showed complete response. 2 of 5 non-injected distance lesions showed response.
Galanis et al 2010 [153]	1	21	Ovarian carcinoma	MV-CEA	Intraperitoneal $TCID_{50}$ .10^3 to 10^9	4 weekly Max 6 cycles	Grade 1-2 Fever, fatigue, abdominal pain most common.	Median survival 12.3 months [1.3-38.4]
Galanis et al 2015 [158]	1	16	Ovarian carcinoma	MV-NIS	Intraperitoneal $TCID_{50}$ .10^8 to 10^9		Grade 1-2	Stable disease 13 patients Median overall survival 26.6 months (7.0-44.4)
Mayo Clinic NCT00390299	1	Recruiting	Glioblastoma multiforme	MV-CEA	Resection cavity or intratumoural $1x10^5$ to $2x10^7$ $TCID_{50}$	One or two doses	No dose limiting toxicities	Awaited

Author/year	Trial phase	No of patients	Type of cancer	Virus strain	Route/Dose	Protocol	Side effects	Efficacy
NCT00450814 Russell et al 2014 [157]	1	Recruiting	Multiple Myeloma	MV-NIS	IV $1x10^6$ to $1x10^{11}$ $TCID_{50}$	Single dose Group 1: MV Group 2: CTX 10mg/kg 2 days prior to MV	Fevers and hypotension at highest dose	2 responses including CR at highest dose.
UARK 2014-21 NCT02192775	2	Recruiting	Multiple myeloma	MV-NIS	IV	One dose and CTX		
Mayo clinic NCT01503177	1	Recruiting - suspended	Mesothelioma	MV-NIS	Intrapleural	Every 28 days, up to 6 cycles		
NCT01846091	1	12	Breast carcinoma Head and neck carcinoma	MV-NIS	Intratumoural	One dose		

Author/year	Trial phase	No of patients	Type of cancer	Virus strain	Route/Dose	Protocol	Side effects	Efficacy
NCT02700230	1	Recruiting	Peripheral nerve sheath tumour	MV-NIS	Intratumourally	One dose		
NCT02068794	1 / 2	Recruiting	Ovarian cancer	MV-NIS	Intraperitoneal Infected adipose tissue MSCs	Every 28 days, up to 6 cycles		
NCT02364713	2	Recruiting	Ovarian, fallopian or peritoneal cancer	MV-NIS	Intraperitoneal Compared to standard cytotoxic chemotherapy	Every 28 days until progression or toxicity		
NCT02919449	1 / 2	Recruiting	NSCLC	MV-NIS	Intratumoural	One dose and Atezolizuma		

1.5 Mechanisms of oncolysis

The mechanisms by which MV causes oncolysis have not been fully elucidated. Our current understanding is that it involves a combination of the direct effect from viral infection of the cell and the host's immune response to that infection. The ability to induce anti-tumour immune responses is emerging as an important determinant of virotherapeutic efficacy [159, 160].

Overexpression of the native MV receptor CD46 on transformed cells gives attenuated strains of MV a natural tropism for cancer cells. Above a certain threshold CD46 density the killing and syncytia formation by MV *in vitro* markedly increases which perhaps explains why normal cells, also expressing CD46, do not undergo oncolysis. The importance of CD46 density *in vivo* is less clear and studies where wild type MV engineered with the H Protein of Edmonston vaccine strain virus infecting macaques did not show expected CD46 tropism [138].

Defective IFN pathways are common in malignant cells thus making them more susceptible to viral infections by evading their host immune system [161]. The variability of this effect has been shown in sarcoma cell lines where three out of eight were MV resistant and strongly up-regulated RIG-I and the interferon-stimulated gene IFIT1. Pre-treatment with IFNβ rendered some of the MV susceptible sarcoma lines more resistant to MV. However increasing the multiplicity of infection (MOI) enabled the resistance to be overcome [162].

When MV infects a cell there is a characteristic cytopathic effect whereby infected cells can interact with neighbouring uninfected 'bystander' cells forming a multinucleate syncytium. Transfection with MV-H and MV-F glycoproteins can affect up to 80 neighbouring cells in a glioblastoma multiforme model U87 [163]. Fusogenic membrane glycoproteins have been explored as they can form syncytia which are effective for local killing and can possibly load DCs more effectively with tumour associated antigens than cells dying from other causes[164]. Replication-deficient viruses and plasmid vectors expressing fusogenic membrane proteins have been reported to cause tumour regression which supports the theory that syncytia formation is an important mechanism of oncolysis [163, 165]

1.5.1 Role of the Immune System

The role of the immune system in oncolytic virotherapy is clearly complex and can be either a benefit or a hindrance. The balance between protecting cells from viral infection and replication which prevents the virus action as an oncolytic, or to help remove infected transformed cells, such as with mechanisms such as antibody dependent phagocytosis or cellular cytotoxicity is not easy to determine. This is particularly challenging to study due to the lack of a murine xenograft that is susceptible to MV infection and also has intact immunity.

The innate immune system is known to have a significant role in MV infection and oncolysis. For many oncolytic viruses, including T-Vec, modifying the virus with granulocyte-macrophage-stimulating factor (GM-CSF) improves the antitumour efficacy by recruiting natural killer cells and dendritic cells to the tumour. However, there is concern that tumour suppressing myeloid-derived cells are also recruited [166, 167]. MV expressing GM-CSF delayed tumour progression and increased overall survival in an immunocompetent murine colon adenocarcinoma model, however the cells recruited were lymphocytes rather than granulocytes. Neutrophil infiltration has been seen in ALL xenografts in our laboratory but as these were immunocompromised murine models it difficult to draw firm conclusions as to their relevance. Plasmacytoid dendritic cells (pDC) express TLR7 and TLR9. Although not susceptible to MV infection the pDCs were activated by MV infected mesothelioma cells and possibly able to cross-present a tumour antigen (NYESO-1) to a CD8+ clone. The pDCs were also able to phagocytose MV infected cells. They demonstrated that MV infected tumour cells induced IFNα production by pDCs which may favour anti-tumour immune responses[168].

Complement is a key component of the innate immune system, quickly acting by opsonisation, neutralization, aiding phagocytosis and clearance of the pathogen from the circulation. Complement inhibition has been used to prevent neutralization of oncolytic vaccinia virus in both immune humans and cynomolgus macaques resulting in an increase in the infectious titre in the blood and appeared to reduce tumour size in the macaques [169]. In contrast, oncolytic vaccinia virus expressing GM-CSF, Pexa-Vec, induced complement-dependent cancer cell cytotoxicity (CDC) in rabbits and humans with a variety

of tumour types [170] . Thus, the overall benefit of complement to oncovirotherapy is controversial and is further complicated by the fact that activation of complement pathways differ between mammalian species [171].

Following infection with wild type MV the appearance of MV specific antibody and T-cell responses appears to coincide with the appearance of the rash, with rash biopsies demonstrating an infiltration of CD4+ and CD8+ lymphocytes [172]. The importance of CD8+ is seen in studies with non-human primates where depletion of CD8+ T cells but not B cells results in a higher and more prolonged viraemia [173]. T cell activation occurs following herpes virus infection. CD8+ T cells limit tumour oncolysis by restricting replication and spread of the virus. An oncolytic virus that expresses a herpesvirus-encoded inhibitor of TAP – transporter associated with antigen processing - has been engineered. By inhibiting TAP, ICP47 downregulates MHC class I expression and allows HSV-1 to complete its replication cycle in the presence of CD8+ T cells resulting in greater efficacy in treating bladder and breast cancer in murine models [174].

The implementation of worldwide measles virus vaccination programs has resulted in widespread immunity to measles. Pre-existing neutralising anti-MV antibodies are perceived to be a barrier to oncolytic virotherapy, and in particular the anamnestic response following repeated exposure to a virus where the antibody titres are augmented can prevent the virus from ever reaching the target cells. A recent report of 170 cancer patients treated with oncolytic adenovirus showed an increased overall survival for patients who did not have neutralizing antibodies at baseline compared with those with pre-existing antibodies (median OS 239 days and 122 day respectively (p=0.022) although no difference was seen when low and high levels groups were compared [175]. These results contrast with a phase 2 trail of oncolytic vaccinia virus where no survival difference was seen [94]. Pre-clinical data have shown that by 'hiding' MV in mesenchymal stem cells to act as cell carriers results in a greater oncolytic effect with overall survival of mice xenografts being increased [176] [177] Other cell carriers such a activated T cells and tumour associated macrophages have also been used. Published early phase clinical trials in MV have either involved local administration of MV (i.e. intratumoral or intaperitoneal), or those that have been given systemically have been in patients with low anti-MV antibody titres [157].

Another approach to overcoming the effect of anti-MV antibodies is immunosuppression. Although induction chemotherapy and corticosteroids are known to have

immunosuppressive effects, the anti-MV IgG titres of 16 patients on the UKALL 14 trial remained largely unchanged with the mean titre between 2000 and 3000 mIU/ml where a level above 200mIU/ml is considered to provide adequate immunity[177] . Hence traditional chemotherapy does not appear to overcome the difficulty of pre-formed antibodies.

1.6 Neutrophils

1.6.1 Neutrophil Biology

The final chapter of this thesis focuses on cellular engulfment or membrane transfer of MV infected ALL cells by neutrophils as a possible mechanism of both MV oncolysis and anti CD20 antibody-dependent cellular phagocytosis (ADCP). Neutrophils are normally the first effector cells to reach an area of infection or inflammation. They mature from myeloid precursors in the bone marrow and are released into the peripheral blood - at a rate of 5-10 $x10^{10}$ per day - where they then comprise 60% of the total white blood cell component of human blood [178]. Granulopoiesis is primarily regulated by G-CSF. Once they are mature, neutrophils are released from the bone marrow in venous sinusoids through decreased CXCR4-CXCL12 signalling and enter the blood circulation. Neutrophils form marginated pools such as in the spleen and the lungs. They are recruited to tissues affected by infection, hypoxia or sterile injury via a carefully orchestrated process of rolling, adhesion, crawling and extravasation from the endothelia. A recently described process of reverse transmigration can also occur where neutrophils are able to upregulate CXCR4 and return to the bone marrow where they are subsequently eliminated [179] .

1.6.2 Neutrophils and phagocytosis

Elie Metchnikoff hypothesised in 1882 that neutrophils contribute to microbe digestion when performing experiments on starfish embryos. Neutrophils, like macrophages can internalize particles that are both opsonized by complement or antibody, or non-opsonized. Neutrophils eliminate bacteria by phagocytosis - in overwhelming bacterial sepsis it is sometimes possible to observe neutrophils containing intracellular bacteria on a peripheral blood smear. Once phagocytosed the chemicals stored in the 4 types of neutrophil

granules, such as proteolytic enzymes, antimicrobial peptides and reactive oxygen species, act to kill and digest the microbe. Neutrophils are also known to phagocytose apoptotic cells [180].

1.6.3 Neutrophils and cancer

The peripheral blood neutrophil-to-lymphocyte (NLR) has been used in solid organ cancers and lymphomas to predict response to treatment, where typically a high NLR is associated with poor outcome. This has been demonstrated in breast carcinoma, gastric cancer, colon carcinoma, hepatocellular carcinoma, and diffuse large B-cell lymphoma [181-184].

There has been controversy surrounding the role of neutrophils in cancer. Determining the involvement of neutrophils is hampered by the existence of myeloid-derived suppressor cells (MDSC) which are morphologically similar to neutrophils and express Gr-1. These cells limit anti-tumour responses by exerting arginase 1 and reactive oxygen species (ROS) dependent immunosuppressive functions that affect T cell proliferation and activation [185]. Neutrophils have been divided into two phenotypically distinct groups - N1 and N2 - where N1 are anti-tumoural and N2 are pro-tumoural. The polarization appears to be driven by interferon gamma (IFNγ) to produce N1 tumour- associated neutrophils that are characterized by production of pro-inflammatory cytokines, and transforming growth factor beta drives the formation of tumour promoting N2 neutrophils which are characterised by and increased arginase content [186]. There is evidence that solid tumours can affect the phenotype of neutrophils by influencing active osteoblasts. The adenocarcinoma appeared to directly affect hematopoiesis by unknown mechanisms that involved the increase in circulating RAGE (receptor for advanced glycation end products) [187]. The division into N1 and N2 neutrophils is now considered less clear-cut with the classifications being an alteration in phenotypic balance rather than the formation of cells with a distinct function. The original experiments describing this division involved treating mice with an oral TGF-β inhibitor SM16 this resulted in an influx of tumour associated neutrophils (TAN) to the murine mesothelioma and lung carcinoma. When these neutrophils were depleted the antitumour effects of treatment were reduced [186]. The majority of studies have been in murine models. In patients with early -stage lung cancer, intratumoural neutrophils had a more activated phenotype. They also identified a small group of TANs which expressed markers typical of antigen presenting cells [188]. Neutrophils can exhibit plasticity and alter

in response to the tumour microenvironment; establishing the exact roles and mechanism of action could potentially influence the development of tumour therapeutics [189].

1.7 Hypothesis and aims of this thesis

The central hypothesis of this thesis is that CD20 is a critical molecule in the outcome of B-cell precursor acute lymphoblastic leukaemia and that it can be effectively targeted with a genetically modified oncolytic measles virus which enters via CD20.

The prognostic value of CD20 in B-cell precursor ALL is unclear. The first results chapter of this thesis - Chapter 3 - aims to determine the impact of CD20 antigen expression on clinical outcome using data obtained from the UKALL14 trial, a large multicentre clinical trial in the United Kingdom. During the course of this research it became clear that some patients did not have cellular specimens available for flow cytometry – a conventional method for determining CD20 expression - and it therefore became important to develop a molecular gene expression assay (RT-qPCR) to determine CD20 bulk from mRNA or cDNA. This would potentially have the dual advantage of improving the statistical power of the UKALL14 trial CD20 analysis and to provide a robust alternative option for future CD20 expression analysis.

Modern therapies are currently not adequate to cure between 50% and 60% of adult patients with ALL so alternative treatments are urgently required. Oncolytic viruses are becoming increasingly recognised as a safe emerging treatment option. Having established the importance of CD20 expression in ALL, Chapter 4 of this thesis aims to determine whether a CD20 targeted oncolytic measles virus could be a possible therapy in ALL. Unwanted effects can limit therapy, particularly in elderly patients, so Chapter 4 also investigates a CD20 targeted oncolytic measles virus that is 'blind' to the native viral receptors CD46 and SLAM.

In the final results chapter of this thesis – Chapter 5 - the mechanisms of MV oncolysis are explored in greater depth. Neutrophils are known to be important for MV oncolysis however their role has yet to be satisfactorily elucidated, with antibody dependent cellular cytotoxicity (ADCC) being largely ruled out as a mechanism by previous work in Prof.

Fielding's laboratory. This thesis entailed investigating an alternative mechanism - neutrophil mediated antibody dependent cellular phagocytosis (ADCP). During the course of the research it became apparent that this FACS based assay may not be measuring neutrophil phagocytosis and thus it became an aim of the project to establish, by imaging techniques, precisely what process was being measured, in order to more fully understand the role of neutrophils in MV oncolysis.

Chapter 2 Methods

2.1 General Cell and Tissue Culture Methods

2.1.1 Tissue culture

Vero cells were grown in Dulbecco's Modified Eagle Medium (DMEM) with 5% fetal bovine serum (FBS), penicillin 100µg/ml , streptomycin 100µg/ml (P/S), and L-glutamine 2mM (L-glut). Vero-SLAM cells required the same media however with 10% FBS and the addition of 0.5mg/ml Geneticin® G418. Suspension cells were grown in Roswell Park Memorial Institute (RPMI) 1640 Medium Gibco™ with 10% FBS, P/S, and L-glut. Cells were incubated at 37°C with 5% CO_2 in humidified air. Cells were generally grown in T75 flasks and passaged in the exponential growth phase at approximately 80-90% confluence.

2.1.2 Cell lines

NALM-6 – human B-cell acute lymphoblastic leukaemia cell line suspension (ACC128; DSMZ)

Raji – human Burkitt lymphoma, suspension (CCL-86; ATCC)

Phoenix AMPHO – human embryonic kidney cell line, adherent (CRL-3213; ATCC)

Vero – African green monkey kidney cell line, adherent (CLL-81; ATCC)

Vero-SLAM – Vero cells that express SLAM, adherent (gifted by Mayo Clinic MN, USA)

2.1.3 Cell culture reagents

Dimethyl Sulfoxide (DMSO) (Sigma Aldrich, Poole, UK).

Dulbecco's Modified Eagle Medium (DMEM) – high glucose 4.5g/L (Invitrogen, Paisley, UK).

Foetal Bovine Serum (FBS), heat inactivated (Invitrogen, Paisley, UK).

L-glutamine 200mM, final concentration in media 2mM (Invitrogen, Paisley, UK).

OptiMEM® medium (Invitrogen, Pailsey, UK).

Penicillin-Streptomycin containing 10,000 units/ml penicillin and 10,000µg/ml streptomycin, final concentration 100 units/ml and 100µg/ml respectively (Invitrogen, Paisley, UK).

Phosphate Buffered Saline (PBS) (Invitrogen, Paisley, UK).

RPMI-1640 medium (Invitrogen, Paisley, UK).

TrypLE™ Express Enzyme (Invitrogen, Paisley, UK).

2.1.4 Cryopreservation and cell recovery

To cryopreserve, cell pellets were resuspended in a freezing mix (10% DMSO and 90% FBS) and aliquoted into polypropylene cryovials (Nunc™, ThermoScientific™) at a concentration of $1x10^6$ – $5x10^6$ cells per ml. They were quickly transferred, in a Mr.Frosty™ freezing container (ThermoScientific™) filled with 100% isopropanol, to the -80°C freezer to achieve approximately 1°C per minute freezing rate. After a minimum of 4 hours, normally the following day, the cryovials were transferred to liquid nitrogen for long term storage.

To thaw and recover cells the cryovials were immersed in a water bath at 37°C until thawing became apparent. 10ml of FBS was added in a dropwise fashion with gentle mixing and then centrifuged at 394*g* for 5 minutes. The resultant cell pellet was then washed with 10ml of a mix of 50% FBS and 50% appropriate culture media to remove any

remaining DSMO. After a further centrifugation the pellet was resuspended in 10ml tissue culture media and transferred to a T25 tissue culture flask (Corning®, NY, USA) and incubated at 37°C, 5% CO_2 until 80-90% confluence was attained, at which time they were transferred to a T75 tissue culture flask (Corning®, NY, USA) and maintained as previously described.

2.1.5 Cell counting and viability

Live cells were counted by trypan blue exclusion method using a glass haemocytometer. 10µl cell suspension was added to 90µl 0.4% trypan blue (Sigma-Adrich®, Poole, UK) and carefully pipetted to the haemocytometer. Using the 10X objective lens of the light microscope, cells were counted in the 4 marked quadrants. Live, unstained cells, and dead, stained cells, were counted with a tally counter. Cell concentration could be estimated by taking an average of the 4 counts, multiplying by 10^4 and then by 10 to correct for the 1:10 trypan blue dilution.

2.2 Flow Cytometry Methods

2.2.1 General method

1-10 x10^5 cells per aliquot were stained with designated antibody and incubated at 4°C for 15 minutes in the dark. They were washed and re-suspended in prepared FACS media or PBS. Brilliant Horizon™ stain buffer (BD Biosciences) was used when 2 or more brilliant violet stains were required for the panel. Where viability staining was required 5µl DAPI or 10µl Propidium Iodide was added immediately prior to acquisition. When cells required fixing, LIVE/DEAD™ aqua was used as per manufacturer's instructions. To fix cells, the cell pellet was resuspended in 150µl BD CellFIX™ diluted at 1/10 in deionized water for 15 minutes and then washed and resuspended in FACS buffer.

Samples were acquired on BD LSR Fortessa™ 20X using BD FACS DIVA™ software. They were subsequently analyzed using FlowJo® 7.4 or latterly FlowJo® 10.

Table 2-1 Antibodies and Isotype Controls used in flow cytometry

Antibodies

Target	***Reactivity***	***Species***	***Ig class***	***Product code***	***Manufacturer***	***Clone***	***Conjugate***
CD10	Human	Mouse	IgG1, κ	332775	BD	HI10a	FITC
CD11b/ MAC-1	Human	Mouse	IgG1, κ	562723	BD Horizon™	ICRF44	BV605
CD13	Human	Mouse	IgG1, κ	347406	BD	L138	PE
CD14	Human	Mouse	IgG_{2a}, κ	561116	BD	M5E2	PerCP- Cy™5.5
CD15	Human	Mouse	IgM, κ	561716	BD	H198	APC
CD15	Human	Mouse	IgM, κ	551376	BD	H198	APC
CD15	Human	Mouse	IgM	17-0158	eBioscience	MMA	APC
CD16	Human	Mouse	IgG1, κ	561308	BD	B73.1	FITC
CD19	Human	Mouse	IgG1, κ	557791	BD	SJ25C1	APC-Cy™7
CD19	Human	Mouse	IgG1, κ	557835	BD	SJ25C1	PE-Cy™7
CD20	Human	Mouse	IgG1, κ	347201	BD	L27	PE Quanitbrite
CD20	Human	Mouse	IgG1, κ	F0799	DAKO A/S, Denmark	B-Ly1	FITC
CD20	Human	Mouse	IgG_{2b},κ	559776	BD	2H7	APC
CD22	Human	Mouse	IgG1	GM-4053	Nordic Mubio	RFB4	PE
CD24	Human	Mouse	IgG_{2a}, κ	658331	BD	ML5	APC-H7
CD25	Human	Mouse	IgG_{2a}	A07774	Beckman Coulter	B1.49.9	PE
CD33	Human	Mouse	IgG1, κ	740400	BD OptiBuild	WM53	BV605
CD34	Human	Mouse	IgG1, κ	347222	BD	8G12	PerCP- Cy™5.5
CD38	Human	Mouse	IgG1, κ	656646	BD	HB7	APC-H7
CD45	Human	Mouse	IgG1, κ	560178	BD	2D1	APC-H7
CD46	Human	Mouse	IgG_{2a}, κ	555949	BD	E4.3	FITC
CD46	Human	Mouse	IgG_{2a}, κ	743778	BD OptiBuild	E4.3	BV605

Target	*Reactivity*	*Species*	*Ig class*	*Product code*	*Company*	*Clone*	*Conjugate*
CD58	Human	Mouse	IgG1, κ	130-101-190	MACS Miltenyi Biotec	TS2/9	APC
CD62L	Human	Mouse	IgG1,κ	560966	BD	DREG-56	PE
CD66b	Human	Mouse	IgM,κ	562940	BD Horizon™	G10F5	BV421
CD81	Human	Mouse	IgG1, κ	656647	BD	JS-81	APC-H7
CD123	Human	Mouse	IgG_{2a}, κ	130-090-901	MACS Miltenyi Biotec	AC145	APC
CD150/SLAM	Human	Mouse	IgG1, κ	559592	BD	A12	PE
CD150/SLAM	Human	Mouse	IgG1, κ	562875	BD Horizon™	A12	BV421
CD193	Human	Mouse	IgG_{2b}, κ	564189	BD	5E8	PerCP- Cy™5.5
CXCR2	Human	Mouse	IgG1, □	555933	BD	6C6	PE
Nectin 4	Human	Mouse	IgG_{2b}, κ	FAB2659P	R&D systems	337516	PE
Nectin 4	Human	Mouse	IgG_{2b}	FAB2659A	R&D systems	337516	APC
NG2	Human	Mouse	IgG1	IM3454U	Beckman Coulter	7.1	PE

Isotype Controls

Fluorophore	*Isotype*	*Clone*	*Immunogen*	*Catalogue Number*	*Manufacturer*
APC-H7	Mouse BALB/c IgG_1 K	X40	Keyhole limpet hemocyanin (KLH)	641401	BD Biosciences
FITC	Mouse BALB/c IgG_1 K	X40	Keyhole limpet hemocyanin (KLH)	345815	BD Biosciences
PE	Mouse BALB/c IgG_1 K	X40	Keyhole limpet hemocyanin (KLH)	345816	BD Biosciences
PerCP-Cy5.5	Mouse BALB/c IgG_1 K	X40	Keyhole limpet hemocyanin (KLH)	347221	BD Biosciences
PE-Cy7	Mouse BALB/c IgG_1 K	X40	Keyhole limpet hemocyanin (KLH)	348808	BD Biosciences
APC	Mouse C.SW IgG_{2b} K	27-35	-	555745	BD Biosciences
BV605	Mouse BALB/c IgG_1 K	X40	Keyhole limpet hemocyanin (KLH)	562652	BD Biosciences
BV421	Mouse BALB/c IgG_1 K	X40	Keyhole limpet hemocyanin (KLH)	562438	BD Biosciences

2.2.2 Compensation

For experiments where the panels included fluorophores in the ultraviolet channel, Utracomp eBeads™ (Invitrogen™) were used for compensation. Otherwise OneComp eBeads™ (Invitrogen™) were used. Compensation with LIVE/DEAD aqua™ (Invitrogen™) required ArC™ Amine Reactive Compensation Bead Kit (Invitrogen™). For experiments using cells transduced to express red fluorescent protein (RFP), positive and negative cells were used for compensation. Where possible, a combination of cells and beads was avoided for compensation.

2.2.3 Estimating molecules per cell (MPC)

BD Quantibrite™ beads were prepared for flow cytometry as per manufacturer's instructions. Beads were run for every occasion MPC estimation was required. At least 10 000 events were captured in the PE channel. BD Quantibrite CD20 PE was used to stain cells to provide a PE:antibody ratio of 1:1. Following acquisition, the geometric mean fluorescence of the 4 peaks obtained was established using FlowJo software, and a standard curve drawn using Microsoft® Excel with $\log_{10}$ fluorescence plotted on the *y*-axis and $\log_{10}$ molecules per bead on the *x*-axis (provided by BD for each batch of Quantibrite beads) Using the equation $y=mx+c$ where y equals $\log_{10}$ fluorescence, and $x=\log_{10}$ molecules per bead. This was then used to determine the MPC for the cells stained with BD Quantibrite CD20 PE.

2.2.4 Fluorescent activated cell sorting

Cell sorting was performed on FACS ARIA III. Initially cells were sorted by RFP expression in the immunology department at the RFH. Following culture they were then sorted by CD20 expression into 3 groups – 'high' 'medium' 'low' at the Cancer Institute.

2.2.5 Imaging Flow cytometry - Imagestream®

ADCP Co-cultures were prepared in an identical manner, using identical antibodies, to those for standard flow cytometry experiments, however, the final concentration of cells was greater at 5 – 10 x10^6/ml. Samples were acquired using Amnis Imagestream® x Mark II Imaging Flow Cytometer with 405nm, 488nm and 642nm lasers. Images were acquired with the 60x objective lens. At least 10 000 events were collected for each sample and data were analysed using Amnis IDEAS software.

2.3 Measles Virus Methods

2.3.1 Measles Virus strain

Edmonston strain vaccine MV-NSe was used. The modified stain MVHαCD20 has been described in the introduction and was rescued from cDNA. Viral stocks were kept at -80°C. Repeated freeze/thaw cycles were avoided.

2.3.2 MV rescue from cDNA

1x10^6 vero-SLAM cells per well were seeded in a 6 well plate and incubated overnight to 80% confluence. Media had been prepared without antibiotic. Veros were then infected with MVA-T7 - modified vaccinia virus expressing T7 RNA polymerase - in 1ml OptiMEM® and incubated for 90 minutes at 37°C with 5% CO2. MV plasmid master mix was prepared in 100µl Opti-MEM® (ThermoFischer Scientific) GlutaMAX™ (Gibco) using 1µg pCG-N, 0.6µg pCG-P, 0.4µg pCG-L, and 10µg full length plasmid. The plasmid mix was added to a mix of Lipofectatamine® 2000 transfection reagent (Invitrogen™) Opti-MEM ® GlutaMAX (8µl and 100µl respectively per well) and incubated at room temperature for at least 20 minutes (stable up to 6 hours). 200µl of the plasmid/lipofectamine mix was added carefully in a dropwise fashion to the vaccinia infected verso. 1ml Opti-MEM® GlutaMAX™ was slowly

added and then incubated overnight at 37°C with 5% CO_2. After 72 hours the supernatant was transferred to fresh Vero-SLAM cells. Once formed, individual syncytia were harvested and propagated.

2.3.3 MV propagation and $TCID_{50}$

Vero, or Vero-SLAM were seeded onto 14cm plates until 100% confluent. MV at 0.01 Multiplicity of infection (MOI) was added in 4ml Opti-MEM® and incubated for 2 hours at 37°C with 5% CO_2. Viral supernatant was replaced with 20ml of appropriately supplemented DMEM media and incubated for 36-48 hours. Once characteristic syncytia were forming and the cells were beginning to lift off the plate, the cells were harvested with a cell lifter into a small volume of Opti-MEM®. Following two freeze-thaw cycles to release intracellular viral particles, viral titre was determined by 50% tissue culture infectious dose ($TCID_{50}$) assay. $5x10^3$ Vero cells per well were seeded in a flat bottom 96-well plate containing 50µl media. Ten fold serial dilutions of MV were prepared and 50µl added with all wells of an 8 well column receiving the same dilution. The plate was then incubated at 37°C with 5% CO_2. The Karber formula was used to calculate the dose.

$$Log_{10}\ TCID_{50} = -\ [log_{10}x - d(p - 0.5)] + log_{10}\ (1/v)$$

x = highest dilution giving 100% wells positive
d = log_{10} of dilution interval (e.g. for 10 fold dilution d=1)
p = sum of values of the proportion of wells positive for infection at all dilutions
v = volume of viral inoculum for each well in ml

Plaque forming units (pfu) per ml was estimated by multiplying $TCID_{50}$ by 0.7 (derived from Poisson distribution)

2.3.4 MV Infection

Suspension cells were initially counted with a haemocytometer. The appropriate number of cells were then washed with phosphate buffered saline (PBS) and re-suspended in Opti-MEM® at the required MOI. Cells were incubated at 37°C with 5% CO_2 for 2 hours before the inoculum was replaced with appropriate media.

Measles virus IgG Enzyme Linked Immunosorbent Assay (ELISA) [IBL international, Hamburg, Germany]

According to manufacturer's instructions, 100µL of each standard, control and diluted sample was pipetted into respective wells of the microtiter plate in duplicate. The plate was covered with adhesive foil and incubated at 37°C for 60 minutes. The solution was then discarded and the plate washed 3x with 300µl per well of diluted wash buffer. Excess solution was removed by tapping the inverted plate on a paper towel. 100µl of enzyme conjugate was then added, the plate covered and incubated at 37°C for 60 minutes. The excess solution was again discarded and washed 3x with 300µl per well of diluted wash buffer. 100µl of TMB substrate solution was added to each well and incubated for 30 mins at 18-25°C in the dark without adhesive foil. The substrate reaction was then stopped by adding 100µL of TMB stop solution into each well. Colour changes were from blue to yellow. The optical density was then measured at 450nm (Reference wavelength 600-650nm) using Tecan Sunrise absorbance reader (Jencon-PLS, UK). Optical density of provided standards was plotted against their concentration to obtain a calibration curve using Excel in order to extrapolate sample concentrations.
Interpretation of results >300 mIU/ml= positive, 200-300 mIU/ml = borderline, <200 mIU/ml = negative.

2.4 Neutrophil Extraction Methods and Cellular Assays

2.4.1 Neutrophil Isolation from Peripheral Blood – Traditional Method

40µl heparin sodium (preservative free) (5000 iu/ml] was pipetted into a 50ml conical tube. 20ml of freshly taken peripheral blood was carefully poured down the side of the tube and gently inverted three times. 12ml of 3% dextran solution was added and inverted several times. The mixture was incubated at room temperature for 45-60 minutes to allow the erythrocytes to sediment to the bottom. The supernatant was then transferred to a 50ml conical tube and centrifuged at 290*g* for 12 minutes at room temperature with no brake. The supernatant was then discarded and the cell pellet treated with hypotonic shock to

remove remaining erythrocytes. This involved re-suspending the cell pellet in 12ml of ice cold ddH20 for 10 seconds, inverting the tube twice to mix then immediately adding 4ml 0.6M KCl to restore isotonicity. The tube was inverted several times to mix and quickly diluted to 50mls with PBS. This was then centrifuged at 363*g* for 5 minutes with normal brake. The hypotonic step was repeated if there was evidence of erythrocytes remaining in the pellet. The supernatant was discarded and the pellet re-suspended in 2.5ml of PBS. The cell suspension was then carefully layered over 3ml Ficoll-Paque™ (GE Healthcare) in a 15ml conical tube. This was centrifuged at 400*g* for 30 minutes at room temperature without brake. The supernatant was discarded and the cell pellet of neutrophils was resuspended and washed 3 times.

2.4.2 Neutrophil Isolation from Peripheral blood – Magnetic Beads - MACSxpress® - Method

Neutrophils were isolated from peripheral blood using MACSxpress® Neutrophil Isolation Kit, human (Miltenyi Biotec Ltd. Surrey) and MACSxpress® Erythrocyte Depletion Kit, human following manufacturers protocol. Fresh peripheral blood was collected in a 10ml BD Vacutainer® K2E (EDTA) using no-touch technique. MACSxpress® Neutrophil Isolation Cocktail lyophilized pellet was reconstituted by addition of 2mL Buffer A and mixed gently by pipetting up and down 3-4 times. Once homogenous, the suspension was added to Buffer B to form a final cocktail. 8ml of anticoagulated blood was transferred to a 15ml tube and 4ml of the final cocktail added. Following gentle inversion, the tube was incubated for 5 minutes at room temperature using a MACSmix® TubeRotator at 12rpm. The open tube was then placed in the magnetic field of a MACSxpress® Separator for 15 minutes. The supernatant containing isolated neutrophils were then collected using top-to-bottom pipetting as described in the manufacturers protocol.

20µl of reconstituted MACSxpress™ Erythrocyte Depletion Reagent was added per 1ml of isolated neutrophil cell suspension. The tube was gently inverted three times and incubated for 5 minutes at room temperature using a MACSmix TubeRotator at 12 rpm. The open tube was then placed in the magnetic field of a MACSxpress Separator for 10 minutes. The supernatant was collected as previously described and the cells washed in RPMI.

2.4.3 Complement Dependent Cytotoxicity (CDC) assay

A total of 8 x 10^6 cells were infected with MV-NSe, MVHαCD20, MVNSeCD46blind, MVHαCD20CD46blind or mock infected. 2 x 10^5 cells of each condition were plated into a round-bottom 96 well tissue culture plate in 200µl RPMI media and either 50µl (i.e. 20%) of human serum (Sigma) or human serum previously heat inactivated at 56°C was added. 10µL/µl of rituximab replaced human serum to act as a positive control. Each condition was replicated thrice. This was then incubated at 37°C, 5% CO_2 for 30 minutes. Cells were washed with FACS buffer (1% BSA (Cell Signalling Technology), and 0.05% sodium azide (Sigma), PBS (Gibco® by Life Technologies™) and transferred to FACS tubes. Prior to flow cytometric acquisition cells were stained with 5µL 4',6-Diamidino-2-Phenylindole, Dihydrochloride (DAPI) (Santa Cruz Biotechnology). Cell death was measured as positive staining by DAPI using BD FACSymphony™.

2.4.4 Neutrophil Mediated Antibody-Dependent Cellular Phagocytosis (ADCP) Assay

For PKH67 (Sigma-Aldrich®) fluorescent cell membrane labelling of target cells, first target cells were washed with PBS then re-suspended in Diluent C to reach 20x10^6 cells/ml. PKH67 was diluted in Diluent C to reach 8µM and then mixed with cell suspension to reach 4µM. Following a 2 minute incubation at room temperature, the staining reaction was stopped by adding an equal volume of FBS for one minute. Cell media was then added and the cells washed three times. The suspension was then incubated on ice until required.

100µl of target cells (normally NALM6) at a concentration of 2 x10^6 /ml (i.e 200 000 cells) were plated in wells of a 96 well clear round bottom ultra-low attachment microplate (Corning®). 50µl of antibody containing media was added, either rituximab to make overall concentration of 10µl/ml, human serum from AB male plasma (Sigma®), heat inactivated human serum (heat inactivated at 56°C for 30 minutes), RPMI or high/low titre anti MV IgG serum and incubated for 10 minutes at room temperature. 100µl of freshly isolated

neutrophil effector cells at a concentration of 0.4 x10^6 /ml (i.e. 40 000 cells) were added and then the co-culture transferred to the incubator at 37°C, 5% CO_2 for 2.5 hours.

Following incubation, cells were transferred to polypropylene 96 well plates V bottom (BD Falcon) and centrifuged at 337*g*. Cells were stained with 50µl antiCD14-APC antibody in FACS buffer (PBS; 2% BSA; 0.1% sodium azide) and incubated at 4°C in the dark for 15 minutes. Cells were washed and resuspended in 150µl FACS buffer and if for immediate FACS acquisition transferred to 1.2ml microtubes (Starlab, Germany). If for next day FACS acquisition then cell pellets were resuspended in 150µl BD CellFIX™ diluted at 1/10 in deionized water for 15 minutes and then washed and resuspended in FACS buffer. If live/dead staining was required but cells needed to be left overnight then cells were first stained with LIVE/DEAD™ aqua (Invitrogen™).

Co-cultures were acquired on Fortessa X20 using FACS DIVA software. Compensation controls were first analysed for PKH67, APC and DAPI (or LIVE/DEAD™ aqua). Events were gated on FSC/SSC to remove debris. A live gate is then created selecting DAPI negative (or LIVE/DEAD™ aqua) events. APC was then used for the y-axis and PKH67 for the x-axis. A rectangular gate was then used to monitor the numbers of neutrophils and at least 1000 events were recorded in this channel.

2.5 Microscopy Methods

2.5.1 Confocal Microscopy

NALM6-high-CD20 cells were stained with PKH67 according to manufacturers instructions (Sigma-Aldrich, St Louis, USA) and made to a concentration of 10x10^6/ml. Neutrophils were extracted from healthy donors using MACSxpress® Neutrophil Isolation Kit, as described previously, and made to a concentration of 5x10^6/ml. Approx 20µg of fibronectin (Sigma-aldrich) was added to each well of ibidi® 15µl-Slide 8 well microscope slides and washed off with PBS after 1 hour. 100µl target cells and 50µl antibody condition (rituximab/anti-MV IgG/Human serum/media) were added to each slide compartment. Immediately prior acquisition, 100µl effector cells (neutrophils) were added. Time-lapse confocal microscopy

imaging acquired with LSM 700 Confocal Microscope (Carl Zeiss Microscopy, Germany), with a definite focusing system, Zen Black software, using a heated stage at 37°C. Images were taken every 20s for the 150min incubation period and analysed using Fiji imaging processing package. In control experiments, 4.5µM Dynabeads coated with CD3/CD28 antibodies (Dynal Biotech ASA, Norway) were added instead of target cells.

2.6 Molecular Biology Methods

2.6.1 mRNA extraction – TRIzol® method

Cell pellets were resuspended with 1ml TRIzol® (Life technologies). A reduced amount was used if the cell number was less than $5x10^6$. The solution was transferred to an RNAse-free eppendorf tube and incubated for 5 minutes at room temperature. 0.2ml chloroform was added and the tube inverted to mix and incubated on ice for 5 minutes. The sample was then centrifuged at 13 151*g* for 15 minutes at 4°C. The upper aqueous phase was then transferred to a new RNAse-free eppendorf tube avoiding the white DNA interphase layer. 0.5ml isopropanol was added and the sample stored at -80°C overnight to facilitate mRNA precipitation. Once thawed, the sample were centrifuged at 13 151*g* for 10 minutes at 4°C. The supernatant was carefully removed, and the pellet washed with 1ml 75% ethanol. This was vortexed and centrifuged at 13 151*g* for 5 minutes at 4°C. The supernatant was carefully removed and the pellet air dried whilst on ice. Concentration and purity of RNA was determined by measuring light absorbance of the samples at 260nm (A260) and 280nm (A280) with NanoDrop™1000 spectrophotometer (Thermo Scientific, Essex, UK).

2.6.2 mRNA extraction – QIAamp® RNA Blood Mini Kit (Quiagen)

mRNA extracted as manufacturers protocol from 'Procedure No.6'. Briefly, either 350µl (or 600µl) of Buffer RLT (containing mercaptoethanol) was added to the cell pellet containing up to 2 $x10^6$ leucocytes (or 2 $x10^6$ to $1x10^7$) to disrupt the cells. Pipetting and vortexing was continued until no cell clumps were visible. Lysate was then directly added into a QIAshredder spin column in a 2ml collection tube and centrifuged at 2 mins at 13 151*g* to homogenize. The homogenized lysate was saved and one volume (350µl or 600µl) of 70% ethanol added and mixed by pipetting. This was carefully pipetted into a new QIAamp spin

column in a 2ml collection tube and centrifuged for 15 seconds at 13 151*g*. If volume exceeded 700µl further spin columns were used. The QIAamp spin column was next transferred into a new 2ml collection tube and 799µl Buffer RW1 applied to the spin column and centrifuged for 15 seconds at 13 151*g* to wash. The spin column was placed in a new 2ml collection tube and 500µl of Buffer RPE pipetted into the QIAamp spin column and centrifuged for 15 seconds at 13 151*g*. The spin column was carefully added and 500µl of Buffer RPE added. After closing the cap, this was centrifuged at 13 151*g* for 3 minutes. The spin column was transferred into a 1.5ml microcentrifuge tube and 330-50µl RNase-free water pipetted directly onto the QIAamp membrane. Finally, this was centrifuged for 1min at 13 151*g* to elute mRNA. mRNA concentration was measured using with NanoDrop™ 1000 spectrophotometer (Thermo Scientific, Essex, UK) and either used immediately or stored at -80°C.

2.6.3 First strand cDNA synthesis – Method A (Used in MV experiments)

0.4-1 µgRNA was diluted to 9µl with ddH20. This was mixed with 2µl (334ng) random hexamers, 1µl 0.1M DTT and 2µl 10mM dNTPs and incubated at 65°C for 5 minutes and on ice for 10-15 minutes. 4µl 5x first strand buffer, 1µl (40 units) RNAsin Plus RNAse Inhibitor and 1µl (200 units) of SuperScript™ II reverse transcriptase was added to each sample and incubated at 25°C for 10 minutes, 50°C for 50 minutes and 70°C for 15 minutes. The product was either used immediately for PCR or stored at -20°C.

2.6.4 First strand cDNA synthesis – Method B (MRD lab method – used for UKALL14 primary patient specimens)

M-MLV Reverse Transcriptase kit (Invitrogen, UK) was used. For each reaction, 1 µg RNA was dispensed into a 1.5 ml micro centrifuge tube and the volume made up to 20µl with DNase/RNase free water. 1µl RNasin was then added to the tube and the mixture was incubated at 65° C for 5 minutes followed by immediate cooling on ice for 5 minutes. For each reaction, the following volumes of each reagent were prepared: 10µl 5×cDNA buffer, 2.5µl 10mM dNTPs,1µl RNasin, 1µl 0.5 µg/ µl pd (N) 6, 2µl Reverse Transcriptase, 0.5µl 100mM DTT and 12µl ddH_2O. The master mix was added to the tube and the tube was

incubated at 37°C for 1 hour followed by 65°C for 10 minutes then cooling on ice for 5 minutes. A non-template control (NTC) reaction was to detect any contamination.

2.6.5 First strand cDNA synthesis – Method C (RT^2 First Strand Kit - Qiagen® – For use with RT^2 Profiler assays)

Following manufacturer's instructions, first the reagents of the RT^2 First Strand Kit were thawed and briefly centrifuged. The genomic DNA elimination mix for each RNA sample was prepared with 0.5μg RNA, 2μl Buffer GE made up to 10μl with RNase-free water. This was mixed by gentle pipetting and then centrifuged briefly. The genomic DNA elimination mix was incubated for 5 min at 42°C and then placed on ice for at least 1 minute. A reverse-transcription mix scaled up and prepared as per volume for 1 reaction – 4μl 5x Buffer BC3, 1μl Control P2, 2μl RE3 Transcriptase Mix, 3μl RNase-free water. 10μl of the reverse-transcription mix was added to each tube containing 10μl genomic DNA elimination mix, mixed by gentle pipetting, nand incubated at 42°C for exactly 15mins and the reaction stopped by incubating at 95°C for 5 minutes. 91μl RNase-free water was added to each reaction and pipetted up and down several times. The reaction was placed on ice for continuation to the real-time PCR protocol or stored at -20°C.

2.7 Cloning Methods

2.7.1 Cloning and Retroviral Transduction of Nalm6 to make Nalm6-CD20

Oligonucleotide primers were designed for CD20 and manufactured by Sigma-Aldrich Co. LLC.; the forward primer also coded a BamH1 restriction site and the reverse coding Xho1 restriction site.

Forward primer 5' TAAGCAGGATCCATGACAACACCCAG 3'
Reverse primer 5' TAAGCACTCGAGTTAAGGAGAGCTGTCATC 3'

BamH1	5'…G^GATCC…3'	Xho1	5'…C^TCGAG…3'
	3'…CCTAG^G…5		3'…GAGCT^C…5'

Human CD20 was amplified from a CD20 containing plasmid – 'CMV sport' - as a 'gradient PCR'.

0.4 µ 10mM dNTP Mix [Promega, Madison, WI USA], 2.0µl 10x ThermoPol® Reaction Buffer [New England Biolabs] 1.0µl Forward primer, 1.0µl Reverse primer, 0.4µl VentR® DNA Polymerase [New England Biolabs]

Temperature range was estimated from the calculated Tm of the oligonucleotide primers. [65.0°C; 65.2°C; 65.7°C; 66.3°C; 67.3°C; 68.5°C; 68.8°C; 71.0°C; 71.8°C; 72.4°C; 72.9°C; 73.0°C].

Initialisation	94°C	3 minutes		
Denaturing	94°C	30 seconds	}	
Annealing	as gradient	30 seconds	}	30 cycles
Extension	72°C	30 seconds	}	
Final elongation	72°C	10 minutes		

This was then repeated using the optimum annealing temperature of 65°C.

The products were run on a 2% TAE (Tris-acetate-EDTA) [Severn Biotech Ltd] agarose gel, with 10µl SYBR®Safe DNA gel stain [Life Technologies]. HyperLadderTM II [Bioline] UV lightbox was used to visualise the CD20 band which was removed using a clean, sharp, disposable scalpel [Swann-Morton®, UK].

2.7.2 Extraction of DNA Fragments from TAE Agarose Gel

The DNA fragments were extracted using QIAEX II® Gel Extraction Kit [Qiagen] as per manufacturers guidelines. Briefly, having removed excess agarose, the slice was weighed in a 1.5ml microcentrifuge tube. 3 volumes of Buffer WX1 were added to 1 volume of gel and resuspended QIAEX II was added. This was then incubated in a water bath at 50°C to solubilise the agarose and bind the DNA. During the incubation period the mixture was briefly vortexed. The sample was centrifuged and the supernatant discarded. The pellet

was washed with 0.5ml Buffer QX1 and subsequently twice with Buffer PE. Following 10-15 mins of air drying the DNA was eluted with dH20.

2.7.3 Restriction Digest

An overnight restriction digest reaction was set up for both MSCV-Ik6-IRES-mRFP and the extracted CD20. The reaction was kept at 37°C overnight and stopped with 20 minutes at 65°C.

1µg DNA
1µl Xho1 restriction enzyme [New England Biolabs Inc]
1µl BamHI-HF restriction enzyme [New England Biolabs Inc]
5µl CutSmart® buffer
dH20 to 50µl

Reaction products were ran on 1.4% TAE agarose gel using HyperLadderTM 1 Kb[Bioline], 7000 bp band from MSCV-Ik6-IRES-mRFP, and the 900 bp band from CD20 were cut and DNA fragments extracted.

2.7.4 Ligase Reaction

10 ligase reactions using ratios insert:vector ranging from 1:1 to 1:7 with 10xT4 DNA Ligase reaction Buffer [New England Biolabs Inc], and T4 DNA Ligase [New England Biolabs Inc]. Reactions were incubated overnight at 16°C and subsequently heat inactivated at 65°C for 10 minutes.

Reaction products were then transformed using NEB 10-beta Competent *E. coli* (High Efficiency) [New England Biolabs, Inc] as per manufacturer's instructions. Resulting bacteria were spread onto freshly made 2xTY agar plates with 100µg/ml ampicillin [Sigma-Aldrich] and incubated at 37°C overnight. Colonies were picked and cultured in 2xTY cultures.

QIAprep® Spin Miniprep Kits [QIAGEN] were used to extract plasmids as per manufacturers instruction.

New oligonucleotide primers were designed and manufactured

Forward primer: 5' TAAGCCTCCGCCTCCTCTTC 3'
Reverse primer: 5' CAAACGCACACCGGCCTTATTC 3'

CD20 insert sequence was confirmed [Eurofins Genomics].

2.7.5 Retroviral Transfection

Day 1: Phoenix™-AMPHO retroviral packaging cells were cultured at 37°C 5% CO_2 in DMEM 10% FBS, L-glutamine, Penicillin and streptomycin. Once they reached 60-80% confluence they were harvested by trypsinisation, washed, resuspended and enumerated. $4x10^9$ cells were plated in 8mls of appropriate media into 10cm culture dishes and incubated over night.

Day 2: The following transfection mix was prepared:-

Solution A: 10µl Fugene®, 150µl Opti-MEM®
Solution B: 1.5µg pCL-ampho retrovirus packaging vector (Imgenex, CA, USA)
n.b.0.5µg/µl, 2.6µg vector construct (MSCV-CD20-IRES- mRFP)
Volume adjusted to 50µl with dH20

Solution B was added to solution A and mixed by gentle pipetting. This was then incubated at room temperature for 15-20 minutes. Phoenix™-AMPHO cells were added in a drop-wise manner and incubated overnight.
Day 3: Supernatant was removed and replaced with 5mls of fresh media.
Day 4: A 6 well tissue culture plate was coated with 2ml/well of RetroNectin® (Clontech, France) at concentration 30ng/ml. This was incubated at room temperature for 2-3 hours. The RetroNectin® was removed and the wells were blocked with 2ml/well 2% filter

sterilised BSA and incubated at room temperature for 30 minutes. The BSA block was removed and the wells washed twice with 3mls PBS. 2.5mls of Nalm-6 cells [$1x10^6$ cells per ml] were then added to each well and incubated at 37°C for 30 minutes.

Viral supernatant from the Phoenix™-AMPHO cells was spun at 340*g* for 5 minutes to remove any remaining cells and cell debris. This was added to the RetroNectin® treated plates in a drop wise manner.

Day 5: Viral supernatant was removed and replaced with 5ml/well of appropriate cell media (RPMI, 10% FBS, 1% L-glutamine, 1% penicillin/streptomycin. The cells were incubated at 37°C, 5% CO_2, for 3 days at which point they were transferred to a T25 flask. Flow cytometry confirmed mRFP and CD20 expression. The cells were then sorted by mRFP using BD FACSaria.

2.8 RT qPCR Methods

2.8.1 MV-N (nucleocapsid) mRNA relative quantification by PCR

To quantify expression of MV-N mRNA a TaqMan® gene expression Real-time PCR assay was used in reactions of 25μl. First strand cDNA was mixed with 0.9M forward and reverse primers and 0.25mM TaqMan® probe labelled with FAM™ reporter dye. 12.5μl TaqMan Universal Master Mix was added to each sample and the remaining volume with RNase/DNase-free water.

PCR conditions were:-
Step 1: 50°C for 2 minutes
Step 2: 95°C for 10 minutes
Step 3: [95°C for 15 seconds, 60°C for 1 minute]x40 cycles

Primer sequences for MV-N:-
MV-N s 5'-GTATCCTGCTCTTGGACTGCAT-3'
MV-N a 5'-GTTCATCAAGGACTCAAGTGTGGAT-3'

The housekeeping gene used was glyceraldehyde 3-phosphate dehydrogenase (GAPDH). The PCR reactions were carried out using Applied Biosystems ABI7500 system. Samples were run in triplicate and non-template controls (NTC) were included where cDNA was replaced with RNase/DNase free water. Relative expression levels were calculated using the formula
ΔCt = Ct(experiment) – Ct(GAPDH)
ΔΔCt = ΔCt – Ct(calibrator)
RQ = 2 (-ΔΔCt)

2.8.2 GeNorm analysis

As per manufacturers protocol, each of 12 lyophilised primer mix was pulse-spun before opening and resuspended in RNAse/DNAse free water. A mix for each reference gene was made up for each reference gene according to the recipe below:-

Resuspended primer mix	1µl
Primerdesign 2x PrecisionPLUS™ Mastermix	10µl
RNAse/DNAse free water	4µl
Final volume	15µl

15µl of mix was pipetted into each plate. 132µl of cDNA for each sample at a concentration of 5ng/µl in RNAse/DNAse free water. 5µl of diluted cDNA was pipetted into each well making a final volume of 20µl.

Plates were run on ABI 7500 fast using the following amplification protocol

Cycling x40	**Step**	**Time**	**Temp**
	Enzyme activation	2min	95°C
	Denaturation	10s	95°C
	Data collection	60s	60°C

Data was analysed using qbase+ real-time PCR data analysis software.

This analysis recommended 4 reference genes ACTB, B2M, GAPDH and 18S.

Initial experiments used the 3 of these genes. Taqman Primers and probes were designed based on the literature, ordered from Sigma Aldrich.

Efficiencies were calculated, desired amplification efficiencies range from 90% to 110%.

$E = -1 + 10^{(-1/\text{gradient})}$

			Tm°C	MW
CD20 Wild type	Forward	5' ATTATTTCCGGATCACTCCT	58.9	6018
	Reverse	5' GAGGCTCAATGAATTCATTA	56.7	6140
	Probe	5' (6FAM)CAACGGAGAAAAACTCCAGG[TAM]	63.5	7314
CD20 D393 Variant	Forward	5' CCTATTGCTATGCAATCTGG	59.7	6083
	Reverse	5' CAGCTATTACAAGTTCCAGT	53.5	6076
	Probe	5' [6FAM]AACCACTCTTCAGGAGGATG[TAM]		
CD20 D657 variant	Forward	5' ATTATTTCCGGATCACTCCT	58.9	6018
	Reverse	5' TCACTGACAAAATGCCCAAA	64.1	6063
	Probe	5' (6FAM)CAACGGAGAAAAACTCCAGG[TAM]	63.5	7314
GAPDH	Forward	5' GAAGGTGAAGGTCGGAGTC	61.3	
	Reverse	5' GAAGATGGTGATGGGATTTC	60.8	6252
	Probe	5' [6FAM]CAAGCTTCCCGTTCTCAGCCT[TAM]	68.8	7454
ACTB	Forward	5' AGCCTCGCCTTTGCCGA	69.6	
	Reverse	5' CTGGTGCCTGGGGCG	68.4	4641
	Probe	5' [6FAM]CCGCCGCCCGTCCACACCCGCC[TAM]	87.7	7684
B2M	Forward	5' AGCGTACTCCAAAGATTCAGGTT	63.9	7048
	Reverse	5' ATGATGCTGCTTACATGTCTCGAT	65.7	7334
	Probe	5' [6FAM]TCCATCCGACATTGAAGTTGACTTACTG[TAM]	70.3	9700
18S	Forward	5' GTAACCCGTTGAACCCCATT	64.5	6037
	Reverse	5' TTACTGGGAATTCCTCGTTC	60.5	6074
	Probe	5' [6FAM]TGATGGGGATCGGGGATTGCAATTATTCC[TAM]	78.1	10165
MS4A1*	Forward	5' CTTCCAAGAGACATGCTGACTTTC	57.8	
	Reverse	5' GCTGCTACAATGGCTACATTCTC	57.5	
	Probe	5' [6FAM]TGAGGTACTCTGCACATACGCACCACA[TAM]	73.8	

Primers and probes from Primerdesign Ltd (sequences of primers and probes for reference genes considered proprietary information)

GAPDH: Accession number: NM_002046, Anchor nucleotide: 1087
18S: Accession number: M10098, Anchor nucleotide: 234
B2M: Accession number: NM_004048, Anchor nucleotide: 362
ACTB: Accession number: NM_1101, Anchor nucleotide: 1194

*MS4A1: Accession number: NM_021950.3.

2.8.3 Real-Time PCR for RT^2 Profiler PCR Arrays

RT^2 Profiler PCR Arrays were prepared as per manufacturers protocol. RT^2 SYBR Green Mastermix (contains HotStart DNA *Taq* Polymerase) was briefly centrifuged to bring the contents to the bottom of the tube. PCR components mix was prepared to a total volume of 2700 µl as follows in a 5ml tube – 1350µl 2x RT^2 SYBR Green Mastermix, 102µl cDNA synthesis reaction [See Methods Chapter - First strand cDNA synthesis – Method C], 1248µl RNase-free water. RT^2 Profiler PCR Array was carefully removed from its sealed bag. 25µl PCR components mix, per well, was carefully dispensed into the RT^2 Profiler PCR Arrays using an 8-channel pipettor. RT^2 Profiler PCR Arrays were either set up immediately or stored at -20°C wrapped in aluminium foil for up to one week.

RT^2 Profiler PCR Arrays were placed in the real-time cycler - Applied Biosystems 7500 fast - sealed with sealing caps and run using the following cycling conditions:-

Cycles	Duration	Temp.	Comments
1	10min	95°C	HotStart DNA *Taq* Polymerase is activated by this step
40	15s	95°C	
	60s	60°C	Perform fluorescence data collection

The threshold cycle was determined using the automatic software and kept constant across plates. The threshold value was above the background signal but within the lower on-third to lower on-half of the linear phase of the amplification plot. The C_r values were exported to and Excel spreadsheet for analysis using SABiosciences PCR Array Data Analysis web-based software. Dissociation (melting) curve analysis was performed to verify PCR specificity with a single peak appearing in each reaction at temperatures greater than 80°C.

Chapter 3 CD20 as a prognostic biomarker in Acute Lymphoblastic Leukaemia

3.1 Introduction

Acute lymphoblastic leukaemia is an aggressive haematological malignancy that is extremely sensitive to chemotherapy but, in adults, a sustained response can be difficult to achieve, with only 40-50% of patients achieving long term remission [5]. It is valuable to be able to predict responses both to limit chemotherapy in those likely gain optimum response, thereby also limiting toxic unwanted effects, and also to predict those likely to have a poor response so that intensive treatments such as allogeneic haematopoietic stem cell transplant (HSCT) or novel, more experimental therapies can be considered.

3.1.1 Prognostic, predictive and therapeutic biomarkers in cancer

Cancer biomarkers can be described as diagnostic, predictive, prognostic or therapeutic. Diagnostic biomarkers enable the early detection of a cancer, normally by non-invasive means. Prognostic biomarkers are clinical or biological characteristics from untreated patients that can provide information on the likely course of the disease and patient outcome. Predictive biomarkers allow the response to a therapy to be predicted by defining sub-populations that will benefit. A therapeutic biomarker is generally a protein that can be used as a target for therapy [190].

3.1.2 Prognostic and predictive factors in ALL

Traditionally, increasing age, male sex and a high white cell count were known to be indicators of poor outcome [191]. With the advent of cytogenetics it became clear that certain chromosomal rearrangements are indicative of a poor prognosis. The classic and most significant example being the Philadelphia (Ph) chromosome t(9;22)(q34;q11) giving rise to the fusion gene *BCR-ABL1*. This is more commonly seen in adult ALL than childhood ALL with 20-30% adult patients affected compared to 2-5% of children [11, 12]. *BCR-ABL1* positivity was previously associated with a dismal prognosis and contributed to the disparity between outcomes in adults and children. However, with the advent of the

tyrosine kinase inhibitors (TKIs) the adverse effect can be largely mitigated [11]. Other unfavourable cytogenetic markers include t(v;11(q13;q23) MLL translocation, t(8;14)(q13;q32), t(14;18)(q32;q21), complex karyotype, low hypoploidy (30-39 chromosomes and near triploidy (60-78 chromosomes). Molecular abnormalities are increasingly investigated with recent interest in a novel subtype of ALL which has a similar gene expression profile to the *BCR-ABL1* positive ALL, but without the translocation. This Philadelphia-like ALL has an unfavourable outcome and is seen in 15-20% of adolescents and young adults. There has also been evidence that the IKZ mutation can also confer a poor prognosis. Current evidence is that the most important predictive biomarker in ALL is the persistence of minimal residual disease following treatment. As described in Chapter 1, MRD is measured by either flow cytometry having identified leukaemia associated phenotype (LAP) at diagnosis, or by molecular methods such as RT-qPCR for patient specific markers – gene fusions and clonal rearrangement of immunoglobulin gene. Patients who have a delayed eradication or persistence of MRD have a higher rate or relapse and poorer overall survival [26].

3.1.3 CD20 as a prognostic marker in ALL

Flow cytometry is mandatory for the diagnosis of BCP-ALL and is widely available, therefore the expression of a marker at diagnosis could be easily and quickly determined. There have been conflicting reports with regards to the prognostic implications of CD20 expression in ALL, and these were discussed in detail in the general introduction. Three large clinical trials indicated CD20 expression above 20% confers poorer prognosis [47, 49, 50] however a Canadian and Italian trial failed to reproduce this finding [52, 57]. Targeted therapy for CD20 already exists and is widely used to successfully treat B-cell haematological malignancies, normally as part of combination chemotherapy.

3.1.4 Rituximab in the treatment of ALL

Rituximab is a chimeric monoclonal antibody directed at surface CD20. Rituximab has been used with promising results in phase II trials for ALL and Burkitt-like leukaemia/lymphoma [58, 192]. Results from a GRAALL-2003 trial [50] and the MD Anderson group [49] were sufficient for the inclusion of rituximab to treat CD20 positive patients – those expressing CD20 on at least 20% of blasts - in their subsequent *BCR-ABL1* negative trial with promising

results. The GRAALL-2005 phase III clinical trial enrolled 220 patients with *BCR-ABL1* negative ALL and randomly assigned them to receive rituximab with standard combination chemotherapy. Overall 16-18 infusions of rituximab at a dose of 375 mg/m^2 of body surface area were given to those in the treatment arm. Those receiving rituximab had a longer event free survival (EFS) than the control group (hazard ratio [HR] 0.66; 95% confidence interval 0.45 to 0.98; p=0.04) however the improvement in overall survival did not reach statistical significance (HR, 0.70; 95% CI, 0.46 to 1.07; P=0.10). It was noted that fewer patients in the rituximab arm experienced allergic reactions to asparaginase, and the incidence of adverse events was similar in the two groups [193].

3.1.5 UKALL14 and Rituximab

The UKALL14 clinical trial is a phase III multicentre clinical trial for ALL in the UK. The B-cell precursor ALL arm of the trial is now finished recruitment having enrolled the required 655 eligible patients. Unlike the GRAALL trial, UKALL14 randomised patients to receive 4 doses of 375mg/m^2 rituximab - irrespective of CD20 expression – during induction phase 1 to determine if the addition of Rituximab improves EFS. The correlative scientific aim is to determine the relationship between CD20 expression on ALL blasts and the response to monoclonal antibody therapy. Figure 3-1 shows a schematic of the UKALL14 treatment.

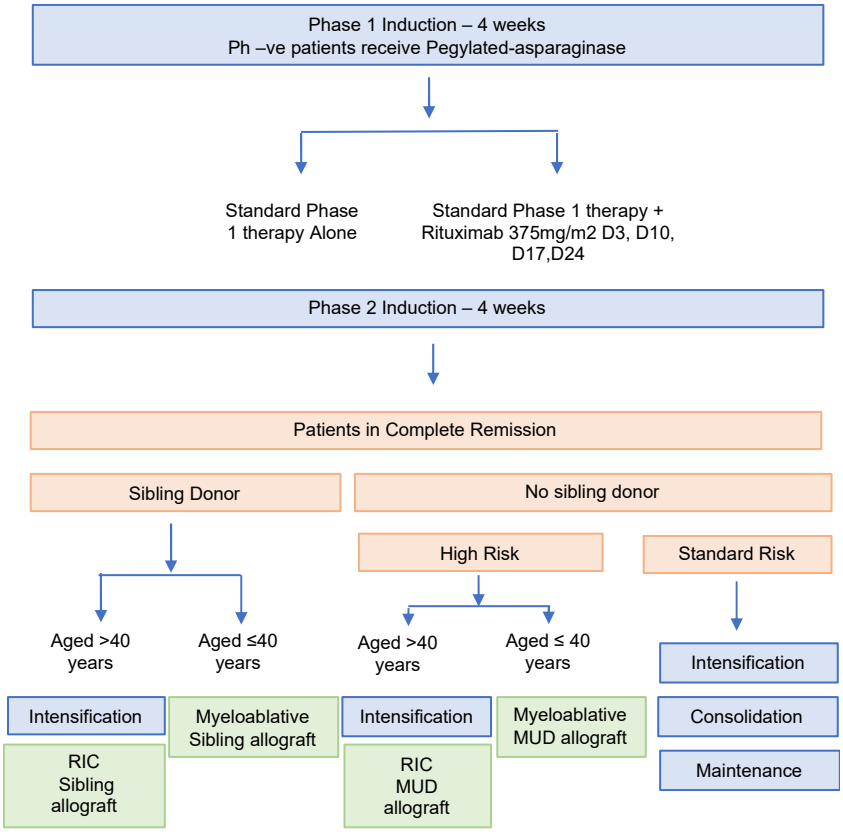

Figure 3-1 UKALL14 Trial Schema *– Precursor B-cell ALL patients. Ph= Philadelphia chromosome t(9;22), High risk features t(9;22), t(4;11), low hypodiploidy, near triploidy or complex cytogenetics, age > 40 years, WBC >= 30 x 109/L, molecular minimal residual disease positivity (>1x104) after Phase 2 Induction. RIC= Reduced intensity conditioning, MUD= Matched Unrelated Donor.*

3.1.6 Clarifying the difference between prognostic and predictive biomarkers

CD20 cannot be used as a diagnostic biomarker because it is expressed on normal and maturing B-lymphocytes. As discussed above, the evidence about its use as a prognostic biomarker is controversial but the overarching aim of this chapter is to establish whether the data from UKALL14 supports this. The promising results from the GRAALL-2005 trial have established CD20 as a therapeutic biomarker but only in those patients with *BCR-ABL1* negative ALL, and with over 20% of leukaemia cells expressing CD20. In order to establish CD20 as a predictive biomarker it is necessary to carry out a randomised controlled clinical trial where patients both expressing and not expressing CD20 are randomised to receive rituximab – such as UKALL14. Unfortunately, the unblinded results for the rituximab randomisation have not been reported at the time of writing this thesis.

3.1.7 How to monitor CD20 expression.

The traditional threshold for considering CD20 expression as positive is 20% of leukaemic blasts expressing the marker. The 20% cut-off is applicable to all markers measured by flow cytometry in the diagnosis of acute leukaemias in order to facilitate standardisation and classification, but this is based on convention rather than evidence [194]. Thomas *et al* investigated outcome at lower levels of CD20 expression, but failed to show a significant difference in outcome to the <10% group [49]. As well as the proportion of cells expressing CD20, the density of CD20 expression can be measured but has been rarely investigated in this context. In 1997 Borowitz et al found that the antigen density of CD20, measured by mean fluorescence intensity (MFI), was of prognostic significant in a retrospective analysis of childhood ALL [47] however this feature has not been explored by any other group with more modern therapy. In order to take into consideration the antigen density in addition to the proportion of leukaemic blasts expressing CD20, the UKALL 14 trial has been designed to use flow cytometry to measure the expression by percentage blasts and by antigen density using BD Quantibrite beads to estimate the CD20 molecules per cell.

3.1.8 Rationale for developing a RT-qPCR assay to measure CD20 expression

A limitation of flow cytometry is that adequate numbers of cells are required, and that ideally this should be carried out on a fresh sample. This provides logistical difficulties for any large trial with a centralised laboratory receiving specimens from geographically distant institutions. The main priority in UKALL14 was for specimens to provide adequate material for MRD, and for the majority of specimens molecular material is extracted and cells then stored if there is adequate remaining material. RT-qPCR is a standard method for diagnostic and monitoring gene expression due to its simplicity, sensitivity, and specificity. This method has rarely been used to measure CD20 expression. A case series investigating whether CD20 is upregulated in diffuse large B cell lymphoma (DLBCL) following treatment with sodium valproate compared CD20 expression by flow cytometry using QuantiBRITE beads and by RT-qPCR measuring the expression of CD20 mRNA relative to GAPDH showed similar results using both methods however they did not attempt to directly compare the two methods [195] Sorro *et al* measured the CD20 expression and CD20 protein in 12 chronic lymphocytic leukaemia (CLL) samples. comparing RT-qPCR CD20 measured by mean fluorescence intensity and mRNA found no correlation measured RT-qPCR CD20 relative to

β-actin (ΔCT) [r=0.16] [196]. This was a small sample size but the main criticism of this publication was there was no validation of the RT-qPCR method used, or rationale for using β-actin as the sole reference gene. A carefully designed RT-qPCR assay could potentially give a better estimation of the quantity of CD20 produced by the leukaemic cells. It would also provide an alternative means to measure CD20 when molecular material is available but fresh cells are not available, making it more amenable to central processing. For more immediate purposes a CD20 RT-qPCR assay could provide a means of measuring CD20 quantity in patient samples in the UKALL14 trial where cellular material is not available.

3.2 Hypotheses:

CD20 expression is a prognostic biomarker that can help predict outcome in adult patients participating in the UKALL14 clinical trial.

3.3 Aims:

To determine CD20 expression in patients participating in the UKALL14 clinical trial by the percentage of leukaemic blasts that express CD20 on their surface and also by the mean density of the CD20 antigen present on each blast.

To determine whether there is an association between CD20 expression and event free survival in UKALL14 patients.

To develop and evaluate a molecular method for the quantification of CD20 as an alternative to flow cytometry.

3.4 Methods

A flow cytometry panel of suitable markers and fluorochromes for the detection of BCP-ALL MRD was designed by the Fielding lab based on Euro-MRD criteria [197-199] (See fi

A

	APC-H7	FITC	PE	Per CP-Cy5.5	PE-Cy7	APC
Channel	R 780/60	B 530/30	YG 586/15	B 695/40	YG 780-60	R 670/30
Tube 1	CD24	CD10	CD13	CD34	CD19	CD15
Tube 2	CD45	CD10	CD20	CD34	CD19	CD33
Tube 3	CD81	CD10	CD22	CD34	CD19	CD123
Tube 4	CD38	CD10	NG2	CD34	CD19	CD58

B

	APC-H7	FITC	PE	Per CP-Cy5.5	PE-Cy7	APC	BV 605	BV421
Channel	R 780/60	B 530/30	YG 586/15	B 695/40	YG 780-60	R 670/30	V 610/30	V 450/50
Tube 1	CD24	CD10	CXCR2	CD34	CD19	CD15	CD13	
Tube 2	CD45	CD10	CD20	CD34	CD19	Nectin 4	CD46	CD150
Tube 3	CD81	CD10	CD25	CD34	CD19	CD123	CD22	
Tube 4	CD38	CD10	NG2	CD34	CD19	CD58	CD33	

Figure 3-2 Flow cytometry antibody panel used for UKALL14 patient specimens

Table [A] Flow cytometry panel used between 2012 – 2015 based on Euro-MRD recommendations. Cells gated on CD10, CD34 and CD19. Acquired using 3 laser BD Fortessa LSR. Table [B] Flow cytometry paned modified to include MV receptors CD45, Nectin 4 and SLAM (CD150), CD25 and CXCR2; used between January 2017 and November 2017. Aquired using 4 laser BD Fortessa X20. Tube 2 contains CD20.

The backbone markers, CD19-PE-Cy7, CD10-FITC, CD34-Per-CPCy5.5, were present in all 4 tubes to enable the identification and gating of B-cell precursor ALL (BCP-ALL) blasts. The remaining markers were chosen to identify patient specific leukaemia-associated phenotypes (LAP). A PE conjugate was combined with CD20 to enable the use of BD Quantibrite™ beads for accurate evaluation of antigen density. Tube 2, which contains CD20-PE, also contained an antibody to CD45 which is currently considered the most useful marker to gate BCP-ALL blasts and to exclude normal cells [198]. During B-cell development CD45 displays increasing levels of expression and can also contribute to deciphering immature subpopulations among normal B-cells. Propidium Iodide (PI) was used as the live/dead stain for the first 57 specimens. A typical example of gating the blasts is shown in Figure 3. Debris was first excluded with a SSC-A/FSC-A dot-plot. Subsequently doublets are excluded by plotting FSC-H against FSC-A, then live cells gated by negative staining of cells with the live-dead stain. In tube 2 gating of the blast cells is first with CD45 ^{dim}, then the 3 backbone markers CD34, CD10 and CD19, with at least one of these expected to be positive. Of note, patients with t(4;11) are known to stain brightly with CD45. A CD20 fluorescence-minus-one (FMO) tube was used to determine the gate for CD20 positive cells, providing a cut-off point between background fluorescence and the positive population. Isotype controls were also analysed to monitor for background staining and used to provide the cut-off if there was greater positivity than the FMO. Controls were run for every specimen.

Between March 2011 and February 2014, 57 fresh and frozen primary patient samples were prepared by members of the MRD laboratory, stained, acquired on BD LSR Fortessa at the Royal Free Hospital. Following the move of the laboratory to the Cancer Institute (UCL) flow cytometers with 4 lasers were readily available making it attractive to expand the panel to analyse more antigen markers. In 2016 the panel was re-designed to include antibodies to the native MV receptors, CD46, SLAM and Nectin 4 with fluorochromes BV605, BV421 and APC respectively. Live/Dead aqua was used to discriminate between live and dead cells, enabling the samples to be fixed prior to acquisition. The results of the MV receptors expression will be discussed in Chapter 4.

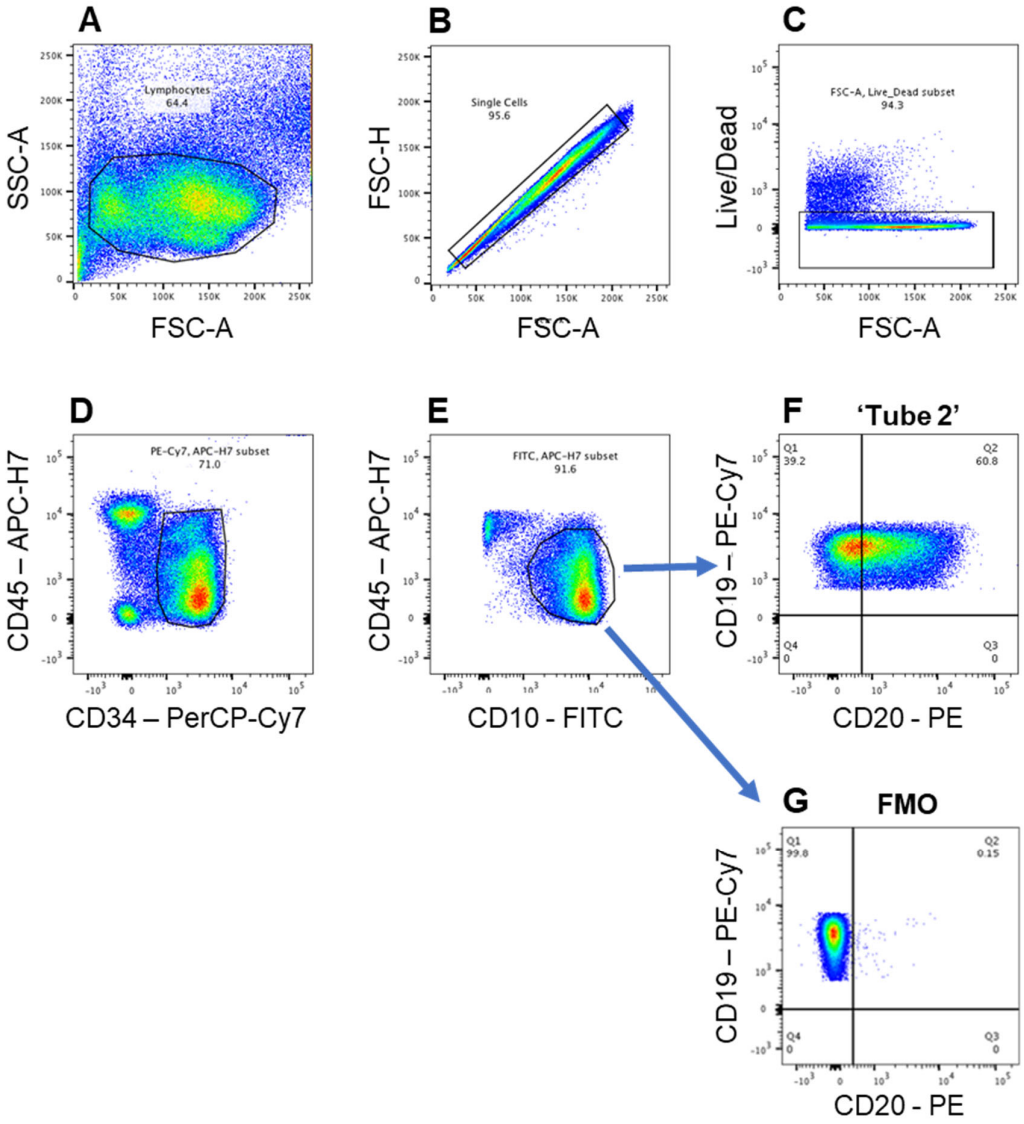

Figure 3-3 Flow cytometry gating strategy for determining CD20 percentage.
[A] *lymphocyte gate defined using forward scatter (x-axis) and side scatter (y-axis).*
[B] *Doublets excluded by FSC-H and FSC-A* ***[C]*** *Dead cells are excluded using PI (live/dead aqua post 2016).* ***[D]*** *CD45 dim (APC-H7) and CD34 (PerCP-Cy7) then* ***[E]*** *FITC* ***[F]*** *Tube 2 stained antibody conjugate to CD20. CD20 determined as 60.8% in this population.* ***[G]*** *FMO (fluorescence minus one) control used to determine CD20 positivity. Quantibrite beads are then used to determine antigen density (molecules per cell) of the CD20 positive population.*

3.5 Results

665 patients were enrolled in the B-cell lineage arm of the UKALL14 trial. Ten were later excluded due to revised diagnosis. Diagnostic bone marrow or peripheral blood specimens were received between December 2010 and July 2017. Where available, cells were extracted and stored in liquid nitrogen if there was sufficient spare diagnostic material. 255 individual patient specimens – 39% of total patients - had either fresh or stored cells available for flow cytometry and have been analysed. Figure 3-4 shows the numbers of patient samples analysed by flow cytometry at the time of writing this thesis.

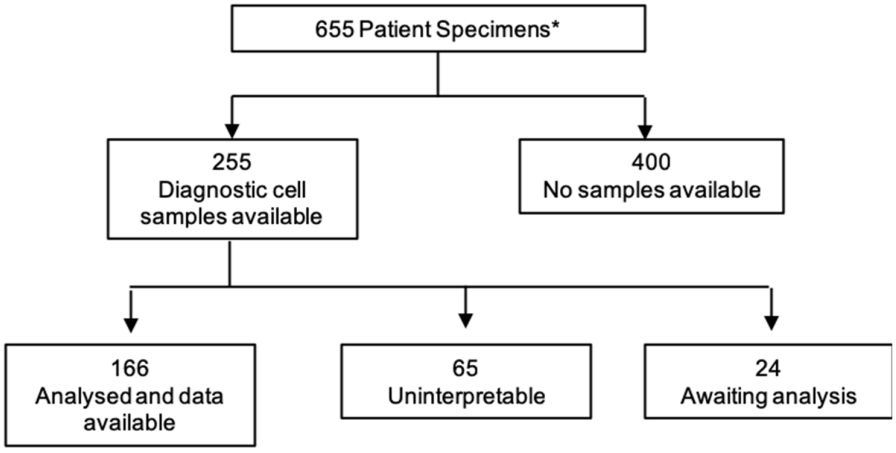

Figure 3-4 Samples from UKALL14 available for flow cytometry*. Chart indicates the number of specimens analysed by flow cytometry including those where the analysis failed and no cellular specimens were available.*

3.5.1 Baseline characteristics of patients analysed for CD20 expression by flow cytometry

Table 3-1 shows the baseline characteristics of patients who had successful flow cytometry compared to and all B-cell patients. There is a small but significant difference in age, with the 166 patients in the flow cytometry cohort having a younger median age at 43 years compared to 46 years for the non-flow cytometry cohort (p=0.017).

Table 3-1 Baseline characteristics of patients with CD20 data by flow cytometry compared to all BCP-ALL patients. *High risk: t(9;22), t(4;11), low hypodiploidy/near triploidy or complex cytogenetics. *patients with missing cytogenetics were assumed standard, **Chi-squared unless otherwise stated. ***Wilcoxon Mann Whitney test*

	Patients with flow data N=166	All B-cell UKALL14 Patients N=655	p-value** (patients with flow data vs those without)
Age			
Median (range) N (%)	43.0 (23 - 65)	46.0 (22 - 65)	0.017***
≤ 40 yr	73 (44.0)	233 (35.6)	0.009
> 40 yr	93 (56.0)	422 (64.4)	
White cell count (x10^9/L)			
Median (range)	25.9(1 - 557.23)	8.0(.11 - 889.6)	<0.001***
<30	89 (53.6)	485 (74.0)	<0.001
30-100	47 (28.3)	101 (15.4)	
≥100	30 (18.1)	69 (10.5)	
Sex			
Male	86 (51.8)	358 (54.7)	0.39
Female	80 (48.2)	297 (45.3)	
Cytogenetic features – N (%)			
BCR-ABL1			
Negative	102 (61.4)	457 (69.8)	0.007
Positive	64 (38.6)	198 (30.2)	
Complex			
Absent	135 (94.4)	488 (95.3)	0.55
Present	8 (5.6)	24 (4.7)	
Missing	23 (16.1)	143 (27.9)	
Low hypodipoidy/near triploidy			
Absent	137 (94.5)	474 (90.6)	0.061
Present	8 (5.5)	49 (9.4)	
Missing	21 (14.5)	132 (25.2)	
t(4;11)(q21;q23)			
Absent	138 (86.8)	567 (92.0)	0.004
Present	21 (13.2)	49 (8.0)	
Missing	7 (4.4)	39 (6.3)	
Risk group at randomisation			
Standard risk*	22 (13.3)	109 (16.6)	0.18
High risk	144 (86.7)	546 (83.4)	

There was a significant difference ($p<0.001$) in the white cell count at diagnosis between groups, where the mean (range) was 25.9 $x10^9$/L (1 – 557 $x10^9$/L) in the analysis group compared to 8 $x10^9$/L (0.11- 890 $x10^9$/L) of the whole B-cell ALL cohort. This could be an unintended consequence of samples with a high white cell count having a greater likelihood of providing a greater quantity of diagnostic material, and thus more likely to have available cells for flow cytometry compared to samples where the white cell count was low. There was also a significant difference ($p=0.007$) in the number of patients who with *BCR-ABL1* positive ALL where 38.6% of patient samples in the tested cohort harboured the translocation, compared to 30.2% of those in the whole group. This could be due to the bias for high white cell counts as patients who are *BCR-ABL1* positive are more likely to have a high white cell count at diagnosis [200]. Older patients are also more likely to have *BCR-ABL1* positive ALL. ALL with the t(4;11) have also been associated with a high presenting white cell count [8]. Overall, these differences did not result in a difference in the risk group at randomisation ($p=0.18$), the high risk group being determined by age ≥ 41 years, white cell count ≥30$x10^9$/L, *BCR-ABL1*, t(4;11), low hypodiploidy/near triploidy or complex cytogenetics.

3.5.2 Distribution of CD20 expression across patient samples in UKALL14

The distribution of CD20 data were investigated across the patient cohort and is illustrated as a histogram (Figure 3-5).

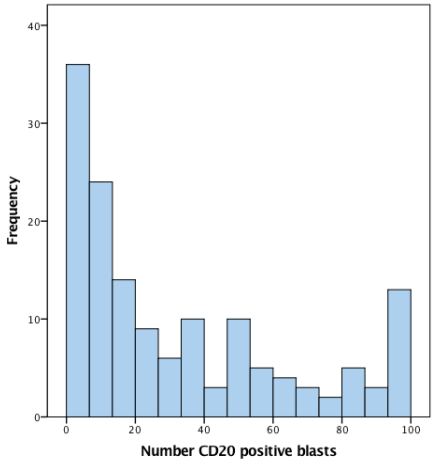

Figure 3-5 CD20 percentage positive blasts in UKALL14 specimens *[A] Histogram of CD20 expression levels by % cells positive for 147 patients in the UKALL14 B-cell population.*

The percentage of leukaemic blasts positive in each patient is seen to vary across the cohort and shows that approximately 50% patients fall into the traditional 'positive' range where the cut-off is 20% of cells with CD20 expression. This is on the higher side of published reports where means range from 32% to 62% (See table 1-2 in Chapter 1). The data also show that CD20 expression is variable across ALL blast populations and given that the 20% cut-off, although universally used in diagnostic flow cytometry, is arbitrary, we are also interested in those below the 'positive' cut-off. In the specimens from UKALL14 where cells could be analysed for flow cytometry, 66% have ≥ 10% cells that express CD20.

3.5.3 CD20 antigen density increases with the proportion of CD20 positive blasts.

An important aim of this project was to investigate the CD20 antigen density of BCP-ALL cells. Figure 3-6 illustrates the CD20 antigen density across the UKALL14 patient samples. The relationship between the antigen density (Molecules per cell, MPC) and the percentage of blasts expressing CD20 was explored. As there appeared to be an exponential relationship between the antigen density and percentage of blasts expressing CD20, a logarithmic transformation was carried out. Following logarithmic transformation of the data a positive correlation can be seen however this is a weak correlation with a R^2 of 0.424. As it is not clear that either measure is a 'better' representation of CD20 expression it seemed reasonable to include both measures within the analysis. Therefore, in order to get a measure of the overall CD20 antigen expression within the blast population, the antigen density was multiplied by the percentage of blasts expressing CD20.

3.5.4 Higher CD20 expression is associated with inferior outcomes in UKALL14

In order to determine the relationship between CD20 expression and clinical outcome (Event free survival (EFS) and overall survival (OS)), Kaplan-Meier survival analysis and cox regression analysis were carried out. Event free survival was measured from the date of randomisation until the date of death or relapse. Patients who were alive and had not relapsed were censored at the date last seen. Overall survival was measured from the date of randomisation until the date of death, with survivors censored at the date last seen. Within the flow cytometry cohort (N=166) the median follow up was 35.9 months. There had been 93 EFS events and 76 deaths giving a 3 year EFS of 38.2 (30.0 to 46.7) and an OS of 48.7% (39.7 to 57.2).

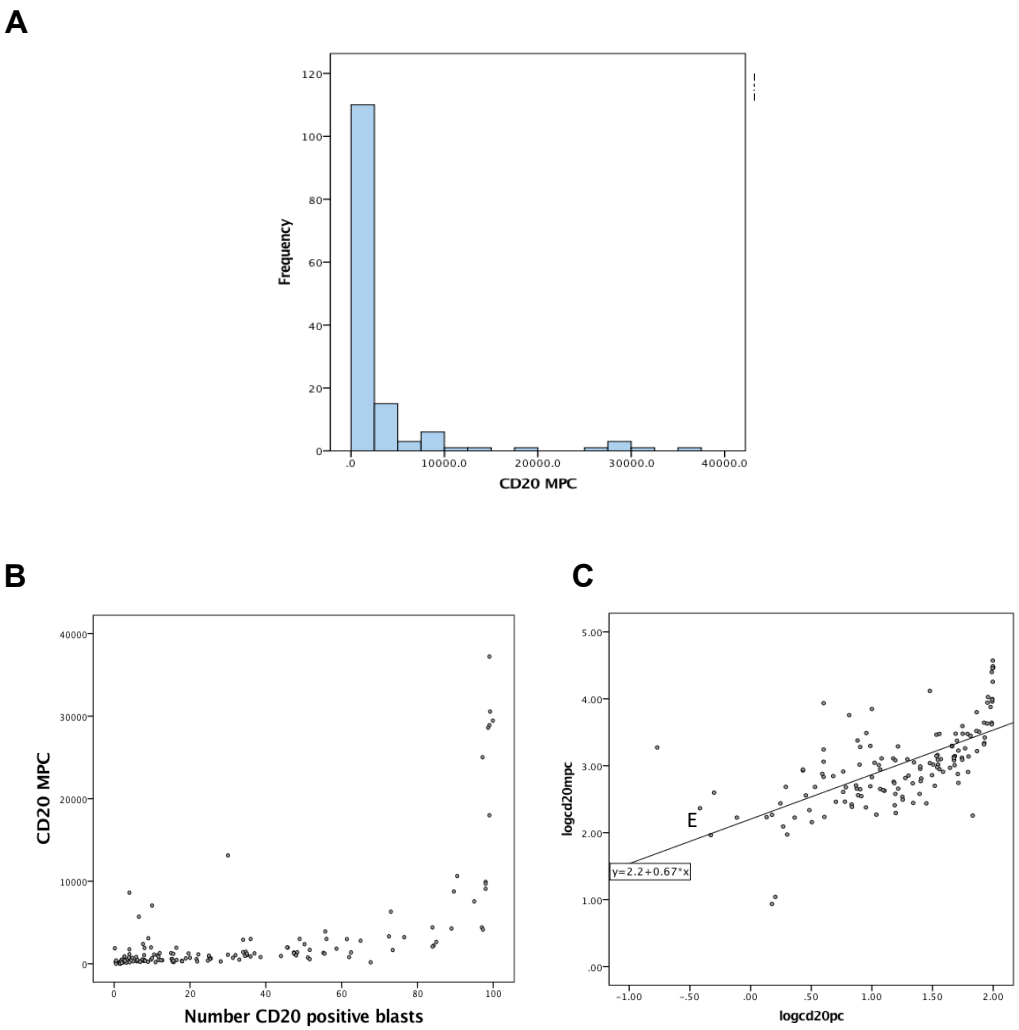

Figure 3-6 Antigen Density of CD20 on B-ALL blasts. *[A] Histogram of CD20 antigen density in UKALL14 specimens. [B] Scattergram of CD20 antigen density (molecules per cell) compared to %CD20 positive blasts. Each point represents an individual patient specimen. [C] Scattergram of logarithmic transformation of data represented in graph D.*
R^2 (coefficient of determination) =0.424.

3.5.5 Event Free Survival and CD20

The percentage of CD20 positive blasts was significantly associated with inferior event free survival (EFS) with a hazard ratio (HR) of 1.21 for the log (%CD20+ blasts) with a 95% Confidence Interval [CI] of 1.04-1.42 [p=0.017].

The data were analysed using 3 different ways of splitting the groups by CD20% (Figure 3-7). First, the traditional 20% CD20 cut-off was used to determine the groups, second, 3 equal sub-groups were taken (tertiles), and third a 10% CD20 cut-off was used. The final grouping was a pragmatic approach as the significance of the lower, <10% CD20 expression on outcome has rarely been evaluated. For the traditional 20% cut off there was a tendency for patients with a greater than 20% blast percentage to have a shorter EFS however this did not reach significance (p=0.086). For patients with <20% CD20 the 3 year survival rates were 45.2% (33.3-56.4) compared to 31.4% (20.2-43.2) for those with CD20 ≥20%. This gave a hazard ratio 1.43 and CI (0.95 – 2.15). When the group was ranked by percentage CD20 positive blasts and then split into 3 equal sub-groups (tertiles), a significant difference is seen between the groups (p=0.037) and the two tertiles with the higher CD20 expression (medium and high) have similar Kaplan-Meier curves with the lowest CD20 expressing group having a reduced risk of relapse. As the lowest tertile was approaching a CD20 level of 10% this led to analysing the group into three sub-groups <10%, 10-20% and ≥20%. This produced similar results to the tertile groups (p=0.038).

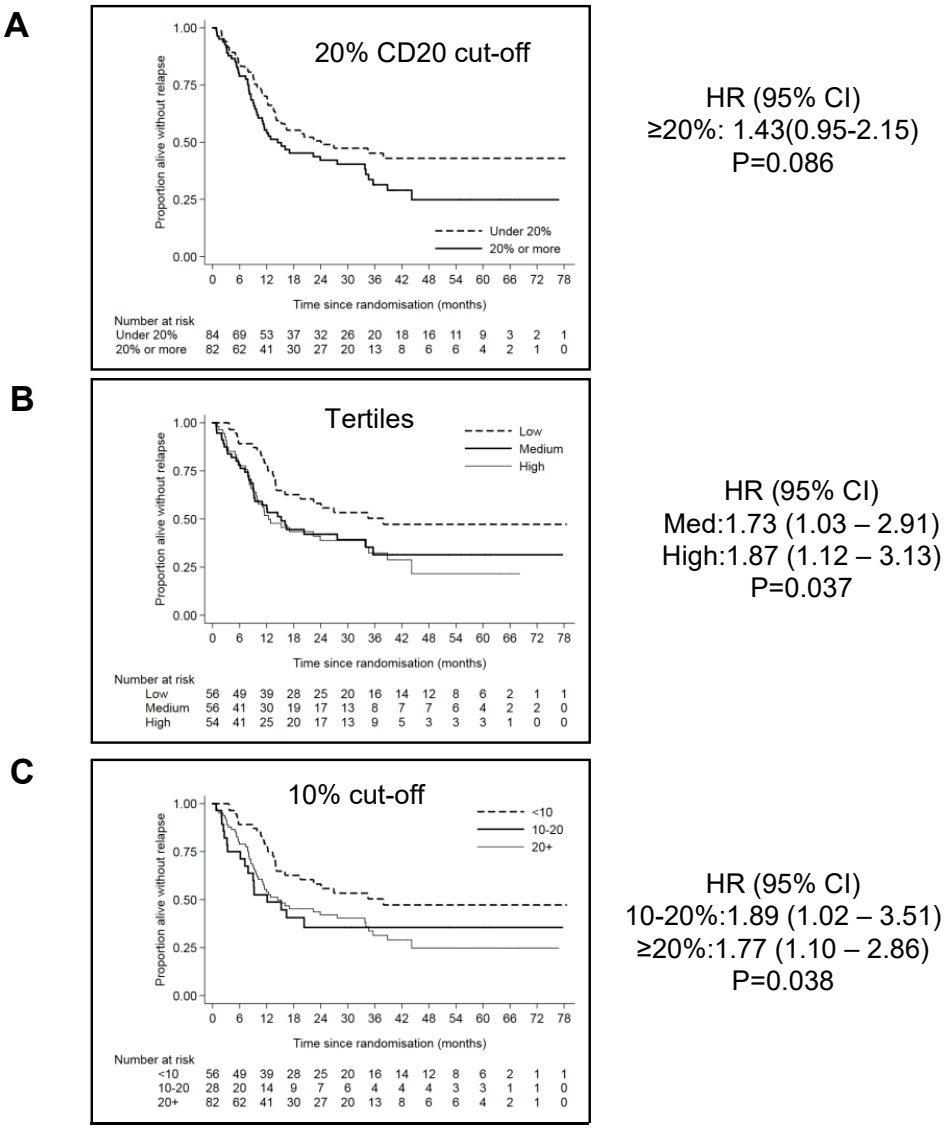

Figure 3-7 Percentage of CD20 positive blasts is significantly associated with inferior event free survival. *Panel A shows the rate of event-free survival over time using the traditional 20% cut-off for a CD20 positive blast population. Panel B shows the rate of EFS over time dividing the cohort into 3 equal groups. Panel C shows the rate of event-free survival over time considering a 10-20% group.*

3.5.6 Overall survival and CD20

The percentage of CD20 positive blasts is also significantly associated with inferior overall survival (figure 3-8). Overall, the logarithmically transformed percent CD20 positive blasts gave a hazard ratio 1.24 with confidence interval (1.04 – 1.47) that was statistically significant p=0.018. As with the event free survival, the three different groupings were used. There was no significant difference in survival when the 20% CD20 cut-off was taken to divide groups, with only a relatively small increase in risk seen (HR 1.23 (0.78 to 1.93) p=0.018) but there was a significant advantage for having low CD20% when groups were divided into tertiles (medium group HR 1.98 (1.11-3.53); high group HR 1.82 (1.02-3.27), p=0.046) or when using the 10% cut-off (10-20% HR 2.51 (1.30-4.84); ≥20% HR 1.72 (1.00-2.97) p=0.017).

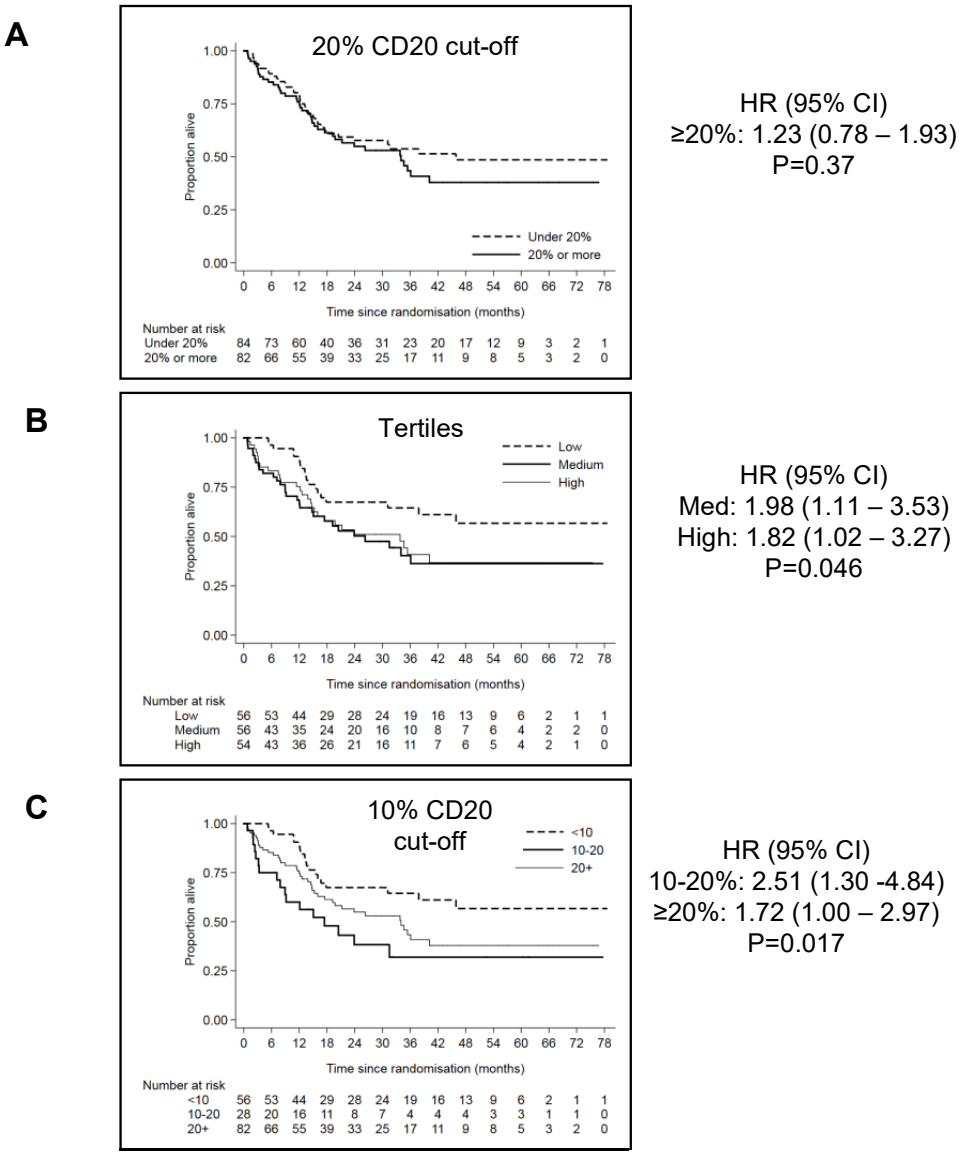

Figure 3-8 Percentage of CD20 positive blasts is significantly associated with inferior overall survival. *Panel A shows the rate of overall survival over time using the traditional 20% cut-off for a CD20 positive blast population. Panel B shows the rate of overall survival over time dividing the cohort into 3 equal groups. Panel C shows the rate of overall survival over time considering the 10-20% group. Median follow up 35.9 months.*

3.5.7 Increasing CD20 antigen density negatively impacts survival

CD20 antigen density multiplied by %CD20 positive blasts was measured to investigate whether this would provide a 'better' means of assessing CD20 cell expression. 162 patients were assessable (4 were missing antigen density data). Again, analysed on the log scale, the HR for event free survival was 1.13 (1.04 – 1.23) p=0.004 (EFS 39% (39.9-47.4)) and the overall survival showed similar results with a HR 1.15 (1.05 – 1.26), p=0.004. The event free survival (figure 3-7) appeared to give a superior separation of the Kaplan-Meier curves compared to percentage CD20 positive blasts (figure 3-8) when the group is divided into tertiles. For the low CD20 group the 3-year EFS was 54.8% (39.5 – 67.7), the medium CD20 group 30.0% (15.1 – 46.6), and the high CD20 group 29.7% (17.2 – 43.3). Compared to the low CD20 group, the HR (CI) for the medium CD20 group was 1.74 (1.00 – 3.00), and for the high CD20 group 2.13 (1.26 – 3.59) (p=0.014). Similarly, for overall survival, when compared to the low CD20 group, the HR (CI) for the medium CD20 group was 2.00 (1.08 – 3.71) and for the high CD20 group was 2.13 (1.17 – 3.88). The low CD20 group had a 3 year overall survival of 70.0% (55.2 – 80.8) compared to the medium group at 39.5% (22.9 – 55.7) and the high CD20 group at 37.9% (23.4 – 52.4).

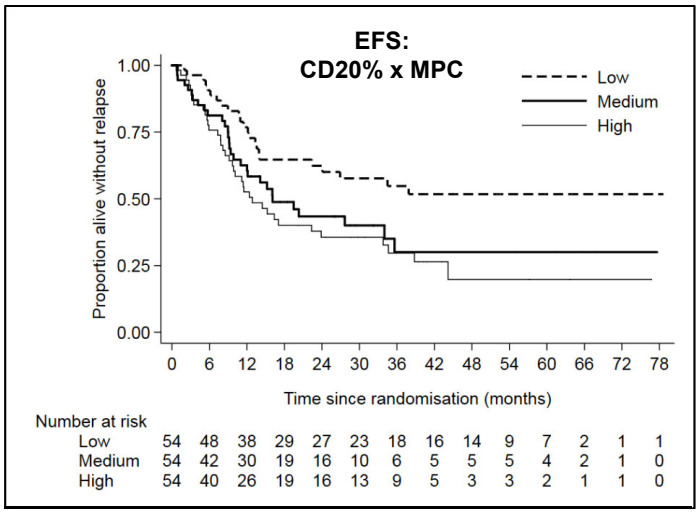

HR (95% CI)
Med:1.74 (1.00 – 3.00)
High: 2.13 (1.26 – 3.59)
P=0.014

Figure 3-9 Percentage of CD20 positive blasts multiplied by CD20 antigen density (MPC) is significantly associated with inferior event free survival.

3.5.8 CD20 expression does not affect outcome in UKALL14 patients with *BCR-ABL1*

Previous studies, such as the GRAALL group, examining the prognostic implications of CD20 expression have been confined to *BCR-ABL1* negative patients, therefore it was important to examine *BCR-ABL1* positive and negative groups. Interestingly, as shown in figure 3-10 and 3-11, CD20 positivity only confers a poorer prognosis in patients who are *BCR-ABL1* negative. This had not been identified in previous published studies. Many clinical trial groups, including GRAALL, treat patients with *BCR-ABL1* positive ALL in separate clinical trials. Figure 3-10 uses the CD20% data, and Figure 3-11 uses this combined with the antigen density data. There is a particularly striking separation between the low CD20%xMPC group and the medium and high group for the *BCR-ABL1* negative patients.

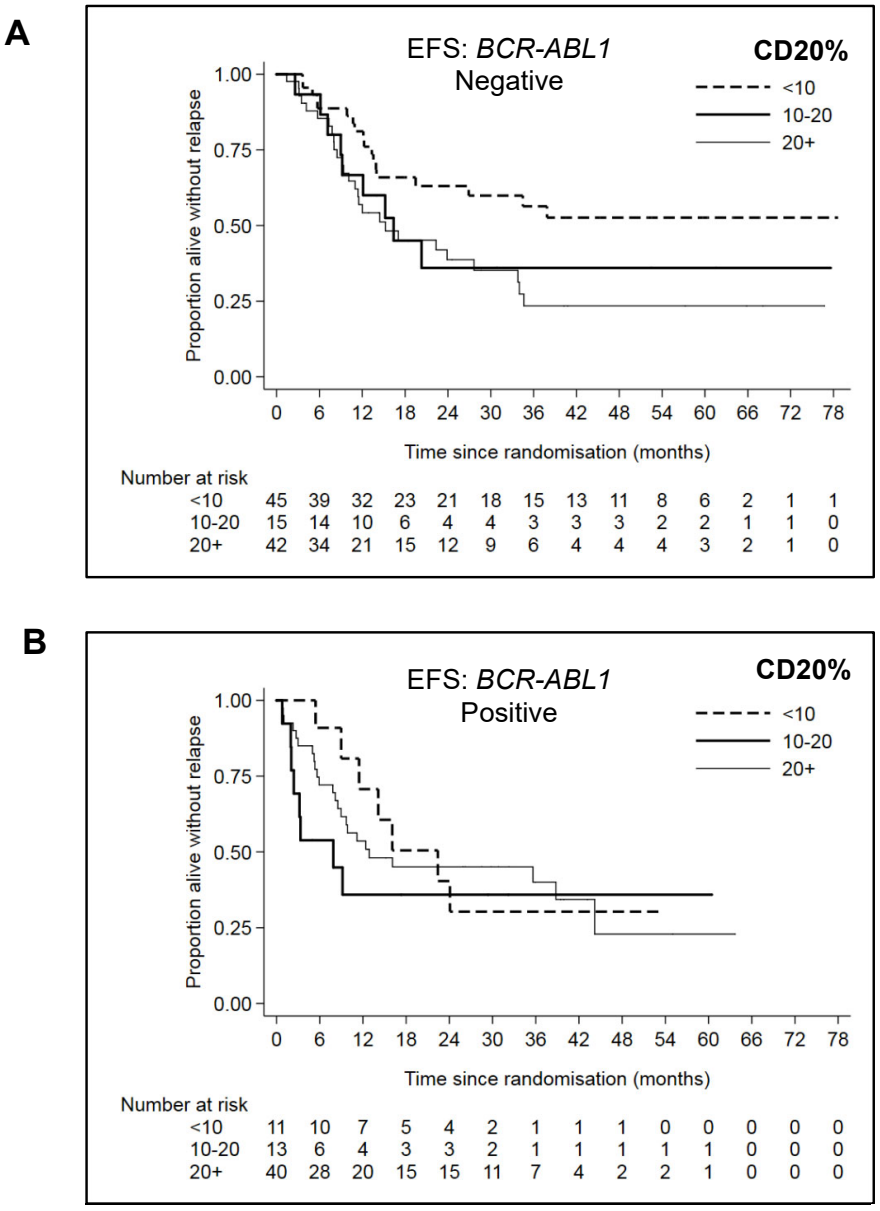

Figure 3-10 Clinical Outcomes in BCR-ABL1 positive and negative groups. *Panel A shows the rate of event-free survival over time in the BCR-ABL1 negative patients. Panel B shows the rate of event-free survival over time in the BCR-ABL1 positive patients.*

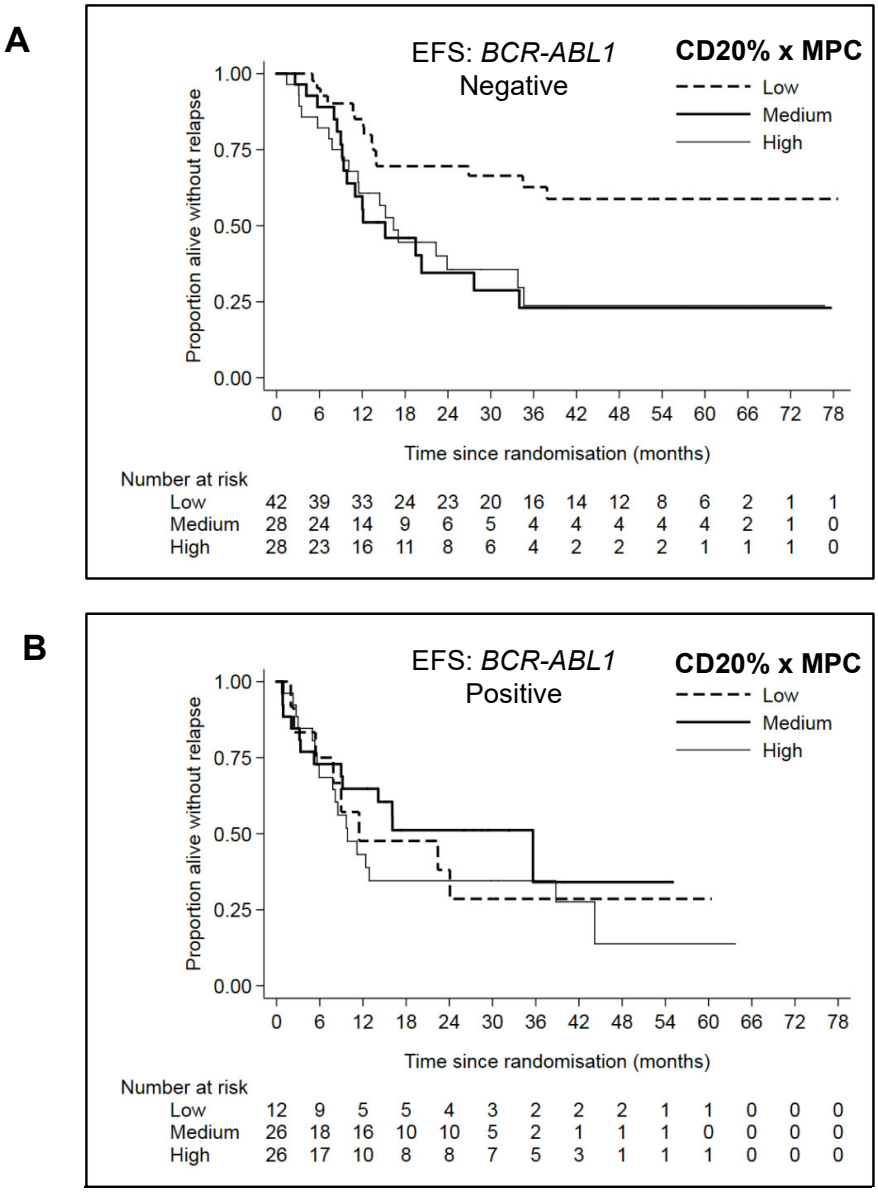

Figure 3-11 Clinical Outcomes in BCR-ABL1 positive and negative groups including CD20 antigen density. *Panel A shows the rate of event-free survival over time in the BCR-ABL1 negative patients. Panel B shows the rate of event-free survival over time in the BCR-ABL1 positive patients.*

3.5.9 Multivariable analysis

The multivariable analysis (table 3-2) indicates that CD20 measured by both flow cytometry methods is an independent risk factor. This is important analysis as the initial baseline characteristics indicated a unintentional bias in the tested samples for age, white cell count, *BCR-ABL1* status and t(4;11), however taking these into account the CD20 remains significant – with the largest effect seen in the *BCR-ABL1* negative patients. 'Post amendment' patients are included as a separate group because prior to the protocol amendment in April 2012, patients who were *BCR-ABL1* positive did badly due to unexpected toxic effects from the combination of pegylated asparaginase, tyrosine kinase inhibitor and intensive chemotherapy [201]. The protocol was modified accordingly for *BCR-ABL1* patients. As this is related to *BCR-ABL1* status, and the risk from CD20 expression appears to be confined to the *BCR-ABL1* negative group, it was important to include this analysis. Taking these changes to protocol into account, increased CD20 expression remains a significant adverse independent risk factor.

Table 3-2 Multivariable analysis of Event Free Survival

	Univariable (complete cases)***		All patients		Post amendment only		*BCR-ABL1* Negative Patients	
	Events/ N	HR (95%CI) p-value	%CD20+ blasts HR(95%CI) p-value	%CD20+ blasts x MPC HR(95%CI) p-value	%CD20+ blasts HR(95%CI) p-value	%CD20+ blasts x MPC HR(95%CI) p-value	%CD20+ blasts HR(95%CI) p-value	%CD20+ blasts x MPC HR(95%CI) p-value
CD20 factor*								
	-	-	1.21 (1.01 – 1.46) p=0.042	1.11 (1.01 – 1.23) p=0.028	1.29 (1.05 – 1.60) p=0.017	1.15 (1.03 – 1.28) p=0.010	1.37 (1.07 – 1.76) p=0.014	1.22 (1.08– 1.38) p=0.002
Age (for an increase of 10 years)								
	90/161	1.41** (1.15 – 1.71) p=0.001	1.35 (1.11 – 1.66) p=0.003	1.37 (1.11 – 1.68) p=0.003	1.39 (1.11 – 1.72) p=0.003	1.42 (1.13 – 1.77) p=0.002	1.31 (1.03 – 1.68) p=0.029	1.33 (1.03– 1.72) p=0.029
Baseline WBC (for an increase of 30 x10^9/L)								
	90/161	1.03 (0.97 – 1.09) p=0.69	1.03 (0.95 – 1.11) p=0.54	1.03 (0.94 – 1.12) p=0.54	1.01 (0.92 – 1.10) p=0.84	1.01 (0.92 – 1.11) p=0.82	0.98 (0.88 – 1.09) p=0.68	0.97 (0.85– 1.10) p=0.61
Cytogenetic Features								
None	16/46	1.00	1.00	1.00	1.00	1.00	-	-
BCR-ABL1	39/64	2.32 (1.29 – 4.15) p=0.005	1.74 (0.97 – 3.13) p=0.062	1.82 (1.00 – 3.33) p=0.048	1.49 (0.80 – 2.79) p=0.21	1.56 (0.82 – 2.97) p=0.18	- -	- -
t(4;11)	12/18	2.26 (1.07 – 4.78) p=0.033	2.52 (0.98 – 6.48) p=0.056	2.12 (0.79 – 5.70) p=0.14	3.12 (1.06 -9.16) p=0.038	2.54 (0.82 – 7.87) p=0.11	4.14 (1.47– 11.57) p=0.007	3.70 (1.28 -10.7) p=0.016
Low hypodiploidy/ near triploidy	6/8	2.48 (0.97 – 6.36) p=0.058	2.04 (0.80 – 5.23) p=0.14	2.14 (0.83 – 5.51) p=0.12	1.97 (0.76 – 5.11) p=0.17	2.00 (0.76 – 5.29) p=0.16	1.96 (0.76 – 5.02) p=0.16	2.06 (0.80– 5.34) p=0.14
Complex	8/8	4.74 (2.01 – 11.22) p<0.001	4.70 (2.00– 11.04) p<0.001	5.02 (2.12– 11.88) p<0.001	5.38 (2.16 – 13.40) p<0.001	5.98 (2.37 – 15.10) p<0.001	5.12 (2.14– 12.24) p<0.001	5.98 (2.45– 14.6) p<0.001

***only patients with non-missing data for all variables are included

3.5.10 Including antigen density improves CD20 as a prognostic biomarker

In order to determine whether including the CD20 antigen density helps to determine patients who are at greater risk, the two methods were compared. Cox regression analysis of event free survival showed a significant effect of CD20 using either method. Harrell C statistic has been used to compare the predictive power of biomarkers or risk score systems[202-204]. A Harrell C score of 0.5 is no better than random chance. Our methods have a marginally better Harrell C of 0.5967 when the antigen density is included compared to 0.5892 for % CD20 positive blasts alone. A similar result is seen when testing the models by receiver operator curve (ROC) analysis where the true positive rate (sensitivity) is plotted as a function of the false positive rate (specificity). The area under this curve (AUC) then gives a measure of how well a parameter can distinguish between the groups. As for Harrell C, an AUC of 0.5 indicates no difference. Figure 3-12 shows ROC curves for both methods. The top two curves are for the entire cohort with flow cytometry data (n=161), the bottom two curves only include patients who are *BCR-ABL1* negative (n=97). In Figure 3-12A and 3-12B we see that including the CD20 antigen density improves the ROC AUC from 0.5943 to 0.6329 but the value is still low, and is illustrated by the curves which do not extend far beyond the diagonal. A ROC AUC of between 0.6 to 0.7 would be considered poor as a discriminatory test. When we exclude patients with *BCR-ABL1* the curves are closer to the ideal curve for a discriminatory test (Figure 3-12C & 3-12D) with AUC 0.6628 using CD20% data only, and AUC 0.7213 when antigen density is included.

The value at which the sensitivity and specificity are optimal can be statistically derived by the Youden index and is called 'Youden's cut off'[205]. For these data Youden's cut off was 11.6% for CD20 positive blasts and a value of 124 for the model including CD20 antigen density. For *BCR-ABL1* negative patients the cut-off is similar at 11.6% for CD20 positive blasts and 69.96 for the model including CD20 antigen density. This is also a similar value for the cut-off of the lower tertile which showed a large difference in event free survival Kaplan-Meier curves (see Figure 3-7).

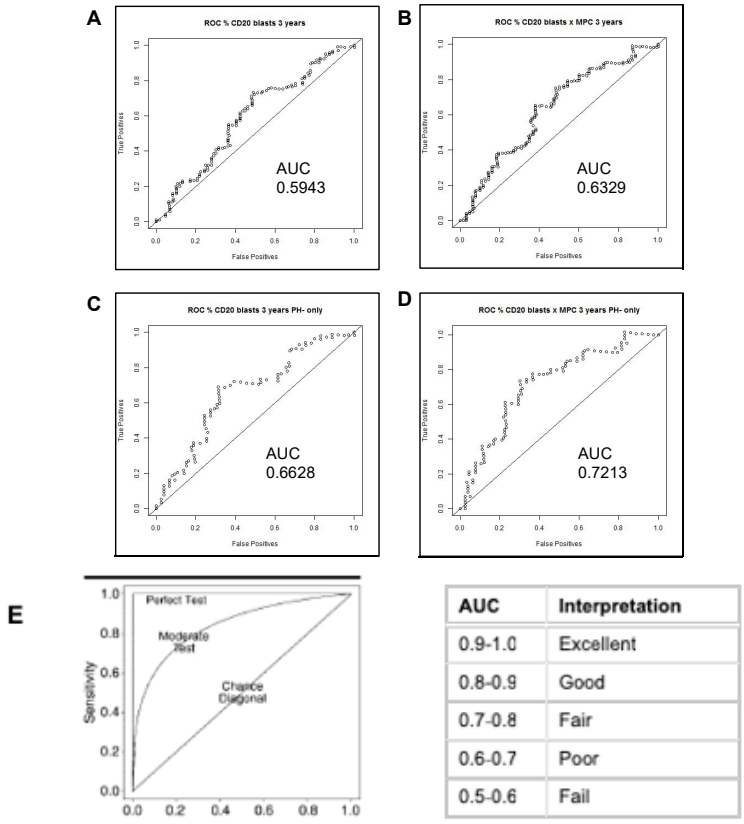

AUC	Interpretation
0.9-1.0	Excellent
0.8-0.9	Good
0.7-0.8	Fair
0.6-0.7	Poor
0.5-0.6	Fail

Figure 3-12 Comparing flow methods: ROC analysis. *Graph [A] shows receiver operator curve (ROC) for %CD20 positive blasts. Graph [B] shows ROC for %CD20 positive blasts multiplied by antigen density (molecules per cell); Graph [C] BCR-ABL1 negative specimens ROC for %CD20 positive blasts; Graph [D] BCR-ABL1 negative specimens shows ROC for %CD20 positive blasts multiplied by antigen density (molecules per cell); Graph [E] shows theoretical curves to illustrate a perfect test, a moderate test and one determined by chance.*

Figure 3-13 (following page) shows Kaplan-Meier EFS dividing the groups using Youden's cut-off. Here we see excellent separation of the curves when this cut-off is used. For the % blasts the cut-off was 11.6% with cox regression hazard ratio 2.18 with a 95% confidence interval (1.36-3.48) p=0.001, The 3 year Kaplan-Meier rate using this cut off was 54.1% (39.1 – 66.9) for the low group and 30.05% (20.0 – 40.6) for the high group. For the %CD20 positive blasts multiplied by antigen density, the hazard ratio was 1.92 (1.25 – 2.96),p=0.003, with Kaplan-Meier rate of 51.3% (38.3 – 62.8) for the low group and 27.2% (16.5 – 39.0) for the high group.

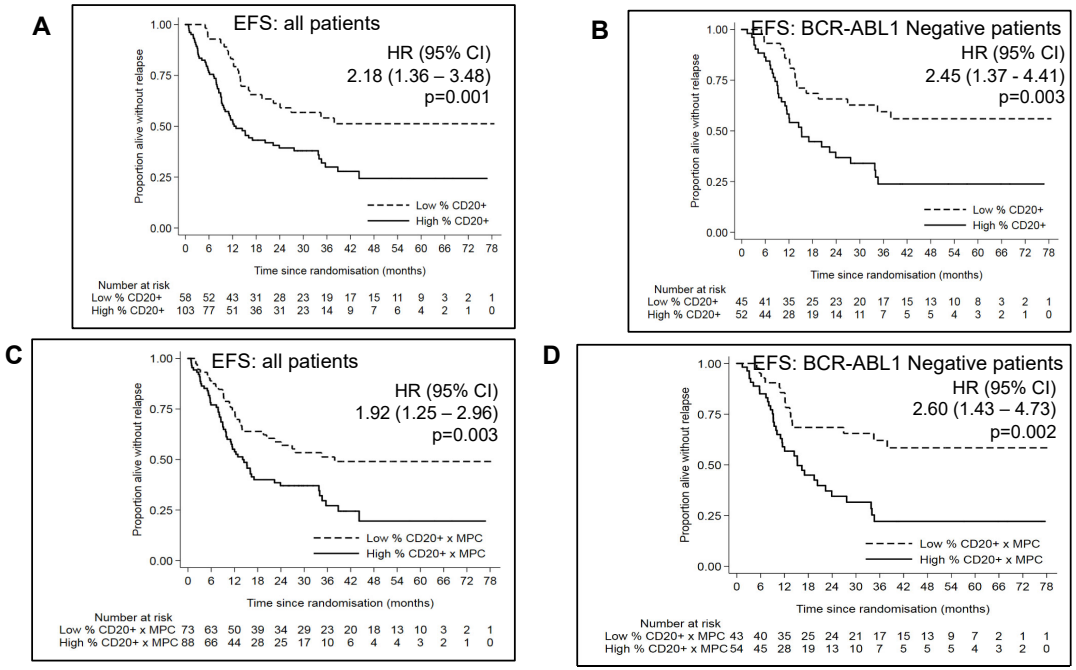

Figure 3-13 ***Clinical outcome when Youden's cut-off is used to determine CD20 positive groups.*** ***Panel A*** *shows the rate of event-free survival (EFS) over time using Youden's cut off for %CD20 positive blasts* ***Panel B*** *shows EFS for BCR-ABL1 negative patients using Youden's cut off for %CD20 positive blasts.* ***Panel C*** *shows the rate of EFS over time using Youden's cut off for %CD20 positive blasts multiplied by molecules per cell* ***Panel D*** *shows EFS for BCR-ABL1 negative patients using Youden's cut off for %CD20 positive blasts multiplied by molecules per cell*

In summary, CD20 appears to be a prognostic biomarker with higher expression of CD20 conferring a worse prognosis in *BCR-ABL1* negative adult ALL. Rather than using the traditional 20% for CD20 positivity, ideally 11.6% would be a better measure. Measuring antigen density appears to add greater discrimination to the measure, detecting a group with more than double the risk of an event, however the low specificity and sensitivity are not ideal for a prognostic biomarker (Figure 3-12 B and D).

3.5.11 CD20 expression together with cytogenetic risk factor can identify very good and very poor risk patients.

Having determined that CD20 shows promise as an independent prognostic biomarker in ALL, it is important to understand how this can be incorporated with the current cytogenetic risk groups i.e. to detect patients who would not otherwise be considered high risk. Kaplan-Meier curves of event free survival measured for groups of high or low CD20 (based on Youden cut offs) combined with high or standard cytogenetic risk groups (Figure 3-14) show that CD20 expression helps to identify those patients that are particularly high risk (High risk/high CD20) and very low risk (standard risk/low CD20). Using antigen density (MPC) instead of CD20% alone, results in 3 more patients in the lowest risk group and 10 fewer in the highest risk group than the method measuring CD20% alone. If high CD20 were added as a risk factor at baseline 11 extra patients out of 166 (using %CD20 blasts) or 7 extra patients out of 161 (using %CD20 blasts x MPC) would be added to the high risk group. High risk is determined by age > 40 years, cytogenetics (t(4;11), low hypodiploidy/near triploidy, complex karyotype or BCR-ABL1) or white cell count $\geq 30 \times 10^9$/L.

A

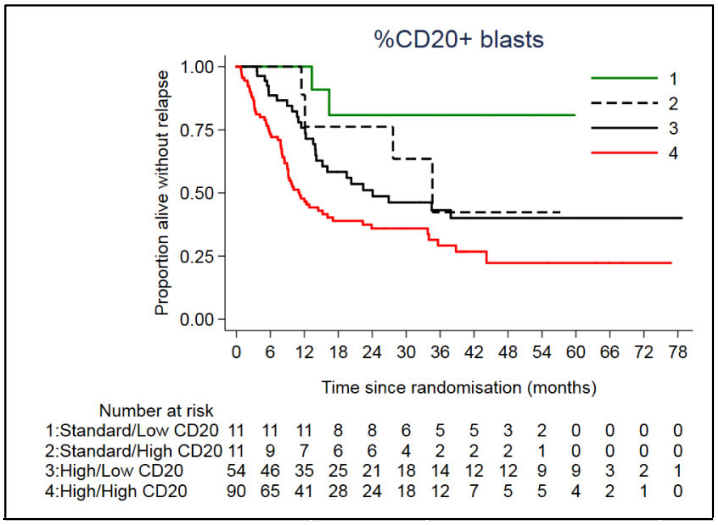

	Events/n	%CD20+ blasts HR(95%CI)	p-value
1 Standard risk/Low CD20	3/11	0.56 (0.36 – 0.89)	0.0011
2 Standard risk/High CD20	3/7	0.40 (0.14 – 1.09)	
3 High risk/Low CD20	31/60	0.15 (0.04 – 0.60)	
4 High risk/High CD20	53/80	1.00	

B

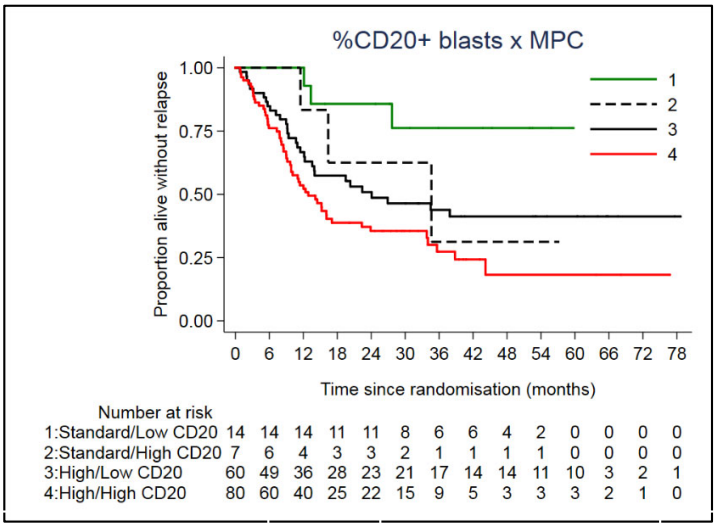

	Events/n	%CD20+ blasts x MPC HR(95%CI)	p-value
1 Standard risk/Low CD20	3/14	0.63 (0.40 – 0.99)	0.0040
2 Standard risk/High CD20	3/7	0.49 (0.15 – 1.58)	
3 High risk/Low CD20	29/57	0.18 (0.06 – 0.58)	
4 High risk/High CD20	55/84	1.00	

Figure 3-14 Clinical Outcomes in for CD20 and standard/high risk groups. Panel A *shows the rate of event-free survival over time with CD20 measured by %CD20 positive blasts.* ***Panel B*** *shows the rate of event-free survival over time with CD20 measured as %CD20 blasts multiplied by antigen density (MPC)*

3.5.12 Developing a molecular method to determine CD20 expression

Limitations of using flow cytometry to determine CD20 quantity include standardisation and timing as ideally the samples should be fresh. An alternate method to assess CD20 expression using molecular methods would enable a greater number of samples to be analysed. It could potentially enable the whole burden of CD20 expression (i.e. antigens per cell and proportion of cells) to be considered in a single, simple method.

3.5.13 GeNorm analysis enables the identification of stable reference genes.

Identifying suitable reference genes is critical to a successful RT-qPCR assay. This can be achieved using GeNorm analysis. The use of reference genes to normalise RT-qPCR is a method that has the benefit of controlling for variation in cDNA quality between samples as the reference genes can act as an internal control. However, reference genes can also vary in their expression between samples. Vandsompele *et al* estimated that reference gene expression can vary by three times in 25% of samples and by six times in 10% of samples. Using mathematical algorithms on RT-qPCR Ct values for representative samples, geNorm analysis enables the ranking of candidate reference genes according to their stability. The analysis software, qBase+ also recommends an optimal number of reference genes for the sample type and provides an assessment of the overall stability of those genes [206].

As recommended by the manufacturer, 14 primary BCP-ALL samples were selected to be run against 12 provided reference genes. It was important that the specimens are as similar to those that will be tested in the assay therefore sequential samples from the UKALL-14 trial, where cDNA was available, were chosen. The reference genes had been pre-selected and provided by Primerdesign Ltd. These were run as per manufacturer's instructions (see methods chapter) and analysed using qBase+ (biogazelle) software. The qBase+ software identifies the most stable reference genes – those genes that vary least between patient specimens – and recommends an adequate number of genes to use. By measuring pairwise variation (V) it determines a candidate reference genes stability (M) compared to all the other reference genes. Figure 15A shows ranking of the candidate genes according to their stability, with the most unstable genes at the left and the most stable to the right. Figure 15B shows a bar chart for determining the optimum number of reference genes.

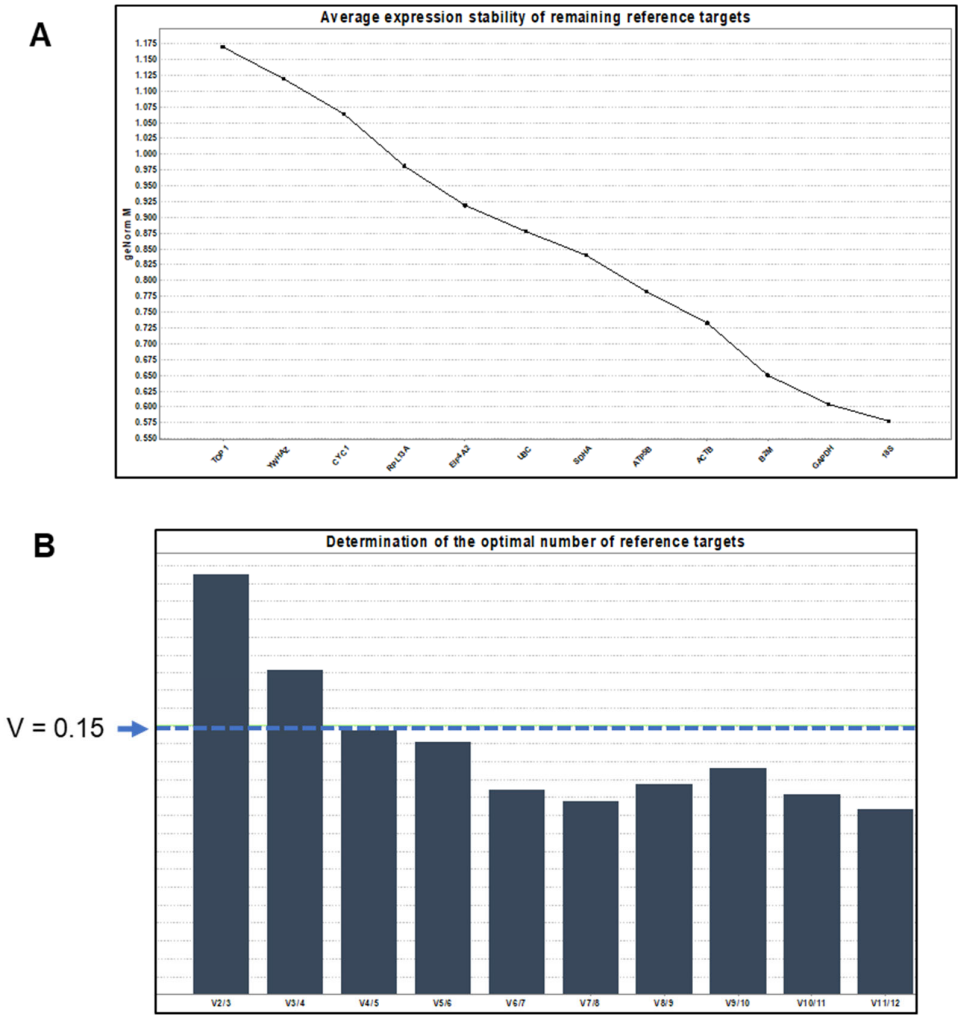

Figure 3-15 ***geNorm analysis to identify the most stable reference genes and the optimum number of reference genes.*** *RT-qPCR was run for a panel of 12 reference targets in 15 UKALL14 patient specimens. Target stability across samples was calculated using qbase+ software. Panel* ***[A]*** *shows the stability of the 12 reference targets. Panel* ***[B]*** *shows the determination of the optimal number of reference targets where geNorm V <0.15 when comparing a normalization factor based on the 4 or 5 most stable targets. GeNorm analysis recommended using 4 reference genes ACTB, B2M, GAPDH and 18S*

The manufacturers recommended that the benefit of adding an extra reference gene is limited as soon as the $V_{n/n+1}$ value drops below a 0.15 threshold. For the UKALL14 specimens, the qBase+ GeNorm analysis recommended using 4 reference genes ACTB, B2M, GAPDH and 18S. Published primer sequences were available for the 3 most stable reference genes, ACTB, B2M, and GAPDH so these were used for a pilot study.

3.5.14 Avoiding increased CD20 expression from normal B-cells – Can CD20 splice variants help exclude normal B-cells?

When the specimens are prepared for molecular analysis in the UKALL14 trial, mononuclear cells are extracted by Ficoll. As diagnostic specimens, it is likely that the majority of cells will be leukaemic blasts but a potential concern was contamination with residual normal mature B-cells or normal B-cell precursors that express CD20. This is not a problem with flow cytometry where specific markers enable the leukaemia cells to be identified and selected for further analysis. Being unable to distinguish blasts from normal cells in the molecular analysis is more likely to be problematic in peripheral blood specimens compared to bone marrow as there are more likely to be normal B-cells present. An alternatively spliced CD20 variant was first reported in 2010 and was expressed in leukaemic B-cells and EBV-transformed cells but not in normal B-cells from healthy donors [207]. The resulting 130 amino acid, truncated protein was thought to be involved in rituximab resistance. More recently, Gamonet *et al* investigated 4 further CD20 splice variants in B cell malignancies and found an association with oncogenesis see Figure 16 [208]. The presence of a CD20 splice variant might distinguish malignant versus benign cellular CD20 expression. If it were possible to quantify this it might act as a means of calculating the proportion of CD20 expression arising from ALL cells to exclude normal cells. The distribution of splice variants in ALL is unknown.

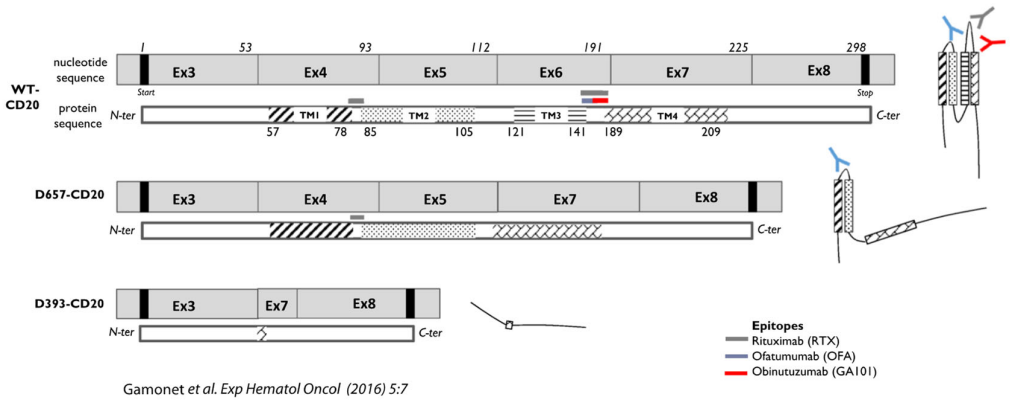

Figure 3-16 ***Schematic representation of CD20 variant coding transcripts****. Transmembrane domains, TM, are positioned on the linear N-ter/C-ter protein. Position of main clinical anti-CD20 antibody eptiopes are indicated. Adapted from Gamonet et al. Exp Hematol Oncol (2016)[208]*

In preliminary experiments using 48 patient samples, Primers and probes from this previously published work for the variants D657-CD20, D393-CD20 were used alongside wt-CD20 and the set of 3 reference genes determined by geNorm analysis. The results were analysed using qBase+ software. Figure 17 shows that the expression of the splice variants was proportional to the expression of the wt-CD20, The D393-CD20 splice variant showed a strong correlation to wt-CD20 with an $r=0.788$ $p<0.001$, and the newly described D657-CD20 splice variant with an $r=0.921$ $p<0.001$. Suggesting that the splice variants were being expressed at a similar level to the wt-CD20. These data indicated that concurrent analysis of the splice variants would not add meaningful information to the qPCR and was not pursued further.

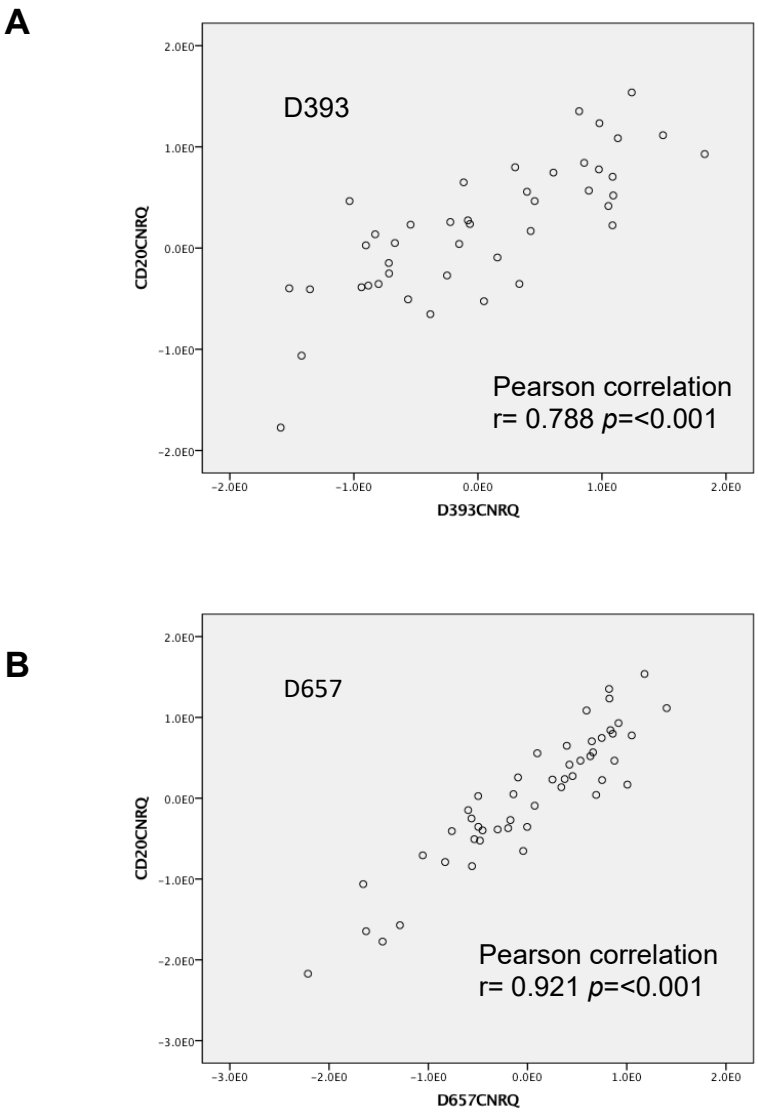

Figure 3-17 ***Expression of CD20 variants in comparison to wild type CD20.*** *Panel* ***[A]*** *shows expression of the first described CD20 variant, D393 which correlates with wild type expression pearsons correlation r=0.788. Panel* ***[B]*** *shows expression of variant D657 which shows strong concordance with expression of wild type CD20. Measured using RT-qPCR, expression of all genes normailsed to reference genes ACTB, B2M, GAPDH and 18S, as determined by geNorm analysis.*

3.5.15 CD20 RT-qPCR assay results correlated strongly with CD20 flow cytometry results

Despite the theoretical possibility of contamination with normal CD20 expressing cells, the RT-qPCR results showed a very strong correlation to CD20 flow cytometry in a pilot of 48 primary specimens (Pearsons correlation r=0.809 p<0.001) Figure 3-18 where material was available for both flow cytometry and RT-qPCR. The histograms in Figure 3-19 show the normalised RT-qPCR results shows a normal distribution and is comparable to the histogram of the logarithmically transformed flow cytometry data including antigen density.

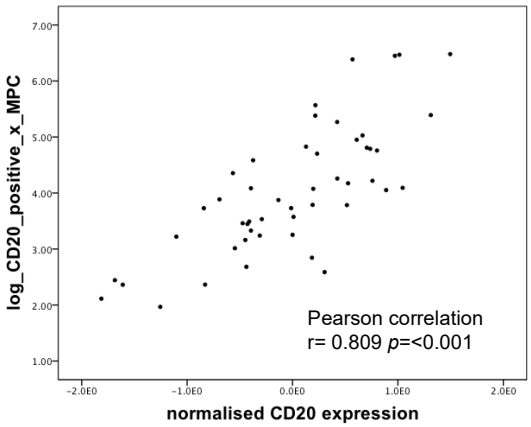

Figure 3-18 ***CD20 gene expression shows a strong correlation to flow cytometry data.*** *RT-qPCR of 48 primary specimens where flow cytometry data was available was carried out. CD20 expression was normalized to reference genes ACTB, B2M, GAPDH and 18S, as determined by geNorm analysis. The is RT-qPCR data showed a strong correlation to the number of CD20 positive cells multiplied by antigen density (molecules per cell). Pearson r=0.809 p<0.001*

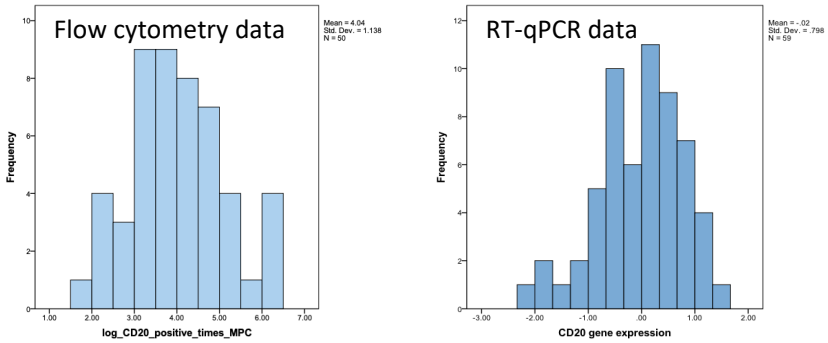

Figure 3-19 Histograms of Flow cytometry and RT-qPCR CD20 expression for UKALL14 specimens in pilot study.

Figure 3-20 shows that when bone marrow samples were analysed as a separate group to the peripheral blood specimens the correlation improved for the bone marrow specimens with an r=0.812 but was considerably worse for the peripheral blood specimens where r=0.654. This would fit with the theory that normal B-cells will 'contaminate' the peripheral blood specimens, however the proportion of blasts in the bone marrow specimen appears adequate to overcome this problem.

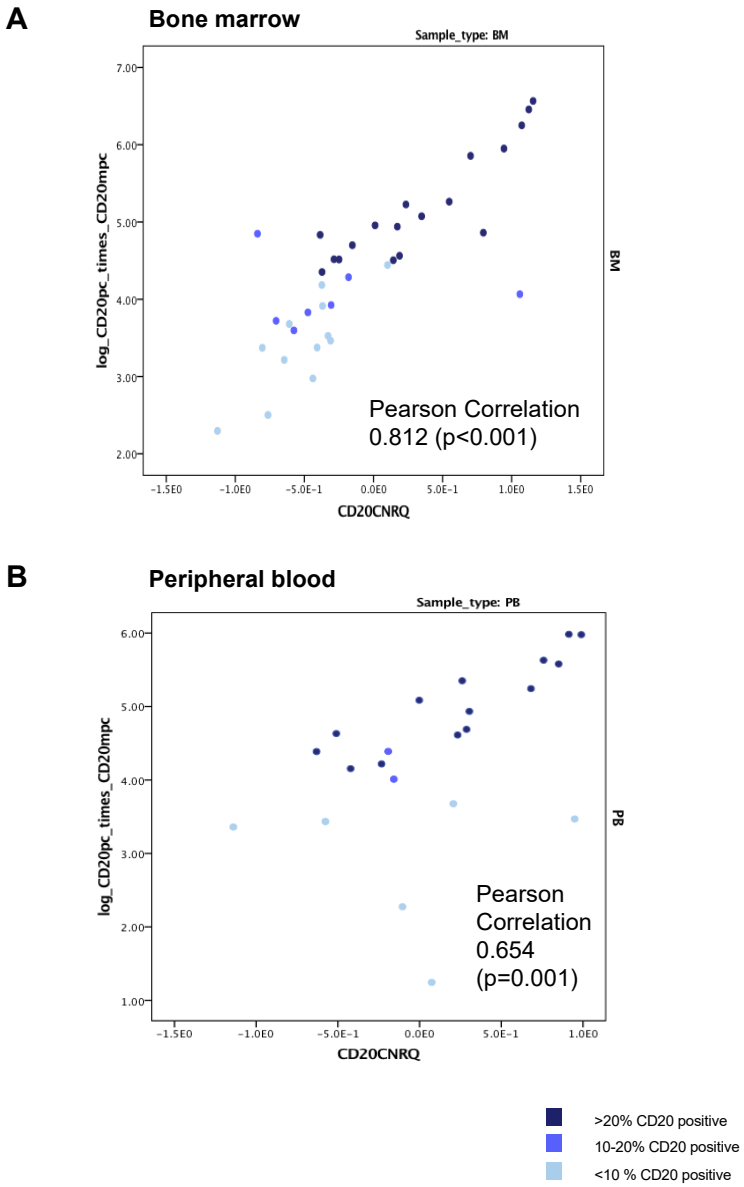

Figure 3-20 ***Concordance of RT-qPCR data to flow data is strengthened when bone marrow samples alone are analysed.*** *Figure A shows the scatterplot for bone marrow specimens. X-axis shows CD20 gene expression, y-axis shows CD20 expression by flow cytometry. This has a high Pearson correlation of 0.812. Figure B shows the scatterplot for peripheral blood specimens. The correlation has a Pearson r=0.654. Colours indicate the %CD20 positive blasts in each patient specimen.*

3.5.16 Further Optimising RT-qPCR Assay performance

The pilot study of the RT-qPCR assay showed promise. Before proceeding to the entire cohort it was important to optimise the RT-qPCR to be as technically robust as possible. Ideally 4 reference genes should be used and also the amplification efficiency should be measured. As the CD20 expression is measured in relation to the mean expression of the reference genes, it is important that the reference genes are amplified by PCR with equal efficiency to the target gene – ideally all at 100% efficiency. 100% indicates that the amount of PCR product doubles every PCR cycle. To validate the method, efficiencies of the genes were measured using a serial dilution of the strongly CD20 expressing cell line, Raji, to create calibration curves, and the efficiencies were calculated using the equation $(10^{-1/gradient} - 1) \times 100$, where the logarithm of the initial template concentration is plotted on the *x*-axis and the C_t is plotted on the *y*-axis. [209, 210] . The acceptable range for qPCR efficiency is between 90-110%. The efficiency for the reference genes fell just below the acceptable level of 90%. Primer/probe mixes were subsequently designed and ordered from PrimerDesign Ltd where 100% efficiency is guaranteed by the manufacturer. This also enabled the purchase of duplex gene expression assays for the reference genes using the two reporter dyes VIC® and FAM™ in the same assay, thus reducing the quantity of cDNA required for each patient sample. As FAM™ is the brighter of the two fluorescent dyes, this was assigned to the lower expressing reference gene, whilst VIC® was assigned to the higher expressing gene. This was determined by the Ct from the pilot study. Thus, assay one: ACTB- FAM™ was amplified with GAPDH- VIC® and assay two: β_2M- FAM™ was amplified with 18S- VIC®. As the gene of interest, CD20 was conjugated with the brighter fluorescent dye FAM™. All duplex dyes were also tested alone and produced comparable Ct values.

3.5.17 Patient characteristic in patients with RT-qPCR data are similar to those with flow cytometry data.

Figure 3-21 shows the fate of specimens used for qPCR. The baseline characteristics of patients with CD20 data measured by both molecular and flow cytometry methods are shown in Table 3-3. Similar to the 166 patients with flow data, the 173 patients with RT-qPCR data have a significantly greater white cell count, and fewer patients with t(4;11) than those without. There is no significant difference in age and *BCR-ABL1* status between the RT-qPCR group and the cohort without.

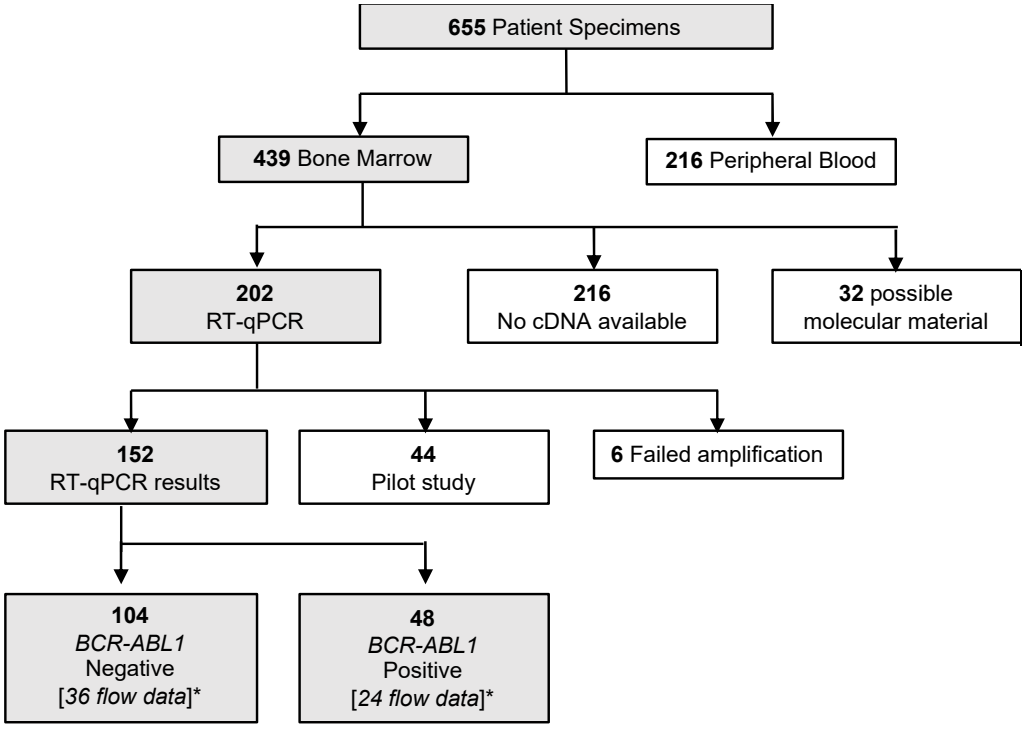

*Indicates flow cytometry CD20 data is also available for patient samples

Figure 3-21 ***Samples from UKALL14 available for RT-qPCR.*** *Chart indicates the number of specimens analysed by RT-qPCR including those where the analysis failed and no specimens available. Overall, 457 patients (70%) were BCR-ABL1 negative and 198 (30%) BCR-ABL1 positive.*

Table 3-3 ***Baseline characteristics of patients with CD20 data by RT-qPCR and flow cytometry compared to all BCP-ALL patients.*** *High risk: t(9;22), t(4;11), low hypodiploidy/near triploidy or complex cytogenetics. *patients with missing cytogenetics were assumed standard, **Chi-squared unless otherwise stated. ***Wilcoxon Mann Whitney test*

	Patients with flow data	Patients with RT-qPCR data	Patients with both	All B-cell Patients	p-value** (patients with flow data vs those without)	p-value** (patients with RT-qPCR data vs those without)
	N=166	N=173	N=84	N=655		
Age						
Median(range)	43.0	45.0	43.0	46.0	0.017***	0.36***
N (%)	(23 - 65)	(25 - 65)	(25 - 62)	(22 - 65)		
≤40 yr	73 (44.0)	63 (36.4)	36 (42.9)	233 (35.6)	0.009	0.79
> 40 yr	93 (56.0)	110 (63.6)	48 (57.1)	422 (64.4)		
White cell count (x10^9/L)						
Median(range)	25.9	21.5	31.7	8.0	<0.001***	<0.001***
N (%)	(1 - 557.23)	(.6 - 453.9)	(1.2- 453.9)	(.11- 889.6)		
<30	89 (53.6)	99 (57.2)	40 (47.6)	485 (74.0)	<0.001	<0.001
30-100	47 (28.3)	44 (25.4)	26 (31.0)	101 (15.4)		
≥100	30 (18.1)	30 (17.3)	18 (21.4)	69 (10.5)		
Sex						
Male	86 (51.8)	89 (51.4)	44 (52.4)	358 (54.7)	0.39	0.32
Female	80 (48.2)	84 (48.6)	40 (47.6)	297 (45.3)		
Cytogenetic features						
BCR-ABL1						
Negative	102 (61.4)	113 (65.3)	48 (57.1)	457 (69.8)	0.007	0.14
Positive	64 (38.6)	60 (34.7)	36 (42.9)	198 (30.2)		
Complex						
Absent	135 (94.4)	141 (95.3)	70 (93.3)	488 (95.3)	0.55	0.98
Present	8 (5.6)	7 (4.7)	5 (6.7)	24 (4.7)		
Missing	23 (16.1)	25 (16.9)	9 (12.0)	143 (27.9)		
Low hypodipoid/near triploidy						
Absent	137 (94.5)	137 (92.6)	74 (97.4)	474 (90.6)	0.061	0.34
Present	8 (5.5)	11 (7.4)	2 (2.6)	49 (9.4)		
Missing	21 (14.5)	25 (16.9)	8 (10.5)	132 (25.2)		
t(4;11)(q21;q23)						
Absent	138 (86.8)	144 (86.7)	69 (85.2)	567 (92.0)	0.004	0.003
Present	21 (13.2)	22 (13.3)	12 (14.8)	49 (8.0)		
Missing	7 (4.4)	7 (4.2)	3 (3.7)	39 (6.3)		
Risk group at randomisation						
Standard risk*	22 (13.3)	22 (12.7)	9 (10.7)	109 (16.6)	0.18	0.11
High risk	144 (86.7)	151 (87.3)	75 (89.3)	546 (83.4)		

3.5.18 RT-qPCR CD20 expression is strongly correlated to flow cytometry CD20

The CD20 RT-qPCR assay was carried out on all available patient bone marrow specimens where cDNA or RNA was available. Figure 3-21 shows the number of specimens available to carry out the assay. As in the pilot, Figure 3-22 shows the results from the samples where both flow cytometry and RT-qPCR data were available (total n=59) and the strength of association measured as Pearsons r=0.796, linear regression analysis gave a coefficient of determination, R^2, of 0.633. Thus, although the correlation between flow cytometry and RT-qPCR is strong, the ability of the qPCR CD20 data to predict the CD20 expression, considering flow cytometry the 'gold standard', may not be sufficient to reliably use for samples where only mRNA/cDNA is available. However, when RT-qPCR and flow cytometry have been compared for the use of MRD similar concordance was found to our results [211, 212]. To put this into a practical clinical context, using the Youden's cut-off established for %CD20 positive cells multiplied by antigen density, in our cohort 4 patients (6.9%) would have remained in a standard risk group when they would have been considered high risk by the flow cytometry method, whilst 8 patients (13.8%) would have been considered high risk by the new method but standard risk if CD20 was determined by flow cytometry (Figure 3-22).

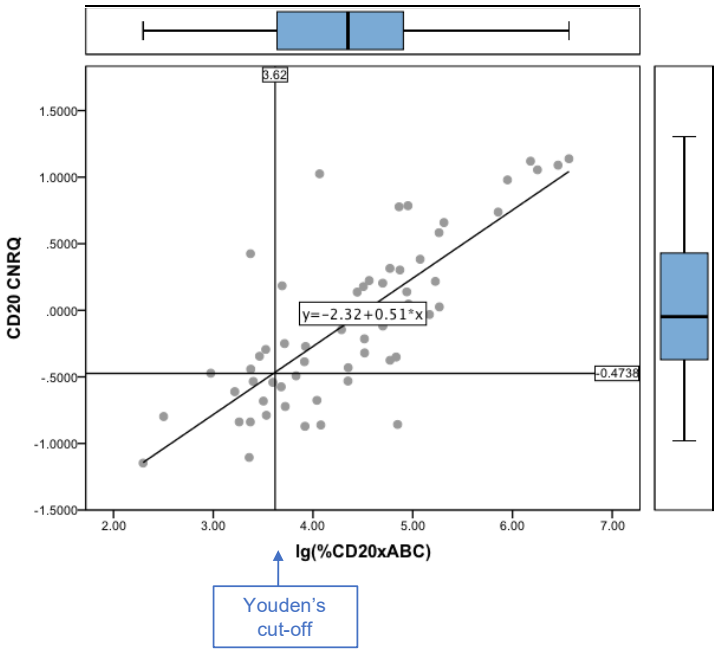

Figure 3-22 59 bone marrow specimens had CD20 data by both flow cytometry (x-axis) and RT-qPCR (y-axis). *Pearson r=0.796, linear regression gave coefficient of determination r^2=0.633. Youden's cut off demonstrates those samples that would be 'false positives' (left upper quadrant) and 'false negatives' (right lower quadrant) if RT-qPCR method used.*

3.5.19 CD20 measured by RT-qPCR does not significantly predict event free survival in UKALL14 BCP-ALL patients

Cox regression analysis failed to show an impact of CD20 expression measured by RT-qPCR on event free survival for 152 UKALL14 patients (HR 1.10, CI 0.74 – 1.62, p=0.64) or when the 103 patients who were negative for *BCR-ABL1* were analysed separately (HR 1.20, CI 0.72 – 1.98), p=0.49). The Harrell's C was also low at 0.5332 for the whole group and 0.5349 for those without *BCR-ABL1*. ROC analysis was carried out and gave a value near 0.5 for both groups. Youden's cut-off was calculated as the best cut-off for sensitivity/specificity. Cox regression analysis using this cut-off to create two groups remained non-significant for the whole group (HR 1.32, CI 0.74 – 2.36, p=0.35) but did reach statistical significance for the *BCR-ABL1* negative group (HR 2.12 ,1.06 – 4.26, p=0.034). (figure 3-23) It is notable that the group size for high risk CD20 is considerably smaller than those identified in the flow cytometry group. 5 of these patients also had flow data and for all of these patients the percentage CD20% blasts was very high (99%, 99%, 98%, 81.4%, and 55.2%). By using Youden cut-off in this population we appear to be selecting very highly expressing CD20 patients. This fits with the estimated low sensitivity 36.4% and higher specificity of 78.8% at this point.

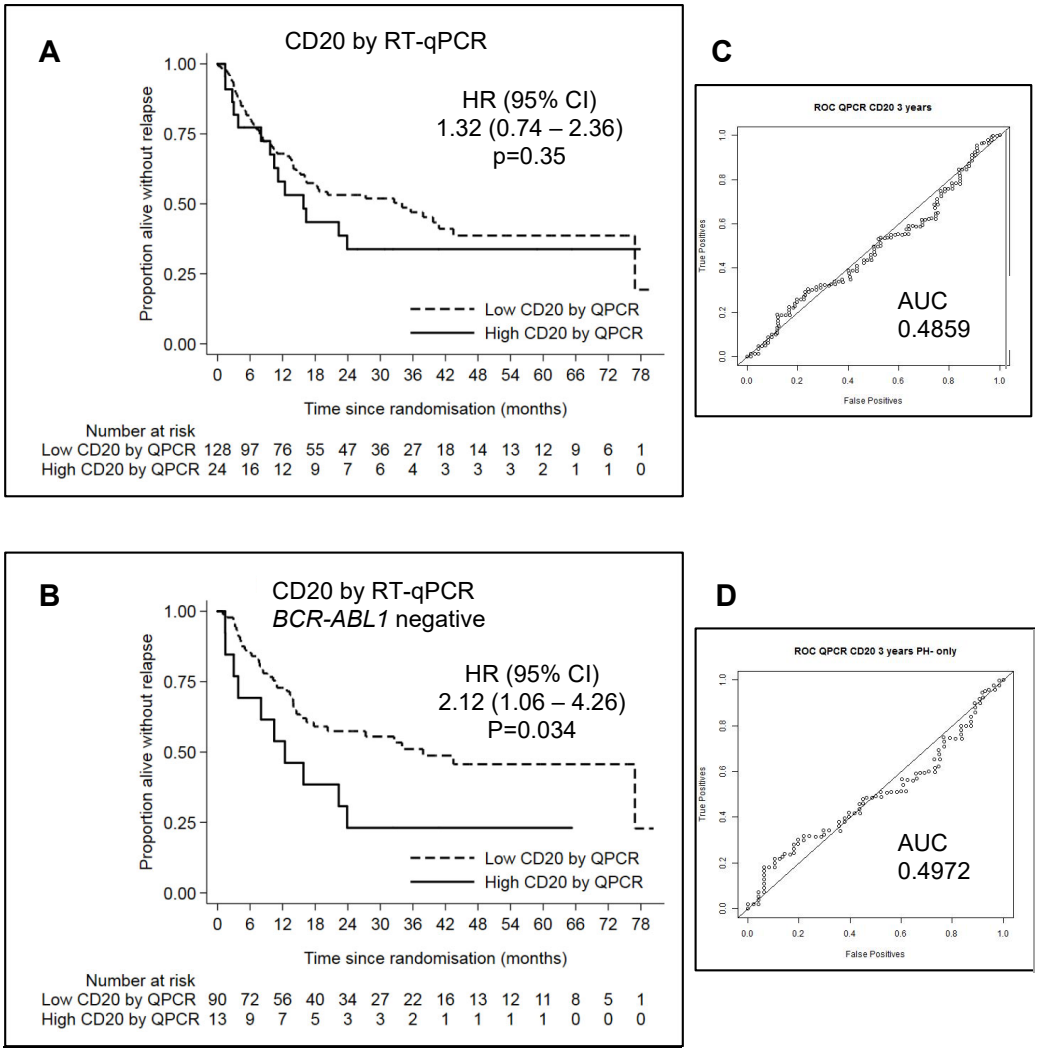

Figure 3-23 ***Clinical outcome Youden's cut-off is used for RT-qPCR CD20 to determine groups.*** ***Panel A*** *shows the rate of event-free survival over time using Youden's cut off for CD20 RT-qPCR data.* ***Panel B*** *shows the rate of EFS over time using Youden's cut off for CD20 RT-qPCR data in patients who were BCR-ABL1 negative.* ***Panel C and D*** *show the ROC analysis for the RT-qPCR data for the entire cohort* ***[C]*** *and BCR-ABL1 negative patients only* ***[D]***

3.5.20 Comparison of RT-qPCR method to flow cytometry methods

Table 3-4 shows the results to analysis comparing the three methods for measuring CD20, the traditional method of percentage positive blasts, the percentage blasts multiplied by the antigen density (MPC) and the RT-qPCR method. The comparison was limited to the 36 specimens that were analysed by all three methods. The risk of an event was consistently higher in the lower expressing CD20 groups with all three methods, and there appeared to be a greater difference in the method using antigen density. As none of the cox regression

analysis of event free survival over 3 years for these samples reached significance, likely due to the small sample size, it is difficult to draw conclusions from this comparison. A larger sample would be required.

Table 3-4 ***Comparing flow data to RT-qPCR data.*** *A similar approach to comparing the 2 flow cytometry methods. Patients included required both flow cytometry and qPCR data.*

	Log(percent CD20+ blasts)	Log(percent CD20+ blasts x MPC)	RT-qPCR
Time to event analysis			
Events/N	18/36	18/36	18/36
Cox regression (EFS) HR (95% CI)	0.98 (0.70 - 1.36) p=0.89	1.01 (0.82 – 1.25) p=0.92	1.05 (0.48 – 2.28) p=0.91
Harrell's C *	0.4922	0.5285	0.4870
Logistic regression/ROC analysis; event at 2 years			
Events/N**	11/27	11/27	11/27
OR (95% CI)	0.96 (0.58 – 1.61) p=0.88	1.03 (0.74 – 1.44) p=0.86	1.25 (0.36 – 4.37) P=0.73
ROC AUC (95% CI)***	0.49 (0.26 – 0.72)	0.54 (0.31 – 0.77)	0.51 (0.28 – 0.74)
Cox regression (EFS) HR (95% CI) – high vs low risk (Youden's cut off and 2 year endpoint) (n=36)	1.38 (0.54 – 3.51) p=0.50	1.49 (0.59 – 3.79) p=0.40	1.95 (0.68 – 5.56) p=0.22
3 year KM rate using this cut off (n=151/103)			
Low group	55.1% (27.7 – 75.8)	59.7% (33.3 – 78.4)	40.4% (14.4 – 65.5)
High group	26.6% (5.6 – 54.4)	23.0% (4.4 – 50.0)	16.7% (0.8 – 51.7)
Using time to event ROC analysis (predicting an event at 3 years)			
Events//N	18/36	18/36	18/36
Cox regression (EFS) HR (95% CI) – high vs low risk (Time to event ROC, 3 years)	1.38 (0.54 – 3.51) p=0.50	1.44 (0.57 – 3.66) p=0.45	1.27 (0.36 – 4.42) p=0.71
3 year KM rate using this cut off (n=151/103)			
Low group	55.1% (27.7 – 75.8)	59.3% (33.0 – 78.1)	43.3% (21.1 – 63.8)
High group	26.6% (5.6 – 54.4)	23.3% (4.5 – 50.4)	25.0% (0.9 – 66.5)

3.6 Discussion

The prognostic significance of CD20 expression has been controversial in both adult and childhood ALL. With a median follow-up of 35.9 months the data from the UKALL14 trial presented in this chapter indicates that increasing CD20 expression is indicative of a worse outcome, when measured as event free survival or overall survival. Measuring the overall burden of CD20 by measuring the proportion of leukaemic cells which were positive for CD20 antigen by flow cytometry and multiplying this by the estimated antigens per cell using BD Quantibrite beads appeared to show a greatest ability to identify this adverse effect. However, it is more difficult to assess whether the added benefit of this method is likely to compensate for the extra time, and expense in routine diagnostic flow cytometry laboratories. We must consider that half of the patients included would have received 4 courses of rituximab, regardless of CD20 expression. If rituximab improves the outcome for those expressing CD20 it would be expected that we would see a reduced adverse effect of CD20 status on outcome. It will be very interesting to see the rituximab sub-analysis data when the UKALL14 trial is unblinded. As well as determining the benefit of rituximab to all patients with BCP-ALL in the UKALL14 trial, it will also enable us to determine how effective rituximab is at differing levels of CD20 expression in overcoming the adverse prognostic effect.

The traditional cut off of 20% cells expressing an antigen indicating positivity is called into question by this data. This is particularly important when considering treating with targeted therapy as patients who only have between 10 and 19% of their leukaemic blasts expressing CD20 could potentially miss out on receiving potentially beneficial targeted therapy. In clinical trials where rituximab is included such as the GRAALL-2005 trial, only patients who were negative for *BCR-ABL1*, and expressed CD20 of at least 20% of their leukaemic blasts received rituximab [193]. This was not an unreasonable choice as there is evidence that the cytotoxic cell killing mechanisms such as CDC, ADCC, are dependent on the quantity of CD20 expressed, and since in our data when a high proportion of blasts expressed CD20 they also tended to have a high antigen density. A counter argument is that there is evidence that the steroid pre-phase can increase the expression of CD20, and thus theoretically increasing the efficacy of rituximab [213]. This will also be relevant for

the next chapter where we consider an alternative treatment for ALL – a CD20 targeted oncolytic measles virus.

3.6.1 CD20 measured by RT-qPCR is a potential prognostic biomarker in *BCR-ABL1* negative patients

The RT-qPCR method held promise as a method of estimating whole CD20 burden from bone marrow mRNA and appeared to correlate strongly with the results from flow cytometry. This technique could potentially overcome issues of obtaining fresh, adequately cellular samples. It can also easily and relatively cheaply be carried out at a central laboratory which would be useful for inclusion in further clinical trials to provide robust data. The CD20 expression seen in flow cytometry is often a 'smear' (See Figure 4-5) and variation between centres in methods, and where positive expression is determined can make a large difference between percentage deemed positive. A molecular method could be considered a less subjective analysis as the cycle at which the DNA is amplified is determined by the computer software, whereas gating of flow cytometry dot plots currently requires human judgement. Analysis of CD20 expression of 152 patients by the RT-qPCR method as a continuous variable on bone marrow specimens did not show a significant effect on outcome. There was a significant effect on the 103 patients who were negative for *BCR-ABL1* but only when the group was split by a cut-off with a very low sensitivity (18.2%). Thus the evidence from the UKALL14 trial suggests that CD20 measured by RT-qPCR could be a potential prognostic biomarker in *BCR-ABL1* negative patients.

3.6.2 Comparing flow cytometry and RT-qPCR

Comparing the two methods – flow cytometry and RT-qPCR – is problematic as it is unknown what influence CD20 expression has on patient outcome. Baseline characteristics showed that the group of patients who had specimens available for flow cytometry was less representative of the whole group in comparison to the patients who had mRNA for qPCR. Although the patients with *BCR-ABL1* were considered separately, Maury et al [50] have shown an influence of CD20 positivity on those with a high white cell burden (WBC >30 $x10^9$/L) where a significant negative impact of CD20 positivity on both cumulative incidence of relapse and EFS was only seen in those with a high white cell count. However,

multivariable analysis of the flow cytometry indicated that CD20 was an independent risk factor so this argument does not hold for the UKALL14 data. The direct comparison for the 2 flow cytometry methods and the RT-qPCR method – in 36 patients in both cohorts - failed to show any significant CD20 adverse prognostic effect for any of the methods. This was a small group of patients as it required patient specimens where there was material for both methods which meant that bone marrow was required, and it was also logical to use patients who were *BCR-ABL1* negative. Up to 30 further samples could be obtained by re-analysing specimens which were run in the pilot study, as these have flow data available. As the pilot study used different primers and probes, and only 3 reference genes, as opposed to the 4 used for the main study, it would not be possible to combine these data. The good correlation between the flow cytometry specimens and the significantly worse outcome seen in *BCR-ABL1* negative patients when measured by the RT-qPCR method does indicate its value as a measure of CD20 expression. It could be considered for use in further trials by prioritising acquisition of mRNA/cDNA.

3.6.3 *BCR-ABL1* and CD20

BCP-ALL patients positive for *BCR-ABL1* traditionally had a dismal outcome. It is now common practice to treat these patients with a tyrosine kinase inhibitor and in UKALL14 imatinib is used. The outcome of UKALL14 is that patients with *BCR-ABL1* are doing as well as those who are negative for the translocation, and the overall survival is perhaps even better, albeit a not-significant difference (unpublished results). CD20 expression does not appear to impact on the outcome of this cohort. A Chinese group has reported that *BCR-ABL1* positive patients with CDKN2 deletion and who are also CD20 positive (≥20% blasts expressing CD20) had a poor overall survival compared to those who were CD20 negative however numbers were small [54]. It should be possible to look at this data from the UKALL14 population. It will be very useful to see if rituximab has made any difference in this population. A group with a particularly high CD20 level may have benefitted from the mAb, improving their survival. Other possibilities include the interaction of the tyrosine kinase inhibitor on downstream effects of CD20. Previous studies have indicated that there is an association between tyrosine kinases with CD20. Stimulating CD20 in resting B cells can result in increased *c-myc*; an effect that can be inhibited by the tyrosine kinase inhibitor herbimycin [214]. There are reports of CD20 expression being decreased by the TKI dasatanib in the CD20 expressing cell line, Raji [215]. This could be due to dasatanib

impairing the binding of a transcription factor PU.1 to the *cd20* gene promotor in Raji cells [216]. Imatinib is a selective Abl kinase inhibitor whereas dasatanib is known to also inhibit Src kinases. As there are no reports of similar effects being investigated using imatinib this would be an interesting area of research to attempt to explain the lack of prognostic impact CD20 has on *BCR-ABL1* positive patients in the UKALL14 trial.

In conclusion, data presented in this chapter has shown that increasing CD20 expression has a significant negative impact on event free survival and overall survival in patients on the UKALL14 clinical trial. It appears that prognostic categories can be more clearly defined by also considering the antigen density using BD quantibrite beads. The UKALL14 trial is unique in that patients are randomised to receive rituximab irrespective of CD20 expression, and it may be that the net benefit to all patients negates a detailed analysis of CD20 expression, and this could theoretically be as a result of CD20 upregulation with steroids during pre- and phase 1 induction. The good level of correlation between flow cytometry data RT-qPCR showed that in the future this could potentially be used to estimate CD20 expression. The correlation between flow cytometry and RT-qPCR is not strong enough to enable the data to be combined. However, we do not know definitely which test gives a better predication of outcome as the cohorts tested were not the same. It is difficult to say whether the concordance between the two tests is not sufficient, or whether for these patients CD20 was not biomarker of poor prognosis. By determining outcome data for a greater proportion of patients this could have added to the power and enabled greater confidence in interpreting the sub-group analysis to determine the benefit of treating with rituximab. Once data is available following the rituximab unblinding it will hopefully be possible to determine if CD20 targeted treatment overcomes the negative prognostic effect of CD20 and to also determine whether the CD20 level is important for deciding on CD20 targeted therapy.

Chapter 4 A CD20 targeted Oncolytic Measles Virus

4.1 Introduction

CD20 is expressed in 30-50% of ALL leukaemic blasts and is currently being targeted using the monoclonal antibody rituximab in several multi-centre international clinical trials with promising results. As seen in the previous chapter, CD20 expression confers adverse survival except in patients who are positive for *BCR-ABL1*, despite approximately half the patients having received CD20 targeting therapy in the form of the monoclonal antibody rituximab. Rituximab is already proving to have value as a therapeutic in CD20 positive ALL resulting in an improved event free survival [193].

This chapter explores the use of a CD20 targeted measles virus - MVHαCD20 - as a potential therapeutic option. As discussed in Chapter 1, MV has been shown to have some efficacy in clinical trials and preclinical work has shown ALL to be sensitive to MV infection and oncolysis. A putative cause for its efficacy in many cancers, ALL included, is the overexpression of the MV receptor CD46. By targeting both CD20 and the native MV receptors we may further enhance the efficacy of the virus. A further theoretical benefit of MV targeted to CD20 is that off-target effects may, perhaps counterintuitively, prove to be beneficial. By infecting and thus eliminating normal CD20 expressing memory B cells, this may reduce the secondary anamnestic antibody response to further treatment with MV.

A MV targeted to CD20, MVHαCD20, has been previously developed by Prof Fielding's laboratory by modifying the H glycoprotein to express a C-terminal single chain (scFv) anti-CD20 antibody as a fusion protein (See Figure 4-1). This targeted virus has previously been shown to be more efficient in supressing the growth of fibrosarcoma tumours expressing CD20 *in vivo* (HT1080CD20) than the native, non-targeted, strain of MV -MVNSe [151]. A CD20 targeted MV that is also blind to the native MV receptors CD46 and SLAM was later generated [217]. Additionally, the targeted and blinded virus has been 'armed' with the prodrug convertase purine nucleoside PNP, resulting in increased survival in xenografts of the Burkitt's lymphoma cell line, Raji, and the Mantle Cell lymphoma cell line, Granta 519, in the presence of F-araAMP [143]. Pre-clinical data has also indicated that prior anti-CD20

therapy does not interfere with infection efficiency or CD20 specificity of the CD20 targeted MV in B cell NHL [218]. A CD20 targeted oncolytic virus has not been evaluated in ALL.

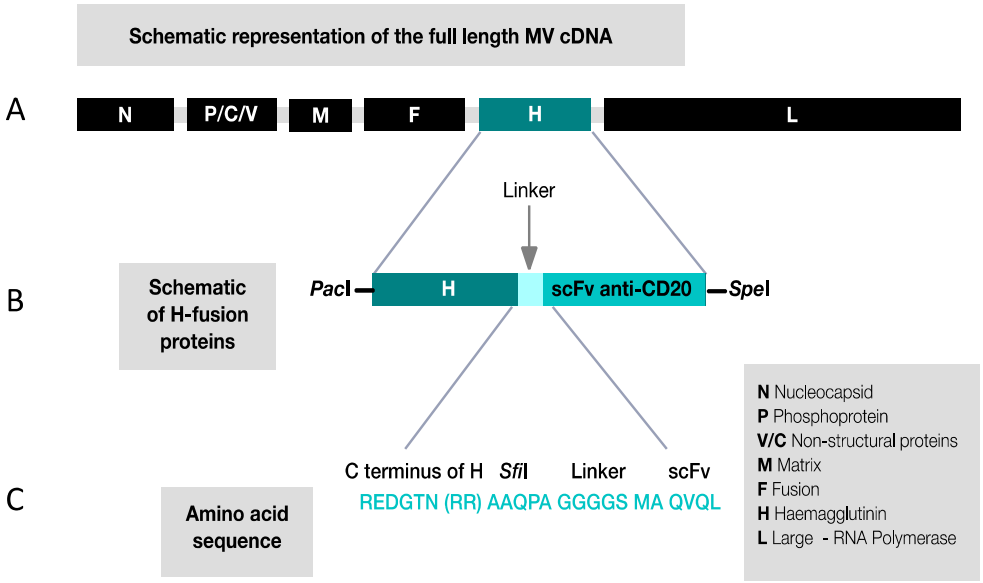

Figure 4-1 ***Schematic representation of MVHαCD20. [A]*** *is a representation of the full MV genome.* ***[B]*** *is an expanded schematic of the H fusion proteins where the scFv anti-CD20 antibody is attached via a linker to the H gene.* ***[C]*** *is the amino acid sequences of the C terminus of MV-H with the Sfi1 restriction site, linker sequence and sequence of the N terminus of the scFV anti-CD20. [Adapted from Bucheit et al, 2003]*

4.1.1 CD46

The MV receptor CD46 is universally expressed on nucleated human cells. CD46 is a negative regulator of complement, acting as a co-factor to Factor-I mediated cleavage of C3b and C4b [219, 220]. There have been numerous reports demonstrating that CD46 is highly expressed in malignancies, with Ong *et al* finding a seven fold difference in CD46 expression on myeloma cells compared to normal plasma cells, and that the high CD46 correlated with MV-induced cytopathic effects [221].

MV infection has been reported to downregulate CD46. Schneider-Schaulies *et al* demonstrated that seven vaccine strains were inhibited by anti-CD46 and resultant down-

regulation of CD46 following infection, and CD46 expression being reduced by 61% from the surface of peripheral blood lymphocytes 16 hours following infection by MV Edmonston. Four of 12 wild type strains tested did not result in CD46 downregulation [222]. This effect is mediated by MV-H - modulation of CD46 can be induced on uninfected cells following contact with MV-H, either on viral particles or infected cells. The downregulation of CD46 by MV-Edm has been shown to enhance the susceptibility of cells, including primary lymphocytes, macrophages, and U937 monocyte cell line, to complement mediated lysis [223].

4.1.2 SLAM (CD150)

SLAM (CD150) is a receptor for both wild type and vaccine strains of measles virus. It is member of the immunoglobulin gene superfamily and is expressed on B-cells, T-cells, dendritic cells, haemopoietic stem cells, and immature thymocytes, and thus may account for the immunosuppressive properties of MV. It is a CD2-related receptor and it functions to enhance T cell proliferation and gamma interferon production (IFN-γ). SLAM engagement also augments the cytotoxic activity of CD4+ and CD8+ T cells.

SLAM is widely expressed on human B-cells, De Salort *et al* measured the expression level of SLAM on normal B cells from human bone marrow (see Table 4-1). Given that nearly 50% of pre-B cells expressed SLAM it seems likely that expression in ALL will vary.

Table 4-1 ***SLAM expression of normal B-cells*** *(from De Salort et al 2011[119])*

	Immunophenotype	**%**	**Mean fluorescence intensity (MFI)**
Pro B	$CD19^{+}CD10^{+}CD34^{+}IgM^{-}$	44	1395
Pre B	$CD19^{+}CD10^{+}CD34^{-}IgM^{-}$	49	733
Immature B	$CD19^{+}CD10^{+}CD34^{-}IgM^{+}$	9	949
Mature B	$CD19^{+}CD10^{-}CD34^{-}IgM^{++}$	83	749

4.1.3 'Blinding' MV to Native receptors

To create 'blinded', or fully retargeted MV, point mutations can be introduced into the CD46 and SLAM binding domains of the MV-H protein. The relevant residues were painstakingly identified by iterative cycles of mutant protein production followed by functional assays [217] Several residues were identified that are required for CD46 dependent fusion (451, 481) and SLAM dependent fusion (529,533). The first demonstration of the oncolytic efficacy of a targeted and then 'blinded' MV was a fully retargeted to CD38. Paired mutations at positions 451 and 529 or 481 and 533 supported fusion via the CD38 but not CD46 or SLAM[154]. In order to rescue such fully 'blinded' virus on vero cells a system whereby a His-Tag – a peptide containing 6 histidine residues at the C terminus of the mutated H protein - was used[155]

A CD20 targeted MV that is unable to infect cells via the native MV receptors CD46 or SLAM is an attractive proposition as it could potentially avoid off target unwanted effects, by avoiding infection of normal cells. Although clinical trials where the MV is administered systemically have shown that the virus is well tolerated, with some immediate effects such as high fevers whilst the infusion is in progress, there are no long-term safety data [224]. The ability of a MV to avoid engaging CD46 is theoretically appealing as CD46 is expressed on all human nucleated cells. Engagement of SLAM can result in MV-related immunosuppression as it is present on B-cells, T-cells, and dendritic cells, thus 'blinding' to this receptor could result in a safer therapy.

A theoretical benefit of retargeting MV is the possibility of reducing neutralization by pre-existing antibodies in human serum. The haemagglutinin attachment is a major target for neutralising antibodies and the modifications to the H-protein could potentially destroy target epitopes from the mutations that have conferred 'blindness' to CD46 or SLAM (Y481A and R533A; or Y481A, R533A, S548L and F549S). Alternatively, the addition of the scFv to confer re-targeting could shield epitopes from antibodies. Lech *et al* (2014) investigated this by cloning MV-H82.αEGFR and using neutralization assays and structural modelling of H. Their data indicated that although the retargeted MV derivative was able

to escape neutralization from antibodies targeted to the receptor-binding surface, they were no better at escaping neutralization by human serum than non-retargeted MV [225].

4.2 Purpose of this chapter.

In this chapter, I investigated the permissiveness and susceptibility of NALM6 cells that have been transduced to express CD20, to both the native, Edmonston, NSe strain of MV and a modified, CD20 targeted MVHαCD20. I investigated the ability of MVHαCD20 to kill ALL cells in a monoculture and determined whether this was influenced by the CD20 antigen density expressed on the surface of NALM6 ALL cells. To investigate the efficacy of viruses targeted to CD20 and 'blinded' to the native receptors of MV, namely CD46 and SLAM, I quantified the expression of CD46 and SLAM on cell lines and primary ALL cells. Given the role of CD46 as a negative regulator of complement, I carried out assays to investigate whether downregulation of CD46 by MV infection will make the ALL cells more susceptible to complement mediated destruction

4.3 Hypotheses

A MV with targeted entry via CD20 will have better oncolytic capability against ALL than the parental virus when CD20 is expressed on ALL cells.

4.4 Aims

To determine the effect of engaging CD20 on MV replication and killing of CD20 'positive' and 'negative' ALL cells.

To determine the anti-ALL effects of MVHαCD20 which is "blind" to either of the native MV receptors SLAM or CD46.

4.5 Results

4.5.1 NALM6 cells can be retrovirally transduced to stably express CD20

In order to investigate the effect that the density of CD20 antigen expression of ALL cells has on MVHαCD20 infection and subsequent oncolysis, first a cell line was created by retrovirally transducing the CD20 negative ALL cell line, NALM6, to express the human CD20 gene. The CD20 retroviral vector was generated by substitution of the IK6 from the MSCV-IK6-IRES-mRFP plasmid (kindly donated by Mulligan laboratory, St Jude Children's Research Hospital, Memphis, TN, USA) with the human CD20 coding sequence to generate MSCV-CD20-IRES-mRFP [Figure 4-2].

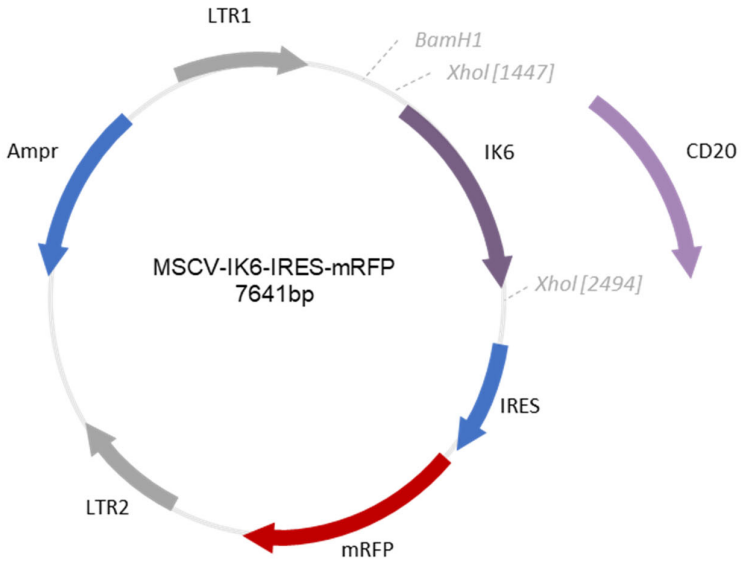

Figure 4-2 ***Schematic of MSCV-IK6-IRES-mRFP replication defective retroviral vector indicating restriction sites and insertion of CD20 gene.*** *LTR= long terminal repeat; Ampr=ampicillin; MSCV=murine stem cell virus; IRES= internal ribosome entry site; mRFP=red fluorescent protein; IK6= ikaros gene. BamH1 and XhoI are restriction sites.*

Phoenix™-AMPHO retroviral packaging cells were subsequently transfected with the CD20 modified MSCV plasmid and NALM6 cells then infected with the retrovirus supernatant

[Figure 4-3]. Successful retroviral transduction of the cloned plasmid was confirmed by flow cytometry measuring both mRFP expression and CD20.

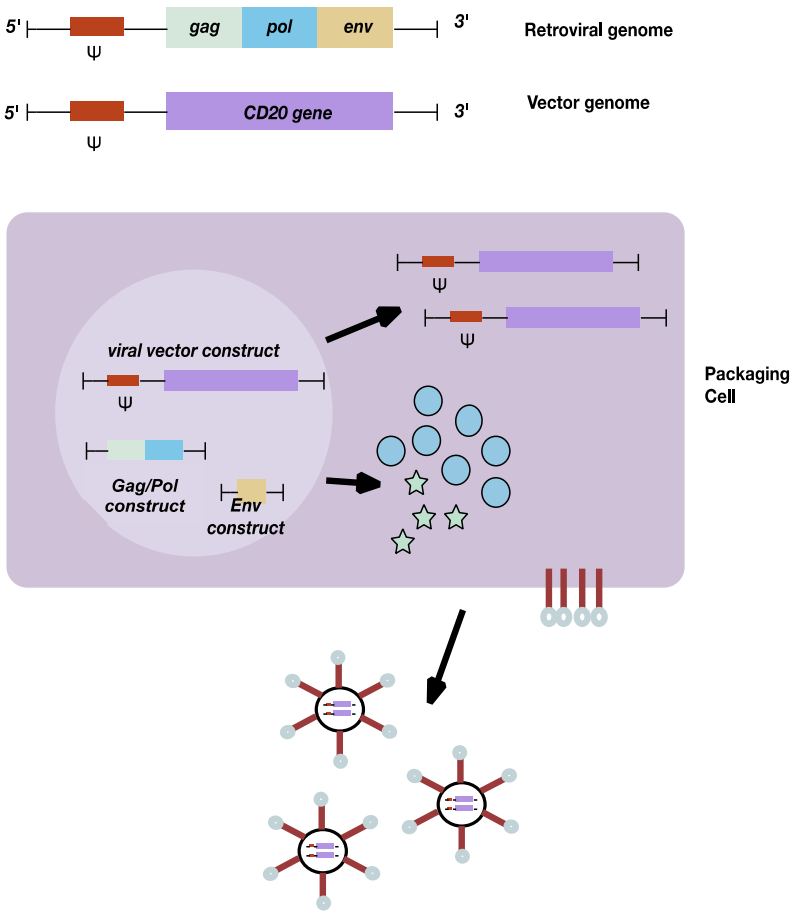

Figure 4-3 ***Schematic of retroviral transduction using Phoenix™-AMPHO packaging cells*** *Phoenix™-AMPHO cells are based on the 293T cell line and are highly transfectable. They are capable of producing gag-pol, the envelope protein for amphotropic viruses - i.e. retrovirus that can replicate in tissue culture but does not produce disease. The transfection mix included the retroviral construct - MSCV-CD20-IRES-mRFP - containing the gene of interest CD20, the pCL-ampho retrovirus packaging vector, and was incubated with the Phoenix™-AMPHO cells. Retroviruses are produced which are able to infect target cells to insert the gene of interest - CD20 - but do not contain the apparatus to replicate.*

gag : structural precursor protein; pol : polymerase; env : envelope; MSCV : murine stem cell virus; IRES : internal ribosome entry site; mRFP : red fluorescent protein

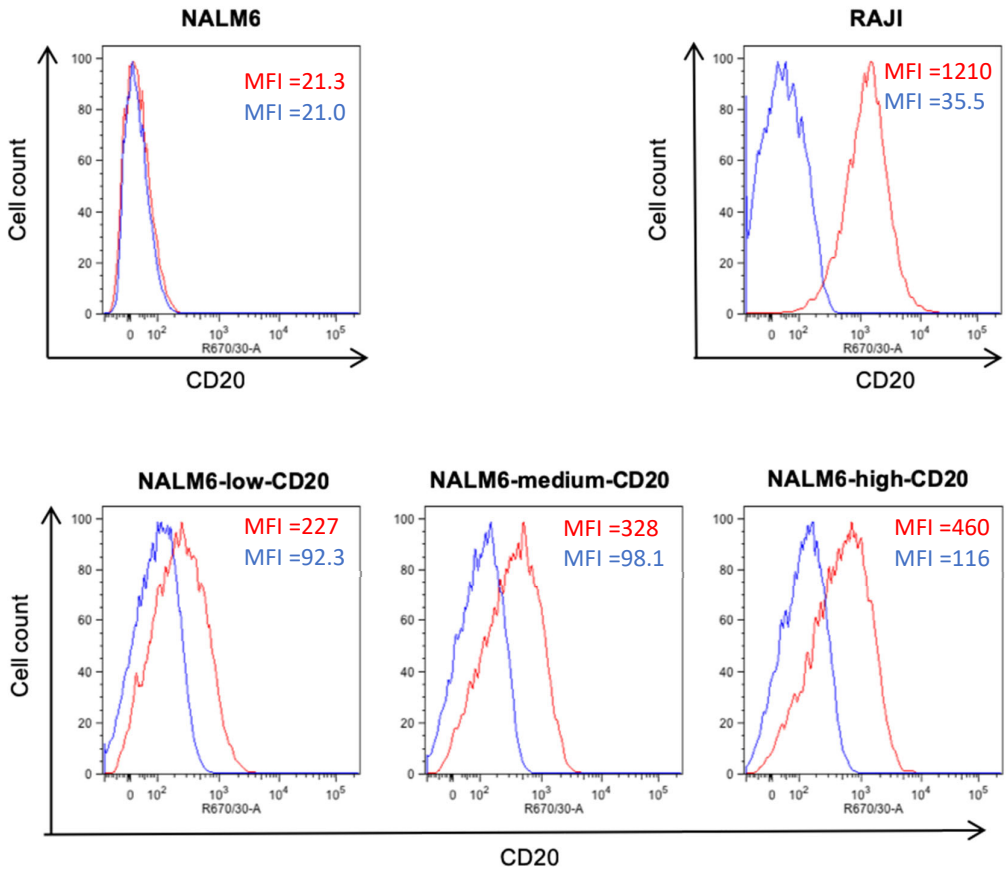

Figure 4-4 ***CD20 expression of NALM6 cells, Raji, NALM6-low-CD20, NALM6-medium-CD20, and NALM6-high-CD20.*** *Cells were analysed following FACS sorting. Events acquired on Fortessa X20 using FACS-DIVA software. Red outline: Cells labelled with CD20-APC Blue outline: Isotype-stained negative control*

The cells were then FACS sorted based on the mean fluorescence intensity (MFI), initially sorting the cells equally into 'low', 'medium' and 'high' expressing populations [Figure 4-4].

4.5.2 CD20 expression on ALL cells can show a broad range of intensity within a leukaemic blast population.

The previous chapter details the flow cytometry of CD20 expression in ALL specimens. The focus of the work was on the mean intensity of expression, however it was noted that there was often a spread of intensity, as opposed to a narrow peak. Figure 4-5 shows the CD20 expression in five representative patient specimens from UKALL14 illustrating that CD20 expression is variable in ALL and that within a leukaemic blast population there is a typical 'smear' pattern indicating a range of expression densities within the population. Although it would be possible to sort cells with a narrower MFI range, by opting to choose a wider range of CD20 positive expression from the sort was similar to that seen in the primary specimens in the previous chapter, and therefore more representative of CD20 expression on ALL blast populations. At several time points following transduction the CD20 expression was reassessed confirming that the cells showed stable expression. At approximately 4 and 8 weeks MFI for NALM6-high-CD20 was 373 then 395, and for NALM6-low-CD20 was 172 then 136 respectively.

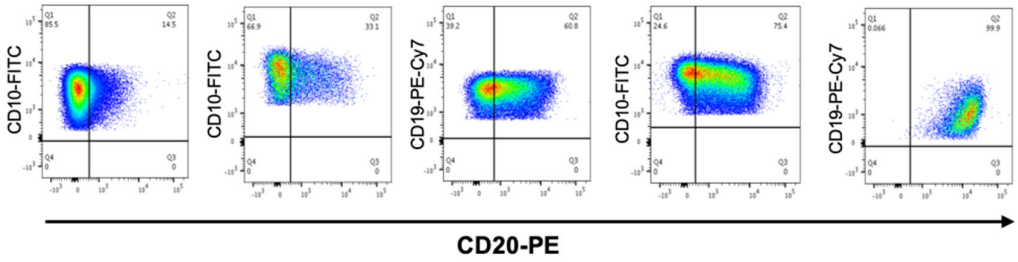

Figure 4-5 ***Examples of CD20 expression in primary ALL specimens.*** *Flow cytometry dot plots often show a 'smear' pattern. Five representative samples from UKALL14 specimens are shown. Flow cytometry was carried out, and blasts have been gated as described in Chapter 3. x-axis indicates fluorescence intensity of PE-CD20. Quadrant Q2 indicates percentage positive determined by the FM0. Specimens are arranged in order of increasing CD20 positivity for illustrative purposes.*

4.5.3 MVHαCD20can infect and replicate in ALL cells

It has previously been demonstrated that MVHαCD20 can enter cells through the CD20 antigen in CHO and HT1080 cells engineered to express CD20 however this has not been shown in ALL [151]. Experiments were carried out to investigate whether NALM6 cells, with or without CD20 expression, are both susceptible and permissive to infection by MVHαCD20. The MVHαCD20 virus was first rescued from the MV plasmid as described in the methods chapter. MVHαCD20 was then successfully propagated on Vero cells. Figure 4-6 shows viral growth curves for NALM6 and NALM6 with 'high' expression of CD20 following infection with either the parent virus MVNSe or with MVHαCD20. The graphs show typical viral growth curves, with similar peaks of viral replication, although the MVHαCD20 appears to replicate for longer in the ALL cells compared to MVNSe. This could reflects a more efficient infection by the native strain virus.

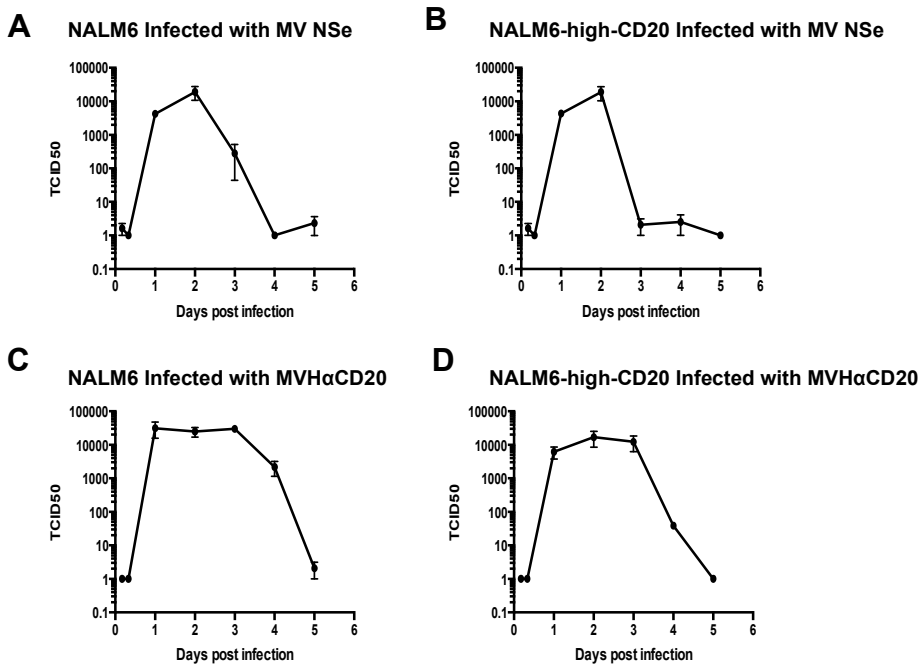

Figure 4-6 ***One-step growth curves for MV-NSe and MVHαCD20***

Growth curve for MV-NSe on ***[A]*** *NALM6 cells and* ***[B]*** *on NALM6-high-CD20 cells. Growth curve for MVHαCD20 on* ***[C]*** *NALM6 cells and* ***[D]*** *on NALM6-high-CD20 cells. In all cases cells were infected at MOI 1.0. N=2 independent experiments. Data shown is mean +/- SEM.*

Further experiments were carried out to investigate the viral replication by quantifying MV-N mRNA. The method of RT-qPCR measuring the expression of the MV nucleocapsid gene (MV-N) using hydrolysis probe (TaqMan™) gene expression assays using GAPDH as a reference gene, has been previously validated [226]. Figure 4-7 shows assessment of the viral genome by RT-qPCR for MV-N mRNA using the uninfected cells as a calibrator at 24 hour time points. The data shows a 5-6 log increase in the MV-N RNA occurring from 24 hours and being maintained for both NALM6 and NALM6-high-CD20 cell lines and for both MVNSe and MVHαCD20 over three days. This is comparable to primary ALL cells infected by MVNSe reached by day 5 [226]. There was no significant difference between the MV-N RNA levels between MVNSe and MVHαCD20 infected cells indicating that the viral replication remained constant over the three days.

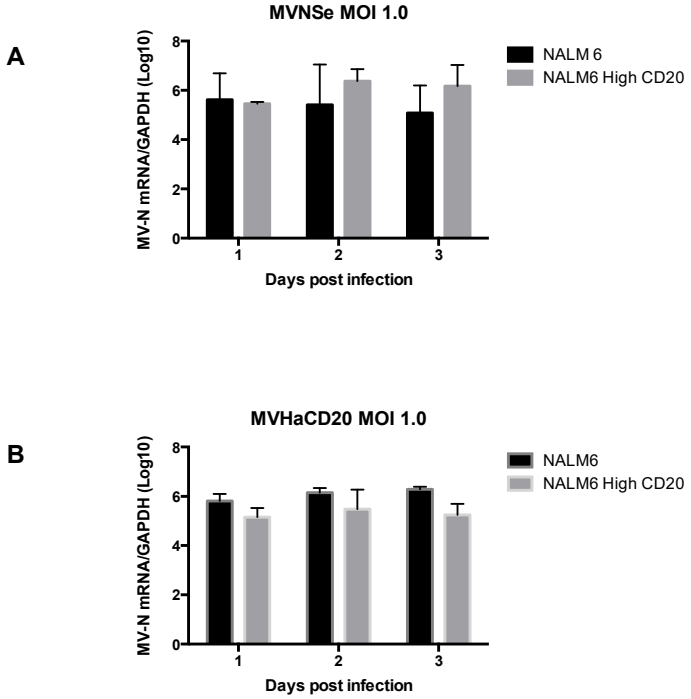

Figure 4-7 ***MV-N mRNA expression of NALM-6 and NALM6-high-CD20 cells following MV infection.*** *NALM6 and NALM6-high-CD20 cells were infected at MOI 1.0 with* ***[A]*** *MVNSe and* ***[B]*** *MVHαCD20. MV-N mRNA was quantified from RNA extracted from cells at 24 hour time points. mRNA extracted from uninfected cells served as the calibrator. GAPDH was used as the reference gene in all cases. Differences did not show statistical significance. Data shown is mean +/- SEM.* N=3.

4.5.4 MVHαCD20 infection results in greater cell death in ALL cells expressing CD20

To assess cell death, cells were stained with trypan blue and live cells subsequently counted. NALM6, NALM6-low-CD20 and NALM6-high-CD20 were infected with MVNSe or MVHαCD20 at an MOI 1.0. The proportion of live cells was calculated as a proportion of the respective uninfected condition. In [Figure 4-8] the data show that infection with the MVHαCD20 causes a comparable amount of cell death to infection with the parent virus - MVNSe - in unmodified NALM6 cells. This indicates that the virus fully retains its ability to infect via native MV receptors despite modification of the haemagglutinin glycoprotein. Infection by the CD20 targeted virus results in a marked increase in cell death in the CD20 expressing cell lines compared to that caused by the parent virus. This appears to be greater in the cells with 'high' expression of CD20 however the difference between the NALM6-high-CD20 and NALM6-low-CD20 expressing cells was not found to be statistically significant when analysed by unpaired student t-tests.

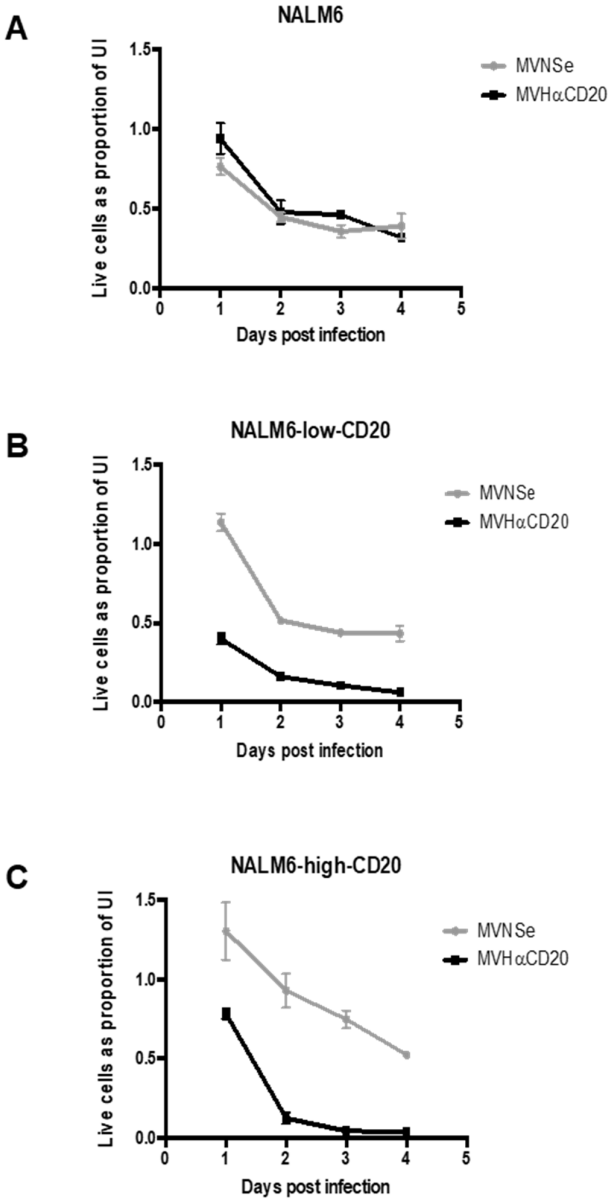

Figure 4-8 ***Live cells as a proportion of uninfected cells following MVHαCD20 infection or MV-NSe on NALM6 cells with differing CD20 expression.***

[A] *NALM6* ***[B]*** *NALM-6-low-CD20 and* ***[C]*** *NALM-6-high-CD20 cells were infected with MVHαCD20 or MV-NSe at MOI 1.0. Live cells were counted by trypan blue staining at 24 hour intervals for 4 days and expressed as a proportion of uninfected cells. Data shown is mean +/- SEM. N=3*

4.5.5 NALM6 cells expresses CD46 but do not express SLAM or Nectin4.

In order to investigate the effect of the blinded CD20 targeted MVs, (MVHαCD20SLAMblind and MVHαCD20CD46blind) it was first important to establish the expression of the native MV receptors on the experimental model cell lines, and on primary ALL cells. CD46 is expressed on all nucleated cells and found to be upregulated in malignant cells so high levels were expected. Nectin 4 is normally expressed on epithelial cells so would be unlikely to be expressed on leukaemia cells. SLAM expression in lymphoid cells is variable. Expression of the native MV receptors, CD46, SLAM and Nectin 4 was established by flow cytometry for the cell lines NALM6 and Raji using the conjugates CD46-FITC, SLAM-PE, and Nectin4-PE. These results (Figure 4-9) show that NALM6 express CD46 but do not express the native receptors SLAM and Nectin4. However, Raji, a Burkitt lymphoma cell line, which has been included due to its high CD20 expression, shows lower expression of SLAM (29%).

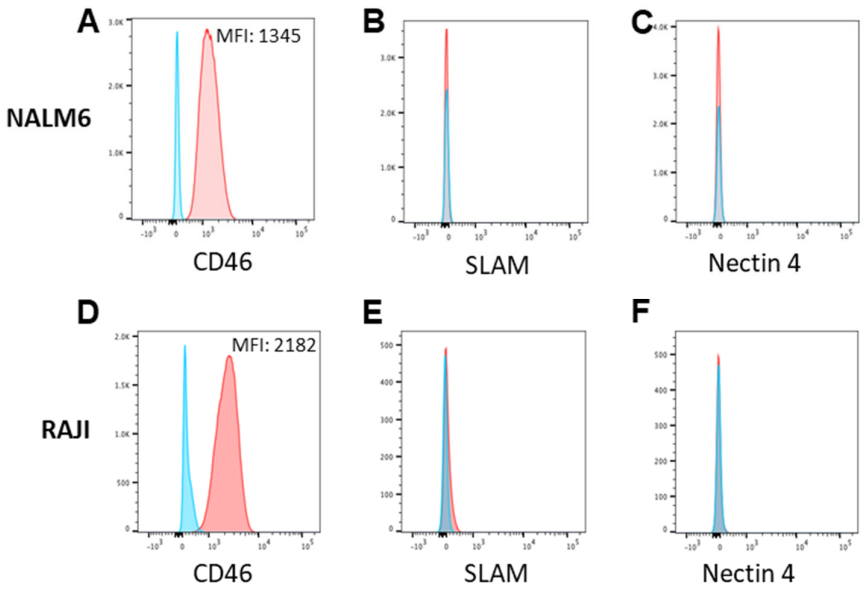

Figure 4-9 ***NALM6 cells express CD46 but not SLAM or Nectin 4.*** *NALM6* ***[A-C]*** *and Raji* ***[D-F]*** *cells were stained for CD46-FITC* ***[A,D]****, SLAM-PE* ***[B,E]*** *and Nectin 4-PE* ***[C,F]*** *. Corresponding isotypes were used as negative controls. Events were acquired with Fortessa X20.*

Red lines: cells labelled with antibody, Blue lines: Cells labelled with Isotype control.

4.5.6 ALL cells universally express CD46 but rarely express SLAM or Nectin 4.

Expression of MV receptors was measured as part of the multicolour flow panels in the previous chapter. There were 101 patients who had adequate viable cells that had been stained with the MV receptor stains CD46-BV605, SLAM-BV421 and Nectin 4-APC. As expected, all 101 patient specimens expressed CD46 (Figure 10A). One patient specimen (1%) expressed Nectin 4 and two patients (2%) expressed SLAM. However, the fluorescence for all three of the Nectin 4 and SLAM positive patient specimens were dim compared to the cell lines used as positive controls; H1975 for Nectin 4 and Vero-SLAM for SLAM (Figure 10B and 10C). Given that de Salort *et al* found 49% of normal pre-B cells, as previously shown in Table 1, expressed SLAM it is interesting that there were not greater numbers expressing SLAM in the primary ALL cells.

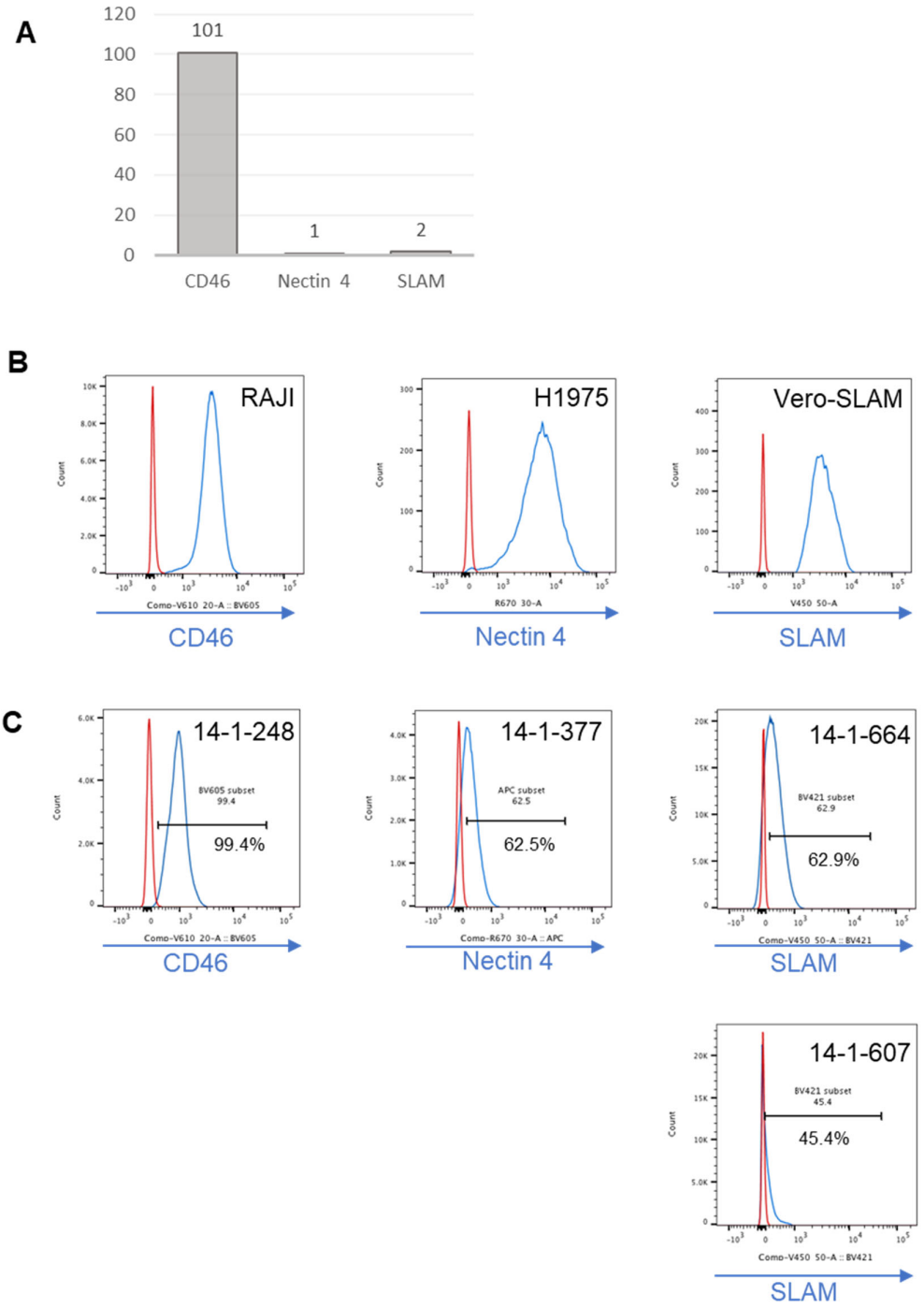

Figure 4-10 ***Expression of MV receptors CD46, Nectin 4 and SLAM of primary ALL cells****.*

101 patient samples were analysed by flow cytometry. Cells were gated on CD45-APC-H7, and the ALL markers CD10-FITC, CD19-PE-Cy7 and CD34-PerCP-Cy5.5 where positive. Dead cells were excluded by LIVE/DEAD™ aqua staining. ***[A]*** *All 101 specimens stained positive for CD46, one expressed Nectin 4 and two expressed SLAM (CD150).* ***[B]*** *Positive controls for CD46 (RAJI), Nectin 4 (H1975) and SLAM (Vero-SLAM)* ***[C]*** *A representative specimen is shown for CD46 expression and all patient samples expressing Nectin 4 or SLAM are shown.*

4.5.7 CD46 expression, as measured by mean fluorescent intensity (MFI) is significantly lower in leukaemic blasts than in normal lymphocytes.

CD46 has been considered a significant receptor for MV oncolysis and it is believed that the upregulation of CD46 in cancer cells provides increased protection from autologous complement destruction which this antigen confers as a negative complement regulator [115]. UKALL14 specimens were analysed using FlowJo software. The gating method is shown in Figure 11A. Leukaemic blasts were identified by dim expression of CD45, and positive expression of at least one of the markers CD10, CD34 and CD19. Normal lymphocytes were identified by high expression of CD45 and negative expression of the ALL blast markers CD10, CD34 and CD19. The geometric mean MFI of CD46-BV605 was measured for the ALL blasts and the normal lymphocytes where possible and the results shown in Figure 11C and 11D. The CD46 expression was significantly higher on normal lymphocytes than their corresponding blast cells. All the leukaemic blast populations had a MFI at least 1000 lower than RAJI, and only 4 patients had higher CD46 expression than NALM6. The difference in means was analysed using a two-tailed paired student t-test, mean of differences =185.5, standard deviation of differences = 308.3, standard error of the mean of differences = 33.84, 95% confidence interval 118.2 to 252.8. $p<0.0001$.

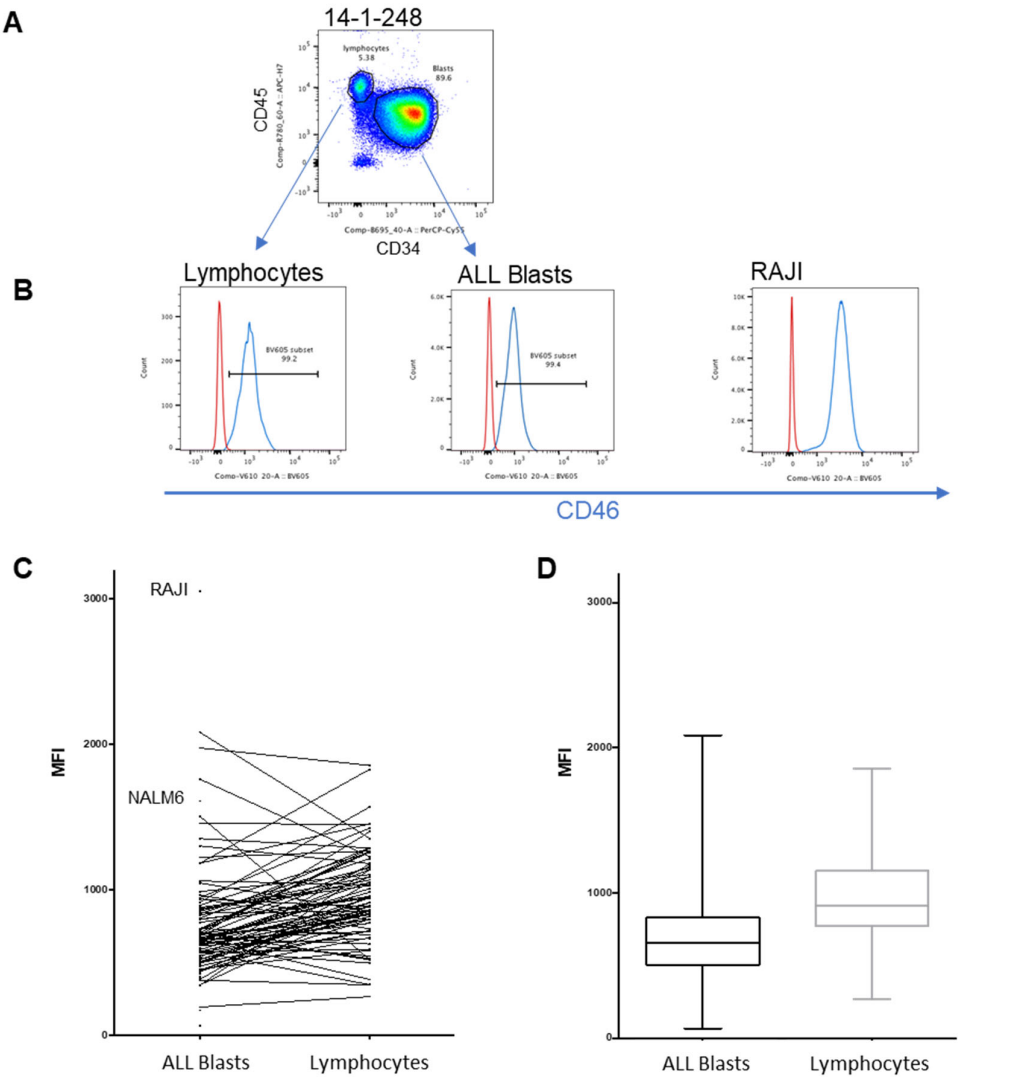

Figure 4-11 ***CD46 expression has a significantly lower MFI in normal lymphocytes compared to ALL blasts in paired patient UKALL14 specimens.*** *UKALL14 patient specimens were analysed by flow cytometry.* ***[A]*** *Normal lymphocytes were identified by high expression of CD45 and negative expression of the blast markers CD34, CD10 and CD19. A representative patient specimen is shown.* ***[B]*** *Histograms of CD46 MFI of lymphocytes and ALL blasts for the representative patient specimen. RAJI histogram represents a positive control. Blue lines represent specimen stained with antibody, red lines with isotype control* ***[C]*** *Graph showing CD46 MFI of paired blasts and lymphocytes in UKALL14 patient specimens. NALM6 and RAJI are included for illustrative purposes and not included in any statistical analysis.* ***[D]*** *The geometric MFI of ALL blasts in all patient samples were compared to that of lymphocytes identified in the same specimens. Student two-tailed paired t tests showed a mean of differences 185.5, p<0.0001.*

4.5.8 MVHαCD20 has greater oncolytic efficacy than MVHαCD20CD46blind

To investigate the efficacy of the blinded viruses compared to the non-blinded viruses, trypan blue counting experiments were carried out using NALM6, NALM6-low-CD20, NALM6-high-CD20, and RAJI cells using a similar experimental design to previously described experiments. The results are shown in Figure 4-12. The non-blinded viruses (in black), MVHαCD20 and MVNSe, showed similar oncolysis to the previous experiments. The CD46 blind virus (in grey) had little oncolytic effect except when it was re-targeted to CD20. The MVHαCD20CD46blind virus produced a comparable killing effect to the MVHαCD20 virus with marginally less efficacy. This could indicate that the efficacy of the CD20 targeting is from selective CD20 entry alone rather than from entry via CD46. Alternatively, it could be that the efficacy is additive with both the availability of CD20 and CD46 as entry receptors conferring an advantage. No significant difference between the low and high expressing CD20 cell lines was seen. Overall the data show that the CD20 targeting has a predominant effect over blinding to CD46.

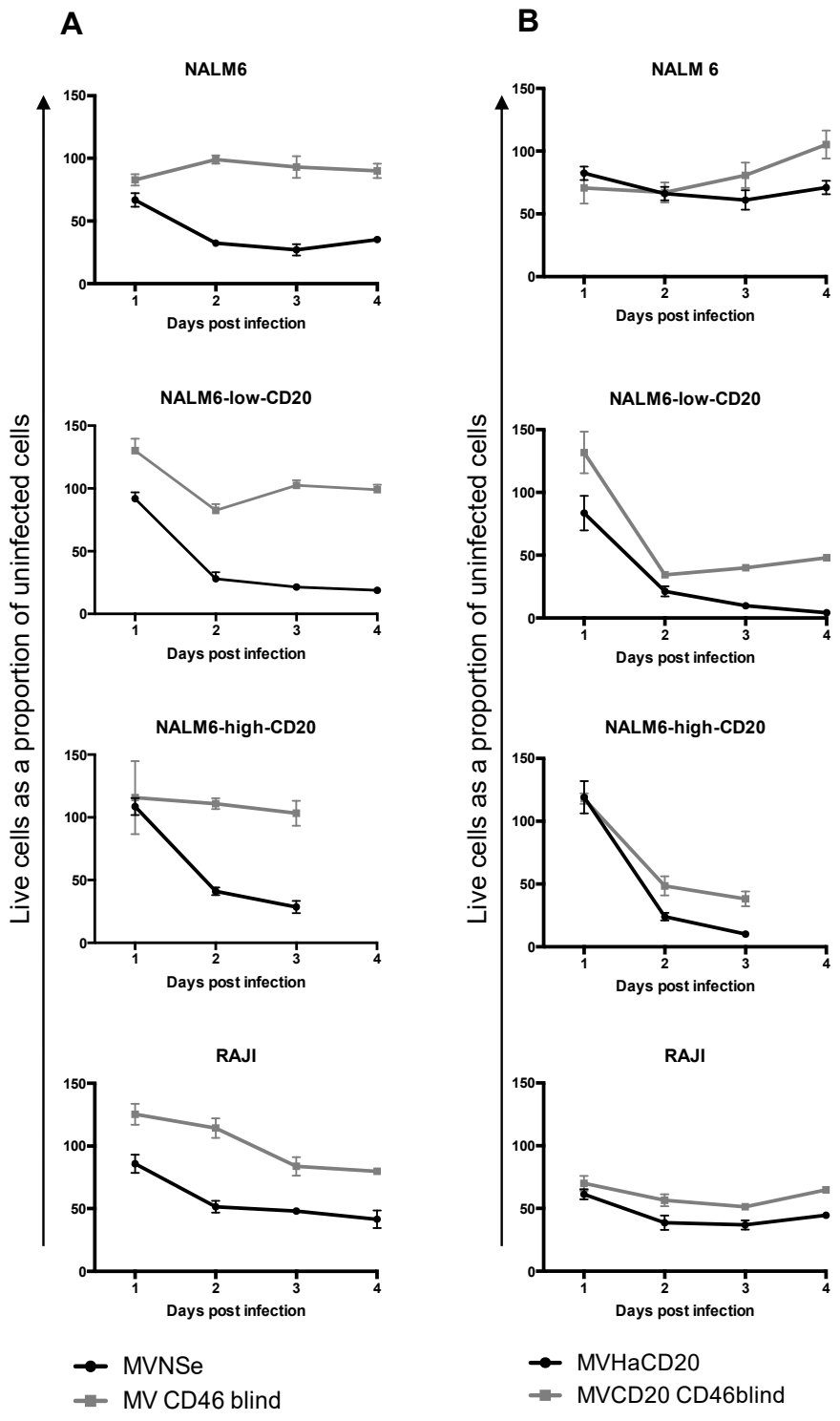

Figure 4-12 ***Live cells over time following infection with CD46 blind MV.*** *Column* ***A*** *shows cells infected by MVNSe and MV CD46 blind****,*** *Column* ***B*** *shows cells infected by MVHαCD20 and MVHαCD20CD46 blind****.*** *Cells were infected with MV at MOI 1.0. Live cells were counted by trypan blue staining at 24 hour intervals for 4 days and expressed as a proportion of uninfected cells. N=2. Data shown is mean +/- SEM of experimental replicates.*

4.5.9 MVHαCD20SLAMblind has similar oncolytic efficacy to MVHαCD20

As seen in Figure 13, the MVHαCD20SLAMblind virus killed target NALM6 cells with comparable efficacy to the MVHαCD20 virus, however there was initially less killing of RAJI. NALM6 cells do not express SLAM whilst RAJI cells do express a small amount of SLAM, so this result was as predicted. There was no significant difference between non-CD20 targeted viruses, MVNSe and MVSLAMblind for the NALM6 cells and NALM6-high-CD20 cells. The MVNSe had a small but significant killing benefit over the MVSLAMblind for the RAJI cells, as expected (Paired t-test, two tailed p=0.007). Overall the results of the trypan blue exclusion assays for CD20 targeted CD46 or SLAM blinded MV were consistent with the known expression of MV receptors on the cell lines.

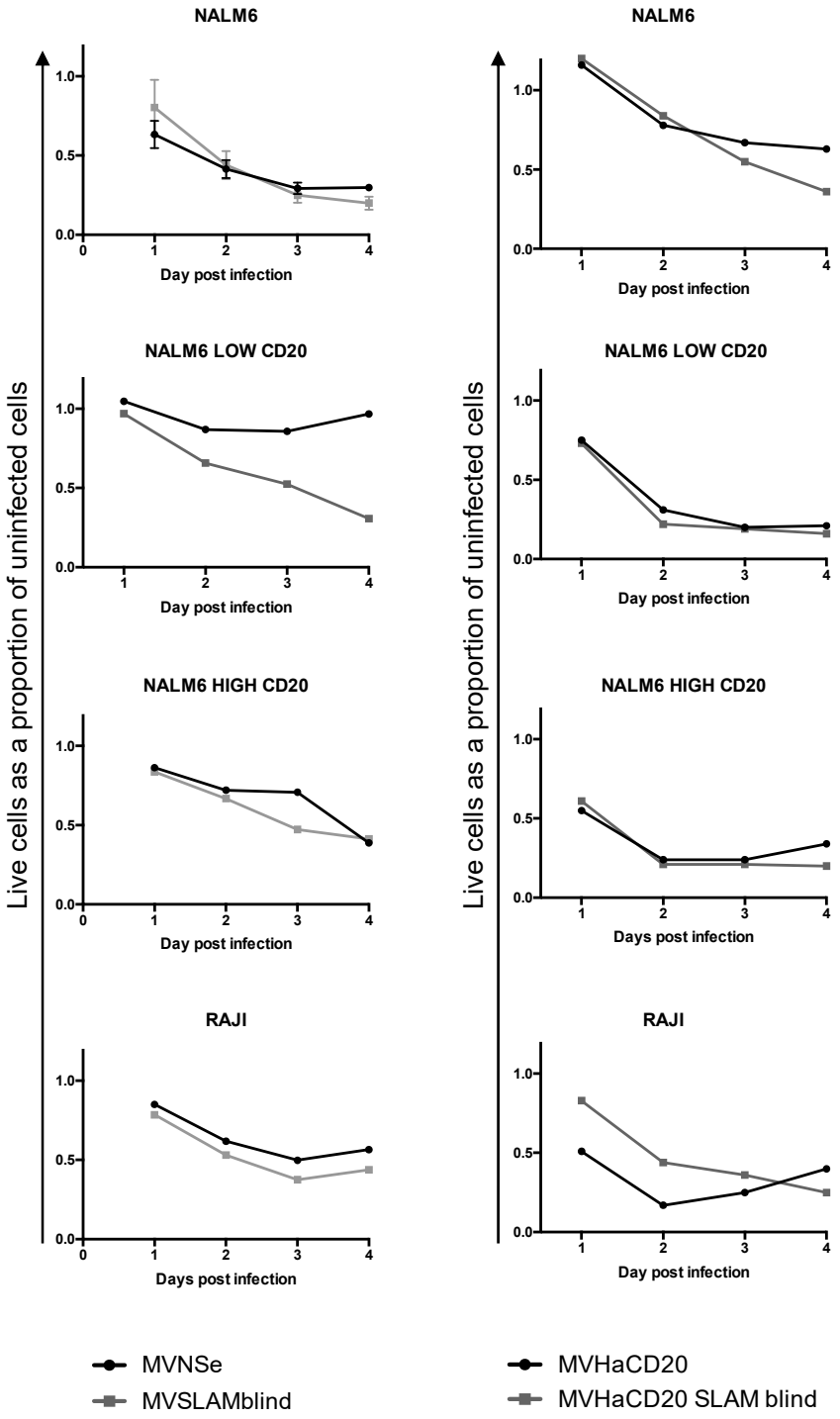

Figure 4-13 ***Live cells over time following infection with SLAM blind MV.*** *Right hand column are cells infected with CD20 targeted viruses. Cells were infected with MVHαCD20, MVNSe, MVHαCD20SLAMblind, or MVSLAMblind at MOI 1.0. Live cells were counted by trypan blue staining at 24 hour intervals for 4 days and expressed as a proportion of uninfected cells. N=1.*

4.5.10 Blinding MV to CD46 results in reduced complement dependent cytotoxicity.

CD46 is a negative regulator of complement, acting as a co-factor to Factor-I mediated cleavage of C3b and C4b. Assays using MV and CD46-blind MV variants were carried out to investigate whether complement dependent cytotoxicity (CDC) is a mechanism of MV mediated oncolysis in ALL cells. Infection with MV is expected to downregulate CD46 making cells more susceptible to CDC destruction. It would therefore be expected that the degree of CDC would be reduced in the CD46-blind viruses compared to its parent, non-blind virus.

CDC is a known mechanism of rituximab cytotoxicity so rituximab was chosen as a positive control for these assays. As shown in Figure 4-14, two timepoints were chosen: 2 hours and 24 hours. The early time point was chosen because complement destruction could theoretically play a role early in MV infection as part of the host's innate antiviral response. However, at 2 hours there was virtually no evidence of CDC as a mechanism in any of the cell line.

At 24 hours (Lower Figure 4-14) a greater amount of CDC was seen, although not quite matching the positive control. A mean of 8.73% specific complement lysis was seen in the NALM6-high-CD20 cells infected by the non-blinded virus MVHαCD20 whereas the blinded virus, MVHαCD20CD46blind, resulted in a mean specific complement lysis of only 3.71% (student t tests p=0.34). The overall amount of CDC was less in the NALM6-low-CD20 cells. MVHαCD20 infection resulted in specific complement lysis of 4.79% compared to 1.29% for MVHαCD20CD46blind. This difference was statistically significant when analysed by student t-test (p=0.03).

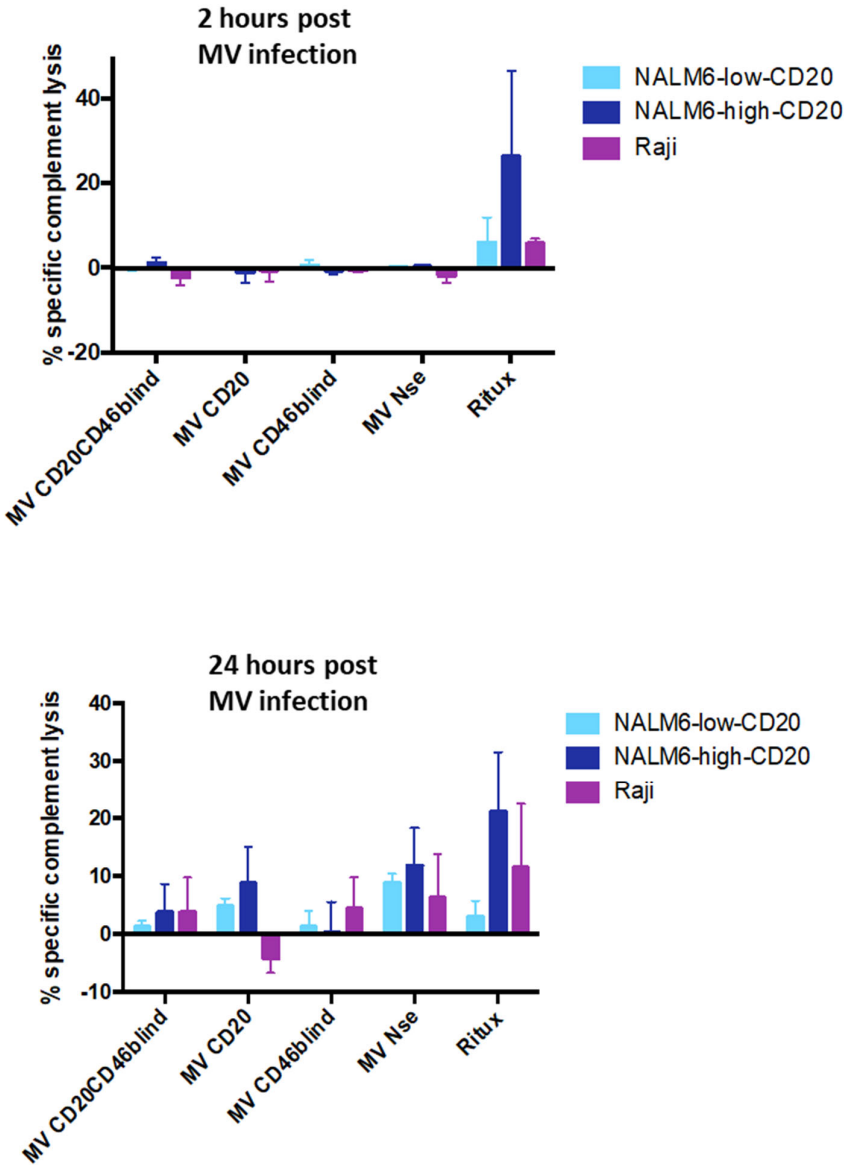

Figure 4-14a Complement Dependent Cytotoxicity (CDC) assay following infection with CD46 blind MV. *CDC after 2 hours (top) and 24 hours (bottom) post infection. Cells were infected with MVHαCD20, MVNSe, MVHαCD20SLAMblind, or MVSLAMblind at MOI 1.0. Rituximab was a positive control. Cell death was estimated with DAPI live/dead staining. Data shown is mean +/- SEM. N=3. The following page shows the gating strategy.*

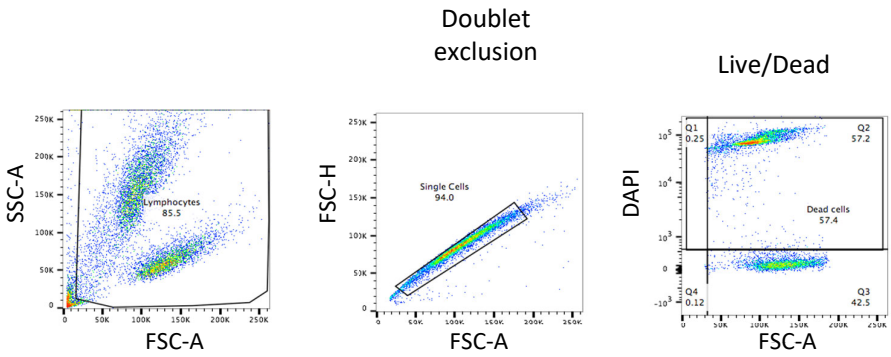

A: Live/Dead control

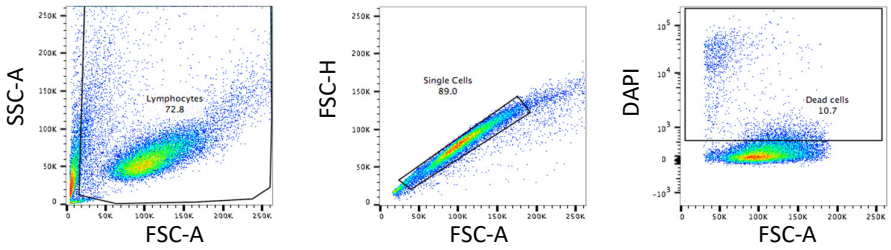

B: Example of CDC gating

Figure 4-14b: Gating Strategy for CDC experiments*. Live/Dead gating is determined from the live/dead control using DAPI staining* ***[A].*** *The identical gate is then applied to determine the proportion of dead cells in the experimental specimens* ***[B]****.*

4.5.11 MVHαCD20CD46blind infection induces less neutrophil-medicated antibody dependent cellular phagocytosis (ADCP) than MVHαCD20 when complement is present.

Antibody-dependent cellular responses may be critical to MV oncolysis and neutrophils have been shown to be a key mediator [149, 227]. A flow cytometry-based ADCP assay was chosen (see chapter 5 for a full explanation and methodological details) and carried out using MVHαCD20CD46blind and MVHαCD20 to determine whether the presence of complement resulted in less ADCP when infected by the CD46 blind virus.

Briefly, MV infected NALM6-high-CD20 cells were stained with the tracking dye PKH-67 and subsequently incubated with freshly isolated neutrophils, +/- complement, for 2.5 hours. The neutrophils were then stained with CD15-APC, and the co-culture analysed by flow cytometry. Events which are positive for both PKH-67 and CD15-APC were taken as a percentage of total CD15-APC staining cells. This is the percentage phagocytosis. Rituximab was used as a positive control, and both low-antiMV IgG antibody and no-serum conditions were negative controls.

The results (Figure 15) demonstrate that for both viruses the percentage phagocytosis was increased when complement was present. However, this effect was significantly blunted when the NALM6-high-CD20 cells were infected by MVHαCD20CD46blind. Where complement was present there was a significant difference between the viruses. The mean ADCP was 39.78% for MVHαCD20 infected cells compared to 31.4% for MVHαCD20CD46blind, (p=0.028). In summary, where complement was present, the non-blind virus, MVHαCD20, induced a greater degree of phagocytosis.

There are limitations to this method. Although doublets are excluded by gating, it cannot simply be determined whether the PKH-67 fluorescence is external or has been phagocytosed by the neutrophil. This is explored in greater depth in Chapter 5.

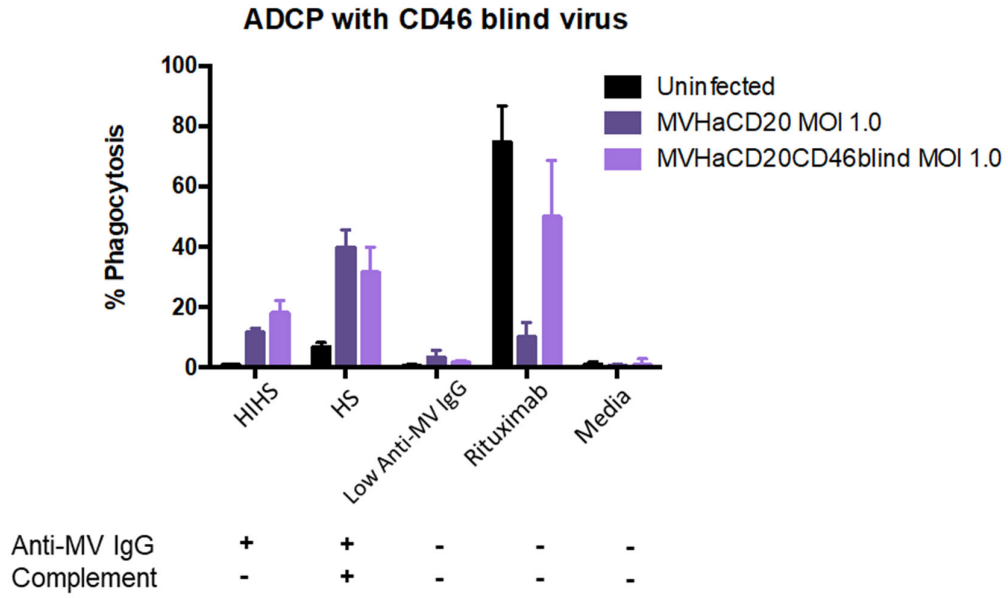

Figure 4-15 ***Neutrophil mediated Antibody dependent cellular phagocytosis (ADCP) assay with CD46 blind MV. Comparing the % phagocytosis in samples +/-complement.*** *NALM6-high-CD20 cells are infected with MVHaCD20 or MVHaCD20CD46 blind at MOI 1.0, 24 hours prior to PKH67 labelling and 2.5 hour co-culture with neutrophils. Heat inactivated human serum is heated to 56℃ for 30 minutes to inactivate complement. Low titre antiMVab HIHS and No ab are negative controls. Rituximab is used as a positive control. Data shows the percentage phagocytosis. Data shown is mean +/- SEM. N=3*

4.6 Discussion

Prof. Fielding's laboratory has previously demonstrated that disseminated pre-B ALL xenografts in severe combined immunodeficient (SCID) mice are highly sensitive to MV oncolysis resulting in prolonged survival and complete bone marrow remission [177, 226]. In this chapter I have explored the use of a MV targeted to CD20, MVHαCD20, which has previously been investigated in CD20 positive malignancies but not in acute lymphoblastic leukaemia [151]. In the previous chapter I have shown that increasing expression of CD20 in the UKALL14 patients confers a shorter event free survival, and as 66% of patients had leukaemic populations that expressed CD20 on greater than 10% of their cells, CD20 is an attractive target. In this chapter I have shown in a simple experiment that*, in vitro*, the targeted virus, MVHαCD20 is as effective at killing ALL cells in a monoculture as the native strain NSe virus even when CD20 is not expressed on the target cells. However, to take this further it would be necessary to investigate in an *in vivo* model whether the added targeting saw a greater oncolytic effect than the parent MVNSe, rather than the simple *in vitro* monoculture.

Given that the expression of CD20 is variable in ALL, it could be of added benefit for the virus to be able to enter target cells via more than one receptor. There is evidence that the efficacy of rituximab is reduced in malignancies that have a lower expression of CD20 [228] so this could apply to a MV that can only enter cells expressing CD20. Although I have shown in this chapter that it appeared that the killing effect of the CD20 targeted virus, MVHαCD20, was lower when infecting cells with a lower density of CD20 expression, it was not possible to demonstrate statistical significance. CD20 is upregulated by steroids. As lymphoblasts are extremely sensitive to steroids, they are routinely included in standard induction therapy for ALL. Dworzak *et al* investigated the CD20 levels of Austrian children treated for Pre-B ALL between 2000 and 2009. They found that, where there were adequate numbers of leukaemic cells to measure, paired diagnostic and follow-up samples on day 8, 15 and 33, showed an increased number of CD20 positive blasts in the follow up samples. They also demonstrated an increase in MFI following the seven-day steroid pre-phase [213].

In this chapter I have shown that the CD20 targeted MV, MVHαCD20, can infect and replicate in both NALM6 cells RAJI cells irrespective of their CD20 expression. Although theoretically able to infect via native MV receptors CD46 and SLAM, when CD20 is expressed there is greater cell death when infected by MHαCD20 than cells where CD20 is not expressed.

The MVHαCD20 could offer an alternative immunotherapy when rituximab resistance occurs, as shown by Yaiw *et al* in a MV re-targeted to CD20[218]. They demonstrated that the infectivity of their fully blinded virus $MV^{green}{}_{H}{}^{blind}$anti-CD20 was not impaired following rituximab administration in specimens from six patients with splenic marginal zone lymphoma and four with mantle cell lymphoma. However, unlike this study, they did not compare $MV^{green}{}_{H}{}^{blind}$anti-CD20 to a non-blinded anti-CD20 MV, but to the native MVNSe virus.

Although blinding the targeted MV to CD46 could potentially mitigate against off-target unwanted effects, maintaining the ability of MV to recognise CD46 may have three possible advantages. First, there is evidence that overexpression of CD46 can enhance oncolysis with Anderson *et al* finding there was a threshold over which CD46 expression, as measured by flow cytometry, resulted in an increase in CPE and cell killing. [115]. This fits with published evidence that malignant cells have a high expression of CD46 [221] However, in this chapter I have shown that although ALL cells in the UKALL14 patients universally express CD46, the expression level is lower than on the respective untransformed lymphocytes. The expression level, as measured by MFI was also considerably lower than the Burkitt's lymphoma cell line, Raji, and 96% of the patient specimen's leukaemia cells had an MFI lower than NALM6. The data in this chapter adds to the evidence that the susceptibility of the malignant cells to MV oncolysis is likely via means other than CD46 receptor density, such as defective interferon pathways [229].

A second advantage of a virus able to recognise and infect via CD46 is the subsequent downregulation of the CD46 antigen [222]. This, in turn, enhances the susceptibility of the cell to complement destruction. Schnorr *et al* also found that complement medicated lysis following MV infection is inversely associated with CD46 expression, as determined by MFI, in seven cell lines. [223] This could help explain the results from the CDC and ADCP experiments described in this chapter, where the non-blind virus had a greater effect than

the CD46 blind virus when complement was present. The importance of CDC has been implicated in vaccinia virus where CDC from humans treated with Pexa-vec (pexastimogene devacirepvec – an oncolytic vaccinia virus) has been measured. In a cohort of 14 patients with diverse malignancies treated with Pexa-vec, survival was inversely correlated with cell viability in a CDC assay (Spearmans r = -0.81, $p<0.001$) and thus positively correlated with CDC. [170] In MV research there is evidence that CDC is a mechanism of MV oncolysis. Nosaki *et al* were investigating a polymer coated MV and found that in mouse models increasing doses of the polymer coated MV resulted in increased CDC [230]. CDC in MV oncolysis is likely to be mediate by anti-MV IgG recognising MV epitopes displayed on the surface of the infected malignant cells. The increasing polymer coating would theoretically enable a greater proportion of MV particles to evade the host's immune system until the target is reached. The data from this chapter suggest that CD46 downregulation could enhance oncolysis. However, the benefit of maintaining CD46 recognition may be not extend to subsequent doses of MV if the downregulation of CD46 persists and thus reduces the cells' future susceptibility to the virus. It would have been interesting to carry out the CDC experiments with a greater proportion of serum – approaching physiological levels of 50% - and to see the effects of the anti-CD20 monoclonal antibody ofatumumab which exhibits higher levels of CDC than rituximab [231].

A third, more controversial advantage of MVHαCD20 compared to the blinded virus or parent virus, could be that the virus has an alternative receptor to CD20. This could provide an alternative means of viral entry both after treatment with CD20 targeted drugs such as rituximab which can result in transient downregulation of CD20 [232], and also for subsequent treatments with MVHαCD20 for the same reason. Yaiw *et al* suggests that this may be unnecessary as a fully blinded virus had efficacy following rituximab [218]. Even in an individual patient with CD20 positive ALL, there is a range of CD20 expression within the leukaemic blast population so some cells will be less susceptible to a fully blinded CD20-targeted virus than others.

The SLAM blind virus, MVHαCD20SLAMblind, produced similar time dependent cell killing to MVHαCD20. It would make a good candidate for further research to investigate whether avoiding the off-target effects MV by not infecting SLAM expressing immune cells, is of potential benefit. It is difficult to investigate the off-target effects that could potentially be mitigated by bypassing the immune cells which express SLAM without an immune

competent murine model [233]. The next chapter in this thesis explores the role of neutrophils in MV oncolysis but as SLAM is not expressed on neutrophils it was not investigated further as part of this project.

In conclusion, the targeted MVHαCD20 virus is a promising candidate for treating CD20 positive ALL and is also likely to be effective in the absence of CD20. Making the targeting more selective by 'blinding' to the native receptors CD46 and SLAM is potentially attractive as a means to avoid off-target effects. The CD20 targeted SLAM blind virus, MVHαCD20SLAMblind, resulted in comparative results to the non-blind virus, MVHαCD20, however the CD46 blind virus, MVHαCD20CD46blind resulted in reduced efficacy *in vitro*. Thus, for MVHαCD20CD46blind, the advantage of avoiding potential side effects, could be offset by the benefits of maintaining this targeting which sees an increase in complement mediated mechanisms of oncolysis *in vitro*. In the next chapter we investigate in more detail, the mechanism of MV oncolysis demonstrated by the neutrophil mediated antibody-dependent cellular phagocytosis (ADCP) assay.

Chapter 5 Antibody-Dependent Neutrophil-Mediated Oncolysis

5.1 Introduction

MV is showing promise as an oncolytic therapy in early phase clinical trials. MV oncolysis is evident in both primary ALL cells and in ALL xenografts [177, 226]. By understanding the mechanism of action, in particular its dependence on immune cells and the tumour microenvironment, we may better understand its role as a therapeutic. Previous work from Prof. Fielding's laboratory and others has demonstrated the importance of neutrophils in virotherapy [147, 227, 234], however their precise role remains elusive.

Neutrophils are the most abundant leucocyte in humans and are important players in innate immunity. Neutrophils can efficiently phagocytose microorganisms that have been opsonized by complement or antibody and can also directly recognise and internalize pathogens via PRRs such as toll-like receptors [235]. Neutrophils can directly phagocytose influenza-A virus *in vitro* and phagocytose influenza-A virus apoptotic infected epithelial cells *in vivo* [236, 237]. Neutrophils have also been shown to phagocytose CMV-infected cells [238] and RSV-infected cells [239].

Human neutrophils constitutively express the low-to-intermediate affinity IgG Fc receptors FcγRIIIb (CD16b) and FcγRIIa (CD32a). They also express the high affinity Fc receptor for IgG FcγRIa (CD64a) which is known to be upregulated in the presence of IFNγ and G-CSF. FcγRIIIb is the most abundant Fcγ receptor on neutrophils however targeting this does not confer efficiency tumour cytotoxicity, in contrast to targeting of the less abundant FcγRIIa [240]. Neutrophils can also be activated via FcαR1 (CD89) and this has been demonstrated with a bispecific antibody to CD20 and FcαR1 [241]. Prof. Fielding's laboratory has also shown that FcαR1 is upregulated by MV infection [242]. When neutrophils and tumour cells are incubated in the presence of IgA monoclonal antibodies the presence of neutrophil extracellular traps (NETs) can also be demonstrated however their significance has yet to be demonstrated in this context [243]. Antibody-dependent neutrophil mediated killing does not appear to depend on reactive oxygen species (ROS) – neutrophils taken from patients with chronic granulomatous disease are unable to produce ROS but are able to mediate tumour killing in the presence of appropriate monoclonal antibodies [244].

There have been reports that neutrophils perform cellular phagocytosis as a mechanism of antibody-based immunotherapy for cancer [245, 246]. Other described mechanisms of neutrophil killing include direct effects, i.e. from degranulation, complement dependent cytotoxicity, antibody dependent cellular cytotoxicity, antibody dependent cellular phagocytosis and neutrophil antibody dependent killing.

5.1.1 Neutrophils and oncolytic virotherapy

Neutrophils are important effector cells in oncolytic virotherapy. When neutrophils were depleted in a BCG model of immunotherapy for bladder cancer this abrogated the anti-tumour efficacy and also resulted in decreased trafficking of CD4+ T cells [247]. Fu *et al* demonstrated that neutrophils are important for tumour lysis. They modified HSV-2 by deleting the N-terminal region of the *ICP10* gene to produce a virus known as FusOn-H2 [248]. Surprisingly some of the 20% of cancer cell lines that were resistant to FusOn-H2 infection *in vitro* responded well to the therapy *in vivo* and saw a massive infiltration of neutrophils throughout the tumour tissue. An infiltration of innate immunity cells and signs of neutrophil-mediated cytotoxicity were also seen by Holl *et al* in breast and prostate cancer xenografts treated with recombinant oncolytic poliovirus PVSRIPO [247, 249].

Previous work in Prof. Fielding's laboratory showed that Raji tumours in mouse models resulted in an infiltration of neutrophils following injection with MV [147]. This study further showed that the oncolytic activity of a MV which was engineered to express GM-CSF was correlated with a greater tumour infiltration by neutrophils, however macrophages and NK cells were not seen. The role of neutrophils was further explored by Zhang *et al* who demonstrated that neutrophils infected by oncolytic MV, but not wild type MV, survived for longer in tissue culture. These neutrophils also produced anti-tumour cytokines such as MCP-1 which is known to recruit both monocytes and T-cells, TNFα, IL8 and IFNα and upregulated neutrophil degranulation markers and the release of TRAIL [227]. Neutrophil depletion also reduced the efficacy of MV oncolysis in a Raji xenograft [149]. To attempt to dissect out the role of neutrophils in MV oncolysis, the Fielding lab investigated neutrophil mediated ADCC as a putative mechanism. However, the results of these experiments indicated that neutrophil ADCC was not a mechanism of oncolysis in B-cell malignancies [250]. Neutrophil-specific lysis was determined by a chromium release

assay and for Nalm-6 cells infected with MVNSe there was no change in neutrophil-specific lysis upon addition of serum containing a high titre of anti-MV antibody in comparison to absence of serum, thus the role of neutrophils in MV oncolysis could not be explained by ADCC [250].

5.1.2 Antibody dependent cellular phagocytosis (ADCP)

ADCP is an important mechanism for the action of therapeutic monoclonal antibodies where cells opsonized by antibody are subsequently recognised and phagocytosed by effector cells. It is recognised as an important mechanism of therapeutic monoclonal antibodies such as rituximab, with the monoclonal antibody acting as a bridge between target and effector cell and is most frequently described with macrophages or monocytes as effector cells. There have been several reports of neutrophil mediated antibody dependent cellular phagocytosis (ADCP) as a mechanism of immunotherapy [245, 246], Most monoclonal antibodies are of the IgG1 isotype and are thus effective at engaging with effector cells such as macrophages, neutrophils or NK cells via Fcγ receptors. Clinical responses to rituximab have been correlated with the polymorphism 131 H/R in FcγRIIa [69] a receptor expressed by neutrophils and macrophages but not by lymphocytes or NK cells. Although this has previously been attributed to the successful ADCP by macrophages, it is possible that this could also be a result of mediation by neutrophils.

To further elucidate the mechanisms of MV oncolysis I carried out antibody dependent phagocytosis assays (ADCP) using freshly isolated human neutrophils as effector cells. The assay was based on a flow cytometry based protocol previously published [251]. During the course of this doctoral research, evidence published showed that the flow based ADCP assays employed to investigate the action of rituximab, similar to those used in my experiments, were not correctly measuring phagocytosis but a phenomenon called trogocytosis. I therefore used imaging techniques to determine whether this was also the case for MV infected NALM6 cells and attempted to investigate the role of neutrophils in the context of the co-culture.

5.2 Hypothesis:

Neutrophil mediated antibody dependent phagocytosis is a mechanism by which neutrophils can kill MV infected ALL cells.

5.3 Aims:

To investigate whether neutrophil mediated ADCP of MV infected ALL cells occurs *in vitro* and whether this is dependent on the concentration of anti-MV antibody.

To determine, using imaging techniques, whether the ADCP assay demonstrates phagocytosis or trogocytosis of MV infected ALL cells and to explore the subsequent effects of neutrophils.

5.4 Results

5.4.1 Neutrophil mediated antibody dependent cellular phagocytosis (ADCP) as a mechanism of MV oncolysis

Experiments were designed to explore the immune response to ALL cells infected with MV. Neutrophils were chosen as effector cells as our laboratory has previously demonstrated that they have an important role in MV-mediated oncolysis [149] The exact mechanism of neutrophil-mediated MV oncolysis has not been elucidated. ADCP is known to be a mechanism in the action of anti-cancer monoclonal antibodies such as rituximab [76] but has yet to be investigated as a possible mechanism for MV oncolysis. A FACS based assay was used to determine the percentage phagocytosis. Neutrophils that have engulfed the PKH67-stained target cells will be positive for both CD15 and PKH67. Figure 5-1 provides an example of the dot plots obtained and the gating strategy. All experiments were carried out using target cells expressing CD20 in order that rituximab could be used as a positive control.

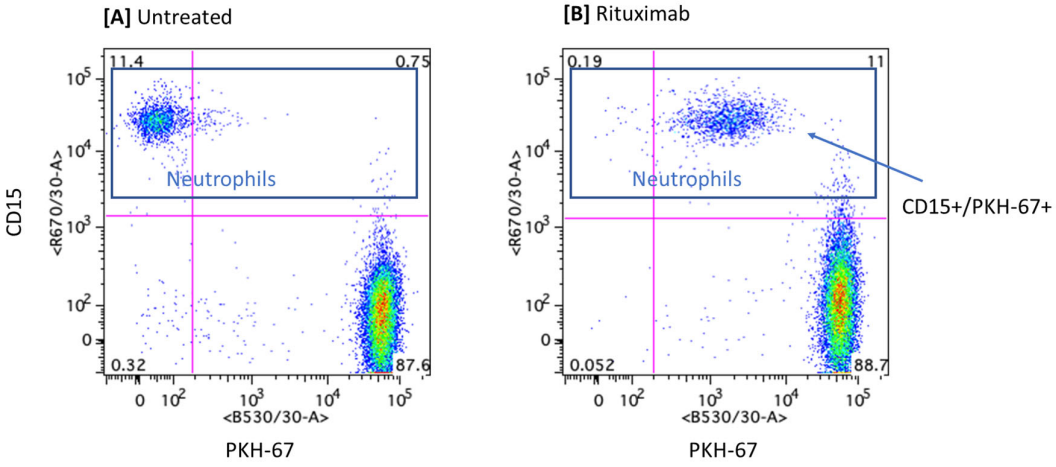

Figure 5-1 ***Representative flow cytometry dot plot of antibody dependent phagocytosis (ADCP) assay with CD15-APC stained neutrophils as effector cells and PKH67 stained NALM6 highCD20 cells [A]*** *untreated* ***[B]*** *with rituximab****.*** *Phagocytosis is calculated as $CD15^{+}PKH67^{+}$ cells as a percentage of total neutrophils. Events were first gated on live cells using DAPI as a live/dead indicator [See Appendix I].*

To determine the performance of the assay, a preliminary experiment was carried out, without MV infection, using rituximab at different concentrations. The level of phagocytosis was seen to be dependent on the level of CD20 expression with only modest levels of around 15% phagocytosis in NALM6-low-CD20 cells but high levels of approximately 60% phagocytosis in NALM6-high-CD20 cells Figure 5-2. Although there was a possible peak of response to rituximab at 1ug/ml overall there was no dose-response. The experiment was only carried out once and acted as a pilot study. Due to their positive results NALM6-high-CD20 cells were chosen for subsequent experiments to investigate whether ADCP is a possible mechanism of MV oncolysis.

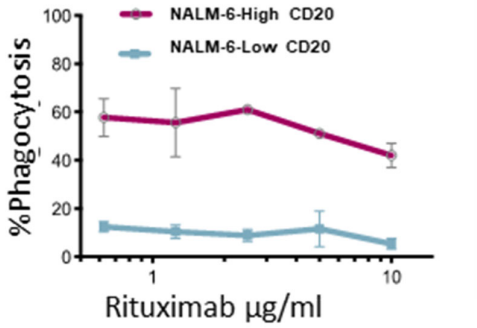

Figure 5-2 ***Neutrophil phagocytosis is increased in higher expressing CD20 cells in the presence of Rituximab at different concentrations.*** *Phagocytic assay carried out with uninfected NALM6-low-CD20 cells and NALM6-high-CD20 cells. Ratio of neutrophils to target cells 1:5, incubated for 2.5 hours. Rituximab concentration ug/mL is recorded on the x-axis as a log_{10} ;% phagocytosis is represented on the y-axis. Data shown is mean +/- SEM of 3 replicates in a single experiment.*

5.4.2 MVNSe and MVHαCD20 infection result in a positive finding in the ADCP assay

To investigate MV-mediated ADCP, NALM6-high-CD20 cells were infected with MV twenty-four hours prior to the co-culture. Human serum containing a high titre of anti-MV antibody (kind gift of Royal Free London NHS Foundation Trust virology laboratory) was added as a source of anti-MV antibodies and heated to 56°C for 30 minutes to inactivate complement. An optimal concentration of 1 in 100 had previously been determined by the lab [250]. Neutrophils from healthy donors were added at a ratio of 1:5, effector : target

cells as this has previously shown measurable levels of phagocytosis in preliminary experiments investigating ADCP against ALL targets in a different context [252].

Figure 5-3A shows that neutrophil phagocytosis of NALM6-high-CD20 cells after infection by MVNSe was evident in the presence of high anti-MV antibody containing human serum in which complement had been heated inactivated. When human serum contained both anti-MV antibodies and active complement the percentage of phagocytosis matched the positive control condition - uninfected NALM6-high-CD20 cells incubated with rituximab. Without antibody, minimal phagocytosis was evident and as with low titre MV antibody.

When the experiment was repeated using MVHαCD20 [Figure 5-3B] a similar trend was seen however the level of rituximab mediated phagocytosis was significantly reduced following MHαCD20 infection.

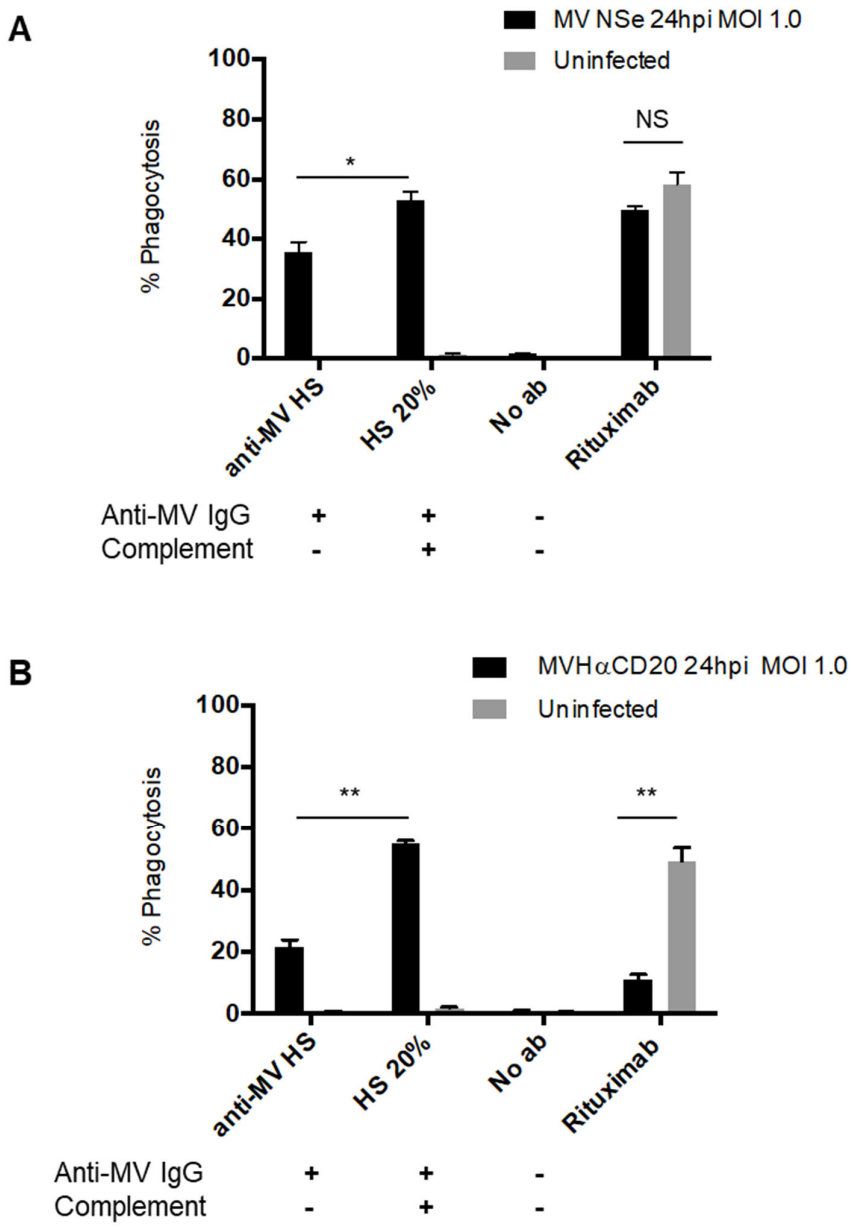

Figure 5-3 ***A positive neutrophil mediated ADCP assay reached similar levels following MV infection to rituximab in the presence of both anti-MV antibody and complement. %*** *Phagocytosis was measured compared in NALM6-high-CD20 cells +/-* ***[A]*** *infection with MV-NSe or* ***[B]*** *Infection with MVHαCD20. Either in the presence of rituximab 10ul/ml, human serum high in anti-MV antibody which has been heated to 56°C to inactivate complement, or human serum 20% as a source of complement. Data shown is mean +/- SEM. Students t-test. *p=0.0024, **p<0.0001. N=3.*

In a separate experiment, NALM6-high-CD20 cells were infected with MVNSe, MHαCD20 at a MOI 1.0, or were uninfected as a monoculture. By measuring the fluorescence intensity of CD20-APC stained NALM6-high-CD20 cells 24 hours following infection, those infected with MHαCD20 had a lower MFI than either MVNSe infected or uninfected cells, suggesting that the CD20 antigen is either masked by the MVHαCD20 or CD20 is downregulated 24 hours post-MV infection, as has been demonstrated following rituximab treatment of chronic lymphocytic leukaemia cells [232] Figure 5-4.

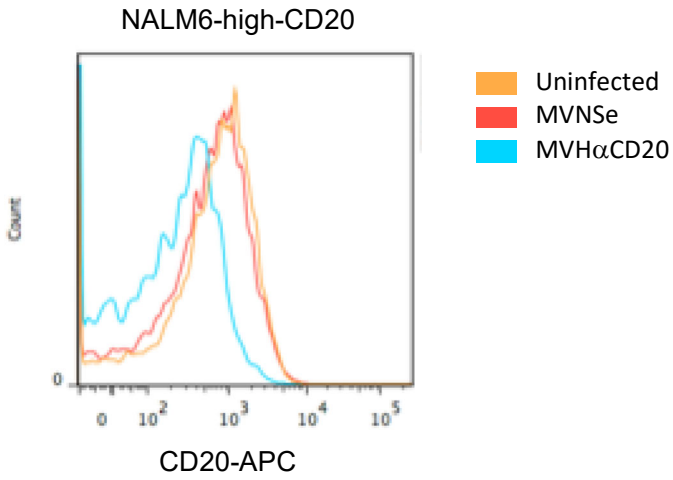

Figure 5-4 ***CD20 MFI decreases following 24 hours post infection MVHaCD20 MOI 1.0.*** *NALM6-high-CD20 were infected with MVHaCD20, MVNSe or were uninfected. 24 hpi the cells were stained with CD20-APC and events acquired on BD Fortessa. N=1*

5.4.3 The proportion of positive cells in the ADCP assay is dependent on the quantity of anti-MV IgG

To determine whether phagocytosis following MV infection was an antibody mediated phenomenon, the relationship of the concentration of MV antibody to ADCP assay was investigated using healthy donor samples of differing anti-MV antibody concentration. In order to obtain negative controls with serum containing IgG, but not anti-MV IgG, nine serum samples were obtained from the UCLH virology department that had tested negative for anti-MV IgG according to their DiaSorin EXCEL Measles IgG chemiluminescent immunoassay – a semiquantitative assay - were collected between April 2016 and

September 2016. These were re-analysed using a MV ELISA kit and the anti-MV IgG of these 'negative' samples ranged from 0 to 1800 mIU/ml with only three specimens <200mIU/ml deemed non-immune according to manufacturer's literature [Figure 5-5A]. The anti-MV IgG concentrations collected from normal healthy donors who had mounted an immune response ranged 2000 – 4000 MIU/ml. The 'best fit' curve was found using Microsoft® Excel software. There was a strong correlation between MV anti-IgG concentration and the degree of phagocytosis demonstrated by this assay with R^2 0.9404 [Figure 5-5B]. These data suggest that the ADCP observed is antibody mediated.

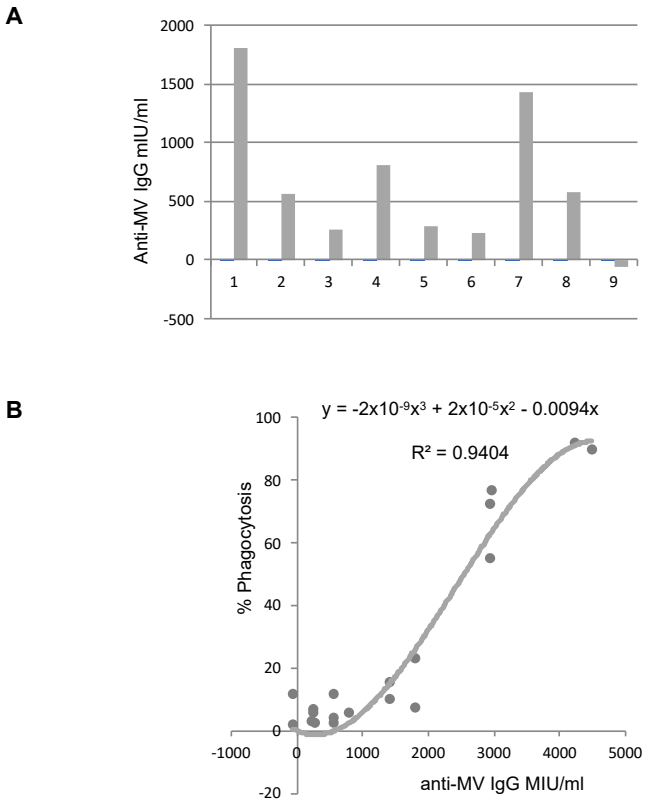

Figure 5-5 ***ADCP assay result is related to concentration of anti-MV IgG [A]*** *Samples which had been 'non-immune' for anti-MV IgG using DiaSorin EXCEL Measles IgG chemiluminescent immunoassay were re-analysed using Measles Virus IgG ELISA (IBL international).*

The graph in figure ***[B]*** *shows the results of the ADCP assay when carried out using human serum with a range of anti-MV IgG concentrations to investigate a dose-dependent response. MV IgG concentrations were determined using the MV IgG ELISA. The best fit curve was determined using Microscoft® Excel.*

5.4.4 Imaging flow cytometry and confocal microscopy show true phagocytosis to be a rare event

During the course of carrying out these experiments, new data was published which shed considerable doubt on whether the flow based ADCP assay used in previous experiments was correctly measuring neutrophil phagocytosis, and suggested a process called 'trogocytosis' or 'shaving' as an explanation for the data [253]. Trogocytosis is a mechanism where a small amount of target cell membrane in 'nibbled' by the effector cell. In order to determine whether the entire target cell was being engulfed by the neutrophil effector cell (phagocytosis) or small amounts of target cell membrane was being transferred to the neutrophil (trogocytosis) imaging flow cytometry and confocal microscopy experiments were carried out to enable direct visualisation of individual cells.

In order to visualise individual cells that would be classified as positive for phagocytosis in previous experiments, Imaging flow cytometry was used in 3 independent experiments. This enabled the ADCP experiment to be carried out using identical staining methods, and DAPI was also added to visualise the nucleus. This was useful to clearly distinguish between target and effector cells as neutrophils have a segmented nucleus whereas NALM6 cells have a large, rounded non-segmented nucleus. Bright field using a x63 objective lens, and fluorescence data for every cell is collected by the cytometer and can form a composite image, thus enabling phagocytosis or trogocytosis to be distinguished. Figure 5-6 shows Imagestream analysis for the co-culture incubated with rituximab (positive control) and Figure 5-7 shows the results where MVHαCD20 infected NALM6-high-CD20 cells have been co-cultured with neutrophils. Overall, the images in both conditions appear similar. The gating strategy for Imagestream is shown in Figure 5-6A and Figure 5-7A. The left hand panel shows how images that are in focus are included, and the right hand panel shows the method for gating singlets. Figure 6B and 7B show the Imagestream data. The top panels indicate the rare events which are strongly double positive for the tracking dye PKH67 (green) and CD15-APC (red). These images could indicate true phagocytosis. The second row shows less 'positive' cells, and they have several convincing areas of PKH67 (green) staining inside the CD15-APC (red) stained neutrophils. The neutrophils in the row below, third row down, also contain small, faint PKH67 staining. Both the second and third row could fit the description for trogocytosis. The fourth, bottom row, show neutrophils where no visible PKH67 tracking dye can be seen. These would also have been counted as

negative in the original ADCP assay. Imagestream analysis showed that true phagocytosis was a rare event.

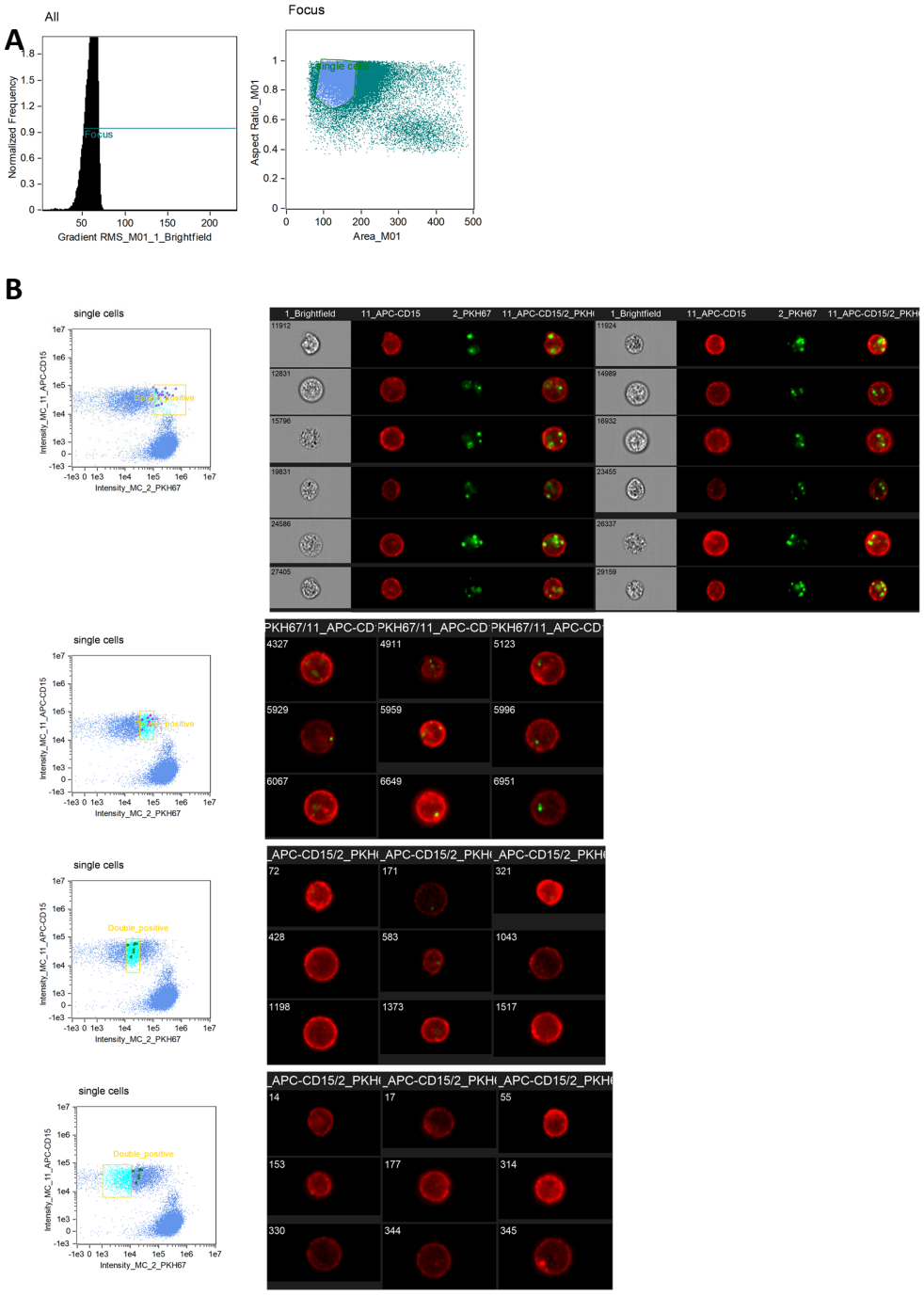

Figure 5-6 ***Imagestream analysis of ADCP assay – rituximab condition. [A]*** *shows gating – left hand gating for cells in focus, right hand – gating for singlets* ***[B]*** *Images showing representative images at differing PKH67 positivity. Top row shows most positive, bottom least positive. Red is APC-CD15 stained neutrophils, Green is PKH67 tracking dye. N=3*

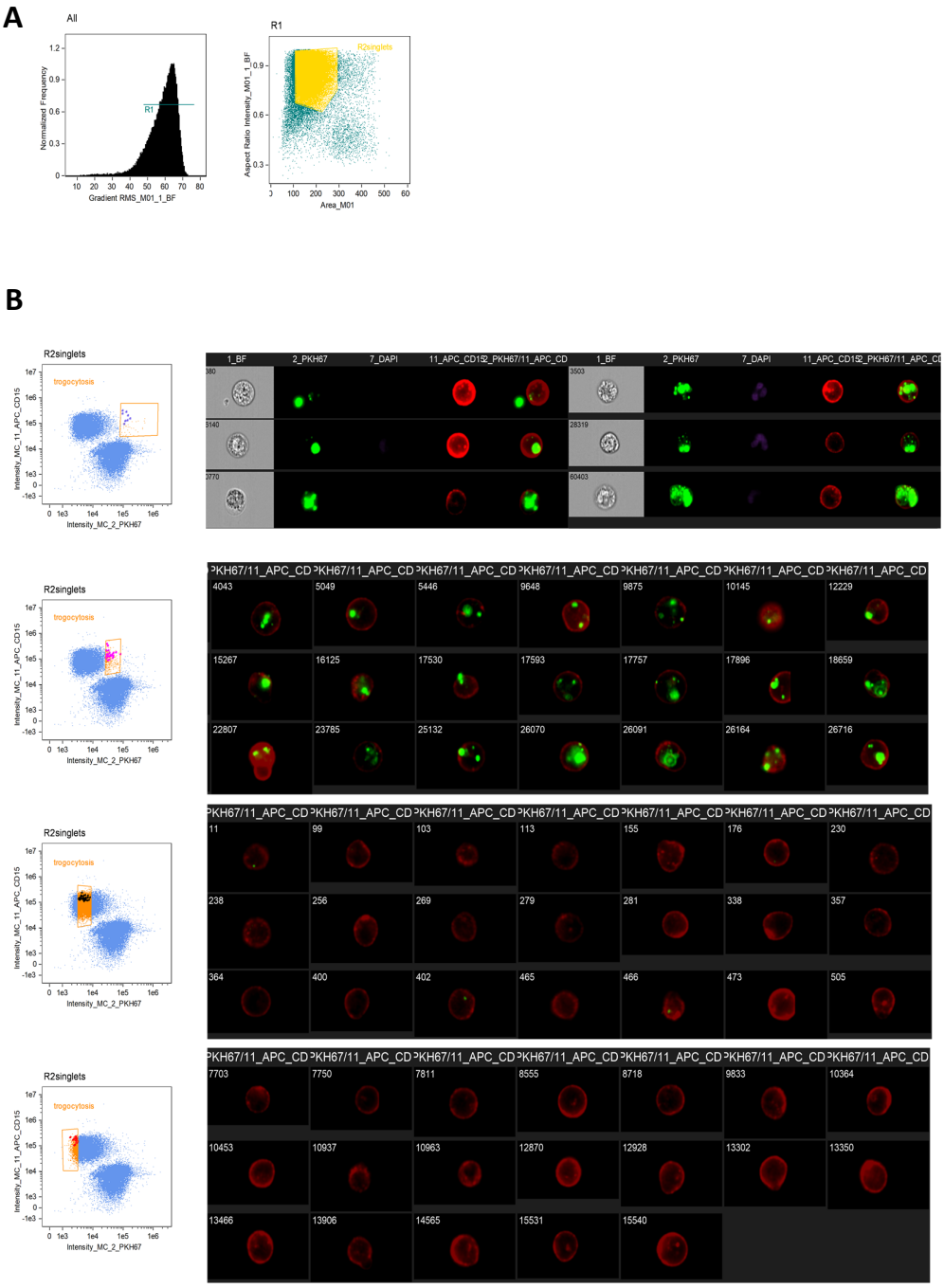

Figure 5-7 Imagestream analysis of ADCP assay – MV infected NALM6 cells. [A] *shows gating – left hand gating for cells in focus, right hand – gating for singlets* ***[B]*** *Images showing representative images at differing PKH67 positivity. Top row shows most positive, bottom least positive. Red is APC-CD15 stained neutrophils, Green is PKH67 tracking dye. N=3*

5.4.5 Neutrophils had increased mobility, morphological changes and showed trogocytosis when ALL cells had previously been infected with MV.

In order to visualise changes for the duration of the co-culture, time-lapse confocal microscopy experiments were carried out. Neutrophils engulfing NALM-6 cells (phagocytosis) was not seen during the time-lapse confocal microscopy experiments in any of the experimental conditions, including the rituximab condition, but phagocytosis of control magnetic beads was clearly demonstrated. [Figure 5-8C]. To analyse the co-culture videos by a semi-quantitative method, each neutrophil was individually assessed for the entire time lapse to assess any transfer of PKH-67 dye to indicate trogocytosis [Figure 5-8A] the number of different ALL cells it touched [Figure 5-8B]

Morphology changes during the time-course were assessed [Figure 5-9]. Neutrophils appeared to be more mobile in conditions where NALM6-high-CD20 cells had been infected with MV and anti-MV IgG was present. PKH67 membrane dye transfer could be seen, indicating trogocytosis, but it was not possible to accurately compare the infected condition with the rituximab condition as the staining of the infected cells where syncytia are present, consistently appeared fainter than in the uninfected conditions

Z-stack analysis enabled a 3-dimensional analysis and showed that the membrane stain was internalised by the neutrophils during the trogocytosis process [Figure 5-10].

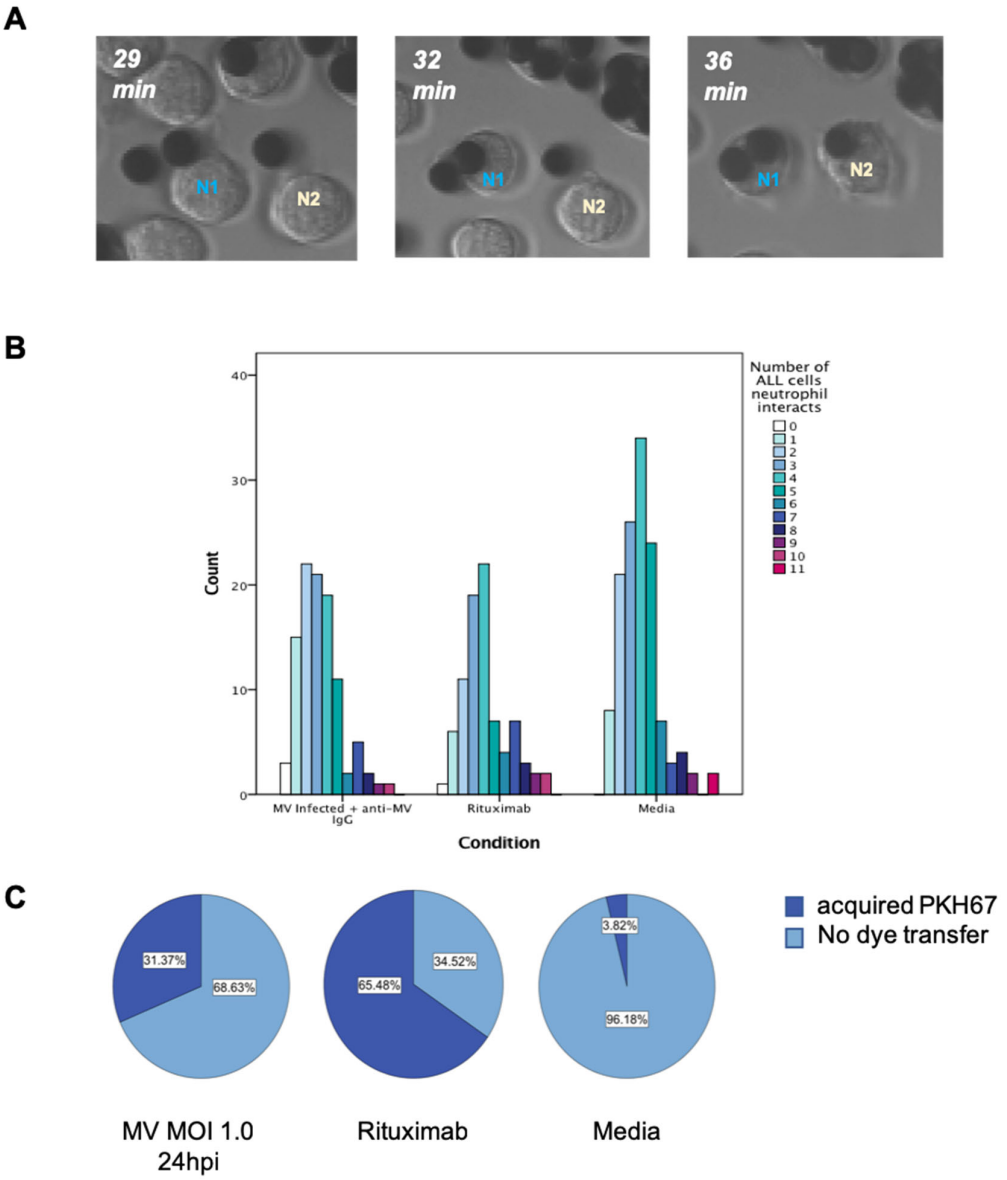

Figure 5-8 ***Neutrophils showed acquisition of of PKH67 dye from NALM6 cells, and greater activity when in co-culture with NALM6-high-CD20 infected by MV-HαCD20 than with uninfected targets alone****. Membrane is internalized. Live time-lapse confocal images of co-cultures were analysed by* ***[A]*** *A control using magnetic beads to test for phagocytosis was run in duplicate* ***[B]*** *counting the number of ALL cells that each neutrophils interacted with during 130 min incubation. Targets were stained with PKH67, Neutrophils were unstained. [C] counting the number of neutrophils that acquired PKH67 tracking dye from ALL cells. All conditions were run in duplicate. Overall 6 donors contributed their neutrophils.*

A

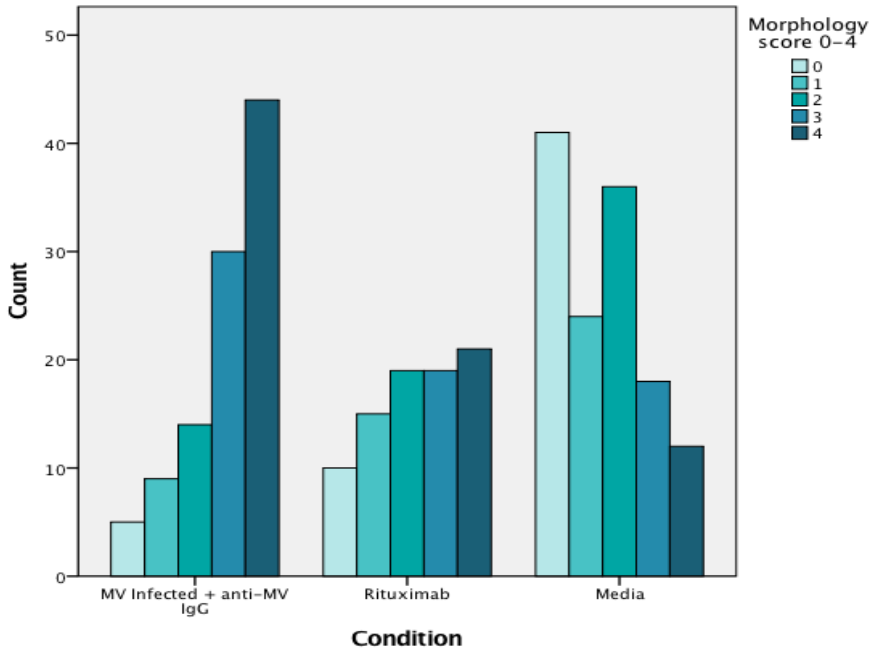

B

0: Remains rounded throughout incubation period

1: Single podocyte visible up to 3 times

2: Often several podocytes but maintains round form

3: Increasing alteration of morphology altering roundness

4 Very active cell often with spindle shape and bizarre forms.

Figure 5-9 ***Neutrophils showed greater morphological changes when in co-culture with NALM6-high-CD20 infected by MVHαCD20 than with uninfected targets alone****. Figure [**A**] shows the results of live time-lapse confocal images of co-cultures that were analysed by assessing with a score of morphological alteration as shown in **[B]** over 130 min incubation. The 3 conditions were run in duplicate with a different donor's neutrophils, NALM6-high-CD20 24hpi MVHαCD20 MOI 1.0 with heat inactivated human serum as a source of anti-MV IgG, uninfected conditions were rituximab and media alone. Target cells were added to the microscope slide approximately 1 hour prior to microscopy, neutrophils were added 20mins prior to image acquisition allow the cells to settle on the slide. Video recordings of the co-culture were later assessed by the author using Fiji (ImageJ) software*

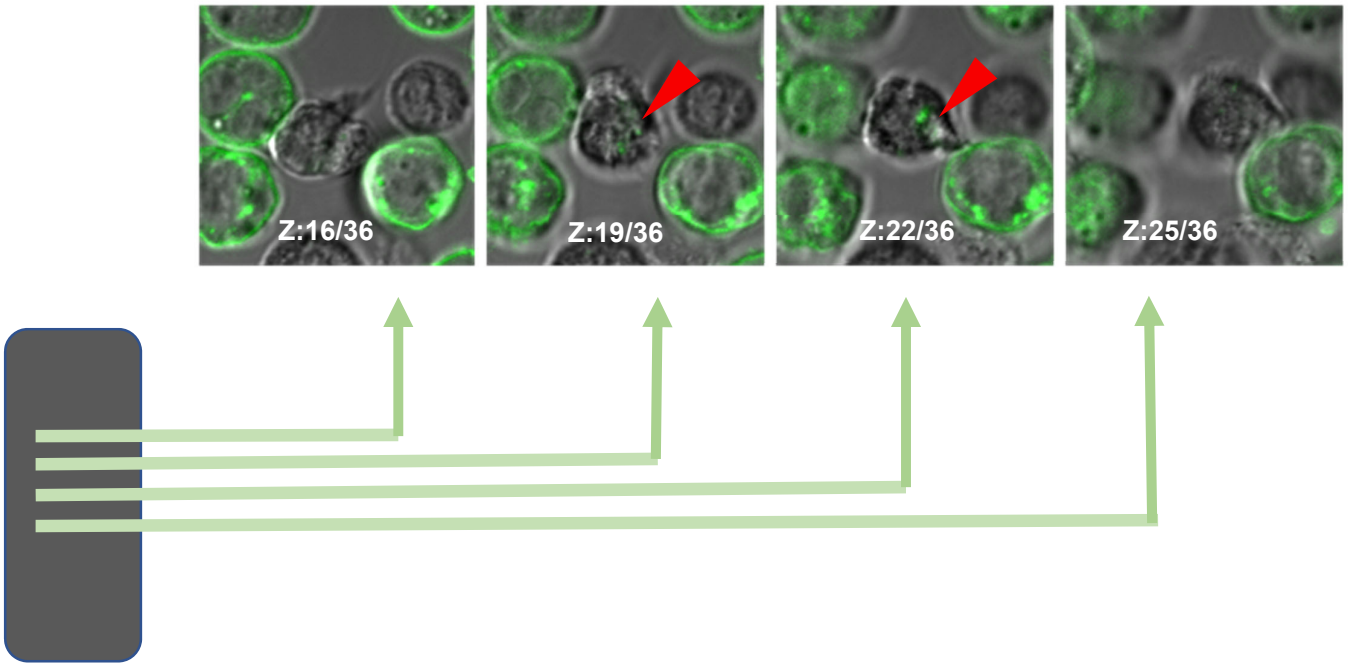

Figure 5-10 ***Confocal imaging Z-stack indicates internalization of PKH67 staining by neutrophil.*** *Z-stack analysis enables visualization in 3 dimensions. This image shows apparent internalization of PKH67 staining by a neutrophil as indicated by the red arrows which is not present in the layers 'above' or 'below' suggesting the stain is inside the cell rather than on the cell membrane. NALM6-high-CD20 cells were stained with PKH67 prior to incubation with unstained, freshly extracted donor neutrophils. Numbers indicate the layer within z-stack (total 36 layers). N=4.*

5.4.6 Trogocytosis does not directly result in increased target cell death.

In order to determine if trogocytosis resulted in target cell death, an analysis of the cell viability during the ADCP assays was performed using viability stains. The data are illustrated in Figure 5-11. There was no significant reduction in the viability of either neutrophils or target cells corresponding with the trogocytosis seen. It is possible that trogocytosis confers a slower mechanism of cell death – for example, by repeated removal of small portions of cell membrane - and that the *in vitro* data does not fully represent the *in vivo* situation. The viability of neutrophils *in vitro* is dramatically reduced at 24 hours so these assays would be difficult to perform.

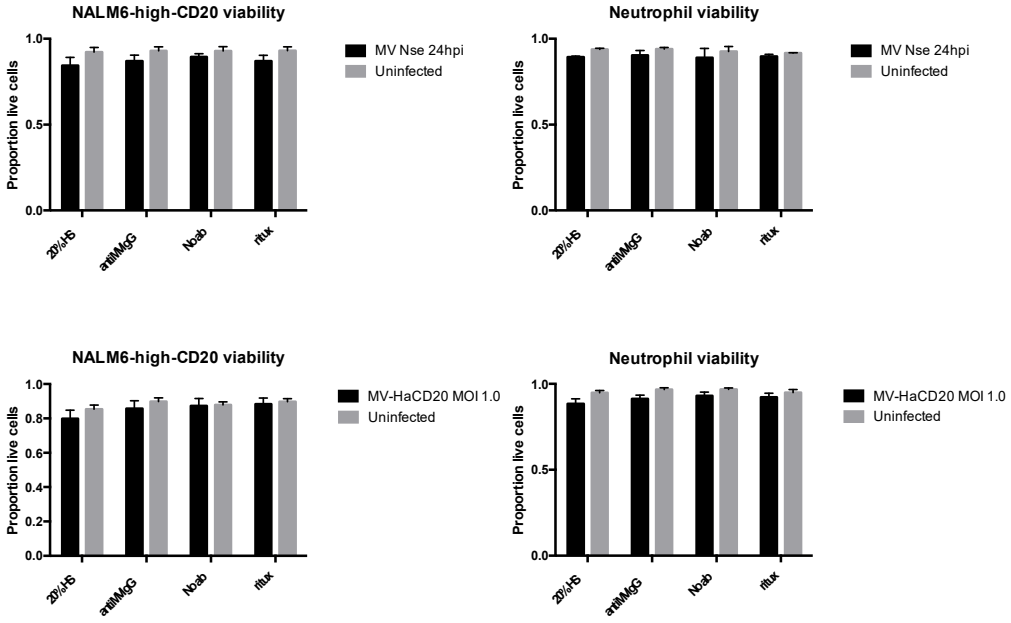

Figure 5-11 ***Live/dead analysis of NALM6-high-CD20 cells and neutrophils in ADCP assays****. Infected NALM6-high-CD20 were co-cultured with freshly extracted neutrophils from healthy donors for 2.5 hours at 37ºC; 5% CO_2, stained and acquired on Fortessa as previously described. In figures* ***[A]*** *and* ***[B]****, ALL cells were infected with MVNSe, in figures* ***[C]*** *and* ***[D]*** *cells were infected with MVHαCD20. There was no significant difference between incubation conditions (2 way ANOVA). Where cells were uninfected the viability is higher both for neutrophils and NALM6-high-CD20. For neutrophils this value only reaches significance when infected by MVHαCD20 (p=0.003) and is approached significance when infected by MV NSe (p=0.066), for the target cells the difference is significant in the MV NSe infected experiments (p=0.016) but not in MVHαCD20 (p=0.234). For MVHαCD20 N=4, for MV NSe N=3*

5.4.7 Relationship of trogocytosis and neutrophil activation

Previous work from Prof. Fielding's laboratory has suggested that neutrophil infection with MV Moraten (a vaccine strain of MV) resulted in the activation of neutrophils [227]. The highly significant morphological changes observed in the previous experiments (Figure 5-10) are also suggestive of activation. To determine the relationship of neutrophil activation to trogocytosis a six multicolour flow cytometry panel was designed to identify neutrophils within the co-culture and concurrently measure the activation markers L-selectin, CD66b and CD11b by MFI [Figure 5-13]. The following antibody-fluorochrome conjugates were used: CD11b-BV605, CD62L(L-selectin)-PE, CD66b-BV421, CD15-APC, PKH-67, and eFluor™ 780 (live/dead stain). When neutrophils are activated, L-selectin (CD62L) is shed from the cell surface so expression would be expected to fall. Conversely CD11b (an integrin family member) and CD66 (a glycoprotein involved in cell adhesion) would be expected to rise. Figure 5-13A shows the gating strategy. Singlets were first gated, then live cells gated as those negative for eFluor™ 780, and finally those staining for CD15-APC (i.e. neutrophils). The CD20 positive cells, NALM6-high-CD20 and Raji were used as a positive control for rituximab mediated trogocytosis. Having both NALM6-high-CD20 and Raji was important because L-selectin was only available as a PE conjugate and therefore could not be used with NALM6-high-CD20 as they expressed RFP and thus there would be a high level of spectral overlap. NALM6 was a negative control for rituximab.

The presence of human serum containing antibody appears to make a difference to the activation markers of the neutrophils in the uninfected conditions. In NALM6 and Raji cells the conditions containing human serum (antiMV IgG and HS) have lower levels of L-selectin compared to the conditions containing media or rituximab. For all three cell lines the level of CD66b is higher in the serum conditions (antiMV IgG and HS) than media alone. The expression level of CD11b is higher for the antiMV IgG in all three conditions. Thus, neutrophils show greater activation when incubated with target cells and human serum, with or without complement.

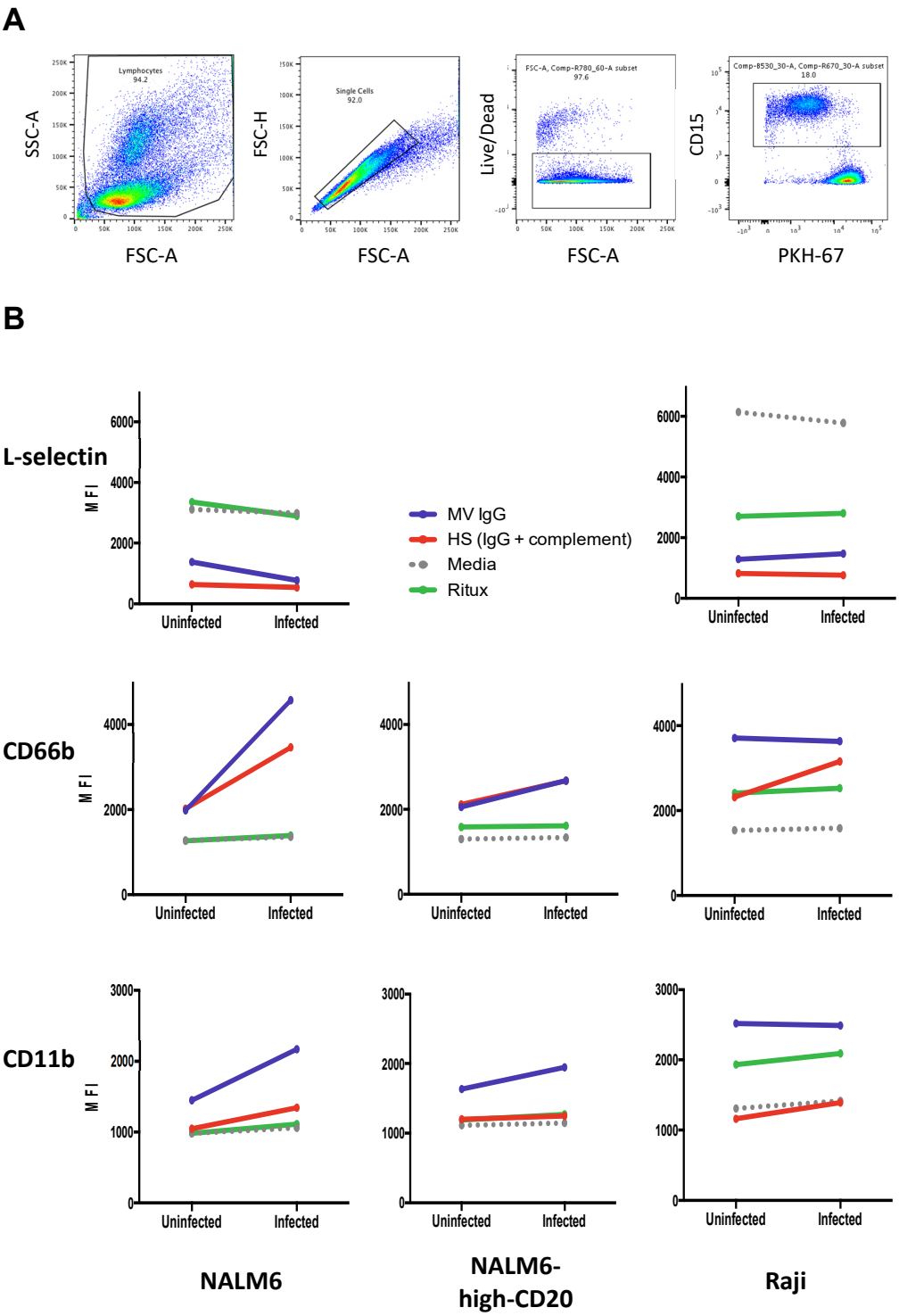

*Figure 5-12 N**eutrophils activation in ADCP assay** Co-cultures were prepared as previously however staining was with a 6 colour neutrophil activation panel. Figure **[A]** shows gating strategy for neutrophils. Figure **[B]** shows geometric (MFI) for activation markers*

L-selectin, CD66b and CD11b. ***Figure [C i-iii]*** *Shows histograms for L-selectin, CD66b and CD11b. N=1*

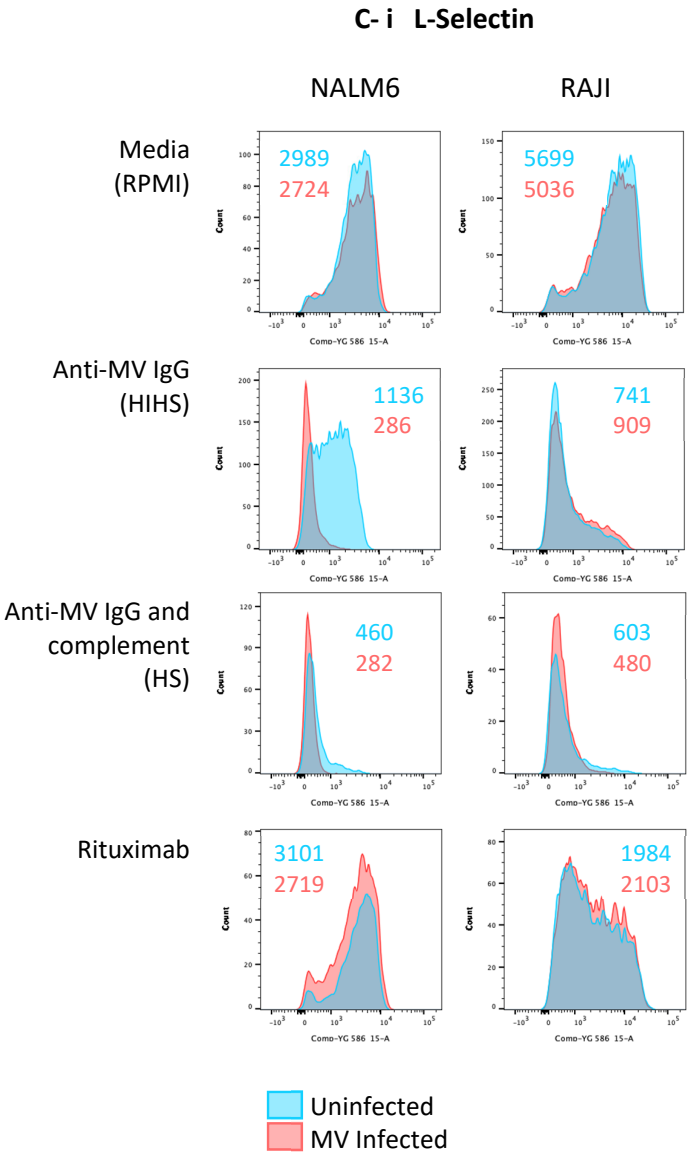

C- ii CD66b

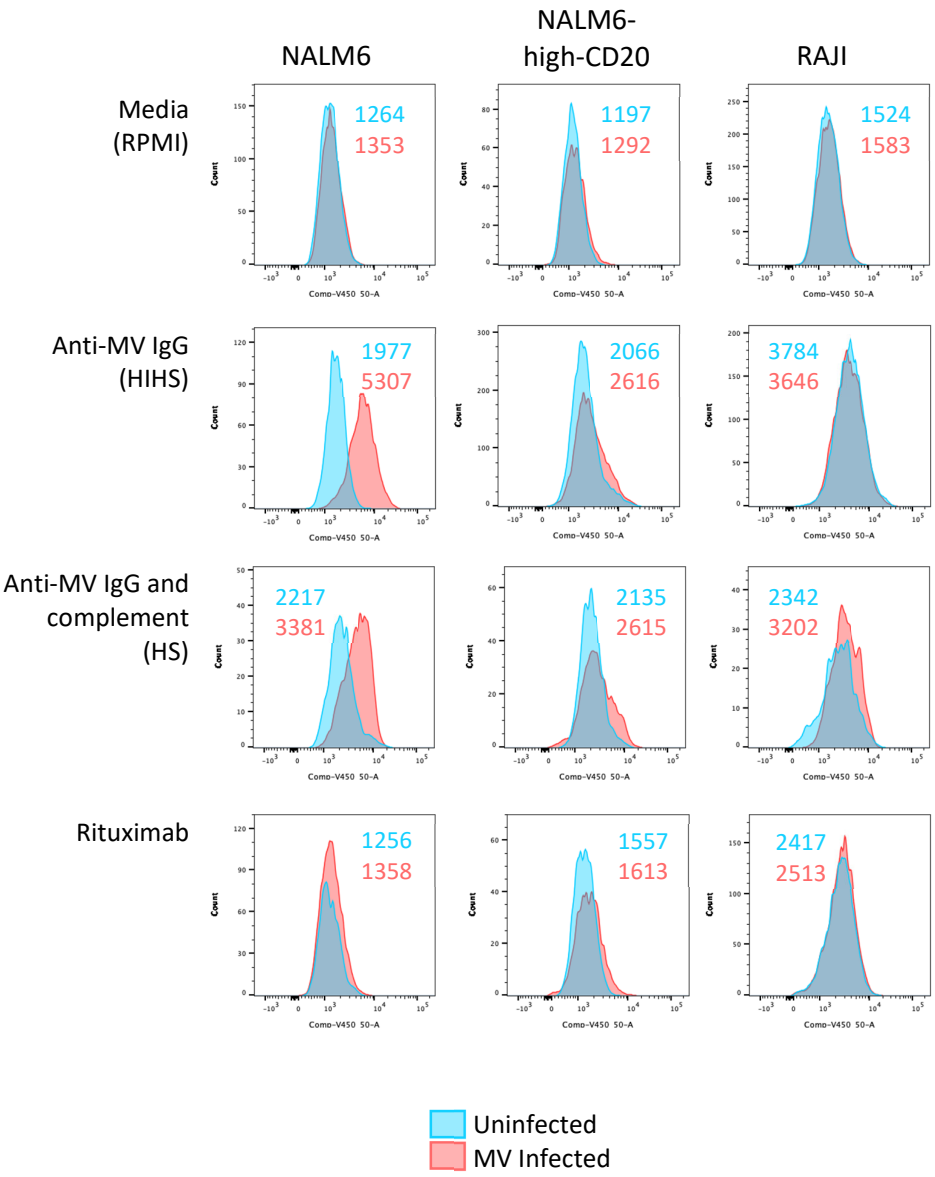
NALM6
NALM6-high-CD20
RAJI
Media (RPMI)
Anti-MV IgG (HIHS)
Anti-MV IgG and complement (HS)
Rituximab
1264
1353
1197
1292
1524
1583
1977
5307
2066
2616
3784
3646
2217
3381
2135
2615
2342
3202
1256
1358
1557
1613
2417
2513
Count
Comp-V450 50-A
Uninfected
MV Infected

C- iii CD11b

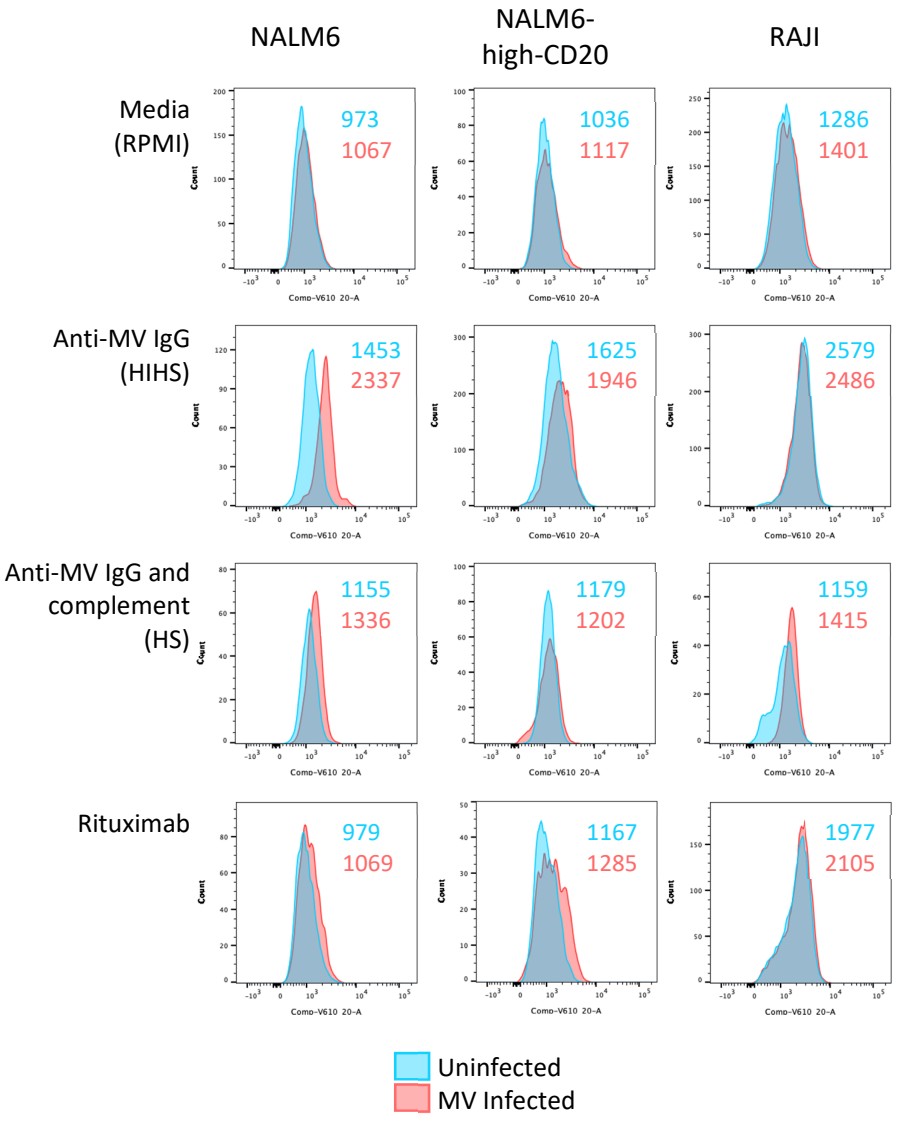
NALM6
NALM6-high-CD20
RAJI
Media (RPMI)
973
1067
1036
1117
1286
1401
Anti-MV IgG (HIHS)
1453
2337
1625
1946
2579
2486
Anti-MV IgG and complement (HS)
1155
1336
1179
1202
1159
1415
Rituximab
979
1069
1167
1285
1977
2105
Count
Como-V610 20-A
Uninfected
MV Infected

Trogocytosis would be expected to occur in conditions where CD20 positive cells are incubated with rituximab (both uninfected and infected), and when infected cells are incubated with anti-MV antibody or complement. The condition with media alone acted as a negative control for trogocytosis. Where neutrophils were co-cultured with NALM6 there was a clear increase in activation following MV infection when MV IgG was available. This is seen in the reduction in L-selectin and the increased expression of CD66b and CD11b. The same trend is seen for the condition containing media, but here the change is not as large. A similar trend is seen for the NALM6-high-cells but not for Raji. Thus, in conditions where trogocytosis would be expected to occur the neutrophils generally have markers indicating increased activation. A limitation of this experiment was that it relied on internal controls of neutrophil activation. The experiment could be improved by including an independent positive control of neutrophil activation, for example, lipopolysaccharide.

5.4.8 Exploring targeted gene expression profiles of neutrophils after trogocytosis.

In order to discover a mechanism for trogocytosis a targeted gene expression profile was carried out using RT-qPCR panels for phagocytosis and chemokine/cytokine panels which were run simultaneously to measure the relative expression of multiple genes. The advantage of this method was that a useful gene-set that been pre-selected by the manufacturer and the laboratory was technically experienced using this method. This was an exploratory experiment which was carried out once. The uninfected co-culture was used as the comparator. The co-culture was cell sorted to collect neutrophils and subsequently mRNA was extracted from the neutrophils using the TRIzol® method. A large number of cells (>500 000) were required in order to extract adequate quantities of mRNA from neutrophils, so four conditions were chosen – uninfected, rituximab, low-titre anti-MVab, and high-titre anti-MVab. The low-titre anti-MVab condition was chosen as the negative control for trogocytosis as this had shown similar low levels of double positive (trogocytosis) events to media alone yet offers a better control given it contains all but the anti-MV IgG. The high-titre anti-MVab condition was the experimental condition for trogocytosis. The rituximab condition was a positive control for trogocytosis without MV infection. The results are shown in Figure 11a and 11b. The uninfected condition was used as the gene expression comparator in the analysis. The previous ADCP assays showed positive results for rituximab and for MV plus anti-MV IgG, therefore it could be expected that the change in expression for these two conditions (the blue and grey bars) would be similar to each other and different to the negative control - MV plus low anti-MV IgG (the orange bar), if that gene expression were important for trogocytosis. If the MV plus anti-MV IgG (blue) showed similar expression to the negative control (orange) but different to the rituximab (grey) then this could be due to MV infection rather than trogocytosis

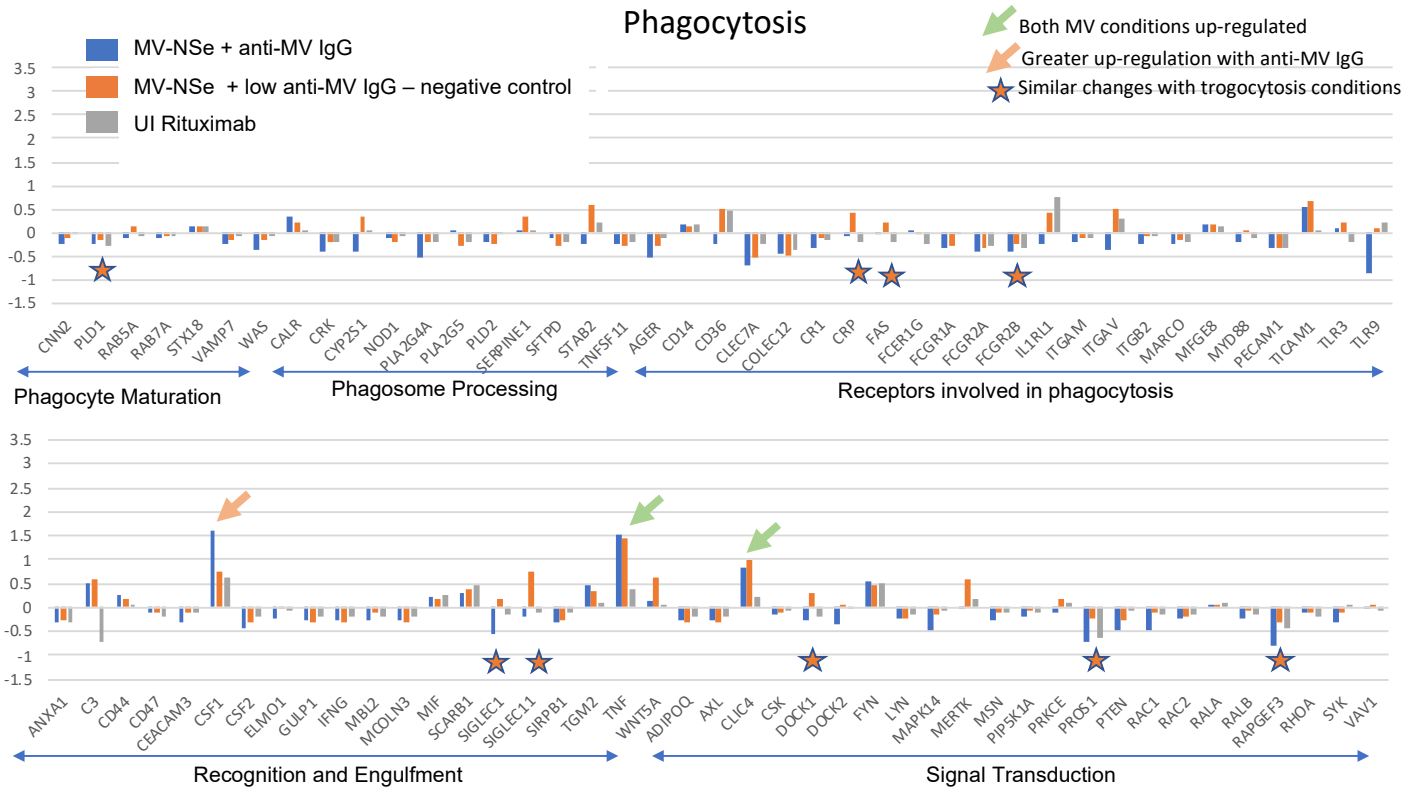

Figure 5-13 ***RT² qPCR Human Phagocytosis gene array****. NALM6-high-CD20 cells were co-cultured with freshly isolated neutrophils and incubated for 2.5 hours. Neutrophils were sorted by cell sorting using BD FACS Aria. >500 000 cells were required for adequate RNA extraction. Figure shows fold up- and down- regulation in comparison to uninfected control. List of genes can be found in Appendix 1.*

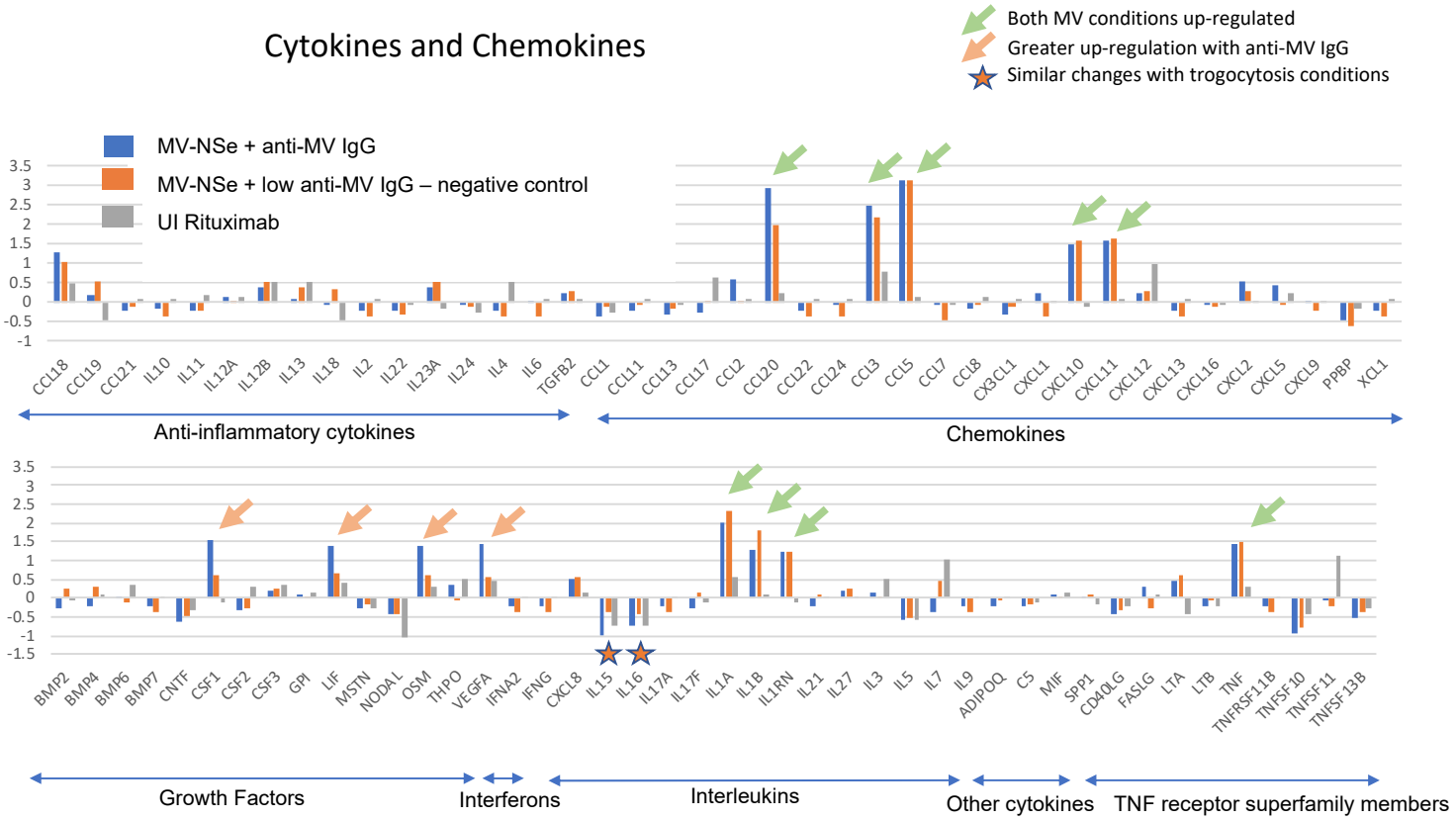

Figure 5-14 ***RT² qPCR Human Cytokine and Chemokine*** *array. NALM6-high-CD20 cells were co-cultured with freshly isolated neutrophils and incubated for 2.5 hours. Neutrophils were sorted by cell sorting using BD FACS Aria. >500 000 cells were required for adequate RNA extraction. Figure shows fold up- and down- regulation in comparison to uninfected control. List of genes can be found in Appendix 1.*

In keeping with the imaging experiments, expression of genes related to phagosome maturation, processing and phagocytosis receptors showed minimal up- and down-regulation of less than 1 fold from the comparator uninfected condition.

The pattern interpreted as possibly representing trogocytosis was where both the rituximab and the positive MV condition (MV-NSe antiMVab + anti-MV-IgG) - i.e. those that would have given a positive result in the flow assay - showed opposing expression to the MV negative condition (MV-NSe + low anti-MV IgG). Thus, in the Phagocytosis panel, the genes which showed a pattern to indicate involvement in trogocytosis were PLD1, CRP, FAS, FCGR2B, SIGLEC1, SiGLEC11, DOCK1, PROS1 RAPGEF3, however the changes in expression are very small so it is difficult to have any real certainty in the meaningfulness of these changes. TLR9 was downregulated in the MV infected with high anti-MV IgG condition whilst marginally upregulated in the low anti-MV IgG condition and with rituximab. M-CSF (CSF1) was upregulated 1.5fold in the high anti-MV IgG and only 0.5 fold in the low anti-MV IgG and with rituximab.

More notable changes were seen in the cytokines and chemokines profiles but not a pattern that suggests they relate to trogocytosis. In particular CCL20, CCL3, CCL5, CXCXL10, CXCXL11, TNF were upregulated in the two infected conditions but not in the rituximab condition. Several of these cytokines have roles in recruiting leucocytes: CCL20 recruits Th17 cells and DCs; CCL5(RANTES) has an active role in recruiting Th1 cells and NK cells. However, changes appeared to be related to prior infection rather than conditions where trogocytosis is expected. If the changes were related purely to trogocytosis we would expect the rituximab condition to produce similar changes in mRNA expression to those seen in the high anti-MV IgG. Examples where this is seen, e.g. PROS1, IL15, IL16, as with the phagocytosis panel the fold difference is very small and therefore unlikely to be biologically relevant. The minimal up- and down-regulation in the phagocytosis panel would support the theory that the ADCP assay is not a true reflection of phagocytosis. However, it does not significantly help provide insight into the mechanism of trogocytosis.

A limitation of this approach was the short time period of 2.5 hours following the initiation of the co-culture at which the neutrophils were sorted. This was for practical purposes and because freshly extracted human neutrophils do not survive for many hours in tissue culture. However, this may not have allowed sufficient time for a significant change in gene

expression to occur. This could explain why the changes that were seen are in keeping with MV infection rather than likely to be attributable to trogocytosis. If this were to be repeated, a later time point after co-culture should be considered.

5.5 Discussion

Neutrophil mediated antibody dependent neutrophil trogocytosis or trogoptysis is a possible mechanism of effector cell MV oncolysis that has not been previously described in published literature however has been suggested as a mechanism of monoclonal antibody therapy in chronic lymphocytic leukaemia and breast cancer. Recent reports published during the course of this work, had cast doubt on the results of flow based ADCP assays being indicative of true phagocytosis. Valgardsdottir *et al* demonstrated - using fluorescent live imaging and confocal microscopy - that rather than whole cell phagocytosis, there was transfer of small sections of plasma cell membrane to the neutrophils from CLL cells in the presence of the anti-CD20 monoclonal antibodies rituximab or obinutuzumab [253]. This alternative mechanism had previously been described as 'shaving' in the context of the T-cell immunosynapse, and also as trogocytosis (trogo- taken from the Greek τρογο 'to gnaw'). Matlung *et al* have more recently investigated this as a mechanism in breast cancer cells and further suggest 'trogoptosis' as the mechanism underlying ADCC [254]. There are contradictions between the two publications, as Valgardsdottir's group show no evidence of increased cell death, in contrast Mutlung's data indicate that neutrophil trogocytosis leads to a lytic form of cell death of the antibody-opsonised cells. They also go further to explore the mechanism and suggest that a CD11b/CD18 integrin dependent conjugate is required. In this chapter I explored whether either neutrophil ADCP or trogocytosis is relevant to MV oncolysis.

In this chapter I have shown that the proportion of cells that are affected by trogocytosis is dependent on the amount of MV antibody present which strongly supports the theory that this is an antibody dependent process. The imaging studies, both imaging flow cytometry and confocal microscopy show that phagocytosis of the ALL cells by neutrophils does not occur, except in very rare cases. The imaging flow cytometry showed that the membrane of the target ALL cells, stained with PKH67 was internalised by the neutrophils, however a convincing internalisation score was not reached as a likely consequence of the staining used. There was no evidence that this caused cell death within the 2.5hr co-culture, however, it would be useful to determine whether this occurs at a later time point. A technical difficulty with investigating this *in vitro* is that fresh neutrophils have a limited survival time in vitro. A pilot experiment in which I attempted to address this indicated that neutrophil viability was considerably reduced after 12 hours incubated in co-culture.

Matlung *et al* demonstrated that neutrophils kill antibody-opsonized cancer cells by trogocytosis, or, as they named it 'trogoptosis'. In their breast cancer model the trogocytosis seen correlated with ADCC, and they therefore interpreted this as trogocytosis eventually resulting in ADCC [254]. In previous work by the Fielding laboratory there was no convincing evidence that ADCC is a mechanism of MV oncolysis in NALM6 cells or Raji cells [250] Thus the fact that the transduced NALM6 cells have convincingly and repeatedly demonstrated neutrophil trogocytosis in the form of positive ADCP assays is unlikely to be explained by ADCC.

As I was unable to establish that the increased amounts of trogocytosis lead to increased target cell death – i.e. oncolysis – I further investigated the effects on neutrophils, with the hypothesis that engulfing target cell membrane could lead to the effector cell recruiting further immune cells to the site. Neutrophils where they were exposed to MV infected target cell and MV antibody, become activated in comparison to control conditions. The phagocytosis RT-qPCR array did not show a great difference to the investigated co-culture conditions compared to the baseline uninfected cells. In fact, many of the phagocyte maturation, phagosome processing and receptors involved in phagocytosis were downregulated. This is in keeping with the evidence that the ADCP assays do not show neutrophil phagocytosis, however should be interpreted with caution as much of the neutrophil components required for phagocytosis are available in pre-formed granules. There is greater upregulation in chemokines and cytokines produced, however if this were due to trogocytosis we would expect to see the greatest change in the conditions with high levels of MV antibody and our positive control rituximab. It appears that neutrophils are important to MV oncolysis however, this is not necessarily due to trogocytosis but rather contact with the MV infected cell in the presence of antibody. The infected conditions resulted in the production of mRNA to cytokines which help recruit Th17 cells, monocytes, dendritic cells, Th1 cells, and NK cells.

In summary, in this chapter I have shown that NALM6 cells infected with MV results in a positive ADCP assay in an anti-MV IgG dependent manner. This is seen more markedly when both anti-MV IgG and complement are present during the co-culture. However, further imaging has shown that the neutrophil ADCP assay does not indicate phagocytosis but a process known as 'trogocytosis' and thus we can surmise that this is seen to occur in ALL cells that have previously been infected with MV and is strongly positively correlated to

the amount of anti-MV IgG. The significance of trogocytosis is not yet clear. It does not appear to be related to ALL cell death, and the cytokines expressed are more indicative of the infection of ALL cells by MV being important for neutrophils to recruit further immune effector cells rather than the process of trogocytosis *per se*. Further research would be required to investigate the process of trogocytosis and the short life span of neutrophils *ex-vivo* makes longer time courses extremely problematic. To overcome this it might be possible to encompass measuring trogocytosis as part of oncolytic MV experiments in murine xenografts as this would enable the process to continue for a longer time. This is beyond the scope of this thesis but could form the basis for future research.

Chapter 6 General Discussion

Adult acute lymphoblastic leukaemia is an aggressive malignancy for which refining current treatment strategies and developing novel non-toxic therapies are urgent priorities. This thesis has focused on CD20 as an antigen which is important, both as a potential prognostic biomarker and also as a target for therapy, specifically in the form of measles oncolytic virotherapy. This chapter will summarise the overall findings presented in this thesis and also discuss this in the broader context of acute lymphoblastic leukaemia and oncolytic virotherapy. The discussion will also consider the limitations of this work and consider future directions for research.

6.1 CD20 as a prognostic marker.

There has been controversy regarding the prognostic impact of CD20 in adult acute lymphoblastic leukaemia with some, but not all, studies suggesting that it confers a poor outcome. This thesis has helped to clarify that CD20 is an important independent biomarker that predicts poorer outcome. It has also clarified that this is only in those who do not harbour the Philadelphia chromosome with its respective fusion gene *BCR-ABL1*. This has been shown by analysing the expression of CD20 on primary ALL cells from the multicentre, phase III clinical trial, UKALL14. This work took the interrogation of CD20 one step further by examining the antigen density along with the percentage of positive cells within each leukaemic population and demonstrated that within a prospective clinical trial including antigen density into the measurement of the antigen could provide a more definitive test.

It is interesting that the adverse prognostic impact of CD20 does not extend to patients who are positive for *BCR-ABL1*. Leukaemic blasts which are positive for *BCR-ABL1* tend to have a greater burden of CD20 expression so based on this observation it would be expected that these patients would be more likely to suffer an adverse prognosis from their CD20 burden. It is vitally important to recognise that these *BCR-ABL1* positive patients received different ALL treatment than their *BCR-ABL1* negative counterparts as they all

received the tyrosine kinase inhibitor (TKI) Imatinib. It is possible that by specifically targeting *BCR-ABL1*, the TKI improved the outcome of these patients to the extent that it can overcome the negative prognosis conferred by CD20. We know that the use of TKIs results in a higher number of patients achieving a complete remission, reduced early death and decreased relapse, thus bringing a greater number of patients to a haematopoietic stem cell transplant and a potential cure. An alternative explanation is that the TKI somehow disrupts downstream effect altering the negative influence of CD20 expression. It would certainly be of interest to investigate these effects further.

Despite widespread use of CD20 as a therapeutic target, relatively little is understood about its role in cell biology. Thus, trying to understand why CD20 should confer a poor prognosis is difficult. As they mature, B-cells express greater quantities of CD20, however the very aggressive Burkitt's lymphoma, which expresses high levels of CD20, responds more favourably to chemotherapy than adult ALL reaching a long-term survival of 70-80%. It is also worth noting that CD20 expression is not readily predictable from underlying genetic abnormalities, however there are notable exceptions. B-ALL with t(12:21)(p13;q22) *TEL-AML1*, offers a very favourable prognosis and rarely expresses CD20 but although seen in 25% of childhood ALL, it is rare in adult ALL affecting only 3% [255, 256].

6.2 Redefining the 'positive' cut-off for CD20

Traditionally the cut-off for positivity has always been taken to be 20% of cells within a population expressing a particular marker. This is internationally accepted, albeit arbitrary. The data presented in this thesis show that the poorer outcome associated with CD20 expression extends below the 20% marker. Statistical analysis to determine the ideal cut-off – known as Youden's cut-off - which establishes those at greater 'risk' from their CD20 expression showed a level of 11.6% to be ideal. This is interesting because it highlights that caution should be always applied to unquestioningly accepted norms, but it remains to be proven whether this makes a difference to the application of targeted therapy. Once the results of the rituximab unblinding are available it will be important to ask the question whether treating patients with the CD20 targeted treatment if expression is above 11.6% confers a survival advantage.

6.3 Improving the quantification of CD20 expression

The best method for predicting outcome appeared to be the combined method of measureing both antigen density and the percentage positive cells. This suggests that adding quantibrite or equivalent flow cytometry beads to measure antigen density, should be considered. Given that this could potentially determine best treatment, although the affected number of patients would be small it could potentially determine the difference between patients undergoing an allogeneic haematopoietic stem cell transplant or experimental therapies, and the associated cost, both financial and in risk to the patient.

6.4 RT-qPCR vs flow cytometry

A benefit of flow cytometry is that it is a widely available technology with multiple centres already carrying out diagnostic analysis. A concern with using a specific quantity to determine treatment for a patient its that there is a large amount of inter-laboratory variation. This can be illustrated from a comparable multicentre UK trial, AML15, where CD33 expression was investigated. They compared expression of the antigen determined locally, to that determined at 3 central reference laboratories and found poor agreement [257]. It is difficult to know whether the added complexity of adding reference beads would improve or worsen the comparability of results between laboratories. A molecular method could potentially overcome this concern and the practicalities of requiring cells to be shipped to a reference centre. The development of the RT-qPCR assay to measure CD20 has highlighted the importance of choosing an adequate number of adequately stable reference genes. In previous literature there has not been a reliable molecular assay for CD20 expression. It is interesting that it best correlated to the function that combined CD20 antigen density to percentage within the blast population, thus giving a surrogate for the amount of antigen within the population. The disadvantage of requiring greater quantities of molecular material to measure a greater number of genes was overcome by the use of duplex assays. A limitation of this method was that it was only reliable for bone marrow specimens. As experiments to measure splice variants failed to provide a method for distinguishing the proportion of leukaemic cells compared to normal cells, It might be possible to combine it with a test for normal cells, such as a T-cell marker to give a surrogate estimation of normal lymphocytes within the sample.

6.5 Exploring the use of a CD20 targeted oncolytic MV

Oncolytic viruses are increasingly being recognised as potential therapies for a wide variety of cancers. In order for a virus to be considered appropriate as a potential therapeutic it has to meet stringent criteria for safety and efficacy. The safety of the live, attenuated vaccine strain of measles virus (MV) has been demonstrated in worldwide vaccination programmes, and only rare incidences of infection have been shown in individuals who are immunocompromised. As it has a negative sense, single stranded unsegmented genome that replicates entirely in the cytoplasm of the host cell, there is little risk of recombination. Early phase clinical trials in patients with multiple myeloma have shown that MV can be infused intravenously with only mild, immediate and transient unwanted effects. Although MV has natural tropism towards malignant cells, a benefit of oncolytic viruses is the ability to genetically modify the virus, and thus adding an extra ability to target the virus. Previous work from Prof Fielding's laboratory has shown that ALL is sensitive to MV and in Chapter 4 of this thesis I explored the use of a CD20 targeted MV. It appeared that this was very effective at killing transformed cells *in vitro* to a greater extent than the parent strain MV-NSe for CD20 expressing cells lines. And the greater the amount of CD20 per cell, as determined by MFI, the greater the amount of oncolysis.

To investigate whether greater sophistication of targeting could be achieved, this thesis explored the utility of a MV which was targeted to CD20 and blind to either the native MV receptors CD46, which is present on all nucleated human cells, and SLAM, which is present on many immune cells. The results of in vitro assays showed that the CD20 targeted, blinded viruses were also effective at killing transformed cells but to a lesser extent than their unblinded counterparts. It would be useful to see the effect so this virus in a murine model, however although the effects of the CD20 targeting would be possible, it is difficult to fully assess the oncolytic immune effects of the virus as only an immune deficient mice can support the human xenograft. A CD46 mouse exists but will not support a xenograft which would be interesting to determine off-target effects of the MVHαCD20 compared to MVHαCD20 blind, although it remains an artificial model. Further experiments could be carried out to investigate the SLAM blind virus perhaps by infecting normal human cells. It was also beyond the scope of this project to investigate a virus blind to both CD46 and SLAM.

Chapter 5 investigated the role of neutrophils in MV oncolysis. Neutrophils have been shown to be important effector cells in oncolysis but the mechanism is unknown. Previous work in Professor fielding's lab failed to show that antibody dependent cellular cytotoxicity (ADCC) was a mechanism for MV oncolysis, so this thesis investigated complement dependent cytotoxicity (CDC) and antibody dependent cellular phagocytosis (ADCP) as possible mechanisms. The CDC assay indicated a small amount of CDC which was reduced when the virus was blinded to CD46, presumably protecting the cells from downregulation of CD46, a negative regulator of complement, that is seen following infection by unmodified MV. The positive neutrophil ADCP assays were very promising as a potential answer to the question of what role neutrophils play, as neutrophil phagocytosis would have indicated definitive destruction of the ALL cells, and thus a mechanism of neutrophil mediated oncolysis. In the light of evidence that cast doubt on the accepted interpretation of the ADCP assay, it was imperative to investigate the meaning of the assay with imaging experiments. Several techniques demonstrated that this was not phagocytosis, but trogocytosis. However, this raised more questions than it answered. It was clear that this was an antibody-dependent mechanism, but it was not clear how trogocytosis leads to the destruction of ALL cell, if this was indeed the case. There appeared to be a suggestion that the neutrophils were more activated in the conditions where trogocytosis is seen, however there was no decrease in viability of the cells over the time period of the experiments. Further work would certainly involved investigating the effects of trogocytosis over longer time courses, however there is a difficulty that neutrophils do not survive for many hours *in vitro*. There was also the suggestion that cytokines which would be involved in further recruiting immune cells, were being produced. Although this appeared to be related to MV rather than trogocytosis. It clearly requires further work to elucidate the role that neutrophils play in MV oncolysis. The interplay between immune cells and virus is clearly complex and untangling the mechanism a challenge.

The neutrophil mediated mechanism seen in the ADCP assay was demonstrated to be MV antibody mediated. This raises a number of questions as there is now substantial evidence that anti-MV antibodies can provide a barrier to MV virotherapy. In order to effectively treat ALL with MV it will be necessary to administer MV intravenously, however as the vast majority of the population has been immunised against MV, it is likely that patients will have circulating antibodies which will neutralise the MV. This has previously been demonstrated to be the case, even following immunosuppressive induction chemotherapy for ALL [177]. Patients who have shown a response from systemic MV therapy in early MV

trials have normally had low levels of circulating anti-MV IgG [224]. Thus, there is a conundrum. If anti-MV antibody is required for oncolysis but prevents MV reaching the transformed cells then how can it be an effective therapy for ALL? One strategy to address this is to 'hide' and transport the MV within mesenchymal stem cells. This has been shown to be theoretically possible in pre-clinical studies of ALL and is being investigated in early clinical trials of ovarian cancer (NCT02068794)[177]. Thus when the virus is handed-off in the bone marrow it can infect transformed cells, and anti-MV IgG will aid in oncolysis. Alternative strategies include increased immunosuppression, and it is not known the effect of increased B-cell destruction following CD20 targeted therapy, whether that is from rituximab or a CD20 targeted virus. Theoretically by destroying normal B-cells it may be possible to mitigate a secondary, or anamnestic response from a therapeutic MV infusion by targeting the cells that produce the antibody. It would be interesting area of research to investigate whether this unwanted effect of a CD20 targeted therapy could enhance the therapeutic effect of oncolytic virotherapy.

6.6 Conclusions

The work presented in this thesis has addressed the utility of CD20 as a prognostic biomarker and as a target for oncolytic measles virus. A higher expression of CD20 appears to confer a poorer prognosis. This data has also suggested CD20 expression cut-off level of 11.6%, below which determines a group with a good prognosis. An RT-qPCR method for quantifying CD20 was developed which shows promise, and could be developed further for use in clinical trials.

A CD20 targeted MV could be a potential therapeutic and can be 'blinded' to reduce off-target effects, however the evidence presented in this thesis suggest that the 'blinding' may also limit its efficacy. Antibody-dependent, neutrophil-mediated trogocytosis appears to be a possible mechanism of oncolysis, however requires further research to fully understand the mechanism. The next step to take the CD20 targeted MV work forward would be to see if the modified virus is effective in a murine xenograft. There is enough collective evidence to consider a clinical trial of MV in ALL using the parent strain MV-NSe. This could help determine the safety of MV in ALL patients, and help unravel the innate and acquired immune response to the virus, in particular the theoretical concerns regarding circulating anti-MV antibody.

References

1. Redaelli, A., et al., *A systematic literature review of the clinical and epidemiological burden of acute lymphoblastic leukaemia (ALL).* Eur J Cancer Care (Engl), 2005. **14**(1): p. 53-62.
2. UK, C.R. *Acute Lymphoblastic Leukaemia (ALL) Incidence by age*. 2018 [cited 2018 18 October]; Acute lymphoblastic leukaemia (ALL) incidence by age]. Available from: https://www.cancerresearchuk.org/health-professional/cancer-statistics/statistics-by-cancer-type/leukaemia-all/incidence#heading-One.
3. Ward, E., et al., *Childhood and adolescent cancer statistics, 2014.* CA Cancer J Clin, 2014. **64**(2): p. 83-103.
4. Bonaventure, A., et al., *Worldwide comparison of survival from childhood leukaemia for 1995-2009, by subtype, age, and sex (CONCORD-2): a population-based study of individual data for 89 828 children from 198 registries in 53 countries.* Lancet Haematol, 2017. **4**(5): p. e202-e217.
5. Pulte, D., et al., *Survival of adults with acute lymphoblastic leukemia in Germany and the United States.* PLoS One, 2014. **9**(1): p. e85554.
6. Bennett, J.M., et al., *Proposals for the classification of the acute leukaemias. French-American-British (FAB) co-operative group.* Br J Haematol, 1976. **33**(4): p. 451-8.
7. Bene, M.C., et al., *Proposals for the immunological classification of acute leukemias. European Group for the Immunological Characterization of Leukemias (EGIL).* Leukemia, 1995. **9**(10): p. 1783-6.
8. Swerdlow, S.H., C. International Agency for Research on, and O. World Health, *WHO classification of tumours of haematopoietic and lymphoid tissues*. World Health Organization classification of tumours. 2008, Lyon: International Agency for Research on Cancer. 439 : ill. (chiefly col.) ; 27 cm.
9. Dores, G.M., et al., *Acute leukemia incidence and patient survival among children and adults in the United States, 2001-2007.* Blood, 2012. **119**(1): p. 34-43.
10. Moorman, A.V., et al., *Karyotype is an independent prognostic factor in adult acute lymphoblastic leukemia (ALL): analysis of cytogenetic data from patients treated on the Medical Research Council (MRC) UKALLXII/Eastern Cooperative Oncology Group (ECOG) 2993 trial.* Blood, 2007. **109**(8): p. 3189-97.
11. Liu-Dumlao, T., et al., *Philadelphia-positive acute lymphoblastic leukemia: current treatment options.* Curr Oncol Rep, 2012. **14**(5): p. 387-94.
12. Bernt, K.M. and S.P. Hunger, *Current concepts in pediatric Philadelphia chromosome-positive acute lymphoblastic leukemia.* Front Oncol, 2014. **4**: p. 54.
13. Secker-Walker, L.M., et al., *Philadelphia positive acute lymphoblastic leukemia in adults: age distribution, BCR breakpoint and prognostic significance.* Leukemia, 1991. **5**(3): p. 196-9.

14. Fielding, A.K., et al., *UKALLXII/ECOG2993: addition of imatinib to a standard treatment regimen enhances long-term outcomes in Philadelphia positive acute lymphoblastic leukemia.* Blood, 2014. **123**(6): p. 843-50.
15. Malagola, M., C. Papayannidis, and M. Baccarani, *Tyrosine kinase inhibitors in Ph+ acute lymphoblastic leukaemia: facts and perspectives.* Ann Hematol, 2016. **95**(5): p. 681-93.
16. ClinicalTrials.gov. *NCT01641107*. 2018; Available from: https://clinicaltrials.gov/ct2/show/NCT01641107.
17. Short, N.J., et al., *Poor outcomes associated with +der(22)t(9;22) and -9/9p in patients with Philadelphia chromosome-positive acute lymphoblastic leukemia receiving chemotherapy plus a tyrosine kinase inhibitor.* Am J Hematol, 2017. **92**(3): p. 238-243.
18. Fielding, A.K., et al., *Prospective outcome data on 267 unselected adult patients with Philadelphia chromosome-positive acute lymphoblastic leukemia confirms superiority of allogeneic transplantation over chemotherapy in the pre-imatinib era: results from the International ALL Trial MRC UKALLXII/ECOG2993.* Blood, 2009. **113**(19): p. 4489-96.
19. Jain, N., et al., *Ph-like acute lymphoblastic leukemia: a high-risk subtype in adults.* Blood, 2017. **129**(5): p. 572-581.
20. Mullighan, C.G., et al., *JAK mutations in high-risk childhood acute lymphoblastic leukemia.* Proc Natl Acad Sci U S A, 2009. **106**(23): p. 9414-8.
21. Mullighan, C.G. and J.R. Downing, *Global genomic characterization of acute lymphoblastic leukemia.* Semin Hematol, 2009. **46**(1): p. 3-15.
22. Tasian, S.K., M.L. Loh, and S.P. Hunger, *Philadelphia chromosome-like acute lymphoblastic leukemia.* Blood, 2017. **130**(19): p. 2064-2072.
23. Roberts, K.G., et al., *Oncogenic role and therapeutic targeting of ABL-class and JAK-STAT activating kinase alterations in Ph-like ALL.* Blood Adv, 2017. **1**(20): p. 1657-1671.
24. Churchman, M.L., et al., *Synergism of FAK and tyrosine kinase inhibition in Ph(+) B-ALL.* JCI Insight, 2016. **1**(4).
25. Churchman, M.L., et al., *Efficacy of Retinoids in IKZF1-Mutated BCR-ABL1 Acute Lymphoblastic Leukemia.* Cancer Cell, 2015. **28**(3): p. 343-56.
26. Bruggemann, M. and M. Kotrova, *Minimal residual disease in adult ALL: technical aspects and implications for correct clinical interpretation.* Blood Adv, 2017. **1**(25): p. 2456-2466.
27. Zach, O. and J. Clausen, *Molecular monitoring of minimal residual disease in acute leukemia*, in *Magazine of European Medical Oncology*. 2014. p. 144-147.
28. Faham, M., et al., *Deep-sequencing approach for minimal residual disease detection in acute lymphoblastic leukemia.* Blood, 2012. **120**(26): p. 5173-80.
29. Sala Torra, O., et al., *Next-Generation Sequencing in Adult B Cell Acute Lymphoblastic Leukemia Patients.* Biol Blood Marrow Transplant, 2017. **23**(4): p. 691-696.
30. Vidriales, M.B., et al., *Minimal residual disease in adolescent (older than 14 years) and adult acute lymphoblastic leukemias: early immunophenotypic evaluation has high clinical value.* Blood, 2003. **101**(12): p. 4695-700.

31. Dhedin, N., et al., *Role of allogeneic stem cell transplantation in adult patients with Ph-negative acute lymphoblastic leukemia.* Blood, 2015. **125**(16): p. 2486-96; quiz 2586.
32. Beldjord, K., et al., *Oncogenetics and minimal residual disease are independent outcome predictors in adult patients with acute lymphoblastic leukemia.* Blood, 2014. **123**(24): p. 3739-49.
33. Bruggemann, M., et al., *Clinical significance of minimal residual disease quantification in adult patients with standard-risk acute lymphoblastic leukemia.* Blood, 2006. **107**(3): p. 1116-23.
34. Bassan, R., et al., *Improved risk classification for risk-specific therapy based on the molecular study of minimal residual disease (MRD) in adult acute lymphoblastic leukemia (ALL).* Blood, 2009. **113**(18): p. 4153-62.
35. Stashenko, P., et al., *Characterization of a human B lymphocyte-specific antigen.* J Immunol, 1980. **125**(4): p. 1678-85.
36. Oettgen, H.C., et al., *Further biochemical studies of the human B-cell differentiation antigens B1 and B2.* Hybridoma, 1983. **2**(1): p. 17-28.
37. Loken, M.R., et al., *Flow cytometric analysis of human bone marrow. II. Normal B lymphocyte development.* Blood, 1987. **70**(5): p. 1316-24.
38. Ginaldi, L., et al., *Levels of expression of CD19 and CD20 in chronic B cell leukaemias.* J Clin Pathol, 1998. **51**(5): p. 364-9.
39. Press, O.W., et al., *Monoclonal antibody 1F5 (anti-CD20) serotherapy of human B cell lymphomas.* Blood, 1987. **69**(2): p. 584-91.
40. Beers, S.A., et al., *Antigenic modulation limits the efficacy of anti-CD20 antibodies: implications for antibody selection.* Blood, 2010. **115**(25): p. 5191-201.
41. Tedder, T.F. and P. Engel, *CD20: a regulator of cell-cycle progression of B lymphocytes.* Immunol Today, 1994. **15**(9): p. 450-4.
42. Eon Kuek, L., et al., *The MS4A family: counting past 1, 2 and 3.* Immunol Cell Biol, 2016. **94**(1): p. 11-23.
43. Anolik, J., et al., *Down-regulation of CD20 on B cells upon CD40 activation.* Eur J Immunol, 2003. **33**(9): p. 2398-409.
44. Uchida, J., et al., *Mouse CD20 expression and function.* Int Immunol, 2004. **16**(1): p. 119-29.
45. O'Keefe, T.L., et al., *Mice carrying a CD20 gene disruption.* Immunogenetics, 1998. **48**(2): p. 125-32.
46. Kuijpers, T.W., et al., *CD20 deficiency in humans results in impaired T cell-independent antibody responses.* J Clin Invest, 2010. **120**(1): p. 214-22.
47. Borowitz, M.J., et al., *Prognostic significance of fluorescence intensity of surface marker expression in childhood B-precursor acute lymphoblastic leukemia. A Pediatric Oncology Group Study.* Blood, 1997. **89**(11): p. 3960-6.
48. Jeha, S., et al., *Prognostic significance of CD20 expression in childhood B-cell precursor acute lymphoblastic leukemia.* Blood, 2006. **108**(10): p. 3302-4.
49. Thomas, D.A., et al., *Prognostic significance of CD20 expression in adults with de novo precursor B-lineage acute lymphoblastic leukemia.* Blood, 2009. **113**(25): p. 6330-7.

50. Maury, S., et al., *Adverse prognostic significance of CD20 expression in adults with Philadelphia chromosome-negative B-cell precursor acute lymphoblastic leukemia.* Haematologica, 2010. **95**(2): p. 324-8.
51. Bachanova, V., et al., *Allogeneic hematopoietic stem cell transplantation overcomes the adverse prognostic impact of CD20 expression in acute lymphoblastic leukemia.* Blood, 2011. **117**(19): p. 5261-3.
52. Mannelli, F., et al., *CD20 expression has no prognostic role in Philadelphia-negative B-precursor acute lymphoblastic leukemia: new insights from the molecular study of minimal residual disease.* Haematologica, 2012. **97**(4): p. 568-71.
53. Naithani, R., et al., *CD20 has no prognostic significance in children with precursor B-cell acute lymphoblastic leukemia.* Haematologica, 2012. **97**(9): p. e31-2.
54. Xu, N., et al., *Correlation between deletion of the CDKN2 gene and tyrosine kinase inhibitor resistance in adult Philadelphia chromosome-positive acute lymphoblastic leukemia.* J Hematol Oncol, 2016. **9**: p. 40.
55. Yang, S., et al., *CD20 expression sub-stratifies standard-risk patients with B cell precursor acute lymphoblastic leukemia.* Oncotarget, 2017. **8**(62): p. 105397-105406.
56. Isshiki, Y., et al., *CD20 positivity and white blood cell count predict treatment outcomes in Philadelphia chromosome-negative acute lymphoblastic leukemia patients ineligible for pediatric-inspired chemotherapy.* Jpn J Clin Oncol, 2017. **47**(11): p. 1047-1054.
57. Chang, H., A. Jiang, and J. Brandwein, *Prognostic relevance of CD20 in adult B-cell precursor acute lymphoblastic leukemia.* Haematologica, 2010. **95**(6): p. 1040-2; author reply 1042.
58. Thomas, D.A., et al., *Chemoimmunotherapy with a modified hyper-CVAD and rituximab regimen improves outcome in de novo Philadelphia chromosome-negative precursor B-lineage acute lymphoblastic leukemia.* J Clin Oncol, 2010. **28**(24): p. 3880-9.
59. Maury, S., et al., *Rituximab in B-Lineage Adult Acute Lymphoblastic Leukemia.* N Engl J Med, 2016. **375**(11): p. 1044-53.
60. Kasi, P.M., et al., *Clinical review: Serious adverse events associated with the use of rituximab - a critical care perspective.* Crit Care, 2012. **16**(4): p. 231.
61. Maloney, D.G., et al., *IDEC-C2B8 (Rituximab) anti-CD20 monoclonal antibody therapy in patients with relapsed low-grade non-Hodgkin's lymphoma.* Blood, 1997. **90**(6): p. 2188-95.
62. Unruh, T.L., et al., *Cholesterol depletion inhibits src family kinase-dependent calcium mobilization and apoptosis induced by rituximab crosslinking.* Immunology, 2005. **116**(2): p. 223-32.
63. Shan, D., J.A. Ledbetter, and O.W. Press, *Signaling events involved in anti-CD20-induced apoptosis of malignant human B cells.* Cancer Immunol Immunother, 2000. **48**(12): p. 673-83.
64. Seyfizadeh, N., et al., *A molecular perspective on rituximab: A monoclonal antibody for B cell non Hodgkin lymphoma and other affections.* Crit Rev Oncol Hematol, 2016. **97**: p. 275-90.

65. Dall'Ozzo, S., et al., *Rituximab-dependent cytotoxicity by natural killer cells: influence of FCGR3A polymorphism on the concentration-effect relationship.* Cancer Res, 2004. **64**(13): p. 4664-9.
66. Lefebvre, M.L., et al., *Ex vivo-activated human macrophages kill chronic lymphocytic leukemia cells in the presence of rituximab: mechanism of antibody-dependent cellular cytotoxicity and impact of human serum.* J Immunother, 2006. **29**(4): p. 388-97.
67. Osinska, I., K. Popko, and U. Demkow, *Perforin: an important player in immune response.* Cent Eur J Immunol, 2014. **39**(1): p. 109-15.
68. Cartron, G., et al., *Therapeutic activity of humanized anti-CD20 monoclonal antibody and polymorphism in IgG Fc receptor FcgammaRIIIa gene.* Blood, 2002. **99**(3): p. 754-8.
69. Weng, W.K. and R. Levy, *Two immunoglobulin G fragment C receptor polymorphisms independently predict response to rituximab in patients with follicular lymphoma.* J Clin Oncol, 2003. **21**(21): p. 3940-7.
70. Harjunpaa, A., S. Junnikkala, and S. Meri, *Rituximab (anti-CD20) therapy of B-cell lymphomas: direct complement killing is superior to cellular effector mechanisms.* Scand J Immunol, 2000. **51**(6): p. 634-41.
71. Bellosillo, B., et al., *Complement-mediated cell death induced by rituximab in B-cell lymphoproliferative disorders is mediated in vitro by a caspase-independent mechanism involving the generation of reactive oxygen species.* Blood, 2001. **98**(9): p. 2771-7.
72. Weng, W.K. and R. Levy, *Expression of complement inhibitors CD46, CD55, and CD59 on tumor cells does not predict clinical outcome after rituximab treatment in follicular non-Hodgkin lymphoma.* Blood, 2001. **98**(5): p. 1352-7.
73. Cragg, M.S. and M.J. Glennie, *Antibody specificity controls in vivo effector mechanisms of anti-CD20 reagents.* Blood, 2004. **103**(7): p. 2738-43.
74. Di Gaetano, N., et al., *Complement activation determines the therapeutic activity of rituximab in vivo.* J Immunol, 2003. **171**(3): p. 1581-7.
75. Uchida, J., et al., *The innate mononuclear phagocyte network depletes B lymphocytes through Fc receptor-dependent mechanisms during anti-CD20 antibody immunotherapy.* J Exp Med, 2004. **199**(12): p. 1659-69.
76. Gul, N. and M. van Egmond, *Antibody-Dependent Phagocytosis of Tumor Cells by Macrophages: A Potent Effector Mechanism of Monoclonal Antibody Therapy of Cancer.* Cancer Res, 2015. **75**(23): p. 5008-13.
77. Vermi, W., et al., *slan(+) Monocytes and Macrophages Mediate CD20-Dependent B-cell Lymphoma Elimination via ADCC and ADCP.* Cancer Res, 2018. **78**(13): p. 3544-3559.
78. Mishima, Y., et al., *High reproducible ADCC analysis revealed a competitive relation between ADCC and CDC and differences between FcgammaRIIIa polymorphism.* Int Immunol, 2012. **24**(8): p. 477-83.
79. Farber, S., *Some observations on the effect of folic acid antagonists on acute leukemia and other forms of incurable cancer.* Blood, 1949. **4**(2): p. 160-7.
80. Hunger, S.P. and C.G. Mullighan, *Acute Lymphoblastic Leukemia in Children.* N Engl J Med, 2015. **373**(16): p. 1541-52.

81. Pelner, L., G.A. Fowler, and H.C. Nauts, *Effects of concurrent infections and their toxins on the course of leukemia.* Acta Med Scand Suppl, 1958. **338**: p. 1-47.
82. Dock, G., *The Influence of complicating diseases upon leukaemia.* The American Journal of the Medical Sciences., 1904. **127**(4): p. 563-592.
83. Kaufman, H.L., F.J. Kohlhapp, and A. Zloza, *Oncolytic viruses: a new class of immunotherapy drugs.* Nat Rev Drug Discov, 2015. **14**(9): p. 642-62.
84. Burke, J.M., et al., *A first in human phase 1 study of CG0070, a GM-CSF expressing oncolytic adenovirus, for the treatment of nonmuscle invasive bladder cancer.* J Urol, 2012. **188**(6): p. 2391-7.
85. Garcia, M., et al., *A Phase 1 Trial of Oncolytic Adenovirus ICOVIR-5 Administered Intravenously to Cutaneous and Uveal Melanoma Patients.* Hum Gene Ther, 2018.
86. Kimball, K.J., et al., *A phase I study of a tropism-modified conditionally replicative adenovirus for recurrent malignant gynecologic diseases.* Clin Cancer Res, 2010. **16**(21): p. 5277-87.
87. Garcia-Carbonero, R., et al., *Phase 1 study of intravenous administration of the chimeric adenovirus enadenotucirev in patients undergoing primary tumor resection.* J Immunother Cancer, 2017. **5**(1): p. 71.
88. Andtbacka, R.H., et al., *Talimogene Laherparepvec Improves Durable Response Rate in Patients With Advanced Melanoma.* J Clin Oncol, 2015. **33**(25): p. 2780-8.
89. Kohlhapp, F.J., A. Zloza, and H.L. Kaufman, *Talimogene laherparepvec (T-VEC) as cancer immunotherapy.* Drugs Today (Barc), 2015. **51**(9): p. 549-58.
90. MacKie, R.M., B. Stewart, and S.M. Brown, *Intralesional injection of herpes simplex virus 1716 in metastatic melanoma.* Lancet, 2001. **357**(9255): p. 525-6.
91. Harrow, S., et al., *HSV1716 injection into the brain adjacent to tumour following surgical resection of high-grade glioma: safety data and long-term survival.* Gene Ther, 2004. **11**(22): p. 1648-58.
92. Nakao, A., et al., *A phase I dose-escalation clinical trial of intraoperative direct intratumoral injection of HF10 oncolytic virus in non-resectable patients with advanced pancreatic cancer.* Cancer Gene Ther, 2011. **18**(3): p. 167-75.
93. Markert, J.M., et al., *A phase 1 trial of oncolytic HSV-1, G207, given in combination with radiation for recurrent GBM demonstrates safety and radiographic responses.* Mol Ther, 2014. **22**(5): p. 1048-55.
94. Heo, J., et al., *Randomized dose-finding clinical trial of oncolytic immunotherapeutic vaccinia JX-594 in liver cancer.* Nat Med, 2013. **19**(3): p. 329-36.
95. Park, S.H., et al., *Phase 1b Trial of Biweekly Intravenous Pexa-Vec (JX-594), an Oncolytic and Immunotherapeutic Vaccinia Virus in Colorectal Cancer.* Mol Ther, 2015. **23**(9): p. 1532-40.
96. van den Driessche, P., *Reproduction numbers of infectious disease models.* Infect Dis Model, 2017. **2**(3): p. 288-303.
97. Griffin, D.E., *Measles virus-induced suppression of immune responses.* Immunol Rev, 2010. **236**: p. 176-89.

98. Enders, J.F. and T.C. Peebles, *Propagation in tissue cultures of cytopathogenic agents from patients with measles.* Proc Soc Exp Biol Med, 1954. **86**(2): p. 277-86.
99. Enders, J.F., et al., *Studies on an attenuated measles-virus vaccine. I. Development and preparations of the vaccine: technics for assay of effects of vaccination.* N Engl J Med, 1960. **263**: p. 153-9.
100. Angel, J.B., et al., *Vaccine-associated measles pneumonitis in an adult with AIDS.* Ann Intern Med, 1998. **129**(2): p. 104-6.
101. Monafo, W.J., et al., *Disseminated measles infection after vaccination in a child with a congenital immunodeficiency.* J Pediatr, 1994. **124**.
102. Rota, J.S., et al., *Comparison of sequences of the H, F, and N coding genes of measles virus vaccine strains.* Virus Res, 1994. **31**(3): p. 317-30.
103. Plemper, R.K., A.L. Hammond, and R. Cattaneo, *Characterization of a region of the measles virus hemagglutinin sufficient for its dimerization.* J Virol, 2000. **74**(14): p. 6485-93.
104. Navaratnarajah, C.K., et al., *The heads of the measles virus attachment protein move to transmit the fusion-triggering signal.* Nat Struct Mol Biol, 2011. **18**(2): p. 128-34.
105. Eckert, D.M. and P.S. Kim, *Mechanisms of viral membrane fusion and its inhibition.* Annu Rev Biochem, 2001. **70**: p. 777-810.
106. Tatsuo, H., et al., *SLAM (CDw150) is a cellular receptor for measles virus.* Nature, 2000. **406**(6798): p. 893-7.
107. Muhlebach, M.D., et al., *Adherens junction protein nectin-4 is the epithelial receptor for measles virus.* Nature, 2011. **480**(7378): p. 530-3.
108. Dorig, R.E., et al., *The human CD46 molecule is a receptor for measles virus (Edmonston strain).* Cell, 1993. **75**(2): p. 295-305.
109. Noyce, R.S. and C.D. Richardson, *Nectin 4 is the epithelial cell receptor for measles virus.* Trends Microbiol, 2012. **20**(9): p. 429-39.
110. Liszewski, M.K., T.W. Post, and J.P. Atkinson, *Membrane cofactor protein (MCP or CD46): newest member of the regulators of complement activation gene cluster.* Annu Rev Immunol, 1991. **9**: p. 431-55.
111. Kemper, C. and J.P. Atkinson, *Measles virus and CD46.* Curr Top Microbiol Immunol, 2009. **329**: p. 31-57.
112. Clifford, H.D., et al., *CD46 measles virus receptor polymorphisms influence receptor protein expression and primary measles vaccine responses in naive Australian children.* Clin Vaccine Immunol, 2012. **19**(5): p. 704-10.
113. Feenstra, B., et al., *Common variants associated with general and MMR vaccine-related febrile seizures.* Nat Genet, 2014. **46**(12): p. 1274-82.
114. Liszewski, M.K. and J.P. Atkinson, *Complement regulator CD46: genetic variants and disease associations.* Hum Genomics, 2015. **9**: p. 7.
115. Anderson, B.D., et al., *High CD46 receptor density determines preferential killing of tumor cells by oncolytic measles virus.* Cancer Res, 2004. **64**(14): p. 4919-26.
116. Tsujimura, A., et al., *Molecular cloning of a murine homologue of membrane cofactor protein (CD46): preferential expression in testicular germ cells.* Biochem J, 1998. **330 (Pt 1)**: p. 163-8.

117. Horvat, B., et al., *Transgenic mice expressing human measles virus (MV) receptor CD46 provide cells exhibiting different permissivities to MV infections.* J Virol, 1996. **70**(10): p. 6673-81.
118. Mrkic, B., et al., *Measles virus spread and pathogenesis in genetically modified mice.* J Virol, 1998. **72**(9): p. 7420-7.
119. De Salort, J., et al., *Expression of SLAM (CD150) cell-surface receptors on human B-cell subsets: from pro-B to plasma cells.* Immunol Lett, 2011. **134**(2): p. 129-36.
120. Hsu, E.C., et al., *CDw150(SLAM) is a receptor for a lymphotropic strain of measles virus and may account for the immunosuppressive properties of this virus.* Virology, 2001. **279**(1): p. 9-21.
121. Cocks, B.G., et al., *A novel receptor involved in T-cell activation.* Nature, 1995. **376**(6537): p. 260-3.
122. Henning, G., et al., *Signaling lymphocytic activation molecule (SLAM) regulates T cellular cytotoxicity.* Eur J Immunol, 2001. **31**(9): p. 2741-50.
123. Yanagi, Y., M. Takeda, and S. Ohno, *Measles virus: cellular receptors, tropism and pathogenesis.* J Gen Virol, 2006. **87**(Pt 10): p. 2767-79.
124. Mateo, M., et al., *Different roles of the three loops forming the adhesive interface of nectin-4 in measles virus binding and cell entry, nectin-4 homodimerization, and heterodimerization with nectin-1.* J Virol, 2014. **88**(24): p. 14161-71.
125. Takano, A., et al., *Identification of nectin-4 oncoprotein as a diagnostic and therapeutic target for lung cancer.* Cancer Res, 2009. **69**(16): p. 6694-703.
126. Zhang, Y., et al., *A novel PI3K/AKT signaling axis mediates Nectin-4-induced gallbladder cancer cell proliferation, metastasis and tumor growth.* Cancer Lett, 2016. **375**(1): p. 179-89.
127. Petralli, J.K., T.C. Merigan, and J.R. Wilbur, *Circulating Interferon after Measles Vaccination.* N Engl J Med, 1965. **273**: p. 198-201.
128. Mitchell, P.S., M. Emerman, and H.S. Malik, *An evolutionary perspective on the broad antiviral specificity of MxA.* Curr Opin Microbiol, 2013. **16**(4): p. 493-9.
129. Caignard, G., et al., *Inhibition of IFN-alpha/beta signaling by two discrete peptides within measles virus V protein that specifically bind STAT1 and STAT2.* Virology, 2009. **383**(1): p. 112-20.
130. Caignard, G., et al., *Measles virus V protein blocks Jak1-mediated phosphorylation of STAT1 to escape IFN-alpha/beta signaling.* Virology, 2007. **368**(2): p. 351-62.
131. Motz, C., et al., *Paramyxovirus V proteins disrupt the fold of the RNA sensor MDA5 to inhibit antiviral signaling.* Science, 2013. **339**(6120): p. 690-3.
132. Davis, M.E., et al., *Antagonism of the phosphatase PP1 by the measles virus V protein is required for innate immune escape of MDA5.* Cell Host Microbe, 2014. **16**(1): p. 19-30.
133. Shaffer, J.A., W.J. Bellini, and P.A. Rota, *The C protein of measles virus inhibits the type I interferon response.* Virology, 2003. **315**(2): p. 389-97.
134. Van Nguyen, N., et al., *Differential induction of type I interferons in macaques by wild-type measles virus alone or with the hemagglutinin*

protein of the Edmonston vaccine strain. Microbiol Immunol, 2016. **60**(7): p. 501-5.
135. Aguilar Hernandez, S., *Observación de un caso de enfermedad de Hodking, con regresión de los säntomas e infartos ganglionares, postsarampión.* Rev Med Quir Oriente, 1948. **9**: p. 75-82.
136. Gross, S., *Measles and leukaemia.* Lancet, 1971. **1**(7695): p. 397-8.
137. Haralambieva, I.H., et al., *Profiling of measles-specific humoral immunity in individuals following two doses of MMR vaccine using proteome microarrays.* Viruses, 2015. **7**(3): p. 1113-33.
138. de Swart, R.L., S. Yuksel, and A.D. Osterhaus, *Relative contributions of measles virus hemagglutinin- and fusion protein-specific serum antibodies to virus neutralization.* J Virol, 2005. **79**(17): p. 11547-51.
139. Radecke, F., et al., *Rescue of measles viruses from cloned DNA.* Embo j, 1995. **14**(23): p. 5773-84.
140. Schneider, H., et al., *Rescue of measles virus using a replication-deficient vaccinia-T7 vector.* J Virol Methods, 1997. **64**(1): p. 57-64.
141. Peng, K.W., et al., *Non-invasive in vivo monitoring of trackable viruses expressing soluble marker peptides.* Nat Med, 2002. **8**(5): p. 527-31.
142. Iankov, I.D., et al., *Converting tumor-specific markers into reporters of oncolytic virus infection.* Mol Ther, 2009. **17**(8): p. 1395-403.
143. Ungerechts, G., et al., *Lymphoma chemovirotherapy: CD20-targeted and convertase-armed measles virus can synergize with fludarabine.* Cancer Res, 2007. **67**(22): p. 10939-47.
144. Dingli, D., et al., *Image-guided radiovirotherapy for multiple myeloma using a recombinant measles virus expressing the thyroidal sodium iodide symporter.* Blood, 2004. **103**(5): p. 1641-6.
145. Msaouel, P., et al., *Noninvasive imaging and radiovirotherapy of prostate cancer using an oncolytic measles virus expressing the sodium iodide symporter.* Mol Ther, 2009. **17**(12): p. 2041-8.
146. Hutzen, B., et al., *Treatment of medulloblastoma using an oncolytic measles virus encoding the thyroidal sodium iodide symporter shows enhanced efficacy with radioiodine.* BMC Cancer, 2012. **12**: p. 508.
147. Grote, D., R. Cattaneo, and A.K. Fielding, *Neutrophils contribute to the measles virus-induced antitumor effect: enhancement by granulocyte macrophage colony-stimulating factor expression.* Cancer Res, 2003. **63**(19): p. 6463-8.
148. Grossardt, C., et al., *Granulocyte-macrophage colony-stimulating factor-armed oncolytic measles virus is an effective therapeutic cancer vaccine.* Hum Gene Ther, 2013. **24**(7): p. 644-54.
149. Dey, A., et al., *The Role of Neutrophils in Measles Virus-mediated Oncolysis Differs Between B-cell Malignancies and Is Not Always Enhanced by GCSF.* Mol Ther, 2016. **24**(1): p. 184-92.
150. Engeland, C.E., et al., *CTLA-4 and PD-L1 checkpoint blockade enhances oncolytic measles virus therapy.* Mol Ther, 2014. **22**(11): p. 1949-59.
151. Bucheit, A.D., et al., *An oncolytic measles virus engineered to enter cells through the CD20 antigen.* Mol Ther, 2003. **7**(1): p. 62-72.

152. Peng, K.W., et al., *Oncolytic measles viruses displaying a single-chain antibody against CD38, a myeloma cell marker.* Blood, 2003. **101**(7): p. 2557-62.
153. Galanis, E., et al., *Phase I trial of intraperitoneal administration of an oncolytic measles virus strain engineered to express carcinoembryonic antigen for recurrent ovarian cancer.* Cancer Res, 2010. **70**(3): p. 875-82.
154. Nakamura, T., et al., *Antibody-targeted cell fusion.* Nat Biotechnol, 2004. **22**(3): p. 331-6.
155. Nakamura, T., et al., *Rescue and propagation of fully retargeted oncolytic measles viruses.* Nat Biotechnol, 2005. **23**(2): p. 209-14.
156. Heinzerling, L., et al., *Oncolytic measles virus in cutaneous T-cell lymphomas mounts antitumor immune responses in vivo and targets interferon-resistant tumor cells.* Blood, 2005. **106**(7): p. 2287-94.
157. Russell, S.J., et al., *Remission of disseminated cancer after systemic oncolytic virotherapy.* Mayo Clin Proc, 2014. **89**(7): p. 926-33.
158. Galanis, E., et al., *Oncolytic measles virus expressing the sodium iodide symporter to treat drug-resistant ovarian cancer.* Cancer Res, 2015. **75**(1): p. 22-30.
159. Bell, J. and G. McFadden, *Viruses for tumor therapy.* Cell Host Microbe, 2014. **15**(3): p. 260-5.
160. Miest, T.S. and R. Cattaneo, *New viruses for cancer therapy: meeting clinical needs.* Nat Rev Microbiol, 2014. **12**(1): p. 23-34.
161. Naik, S. and S.J. Russell, *Engineering oncolytic viruses to exploit tumor specific defects in innate immune signaling pathways.* Expert Opin Biol Ther, 2009. **9**(9): p. 1163-76.
162. Berchtold, S., et al., *Innate immune defense defines susceptibility of sarcoma cells to measles vaccine virus-based oncolysis.* J Virol, 2013. **87**(6): p. 3484-501.
163. Galanis, E., et al., *Use of viral fusogenic membrane glycoproteins as novel therapeutic transgenes in gliomas.* Hum Gene Ther, 2001. **12**(7): p. 811-21.
164. Bateman, A.R., et al., *Viral fusogenic membrane glycoproteins kill solid tumor cells by nonapoptotic mechanisms that promote cross presentation of tumor antigens by dendritic cells.* Cancer Res, 2002. **62**(22): p. 6566-78.
165. Allen, C., et al., *Adenoviral vectors expressing fusogenic membrane glycoproteins activated via matrix metalloproteinase cleavable linkers have significant antitumor potential in the gene therapy of gliomas.* J Gene Med, 2004. **6**(11): p. 1216-27.
166. Mastrangelo, M.J., et al., *Intratumoral recombinant GM-CSF-encoding virus as gene therapy in patients with cutaneous melanoma.* Cancer Gene Ther, 1999. **6**(5): p. 409-22.
167. Parviainen, S., et al., *GMCSF-armed vaccinia virus induces an antitumor immune response.* Int J Cancer, 2015. **136**(5): p. 1065-72.
168. Guillerme, J.B., et al., *Measles virus vaccine-infected tumor cells induce tumor antigen cross-presentation by human plasmacytoid dendritic cells.* Clin Cancer Res, 2013. **19**(5): p. 1147-58.

169. Evgin, L., et al., *Complement inhibition prevents oncolytic vaccinia virus neutralization in immune humans and cynomolgus macaques.* Mol Ther, 2015. **23**(6): p. 1066-76.
170. Kim, M.K., et al., *Oncolytic and immunotherapeutic vaccinia induces antibody-mediated complement-dependent cancer cell lysis in humans.* Sci Transl Med, 2013. **5**(185): p. 185ra63.
171. Wakimoto, H., et al., *The complement response against an oncolytic virus is species-specific in its activation pathways.* Mol Ther, 2002. **5**(3): p. 275-82.
172. Griffin, D.E., W.H. Lin, and C.H. Pan, *Measles virus, immune control, and persistence.* FEMS Microbiol Rev, 2012. **36**(3): p. 649-62.
173. Permar, S.R., et al., *Limited contribution of humoral immunity to the clearance of measles viremia in rhesus monkeys.* J Infect Dis, 2004. **190**(5): p. 998-1005.
174. Pourchet, A., et al., *CD8(+) T-cell Immune Evasion Enables Oncolytic Virus Immunotherapy.* EBioMedicine, 2016. **5**: p. 59-67.
175. Taipale, K., et al., *Predictive and Prognostic Clinical Variables in Cancer Patients Treated With Adenoviral Oncolytic Immunotherapy.* Mol Ther, 2016. **24**(7): p. 1323-32.
176. Ong, H.T., et al., *Systemically delivered measles virus-infected mesenchymal stem cells can evade host immunity to inhibit liver cancer growth.* J Hepatol, 2013. **59**(5): p. 999-1006.
177. Castleton, A., et al., *Human mesenchymal stromal cells deliver systemic oncolytic measles virus to treat acute lymphoblastic leukemia in the presence of humoral immunity.* Blood, 2014. **123**(9): p. 1327-35.
178. Summers, C., et al., *Neutrophil kinetics in health and disease.* Trends Immunol, 2010. **31**(8): p. 318-24.
179. Wang, J., et al., *Visualizing the function and fate of neutrophils in sterile injury and repair.* Science, 2017. **358**(6359): p. 111-116.
180. Underhill, D.M. and A. Ozinsky, *Phagocytosis of microbes: complexity in action.* Annu Rev Immunol, 2002. **20**: p. 825-52.
181. Ozyalvacli, G., et al., *Diagnostic and prognostic importance of the neutrophil lymphocyte ratio in breast cancer.* Asian Pac J Cancer Prev, 2014. **15**(23): p. 10363-6.
182. Lian, L., et al., *Application of platelet/lymphocyte and neutrophil/lymphocyte ratios in early diagnosis and prognostic prediction in patients with resectable gastric cancer.* Cancer Biomark, 2015. **15**(6): p. 899-907.
183. Yildirim, M.A., et al., *Roles of neutrophil/lymphocyte and platelet/lymphocyte ratios in the early diagnosis of malignant ovarian masses.* Asian Pac J Cancer Prev, 2014. **15**(16): p. 6881-5.
184. Troppan, K., et al., *The derived neutrophil to lymphocyte ratio is an independent prognostic factor in patients with diffuse large B-cell lymphoma.* Br J Cancer, 2014. **110**(2): p. 369-74.
185. Marvel, D. and D.I. Gabrilovich, *Myeloid-derived suppressor cells in the tumor microenvironment: expect the unexpected.* J Clin Invest, 2015. **125**(9): p. 3356-64.

186. Fridlender, Z.G., et al., *Polarization of tumor-associated neutrophil phenotype by TGF-beta: "N1" versus "N2" TAN.* Cancer Cell, 2009. **16**(3): p. 183-94.
187. Engblom, C., et al., *Osteoblasts remotely supply lung tumors with cancer-promoting SiglecF(high) neutrophils.* Science, 2017. **358**(6367).
188. Eruslanov, E.B., et al., *Tumor-associated neutrophils stimulate T cell responses in early-stage human lung cancer.* J Clin Invest, 2014. **124**(12): p. 5466-80.
189. Powell, D.R. and A. Huttenlocher, *Neutrophils in the Tumor Microenvironment.* Trends Immunol, 2016. **37**(1): p. 41-52.
190. Carlomagno, N., et al., *Diagnostic, Predictive, Prognostic, and Therapeutic Molecular Biomarkers in Third Millennium: A Breakthrough in Gastric Cancer.* Biomed Res Int, 2017. **2017**: p. 7869802.
191. Terwilliger, T. and M. Abdul-Hay, *Acute lymphoblastic leukemia: a comprehensive review and 2017 update.* Blood Cancer J, 2017. **7**(6): p. e577.
192. Hoelzer, D., et al., *Improved outcome of adult Burkitt lymphoma/leukemia with rituximab and chemotherapy: report of a large prospective multicenter trial.* Blood, 2014. **124**(26): p. 3870-9.
193. Maury, S., et al., *Rituximab in B-Lineage Adult Acute Lymphoblastic Leukemia.* N Engl J Med, 2016. **375**(11): p. 1044-53.
194. Leach, R.M., M.P. Drummond, and A. Doig, *Practical flow cytometry in haematology diagnosis*. 2013, Oxford: Wiley-Blackwell. viii, 248 pages : illustrations ; 26 cm.
195. Damm, J.K., et al., *Pharmacologically relevant doses of valproate upregulate CD20 expression in three diffuse large B-cell lymphoma patients in vivo.* Exp Hematol Oncol, 2015. **4**: p. 4.
196. Sarro, S.M., et al., *Quantification of CD20 mRNA and protein levels in chronic lymphocytic leukemia suggests a post-transcriptional defect.* Leuk Res, 2010. **34**(12): p. 1670-3.
197. Kalina, T., et al., *EuroFlow standardization of flow cytometer instrument settings and immunophenotyping protocols.* Leukemia, 2012. **26**(9): p. 1986-2010.
198. van Dongen, J.J., et al., *EuroFlow antibody panels for standardized n-dimensional flow cytometric immunophenotyping of normal, reactive and malignant leukocytes.* Leukemia, 2012. **26**(9): p. 1908-75.
199. van Dongen, J.J., A. Orfao, and C. EuroFlow, *EuroFlow: Resetting leukemia and lymphoma immunophenotyping. Basis for companion diagnostics and personalized medicine.* Leukemia, 2012. **26**(9): p. 1899-907.
200. Bloomfield, C.D., et al., *Prognostic significance of the Philadelphia chromosome in acute lymphocytic leukemia.* Cancer Genetics and Cytogenetics, 1980. **1**(3): p. 229-238.
201. Patel, B., et al., *Pegylated-asparaginase during induction therapy for adult acute lymphoblastic leukaemia: toxicity data from the UKALL14 trial.* Leukemia, 2017. **31**(1): p. 58-64.
202. Harrell, F.E., Jr., et al., *Evaluating the yield of medical tests.* JAMA, 1982. **247**(18): p. 2543-6.

203. Harrell, F.E., Jr., et al., *Regression modelling strategies for improved prognostic prediction.* Stat Med, 1984. **3**(2): p. 143-52.
204. Harrell, F.E., Jr., K.L. Lee, and D.B. Mark, *Multivariable prognostic models: issues in developing models, evaluating assumptions and adequacy, and measuring and reducing errors.* Stat Med, 1996. **15**(4): p. 361-87.
205. Youden, W.J., *Index for rating diagnostic tests.* Cancer, 1950. **3**(1): p. 32-5.
206. Hellemans, J., et al., *qBase relative quantification framework and software for management and automated analysis of real-time quantitative PCR data.* Genome Biol, 2007. **8**(2): p. R19.
207. Henry, C., et al., *Identification of an alternative CD20 transcript variant in B-cell malignancies coding for a novel protein associated to rituximab resistance.* Blood, 2010. **115**(12): p. 2420-2429.
208. Gamonet, C., et al., *New CD20 alternative splice variants: molecular identification and differential expression within hematological B cell malignancies.* Exp Hematol Oncol, 2016. **5**.
209. Bustin, S.A., *Why the need for qPCR publication guidelines?--The case for MIQE.* Methods, 2010. **50**(4): p. 217-26.
210. Bustin, S.A., et al., *The MIQE guidelines: minimum information for publication of quantitative real-time PCR experiments.* Clin Chem, 2009. **55**(4): p. 611-22.
211. Thorn, I., et al., *Minimal residual disease assessment in childhood acute lymphoblastic leukaemia: a Swedish multi-centre study comparing real-time polymerase chain reaction and multicolour flow cytometry.* Br J Haematol, 2011. **152**(6): p. 743-53.
212. Alm, S.J., et al., *Minimal residual disease monitoring in childhood B lymphoblastic leukemia with t(12;21)(p13;q22); ETV6-RUNX1: concordant results using quantitation of fusion transcript and flow cytometry.* Int J Lab Hematol, 2017. **39**(2): p. 121-128.
213. Dworzak, M.N., et al., *CD20 up-regulation in pediatric B-cell precursor acute lymphoblastic leukemia during induction treatment: setting the stage for anti-CD20 directed immunotherapy.* Blood, 2008. **112**(10): p. 3982-8.
214. Deans, J.P., et al., *Association of tyrosine and serine kinases with the B cell surface antigen CD20. Induction via CD20 of tyrosine phosphorylation and activation of phospholipase C-gamma 1 and PLC phospholipase C-gamma 2.* J Immunol, 1993. **151**(9): p. 4494-504.
215. Winiarska, M., et al., *Inhibitors of SRC kinases impair antitumor activity of anti-CD20 monoclonal antibodies.* MAbs, 2014. **6**(5): p. 1300-13.
216. Winiarska, M., et al., *Src Family Tyrosine Kinases Are Involved in the Transcriptional Regulation of CD20 Levels.* Blood, 2011. **118**(21): p. 1661-1661.
217. Vongpunsawad, S., et al., *Selectively receptor-blind measles viruses: Identification of residues necessary for SLAM- or CD46-induced fusion and their localization on a new hemagglutinin structural model.* J Virol, 2004. **78**(1): p. 302-13.
218. Yaiw, K.C., et al., *CD20-targeted measles virus shows high oncolytic specificity in clinical samples from lymphoma patients independent of prior rituximab therapy.* Gene Ther, 2011. **18**(3): p. 313-7.

219. Liszewski, M.K. and J.P. Atkinson, *Membrane cofactor protein.* Curr Top Microbiol Immunol, 1992. **178**: p. 45-60.
220. Oglesby, T.J., et al., *Membrane cofactor protein (CD46) protects cells from complement-mediated attack by an intrinsic mechanism.* J Exp Med, 1992. **175**(6): p. 1547-51.
221. Ong, H.T., et al., *Oncolytic measles virus targets high CD46 expression on multiple myeloma cells.* Exp Hematol, 2006. **34**(6): p. 713-20.
222. Schneider-Schaulies, J., et al., *Receptor usage and differential downregulation of CD46 by measles virus wild-type and vaccine strains.* Proc Natl Acad Sci U S A, 1995. **92**(9): p. 3943-7.
223. Schnorr, J.J., et al., *Measles virus-induced down-regulation of CD46 is associated with enhanced sensitivity to complement-mediated lysis of infected cells.* Eur J Immunol, 1995. **25**(4): p. 976-84.
224. Dispenzieri, A., et al., *Phase I trial of systemic administration of Edmonston strain of measles virus genetically engineered to express the sodium iodide symporter in patients with recurrent or refractory multiple myeloma.* Leukemia, 2017. **31**(12): p. 2791-2798.
225. Lech, P.J., et al., *Antibody neutralization of retargeted measles viruses.* Virology, 2014. **454-455**: p. 237-46.
226. Patel, B., et al., *Differential cytopathology and kinetics of measles oncolysis in two primary B-cell malignancies provides mechanistic insights.* Mol Ther, 2011. **19**(6): p. 1034-40.
227. Zhang, Y., et al., *Attenuated, oncolytic, but not wild-type measles virus infection has pleiotropic effects on human neutrophil function.* J Immunol, 2012. **188**(3): p. 1002-10.
228. Singh, V., et al., *Surface levels of CD20 determine anti-CD20 antibodies mediated cell death in vitro.* PLoS One, 2014. **9**(11): p. e111113.
229. Kurokawa, C., et al., *Constitutive Interferon Pathway Activation in Tumors as an Efficacy Determinant Following Oncolytic Virotherapy.* J Natl Cancer Inst, 2018. **110**(10): p. 1123-1132.
230. Nosaki, K., et al., *A novel, polymer-coated oncolytic measles virus overcomes immune suppression and induces robust antitumor activity.* Mol Ther Oncolytics, 2016. **3**: p. 16022.
231. Barth, M.J., et al., *Ofatumumab Exhibits Enhanced In Vitro and In Vivo Activity Compared to Rituximab in Preclinical Models of Mantle Cell Lymphoma.* Clin Cancer Res, 2015. **21**(19): p. 4391-7.
232. Jilani, I., et al., *Transient down-modulation of CD20 by rituximab in patients with chronic lymphocytic leukemia.* Blood, 2003. **102**(10): p. 3514-20.
233. Marty, R.R., et al., *An immune competent mouse model for the characterization of recombinant measles vaccines.* Hum Vaccin Immunother, 2015. **11**(1): p. 83-90.
234. Dey, A., et al., *The Role of Neutrophils in Measles Virus-mediated Oncolysis Differs Between B-cell Malignancies and Is Not Always Enhanced by GCSF.* Mol Ther, 2015.
235. Prince, L.R., et al., *The role of TLRs in neutrophil activation.* Curr Opin Pharmacol, 2011. **11**(4): p. 397-403.

236. Hashimoto, Y., et al., *Evidence for phagocytosis of influenza virus-infected, apoptotic cells by neutrophils and macrophages in mice.* J Immunol, 2007. **178**(4): p. 2448-57.
237. Ratcliffe, D.R., S.L. Nolin, and E.B. Cramer, *Neutrophil interaction with influenza-infected epithelial cells.* Blood, 1988. **72**(1): p. 142-9.
238. Grundy, J.E., et al., *Cytomegalovirus-infected endothelial cells recruit neutrophils by the secretion of C-X-C chemokines and transmit virus by direct neutrophil-endothelial cell contact and during neutrophil transendothelial migration.* J Infect Dis, 1998. **177**(6): p. 1465-74.
239. Kurt-Jones, E.A., et al., *Pattern recognition receptors TLR4 and CD14 mediate response to respiratory syncytial virus.* Nat Immunol, 2000. **1**(5): p. 398-401.
240. Heemskerk, N. and M. van Egmond, *Monoclonal antibody-mediated killing of tumour cells by neutrophils.* Eur J Clin Invest, 2018. **48 Suppl 2**: p. e12962.
241. Stockmeyer, B., et al., *Triggering Fc alpha-receptor I (CD89) recruits neutrophils as effector cells for CD20-directed antibody therapy.* J Immunol, 2000. **165**(10): p. 5954-61.
242. Zhang, Y., *Investigation into the effects of oncolytic measles virotherapy on neutrophil function*, in *Haematology*. 2012, University College London: London.
243. Aleyd, E., et al., *IgA enhances NETosis and release of neutrophil extracellular traps by polymorphonuclear cells via Fcalpha receptor I.* J Immunol, 2014. **192**(5): p. 2374-83.
244. Horner, H., et al., *Intimate cell conjugate formation and exchange of membrane lipids precede apoptosis induction in target cells during antibody-dependent, granulocyte-mediated cytotoxicity.* J Immunol, 2007. **179**(1): p. 337-45.
245. Shibata-Koyama, M., et al., *Nonfucosylated rituximab potentiates human neutrophil phagocytosis through its high binding for FcgammaRIIIb and MHC class II expression on the phagocytotic neutrophils.* Exp Hematol, 2009. **37**(3): p. 309-21.
246. Golay, J., et al., *Glycoengineered CD20 antibody obinutuzumab activates neutrophils and mediates phagocytosis through CD16B more efficiently than rituximab.* Blood, 2013. **122**(20): p. 3482-91.
247. Suttmann, H., et al., *Neutrophil granulocytes are required for effective Bacillus Calmette-Guerin immunotherapy of bladder cancer and orchestrate local immune responses.* Cancer Res, 2006. **66**(16): p. 8250-7.
248. Fu, X., et al., *Virotherapy induces massive infiltration of neutrophils in a subset of tumors defined by a strong endogenous interferon response activity.* Cancer Gene Ther, 2011. **18**(11): p. 785-94.
249. Holl, E.K., et al., *Recombinant oncolytic poliovirus, PVSRIPO, has potent cytotoxic and innate inflammatory effects, mediating therapy in human breast and prostate cancer xenograft models.* Oncotarget, 2016. **7**(48): p. 79828-79841.
250. Dey, A., *Enhancing the neutrophil-mediated anti-cancer response after oncolytic measles virus therapy in B-cell malignancy: Dissecting out the mechanism*, in *Research Department of Haematology*. 2016, UCL.

251. Dheilly, E., et al., *Selective Blockade of the Ubiquitous Checkpoint Receptor CD47 Is Enabled by Dual-Targeting Bispecific Antibodies.* Mol Ther, 2017. **25**(2): p. 523-533.
252. Buatois, V., et al., *Preclinical Development of a Bispecific Antibody that Safely and Effectively Targets CD19 and CD47 for the Treatment of B-Cell Lymphoma and Leukemia.* Mol Cancer Ther, 2018. **17**(8): p. 1739-1751.
253. Valgardsdottir, R., et al., *Human neutrophils mediate trogocytosis rather than phagocytosis of CLL B cells opsonized with anti-CD20 antibodies.* Blood, 2017. **129**(19): p. 2636-2644.
254. Matlung, H.L., et al., *Neutrophils Kill Antibody-Opsonized Cancer Cells by Trogoptosis.* Cell Rep, 2018. **23**(13): p. 3946-3959 e6.
255. Borowitz, M.J., et al., *Surface antigen phenotype can predict TEL-AML1 rearrangement in childhood B-precursor ALL: a Pediatric Oncology Group study.* Leukemia, 1998. **12**(11): p. 1764-70.
256. Olsen, M., et al., *Preleukemic TEL-AML1-positive clones at cell level of 10(-3) to 10(-4) do not persist into adulthood.* J Pediatr Hematol Oncol, 2006. **28**(11): p. 734-40.
257. Khan, N., et al., *Expression of CD33 is a predictive factor for effect of gemtuzumab ozogamicin at different doses in adult acute myeloid leukaemia.* Leukemia, 2017. **31**(5): p. 1059-1068.

Appendix 1: Full gating strategy for ADCP assay

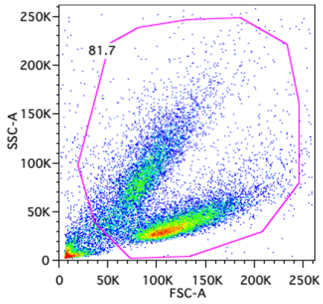

Live/Dead Staining

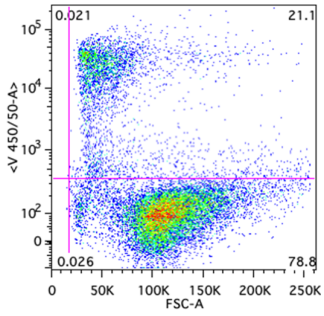

Live/Dead CONTROL

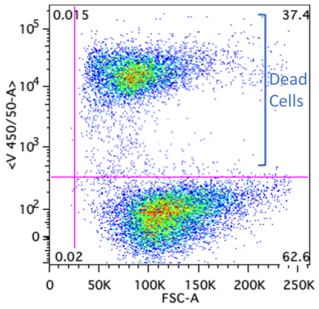

Doublet exclusion

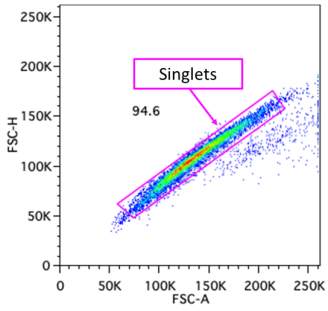

Double positives [CD15+/PKH67+] taken as proportion of total neutrophils [CD15+]

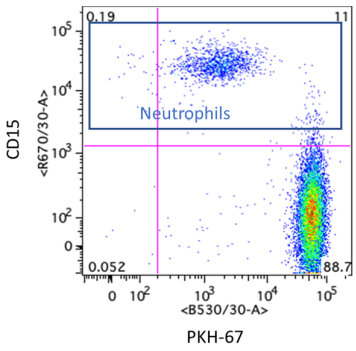

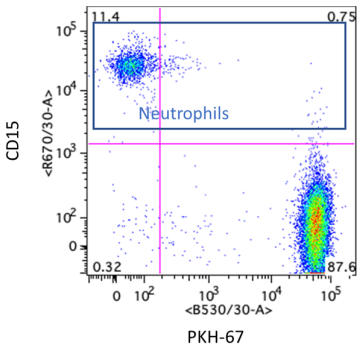

Appendix 2: RT^2 profiler gene lists – Human Phagocytosis

Position	UniGene	GenBank	Symbol	Description
A01	Hs.80485	NM_004797	ADIPOQ	Adiponectin, C1Q and collagen domain containing
A02	Hs.534342	NM_001136	AGER	Advanced glycosylation end product-specific receptor
A03	Hs.494173	NM_000700	ANXA1	Annexin A1
A04	Hs.590970	NM_001699	AXL	AXL receptor tyrosine kinase
A05	Hs.529053	NM_000064	C3	Complement component 3
A06	Hs.515162	NM_004343	CALR	Calreticulin
A07	Hs.163867	NM_000591	CD14	CD14 molecule
A08	Hs.120949	NM_000072	CD36	CD36 molecule (thrombospondin receptor)
A09	Hs.502328	NM_000610	CD44	CD44 molecule (Indian blood group)
A10	Hs.446414	NM_001777	CD47	CD47 molecule
A11	Hs.11	NM_001815	CEACAM3	Carcinoembryonic antigen-related cell adhesion molecule 3
A12	Hs.143929	NM_022570	CLEC7A	C-type lectin domain family 7, member A
B01	Hs.440544	NM_013943	CLIC4	Chloride intracellular channel 4
B02	Hs.651512	NM_004368	CNN2	Calponin 2
B03	Hs.464422	NM_130386	COLEC12	Collectin sub-family member 12
B04	Hs.334019	NM_000573	CR1	Complement component (3b/4b) receptor 1 (Knops blood group)
B05	Hs.461896	NM_016823	CRK	V-crk sarcoma virus CT10 oncogene homolog (avian)
B06	Hs.709456	NM_000567	CRP	C-reactive protein, pentraxin-related
B07	Hs.173894	NM_000757	CSF1	Colony stimulating factor 1 (macrophage)
B08	Hs.1349	NM_000758	CSF2	Colony stimulating factor 2 (granulocyte-macrophage)
B09	Hs.77793	NM_004383	CSK	C-src tyrosine kinase
B10	Hs.98370	NM_030632	CYBB	Cytochrome B-245, beta polypeptide

B10	Hs.98370	NM_030622	CYP2S1	Cytochrome P450, family 2, subfamily S, polypeptide 1
B11	Hs.159195	NM_001380	DOCK1	Dedicator of cytokinesis 1
B12	Hs.586174	NM_004946	DOCK2	Dedicator of cytokinesis 2
C01	Hs.656638	NM_130442	ELMO1	Engulfment and cell motility 1
C02	Hs.667309	NM_000043	FAS	Fas (TNF receptor superfamily, member 6)
C03	Hs.433300	NM_004106	FCER1G	Fc fragment of IgE, high affinity I, receptor for; gamma polypeptide
C04	Hs.77424	NM_000566	FCGR1A	Fc fragment of IgG, high affinity Ia, receptor (CD64)
C05	Hs.352642	NM_021642	FCGR2A	Fc fragment of IgG, low affinity IIa, receptor (CD32)
C06	Hs.654395	NM_004001	FCGR2B	Fc fragment of IgG, low affinity IIb, receptor (CD32)
C07	Hs.390567	NM_002037	FYN	FYN oncogene related to SRC, FGR, YES
C08	Hs.470887	NM_016315	GULP1	GULP, engulfment adaptor PTB domain containing 1
C09	Hs.856	NM_000619	IFNG	Interferon, gamma
C10	Hs.66	NM_016232	IL1RL1	Interleukin 1 receptor-like 1
C11	Hs.172631	NM_000632	ITGAM	Integrin, alpha M (complement component 3 receptor 3 subunit)
C12	Hs.436873	NM_002210	ITGAV	Integrin, alpha V (vitronectin receptor, alpha polypeptide, antigen CD51)
D01	Hs.375957	NM_000211	ITGB2	Integrin, beta 2 (complement component 3 receptor 3 and 4 subunit)
D02	Hs.491767	NM_002350	LYN	V-yes-1 Yamaguchi sarcoma viral related oncogene homolog
D03	Hs.485233	NM_001315	MAPK14	Mitogen-activated protein kinase 14
D04	Hs.67726	NM_006770	MARCO	Macrophage receptor with collagenous structure
D05	Hs.499674	NM_000242	MBL2	Mannose-binding lectin (protein C) 2, soluble
D06	Hs.535239	NM_018298	MCOLN3	Mucolipin 3
D07	Hs.306178	NM_006343	MERTK	C-mer proto-oncogene tyrosine kinase
D08	Hs.3745	NM_005928	MFGE8	Milk fat globule-EGF factor 8 protein
D09	Hs.407995	NM_002415	MIF	Macrophage migration inhibitory factor (glycosylation-inhibiting factor)

Position	UniGene	GenBank	Symbol	Description
D10	Hs.713679	NM_002444	MSN	Moesin
D11	Hs.82116	NM_002468	MYD88	Myeloid differentiation primary response gene (88)
D12	Hs.738731	NM_006092	NOD1	Nucleotide-binding oligomerization domain containing 1
E01	Hs.514412	NM_000442	PECAM1	Platelet/endothelial cell adhesion molecule
E02	Hs.655131	NM_003557	PIP5K1A	Phosphatidylinositol-4-phosphate 5-kinase, type I, alpha
E03	Hs.497200	NM_024420	PLA2G4A	Phospholipase A2, group IVA (cytosolic, calcium-dependent)
E04	Hs.319438	NM_000929	PLA2G5	Phospholipase A2, group V
E05	Hs.732969	NM_002662	PLD1	Phospholipase D1, phosphatidylcholine-specific
E06	Hs.104519	NM_002663	PLD2	Phospholipase D2
E07	Hs.580351	NM_005400	PRKCE	Protein kinase C, epsilon
E08	Hs.64016	NM_000313	PROS1	Protein S (alpha)
E09	Hs.729457	NM_000314	PTEN	Phosphatase and tensin homolog
E10	Hs.475663	NM_004162	RAB5A	RAB5A, member RAS oncogene family
E11	Hs.684374	NM_004637	RAB7A	RAB7A, member RAS oncogene family
E12	Hs.413812	NM_006908	RAC1	Ras-related C3 botulinum toxin substrate 1 (rho family, small GTP binding protein Rac1)
F01	Hs.517601	NM_002872	RAC2	Ras-related C3 botulinum toxin substrate 2 (rho family, small GTP binding protein Rac2)
F02	Hs.6906	NM_005402	RALA	V-ral simian leukemia viral oncogene homolog A (ras related)
F03	Hs.469820	NM_002881	RALB	V-ral simian leukemia viral oncogene homolog B (ras related; GTP binding protein)
F04	Hs.8578	NM_006105	RAPGEF3	Rap guanine nucleotide exchange factor (GEF) 3
F05	Hs.247077	NM_001664	RHOA	Ras homolog gene family, member A
F06	Hs.731377	NM_005505	SCARB1	Scavenger receptor class B, member 1
F07	Hs.414795	NM_000602	SERPINE1	Serpin peptidase inhibitor, clade E (nexin, plasminogen activator inhibitor type 1), member 1
F08	Hs.253495	NM_003019	SFTPD	Surfactant protein D

F09	Hs.31869	NM_023068	SIGLEC1	Sialic acid binding Ig-like lectin 1, sialoadhesin
F10	Hs.661852	NM_052884	SIGLEC11	Sialic acid binding Ig-like lectin 11
F11	Hs.664861	NM_006065	SIRPB1	Signal-regulatory protein beta 1
F12	Hs.408249	NM_017564	STAB2	Stabilin 2
G01	Hs.584913	NM_016930	STX18	Syntaxin 18
G02	Hs.371720	NM_003177	SYK	Spleen tyrosine kinase
G03	Hs.517033	NM_004613	TGM2	Transglutaminase 2 (C polypeptide, protein-glutamine-gamma-glutamyltransferase)
G04	Hs.29344	NM_182919	TICAM1	Toll-like receptor adaptor molecule 1
G05	Hs.657724	NM_003265	TLR3	Toll-like receptor 3
G06	Hs.87968	NM_017442	TLR9	Toll-like receptor 9
G07	Hs.241570	NM_000594	TNF	Tumor necrosis factor
G08	Hs.333791	NM_003701	TNFSF11	Tumor necrosis factor (ligand) superfamily, member 11
G09	Hs.24167	NM_005638	VAMP7	Vesicle-associated membrane protein 7
G10	Hs.116237	NM_005428	VAV1	Vav 1 guanine nucleotide exchange factor
G11	Hs.2157	NM_000377	WAS	Wiskott-Aldrich syndrome (eczema-thrombocytopenia)
G12	Hs.643085	NM_003392	WNT5A	Wingless-type MMTV integration site family, member 5A
H01	Hs.520640	NM_001101	ACTB	Actin, beta
H02	Hs.534255	NM_004048	B2M	Beta-2-microglobulin
H03	Hs.592355	NM_002046	GAPDH	Glyceraldehyde-3-phosphate dehydrogenase
H04	Hs.412707	NM_000194	HPRT1	Hypoxanthine phosphoribosyltransferase 1
H05	Hs.546285	NM_001002	RPLP0	Ribosomal protein, large, P0
H06	N/A	SA_00105	HGDC	Human Genomic DNA Contamination
H07	N/A	SA_00104	RTC	Reverse Transcription Control
H08	N/A	SA_00104	RTC	Reverse Transcription Control
H09	N/A	SA_00104	RTC	Reverse Transcription Control
H10	N/A	SA_00103	PPC	Positive PCR Control
H11	N/A	SA_00103	PPC	Positive PCR Control
H12	N/A	SA_00103	PPC	Positive PCR Control

RT^2 profiler gene lists: Human cytokines and chemokines

Position	UniGene	GenBank	Symbol	Description
A01	Hs.80485	NM_004797	ADIPOQ	Adiponectin, C1Q and collagen domain containing
A02	Hs.73853	NM_001200	BMP2	Bone morphogenetic protein 2
A03	Hs.68879	NM_130851	BMP4	Bone morphogenetic protein 4
A04	Hs.285671	NM_001718	BMP6	Bone morphogenetic protein 6
A05	Hs.473163	NM_001719	BMP7	Bone morphogenetic protein 7
A06	Hs.494997	NM_001735	C5	Complement component 5
A07	Hs.72918	NM_002981	CCL1	Chemokine (C-C motif) ligand 1
A08	Hs.54460	NM_002986	CCL11	Chemokine (C-C motif) ligand 11
A09	Hs.414629	NM_005408	CCL13	Chemokine (C-C motif) ligand 13
A10	Hs.546294	NM_002987	CCL17	Chemokine (C-C motif) ligand 17
A11	Hs.143961	NM_002988	CCL18	Chemokine (C-C motif) ligand 18 (pulmonary and activation-regulated)
A12	Hs.50002	NM_006274	CCL19	Chemokine (C-C motif) ligand 19
B01	Hs.303649	NM_002982	CCL2	Chemokine (C-C motif) ligand 2
B02	Hs.75498	NM_004591	CCL20	Chemokine (C-C motif) ligand 20
B03	Hs.57907	NM_002989	CCL21	Chemokine (C-C motif) ligand 21
B04	Hs.534347	NM_002990	CCL22	Chemokine (C-C motif) ligand 22
B05	Hs.247838	NM_002991	CCL24	Chemokine (C-C motif) ligand 24
B06	Hs.514107	NM_002983	CCL3	Chemokine (C-C motif) ligand 3
B07	Hs.514821	NM_002985	CCL5	Chemokine (C-C motif) ligand 5
B08	Hs.251526	NM_006273	CCL7	Chemokine (C-C motif) ligand 7
B09	Hs.271387	NM_005623	CCL8	Chemokine (C-C motif) ligand 8

B10	Hs.592244	NM_000074	CD40LG	CD40 ligand
B11	Hs.715806	NM_000614	CNTF	Ciliary neurotrophic factor
B12	Hs.591402	NM_000757	CSF1	Colony stimulating factor 1 (macrophage)
C01	Hs.1349	NM_000758	CSF2	Colony stimulating factor 2 (granulocyte-macrophage)
C02	Hs.2233	NM_000759	CSF3	Colony stimulating factor 3 (granulocyte)
C03	Hs.531668	NM_002996	CX3CL1	Chemokine (C-X3-C motif) ligand 1
C04	Hs.789	NM_001511	CXCL1	Chemokine (C-X-C motif) ligand 1 (melanoma growth stimulating activity, alpha)
C05	Hs.632586	NM_001565	CXCL10	Chemokine (C-X-C motif) ligand 10
C06	Hs.632592	NM_005409	CXCL11	Chemokine (C-X-C motif) ligand 11
C07	Hs.522891	NM_000609	CXCL12	Chemokine (C-X-C motif) ligand 12
C08	Hs.100431	NM_006419	CXCL13	Chemokine (C-X-C motif) ligand 13
C09	Hs.708201	NM_022059	CXCL16	Chemokine (C-X-C motif) ligand 16
C10	Hs.590921	NM_002089	CXCL2	Chemokine (C-X-C motif) ligand 2
C11	Hs.89714	NM_002994	CXCL5	Chemokine (C-X-C motif) ligand 5
C12	Hs.77367	NM_002416	CXCL9	Chemokine (C-X-C motif) ligand 9
D01	Hs.2007	NM_000639	FASLG	Fas ligand (TNF superfamily, member 6)
D02	Hs.466471	NM_000175	GPI	Glucose-6-phosphate isomerase
D03	Hs.211575	NM_000605	IFNA2	Interferon, alpha 2
D04	Hs.856	NM_000619	IFNG	Interferon, gamma
D05	Hs.193717	NM_000572	IL10	Interleukin 10
D06	Hs.467304	NM_000641	IL11	Interleukin 11
D07	Hs.673	NM_000882	IL12A	Interleukin 12A (natural killer cell stimulatory factor 1, cytotoxic lymphocyte maturation factor 1, p35)
				Interleukin 12B (natural killer cell stimulatory factor 2, cytotoxic lymphocyte

Position	UniGene	GenBank	Symbol	Description
D08	Hs.674	NM_002187	IL12B	maturation factor 2, p40)
D09	Hs.845	NM_002188	IL13	Interleukin 13
D10	Hs.654378	NM_000585	IL15	Interleukin 15
D11	Hs.459095	NM_004513	IL16	Interleukin 16
D12	Hs.41724	NM_002190	IL17A	Interleukin 17A
E01	Hs.272295	NM_052872	IL17F	Interleukin 17F
E02	Hs.83077	NM_001562	IL18	Interleukin 18 (interferon-gamma-inducing factor)
E03	Hs.1722	NM_000575	IL1A	Interleukin 1, alpha
E04	Hs.126256	NM_000576	IL1B	Interleukin 1, beta
E05	Hs.81134	NM_000577	IL1RN	Interleukin 1 receptor antagonist
E06	Hs.89679	NM_000586	IL2	Interleukin 2
E07	Hs.567559	NM_021803	IL21	Interleukin 21
E08	Hs.287369	NM_020525	IL22	Interleukin 22
E09	Hs.98309	NM_016584	IL23A	Interleukin 23, alpha subunit p19
E10	Hs.411311	NM_006850	IL24	Interleukin 24
E11	Hs.528111	NM_145659	IL27	Interleukin 27
E12	Hs.694	NM_000588	IL3	Interleukin 3 (colony-stimulating factor, multiple)
F01	Hs.73917	NM_000589	IL4	Interleukin 4
F02	Hs.2247	NM_000879	IL5	Interleukin 5 (colony-stimulating factor, eosinophil)
F03	Hs.654458	NM_000600	IL6	Interleukin 6 (interferon, beta 2)
F04	Hs.591873	NM_000880	IL7	Interleukin 7
F05	Hs.624	NM_000584	IL8	Interleukin 8
F06	Hs.960	NM_000590	IL9	Interleukin 9
F07	Hs.2250	NM_002309	LIF	Leukemia inhibitory factor (cholinergic differentiation factor)
F08	Hs.36	NM_000595	LTA	Lymphotoxin alpha (TNF superfamily, member 1)
F09	Hs.376208	NM_002341	LTB	Lymphotoxin beta (TNF superfamily, member 3)

F10	Hs.407995	NM_002415	MIF	Macrophage migration inhibitory factor (glycosylation-inhibiting factor)
F11	Hs.41565	NM_005259	MSTN	Myostatin
F12	Hs.370414	NM_018055	NODAL	Nodal homolog (mouse)
G01	Hs.248156	NM_020530	OSM	Oncostatin M
G02	Hs.2164	NM_002704	PPBP	Pro-platelet basic protein (chemokine (C-X-C motif) ligand 7)
G03	Hs.313	NM_000582	SPP1	Secreted phosphoprotein 1
G04	Hs.133379	NM_003238	TGFB2	Transforming growth factor, beta 2
G05	Hs.1166	NM_000460	THPO	Thrombopoietin
G06	Hs.241570	NM_000594	TNF	Tumor necrosis factor
G07	Hs.81791	NM_002546	TNFRSF11B	Tumor necrosis factor receptor superfamily, member 11b
G08	Hs.478275	NM_003810	TNFSF10	Tumor necrosis factor (ligand) superfamily, member 10
G09	Hs.333791	NM_003701	TNFSF11	Tumor necrosis factor (ligand) superfamily, member 11
G10	Hs.525157	NM_006573	TNFSF13B	Tumor necrosis factor (ligand) superfamily, member 13b
G11	Hs.73793	NM_003376	VEGFA	Vascular endothelial growth factor A
G12	Hs.546295	NM_002995	XCL1	Chemokine (C motif) ligand 1
H01	Hs.520640	NM_001101	ACTB	Actin, beta
H02	Hs.534255	NM_004048	B2M	Beta-2-microglobulin
H03	Hs.592355	NM_002046	GAPDH	Glyceraldehyde-3-phosphate dehydrogenase
H04	Hs.412707	NM_000194	HPRT1	Hypoxanthine phosphoribosyltransferase 1
H05	Hs.546285	NM_001002	RPLP0	Ribosomal protein, large, P0
H06	N/A	SA_00105	HGDC	Human Genomic DNA Contamination
H07	N/A	SA_00104	RTC	Reverse Transcription Control
H08	N/A	SA_00104	RTC	Reverse Transcription Control
H09	N/A	SA_00104	RTC	Reverse Transcription Control
H10	N/A	SA_00103	PPC	Positive PCR Control
H11	N/A	SA_00103	PPC	Positive PCR Control
H12	N/A	SA_00103	PPC	Positive PCR Control